

**KINEMATIC AND INERTIAL RESPONSE OF PILED RAFT
FOUNDATIONS: NUMERICAL AND EXPERIMENTAL STUDIES**

A THESIS

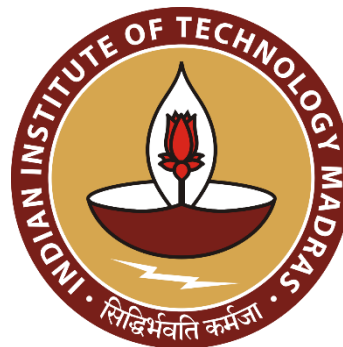
Submitted by

RAMON VARGHESE

for the award of the degree

of

DOCTOR OF PHILOSOPHY



**DEPARTMENT OF CIVIL ENGINEERING
INDIAN INSTITUTE OF TECHNOLOGY MADRAS**

CHENNAI, INDIA

SEPTEMBER 2020

To the spirit of inquiry

THESIS CERTIFICATE

This is to certify that the thesis titled “**KINEMATIC AND INERTIAL RESPONSE OF PILED RAFT FOUNDATIONS: NUMERICAL AND EXPERIMENTAL STUDIES**” submitted by **Ramon Varghese**, to the Department of Civil Engineering, Indian Institute of Technology Madras, Chennai, for the award of the degree of Doctor of Philosophy is a bonafide record of research work carried out by him under my supervision. The contents of this thesis, in full or in parts, have not been submitted and will not be submitted to any other Institute or University for the award of any degree or diploma.

Chennai, India

6th August 2020

Prof. A. Boominathan

Research Guide

Associate Professor

Department of Civil Engineering

Indian Institute of Technology

Madras

Chennai - 600 036, India

Dr. Subhadeep Banerjee

Research Co-guide

Associate Professor

Department of Civil Engineering

Indian Institute of Technology

Madras

Chennai - 600 036, India

ACKNOWLEDGEMENTS

The journey that led me to this day with a dissertation in hand has been remarkable. I wouldn't have made it here had it not been for the individuals whom I wish to acknowledge.

I had the good fortune to work with supportive supervisors at IIT Madras. I wish to wholeheartedly thank my supervisor Prof. A. Boominathan for his enduring support. He exposed me to the world of research and professional consultancy, which has broadened my perspective. I also remember with gratitude the constant encouragement, and care from my co-supervisor, Dr Subhadeep Banerjee. His support during the entire duration of my research at IIT Madras will be remembered.

I wish to thank the faculty members of the Geotechnical Division, and Heads of the Civil Engineering Department who were supportive and generous. I wish to thank my doctoral committee members, Prof. Sathish Kumar, Prof. S. Nallayarasu, and Prof R.G Robinson, for their valuable comments on my work. I also wish to wholeheartedly thank Dr Arun Menon for his support and guidance during the experimental program using the new biaxial shaking table at the Structural Engineering laboratory. The help extended by technical staff, namely Mr Om Prakash, Mr Suresh P., and Mr Soundarapandian of the Geotechnical Engineering laboratory is thankfully remembered. I wish to express my sincere thanks to Mr Aravindraaj, technician at the Soil Dynamics and Earthquake Engineering laboratory, for his valuable help towards laboratory experiments as well as instrumentation for shaking table tests.

The support received from industry professionals was immense. The expensive computational tools used in this research and the procurement of undisturbed soil samples were made possible by a sponsored research project funded by the Nuclear Power Corporation of India Limited, Mumbai. I wish to thank Dr Rajiv Ranjan and Abhishek Tripathi for the many thought-provoking discussions and the finite element model of the nuclear building foundation used in this study. I also acknowledge the support received from engineers at Reliance Industries Ltd, Hazira, towards conducting dynamic pile load tests at their site.

Friends were instrumental in my well-being during my stay in the IIT Madras campus. I remember with sincere gratitude, the support and care extended by V. Jyothsna. I thank Senthen Amuthan, and Dhanya J.S for the thought-provoking discussions and encouragement. Friends

from my lab, Vijaya Ramanathan, Priya Sudevan, and Vineetha K. will be fondly remembered for all the happy occasions and coffee breaks. I remember with love friends such as Jerin Jose, Amal Azad, Malavika Varma, Dinesh N., Nikhil John, S.R Kumar, George Rahul, and Anju Leela Thomas for all the meaningful discussions and support. I also thankfully remember the lot many folks at IITM, from the security guards to mess staff who made my stay in campus pleasant and memorable.

I also graciously remember my family, that patiently supported me through the many years of college education. I graciously remember my father George Varghese for igniting the fire in a high school kid. I fondly remember my mother Susamma Varghese, sister Ria Rachel, and niece Christine for standing by my side as always.

Ramon Varghese

ABSTRACT

Keywords: Piled raft, SSI, Substructuring method, SASSI, Kinematic response, Pile impedance, Shaking table

Piles are columnar foundation elements that are primarily used to transmit vertical loads from structures to deeper, competent strata. In addition to vertical loads, pile foundations can also be subjected to lateral loads, uplift forces, and dynamic forces. There has been an increasing trend towards the design philosophy where the load is transferred to the soil from the pile cap, in parallel to the pile group, which proves economical for heavily loaded structures. Such a foundation where the total load is shared between the pile cap and the pile group is called pile raft foundation. Past experiences have shown that earthquakes can cause permanent and devastating damages to pile supported structures. However, the effect of a thick raft on the foundation input motion, dynamic stiffness, and pile forces, which are relevant in the case of piled rafts, have not been comprehensively studied in the past.

In the present study, the Flexible Volume Substructuring Methodology (FVSM) was adopted for rigorous 3D analysis of the soil-piled raft interaction problem. An algorithm for finite element mesh partitioning and merging of data for execution using the ACS SASSI program was developed. The methodology was verified using standard analytical solutions on the kinematic and dynamic response of single and group piles. A centrifuge shaking table test on a piled raft clay system reported in literature was also simulated. The methodology was then extended to an extensive numerical study on the kinematic and inertial response of piled rafts.

From studies on 2x2 piled raft-clay models, it was found that the translational and rocking response of piled rafts and pile groups do not differ considerably at low frequencies. However, the ratio of translational response of piled raft to pile group was found to increase with increasing pile spacing, at intermediate to high frequencies. A clear trend of increasing filtering of translational response with increasing raft embedment was found from kinematic response factor plots of 3x3, and 5x3 piled rafts in four different soil profiles. An increasing embedment depth was found to increase the rocking response for the 3x3 piled rafts. This effect, however, diminished when the number of piles in the direction of motion was increased. From studies on transient response using eight different ground motion time histories, it was found that the

embedment of the raft influenced all of the critical parameters that define the spectral ratio curve.

The presence of a circular ground contacting cap on a single pile was found to have a significant influence on the stiffness and damping coefficients in stiff soils. In the case of a 2x2 piled raft, the amplitude and phase of the dynamic piled raft interaction factor were found to be strongly influenced by both pile-soil modulus ratio and area ratio of the piled raft, in both vertical and horizontal modes. The ratio of the load carried by the pile in a capped pile was found to be primarily dependent on the relative pile-soil stiffness and frequency of vibration, in the vertical mode of vibration. However, the dependency on frequency was mild in the horizontal mode of vibration. Results from the study suggest that the design of a piled raft for high frequency dynamic loads has to consider the deviation from static load sharing at high frequencies.

The influence of an embedded raft on the kinematic response factor in translation was then studied by carrying out a shaking table test on a scaled down soil-foundation model. The test program consisted of a 2x2 piled raft and a 2x2 pile group model embedded in clay subjected to harmonic input motion. The kinematic interaction factor in translation, calculated from the experimental results was in agreement with the numerically obtained trend. The pile head bending strains in the piled raft and pile group were found to be close to each other up to a frequency of 15 Hz.

The study was then extended to two practical case studies on seismic response of piled rafts. The first case study dealt with the seismic response of an idealized single degree of freedom system supported by a 2x2 piled raft in layered soil. A novel non-dimensional axial force factor was proposed to quantify the role of piles in resisting overturning moments acting on a piled raft. The second case study dealt with a large 100m x 100m piled raft foundation designed for an upcoming nuclear reactor building in India. It was found that a stiff improved layer below the raft alters the kinematic response factors in translation and rotation significantly when compared to the natural soil profile. From a transient ground motion analysis using eight different earthquake time histories, it was found that the improved layer causes an increase in the spectral ratio at zero period by a factor of 1.13 and a reduction in the critical structural period by a factor of 0.25.

TABLE OF CONTENTS

ACKNOWLEDGEMENTS	i
ABSTRACT.....	iii
TABLE OF CONTENTS	v
LIST OF TABLES	x
LIST OF FIGURES.....	xi
NOTATIONS AND ABBREVIATIONS	xviii
CHAPTER 1 INTRODUCTION	1
1.1 BACKGROUND.....	1
1.2 SOIL-PILE-STRUCTURE INTERACTION.....	2
1.2.1 Soil Structure Interaction-An Overview	2
1.2.2 Kinematic Response of Pile Foundations.....	5
1.2.3 Dynamic Response of Pile Foundations.....	7
1.3 THE PILED RAFT FOUNDATION.....	8
1.4 MOTIVATION AND RESEARCH OBJECTIVES.....	12
1.4.1 Research Questions	12
1.4.2 Research Objectives	13
1.5 ORGANIZATION OF THE THESIS.....	13
CHAPTER 2 LITERATURE REVIEW	15
2.1 INTRODUCTION.....	15
2.2 DYNAMIC SOIL-PILE INTERACTION: ANALYTICAL AND NUMERICAL METHODS.....	15
2.2.1 Semi Analytical Methods.....	15
2.2.2 Methods based on Dynamic Winkler Foundation.....	16
2.2.3 Continuum based Analytical Methods	17
2.2.4 Pile-Soil-Pile Interaction.....	18
2.2.5 Effect of Soil Nonlinearity	18
2.3 DYNAMIC SOIL-PILE INTERACTION: EXPERIMENTAL STUDIES..	20
2.4 INFLUENCE OF PILE CAP ON DYNAMIC STIFFNESS	22

2.5	KINEMATIC SOIL-PILE INTERACTION: ANALYTICAL AND NUMERICAL METHODS	23
2.5.1	Overview	23
2.5.2	Semi Analytical Methods	24
2.5.3	Methods Based on the Dynamic Winkler Foundation	27
2.5.4	Studies using the Finite Element Method	29
2.6	KINEMATIC SOIL-PILE INTERACTION: EXPERIMENTAL EVIDENCE.....	32
2.6.1	1-g Shaking Table Tests.....	32
2.6.2	Centrifuge Model Tests.....	34
2.7	SEISMIC RESPONSE OF PILED RAFT FOUNDATIONS	35
2.7.1	Overview	35
2.7.2	Numerical Modelling of Dynamic Response.....	35
2.7.3	Numerical Modelling of Seismic Response.....	37
2.7.4	Physical Modelling.....	38
2.7.5	Field Observations.....	39
2.8	CODAL PROVISIONS ON SSI.....	40
2.9	SUMMARY	42
CHAPTER 3 SOIL-STRUCTURE INTERACTION: NUMERICAL		
	MODELLING IN THE FREQUENCY DOMAIN	44
3.1	INTRODUCTION.....	44
3.2	METHODS OF ANALYSIS FOR SSI PROBLEMS	45
3.3	A HYBRID FEM-BEM TECHNIQUE FOR SSI PROBLEMS: THE SASSI METHODOLOGY	47
3.3.1	Overview	47
3.3.2	The Flexible Volume Substructuring Method.....	48
3.3.3	The Site Response Problem.....	51
3.3.4	Impedance Analysis	52
3.3.5	Algorithm for Meshing and Node numbering.....	53
3.3.6	Modelling Piled Rafts.....	55
3.3.7	Verification with Standard Results	57

3.4	CONCLUDING REMARKS	61
CHAPTER 4 KINEMATIC RESPONSE OF PILED RAFT		
	FOUNDATIONS	63
4.1	INTRODUCTION.....	63
4.2	CASE STUDY OF A PILED RAFT IN CLAY	65
4.2.1	Foundation and Soil Properties	65
4.2.2	Finite Element Model of the Foundation-Soil System.....	66
4.2.3	Simulation of the Experiment	68
4.2.4	Effect of Pile Spacing on Kinematic Response Factors.....	73
4.3	INFLUENCE OF RAFT EMBEDMENT ON KINEMATIC RESPONSE ..	77
4.3.1	Case Study of a Rectangular Piled Raft System	78
4.3.2	Frequency Response.....	80
4.3.3	Transient Response	91
4.4	CONCLUDING REMARKS	106
CHAPTER 5 DYNAMIC STIFFNESS CHARACTERISTICS OF PILED		
	RAFT FOUNDATIONS.....	109
5.1	INTRODUCTION.....	109
5.2	DYNAMIC STIFFNESS OF PILED RAFT FOUNDATIONS	111
5.2.1	Case Study of a Compressor foundation	111
5.2.2	Capped Pile Model: Vertical and horizontal Vibrations	121
5.2.3	Piled raft: vertical and horizontal vibration.....	125
5.3	DYNAMIC LOAD SHARING IN PILED RAFTS.....	131
5.3.1	Capped Pile: Vertical and Horizontal Vibration	131
5.3.2	Piled raft: Vertical and Horizontal Vibration.....	133
5.4	CONCLUDING REMARKS	137
CHAPTER 6 1-G SHAKING TABLE EXPERIMENT ON MODEL PILED		
	RAFT IN CLAY.....	139
6.1	INTRODUCTION.....	139
6.2	SCALE MODEL SIMILITUDE IN 1-G ENVIRONMENT	140
6.3	MODEL SOIL.....	141
6.3.1	Synthetic Clay	141

6.3.2	Shear Wave Velocity of Synthetic Clay.....	143
6.3.3	Strain Dependent Shear Modulus and Damping.....	146
6.4	MODEL PILED RAFT AND PILE GROUP	150
6.5	LAMINAR BOX AND SHAKING TABLE.....	154
6.6	INSTRUMENTATION AND DATA ACQUISITION.....	158
6.7	MODEL CONSTRUCTION.....	160
6.8	TEST PROGRAM.....	162
6.9	RESULTS AND DISCUSSION.....	162
6.10	CONCLUDING REMARKS	169
CHAPTER 7 SEISMIC RESPONSE OF PILED RAFTS:		
	CASE STUDIES	170
7.1	INTRODUCTION.....	170
7.2	CASE STUDY OF A 2X2 PILED RAFT IN CLAY	170
7.2.1	The Soil-Foundation-Structure System.....	170
7.2.2	Input Motion.....	173
7.2.3	Results and Discussion.....	173
7.3	CASE STUDY OF A LARGE PILED RAFT FOR A NUCLEAR BUILDING IN A DEEP SOIL SITE	178
7.3.1	Overview	178
7.3.2	Soil Properties for SSI Analysis.....	178
7.3.3	Piled Raft Foundation and Numerical Model	185
7.3.4	Kinematic Response Characteristics of the Piled Raft.....	187
7.4	SUMMARY	192
CHAPTER 8 SUMMARY AND CONCLUSIONS		
8.1	SUMMARY	193
8.2	CONCLUSIONS.....	195
8.2.1	SSI Analysis using the FVSM Based 3D Models.....	195
8.2.2	Kinematic Response of Piled Rafts.....	195
8.2.3	Dynamic Response of Piled Rafts.....	196
8.2.4	Experimental Evidence	196
8.2.5	Case Studies of Piled Raft-Structure Systems.....	197

8.3	RECOMMENDATIONS FOR FUTURE RESEARCH.....	197
	REFERENCES.....	199

LIST OF TABLES

Table 4.1 Material properties used in the piled raft model	66
Table 4.2 Details of the foundation systems analysed	81
Table 4.3 Details of the input ground motions.....	92
Table 5.1 Soil properties at the site.....	113
Table 5.2 Magnitude of quadratic excitation force from the oscillator.....	116
Table 5.3 Damped natural frequency of the pile-soil system.....	117
Table 5.4 Details of the piled raft foundations analysed.....	120
Table 6.1 Scaling relations for primary variables	141
Table 6.2 Properties of the clay mix after 36 hours of curing.....	145
Table 6.3 Characteristics of the model pile.....	152
Table 7.1 Details of the earthquake motion scaled to 0.16g	173
Table 7.2 Index properties of the soils	182
Table 7.3 Maximum shear modulus of soil at different depths	184

LIST OF FIGURES

Fig. 1.1 (a) Illustration showing a SDOF system with fixed and flexible base, and (b) SSI effects on spectral acceleration (modified from Stewart et al. 2012)	3
Fig. 1.2 Illustration showing the three stages of substructure method of SSI analysis.....	4
Fig. 1.3 General trend of the kinematic displacement factor of single and group piles (Modified from Fan et al. 1991)	6
Fig. 1.4 Soil structure interaction in piled rafts.....	9
Fig. 1.5 Simplified load settlement curve of a piled raft (Modified from Poulos 2001)	10
Fig. 1.6 Settlement reduction as a function of load sharing ratio (From Katzenbach et al. 1998)	11
Fig. 2.1 Effect of soil nonlinearity on dynamic (a) stiffness and (b) damping of pile (Modified from Michaelides et al. 1998).....	20
Fig. 2.2 Influence of E_p/E_s on (a,b) kinematic amplification factors and (c,d) kinematic interaction factors ($L/d=40$, $\beta_s=0.05$, $v_s=0.40$, $\rho_p/\rho_s=1.60$, soil model A)(Gazetas 1984)	26
Fig. 2.3 Typical mean spectral ratios for single pile in homogeneous soil (from Di Laora and de Sanctis, 2013)	31
Fig. 2.4 Frequency dependent variation in the load sharing between piles and raft for $L/d=20$ (from Liu and Ai 2017).....	36
Fig. 3.1 Substructuring in flexible volume method (Modified from Ostadan and Deng, 2012)	50
Fig. 3.2 Halfspace simulation using additional layers and viscous boundary (From Lysmer et al. (1981a)).....	52
Fig. 3.3 Algorithm to generate FVSM model from FE data	54
Fig. 3.4 Images of the (a) total FE mesh of a 2x2 pile group, (b) the excavated soil mesh (c) the near field soil mesh and (d) the foundation mesh.....	55
Fig. 3.5 Illustration of the central beam and rigid link method for pile modelling.....	56
Fig. 3.6 Normalized (a) stiffness and (b) damping coefficients for single and 2x2 pile group in vertical vibration.....	58
Fig. 3.7 Kinematic response factors for single free headed piles in homogeneous soil; comparison of results with Fan et al. (1991).....	60

Fig. 3.8 Kinematic response factors for a fixed head 2x2 pile group in homogeneous soil; comparison of results with Fan et al. (1991).....	61
Fig. 4.1 Schematic diagram of the PR-clay system	65
Fig. 4.2 (a) Finite element mesh of Model 1 (b) Model 2 showing structural elements with near field soil elements (c) Model 2 without near field soil elements.....	68
Fig. 4.3 Time histories & Fourier spectra of (a) Earthquake-1, (b) Earthquake-2, and (c) Earthquake-3	69
Fig. 4.4 Response spectra comparison at the top of raft for (a) Earthquake-1, (b) Earthquake-2, and (c) Earthquake-3 input motion.....	71
Fig. 4.5 Comparison of time histories at the top of raft for (a) Earthquake-1, (b) Earthquake-2, and (c) Earthquake-3 input motion.....	72
Fig. 4.6 Maximum bending moment envelope in pile vs depth for (a) Earthquake -1, (b) Earthquake -2, and (c) Earthquake -3 input motion.....	73
Fig. 4.7 (a) Schematic diagram showing the piled raft soil system and (b) the shear wave velocity profile	74
Fig. 4.8 Kinematic response factor in translation, for PR obtained at top of raft for different pile spacing.....	75
Fig. 4.9 Comparison of transfer functions in rotation for piled rafts and the corresponding pile groups, for different pile spacing	75
Fig. 4.10 Kinematic interaction factor ratio in (a) translation and (b) rotation.....	77
Fig. 4.11 Schematic diagram showing the piled rafts with (a) 3x3 and (b) 5x3 pile configurations	79
Fig. 4.12 Variation of V_s with depth for exponential soil profile.....	80
Fig. 4.13 Finite element mesh of the 5x3 piled raft ($t=5d$) (a) with near field soil elements and (b) without near field elements	81
Fig. 4.14 Kinematic response factor in (a) translation and (b) rotation for the 3x3 piled raft in homogeneous soil with $E_p/E_s=1500$	83
Fig. 4.15 Kinematic response factor in (a) translation and (b) rotation for the 3x3 piled raft in homogeneous soil with $E_p/E_s=500$	84

Fig. 4.16 Comparison of kinematic response factor in (a) translation and (b) rotation for 3x3 piled raft and corresponding fixed head single pile, raft, and pile group models in homogeneous soil with $E_p/E_s=1000$	86
Fig. 4.17 Comparison of kinematic response factor in (a) translation and (b) rotation for 3x3 piled raft and corresponding fixed head single pile, raft, and pile group models in layered soil profile with exponential variation in stiffness	87
Fig. 4.18 Kinematic response factor in (a) translation and (b) rotation for the 5x3 piled raft in homogeneous soil with $E_p/E_s=1000$	89
Fig. 4.19 Kinematic response factor in (a) translation and (b) rotation for the 5x3 piled raft in homogeneous soil with $E_p/E_s=500$	90
Fig. 4.20 Kinematic response factor in (a) translation and (b) rotation for the 5x3 piled raft in layered soil profile with exponential variation in stiffness	91
Fig. 4.21 Variation of frequency content in the selected input ground motions.....	93
Fig. 4.22 Acceleration time histories and corresponding Fourier spectra considered in the study	95
Fig. 4.23 (a) Time history of responses, (b) response spectra at the raft level and (c) spectral ratio for models with 3x3 pile configuration in exponential soil profile subjected to the Norcia 2016 ground motion.....	96
Fig. 4.24 (a) Time history of responses, (b) response spectra at the raft level and (c) spectral ratio for models with 3x3 pile configuration in exponential soil profile subjected to the Central Mexico 2017 ground motion.....	97
Fig. 4.25 Mean spectral ratio curve (grey line) plotted with idealised curve (blue line) for 3x3 pile group models in homogeneous soil stratum with $E_p/E_s=1000$	98
Fig. 4.26 Spectral ratio for single pile for (a) Norcia 2016, (b) Landers 1992, and (c) Valparaiso 2017 ground motions.....	100
Fig. 4.27 Variation in spectral ratio for 3x3 piled rafts in homogeneous soil layer with $E_p/E_s=1000$, obtained for (a) Amberley 2016 and (b) Christchurch 2011 ground motions.....	101
Fig. 4.28 Mean spectral ratio for 3x3 piled rafts in homogeneous soil layer with $E_p/E_s=1000$	102

Fig. 4.29 Mean spectral ratio for 3x3 piled rafts in layered soil with exponential stiffness profile.....	102
Fig. 4.30 Variation in spectral ratio for 5x3 piled rafts in homogeneous soil layer with $E_p/E_s=1000$, obtained for (a) Amberley 2016 and (b) Christchurch 2011 ground motions.....	104
Fig. 4.31 Mean spectral ratio for 5x3 piled rafts in homogeneous soil layer with $E_p/E_s=1000$	104
Fig. 4.32 Mean spectral ratio for 5x3 piled rafts in layered soil with exponential stiffness profile.....	105
Fig. 4.33 Maximum bending moment profile of pile P8 for (a) Norcia 2016, (b) Amberley 2016 and (c) Christchurch 2011 input motion	106
Fig. 4.34 Maximum bending moment profile of pile P1 for (a) Norcia 2016, (b) Amberley 2016 and (c) Christchurch 2011 input motion	107
Fig. 5.1 Layout of the compressor unit and base pad.....	112
Fig. 5.2 Soil layering along with shear wave velocity and SPT N profile at the site.....	112
Fig. 5.3 An illustration of the experimental setup.....	114
Fig. 5.4 Photograph showing the pile and oscillator assembly	115
Fig. 5.5 FE model of the single pile-soil system considered in the experiment	117
Fig. 5.6 Free vibration response from (a)-(b) experiments and (c) simulation	118
Fig. 5.7 Frequency response curve of the pile in horizontal vibration, for varying eccentricity of oscillator mass.....	118
Fig. 5.8 Illustrations showing (a) capped pile, (b) the 2x2 PR foundation and (c) the three foundation types analyzed.....	120
Fig. 5.9 Variation of (a) vertical stiffness and (b) damping coefficients of capped piles with area ratio	122
Fig. 5.10 Vertical stiffness and damping coefficients of capped piles normalized with corresponding single pile coefficients for (a)-(b) layered, (c)-(d) homogeneous; $E_p/E_s =100$, (e)-(f) homogeneous; $E_p/E_s =500$, and (g)-(h) homogeneous; $E_p/E_s =1000$ soil profiles	123

Fig. 5.11 Horizontal stiffness and damping coefficients of capped piles normalized with corresponding single pile coefficients for (a)-(b) layered, (c)-(d) homogeneous; $E_p/E_s = 100$, (e)-(f) homogeneous; $E_p/E_s = 500$, and (g)-(h) homogeneous; $E_p/E_s = 1000$ soil profiles	124
Fig. 5.12 (a) FE mesh of the PR model with $A_r=0.25$ (b) the PR model shown without near field soil elements and (c) the corresponding PG model	125
Fig. 5.13 Amplitude and phase of the dynamic interaction factor for piled rafts in (a)-(b) layered, (c)-(d) homogeneous; $E_p/E_s = 100$, (e)-(f) homogeneous; $E_p/E_s = 500$, and (g)-(h) homogeneous; $E_p/E_s = 1000$ soil profiles	128
Fig. 5.14 Amplitude and phase of the horizontal dynamic interaction factor for piled rafts in homogeneous soil profile with (a)-(b) $E_p/E_s = 500$, (c)-(d) $E_p/E_s = 1000$.	129
Fig. 5.15 Comparison of amplitude and phase of dynamic interaction factor for piled rafts from the analysis and prediction equations for (a)-(b) $A_r=0.25$ and (c)-(d) $A_r=0.75$	130
Fig. 5.16 Vertical load ratio for capped pile models in (a) layered, (b) homogeneous; $E_p/E_s = 100$, (c) homogeneous; $E_p/E_s = 500$, and (d) homogeneous; $E_p/E_s = 1000$ soil profiles.....	132
Fig. 5.17 Horizontal load ratio for capped pile models in (a) layered, (b) homogeneous; $E_p/E_s = 100$, (c) homogeneous; $E_p/E_s = 500$, and (d) homogeneous; $E_p/E_s = 1000$ soil profiles.....	133
Fig. 5.18 Load ratio in vertical vibration for 2x2 PR in (a) layered, (b) homogeneous; $E_p/E_s = 100$, (c) homogeneous; $E_p/E_s = 500$, and (d) homogeneous; $E_p/E_s = 1000$	134
Fig. 5.19 Load ratio in vertical vibration for 2x2 PR with $A_r=0.25$ plotted with phase difference $\Delta\theta$ for (a) layered, (b) homogeneous ($E_p/E_s = 100$), (c) homogeneous ($E_p/E_s = 500$), and (d) homogeneous ($E_p/E_s = 1000$) soil profiles	135
Fig. 5.20 Load ratio in horizontal vibration for 2x2 PR in (a) Layered, (b) $E_p/E_s = 100$, (c) $E_p/E_s = 500$, and (d) $E_p/E_s = 1000$	136
Fig. 6.1 Variation of undrained shear strength with time	143
Fig. 6.2 Photographs showing (a) the bender element apparatus with specimen, and (b) a close up of the bender element.....	144
Fig. 6.3 A Plot of the transmitted and received signals recorded	144

Fig. 6.4 Variation of shear wave velocity with time	145
Fig. 6.5 Photograph of the Cyclic Triaxial Test Setup.....	147
Fig. 6.6 Schematic diagram showing the multistage testing process.....	147
Fig. 6.7 (a) Hysteresis loops for 1% strain and (b) 5 th cycle loop for 0.3% axial strain	148
Fig. 6.8 (a) Modulus reduction and (b) Damping ratio curve obtain from cyclic triaxial tests	149
Fig. 6.9 (a) Schematic diagram of the parallel plate test and (b) photographs of the specimens made of Acrylic glass (left) and PVC (right) and (c) Typical load-deflection curve obtained for a PVC specimen.....	151
Fig. 6.10 An illustration of the model piled raft	153
Fig. 6.11 Photographs showing the raft (left) and the pile cap (right).....	153
Fig. 6.12 Schematic diagram showing the (a) piled raft and (b) pile group models.....	154
Fig. 6.13 Plan and elevation views of the laminar shear box and outer frame	156
Fig. 6.14 The laminar shear box and the outer frame	157
Fig. 6.15 The biaxial shaking table at IIT Madras	157
Fig. 6.16 Feedback to command ratio of displacement response	158
Fig. 6.17 Piezoelectric accelerometers attached to the pile cap.....	159
Fig. 6.18 Schematic diagram of the instrumentation scheme	159
Fig. 6.19 (a) Wet mixing using power mixer, and (b) finished clay bed	160
Fig. 6.20 Layout of the foundation models inside the laminar box	161
Fig. 6.21 The clay bed with instrumented foundation models.....	161
Fig. 6.22 Acceleration time histories recorded at various depths of the clay bed for (a) 5 Hz, (b) 10 Hz and (c) 15 Hz frequencies	163
Fig. 6.23 Acceleration time histories recorded at the top of foundations for (a) 2.5 Hz, (b) 5 Hz and (c) 7.5 Hz frequencies.....	164
Fig. 6.24 Raw and filtered signal recorded at the free field for 5 Hz input motion.....	165
Fig. 6.25 Kinematic response factors in translation obtained from the experimental data	166
Fig. 6.26 Bending strain profile in PR and PG models for (a) 1 Hz, (b) 2.5 Hz, and (c) 5 Hz.....	167
Fig. 6.27 Normalised bending strain profile of piled raft model with varying frequency of input motion.....	168

Fig. 7.1 (a) Schematic diagram and (b) simplified model of the structure-piled raft-soil system (c) FE model of the structure–PR–soil system	171
Fig. 7.2 Time history and Fourier spectra of scaled input motions from (a) Christchurch 2011, (b) Nepal 2015, and (c) Mexico 2017 earthquakes.....	174
Fig. 7.3 Response spectra at the mass level for (a) Christchurch 2011, (b) Nepal 2015 and (c) Mexico 2017 earthquakes	175
Fig. 7.4 Variation of axial force factor with pile spacing, for three earthquake input motion	176
Fig. 7.5 Maximum BM profile in piles for (a) Christchurch 2011, (b) Nepal 2015 and (c) Mexico 2017 earthquakes.....	177
Fig. 7.6 (a) Elevation of the structure with foundation and (b) plan view at raft level.....	179
Fig. 7.7 Soil profile at the site	180
Fig. 7.8 Photographs of (a) intact sample from 10m depth and (b) the sample trimmed to size	181
Fig. 7.9 Grain size distribution of the UDS sample from different depths	181
Fig. 7.10 Photographs of the Bender Element test setup (inset shows the bottom pedestal with bender)	183
Fig. 7.11 Source and receiver signals recorded in the Bender scope.....	184
Fig. 7.12 Soil profile developed for SSI analysis	185
Fig. 7.13 Arrangement of piles in the piled raft.....	186
Fig. 7.14 Finite element model of the piled raft.....	187
Fig. 7.15 Kinematic response factors for (a) translation and (b) rotation.....	188
Fig. 7.16 Spectral ratio obtained for the input time histories.....	189
Fig. 7.17 Comparison of spectral ratio for (a) Norcia 2016 and (b) Christchurch 2011 input motions	190
Fig. 7.18 Mean spectral ratio at the top of raft.....	191

NOTATIONS AND ABBREVIATIONS

English Symbols

a_o	dimensionless frequency
A	area of raft
A_g	area circumscribed by pile group
A_r	area ratio of piled raft
c_u	undrained shear strength
C_{PG}	damping coefficient of pile group
C_{PR}	damping coefficient of piled raft
C_{SP}	damping coefficient of single pile
d	diameter of pile
E_p	modulus of elasticity of pile
E_s	modulus of elasticity of soil
f	frequency of vibration
f_p	axial force factor
FIM	foundation input motion
F_{axi}	axial force on pile
G	secant shear modulus
G_{max}	low strain shear modulus
I	moment of inertia
I_u	kinematic response factor for translation
I_φ	kinematic response factor for rotation
k_{PG}	impedance of pile group

k_{PR}	impedance of piled raft
k_R	impedance of raft foundation
K_{PG}	stiffness coefficient of pile group
K_{PR}	stiffness coefficient of piled raft
K_{SP}	stiffness coefficient of single pile
k_{SP}	impedance of single pile
l	length of pile
LR	load ratio
M_{OT}	overturning moment
PI	plasticity index
PG	pile group
PR	piled raft
r_o	radius of axisymmetric soil column in impedance calculation
s	pile spacing
$S_{a,p}$	spectral ordinate at the top of piled raft
$S_{a,g}$	spectral ordinate at the free field ground
T_{min}	Threshold period corresponding to minimum spectral ratio
T_{crit}	Critical period after which spectral ratio is unity
V_s	Shear wave velocity

Greek Symbols

α_d	dynamic piled raft interaction factor
$\Delta\theta$	phase difference between piled raft and pile group
ε'_{pr}	ratio of bending strain of PR to bending strain of PG
λ	Geometric scale factor

ξ_0	spectral ratio at zero period
ξ_{\min}	minimum spectral ratio
φ	phase angle
ρ	density of soil

CHAPTER 1

INTRODUCTION

1.1 BACKGROUND

Piles are columnar foundation elements that are primarily used to transmit vertical loads from structures to deeper, competent strata. Pile foundations are known to be used to support buildings and bridges right from medieval times. From the early twentieth century onwards, reinforced concrete and steel piles have gained recognition over their timber counterparts owing to the higher capacities and ease of construction. In addition to vertical loads, pile foundations can also be subjected to lateral loads, uplift forces, and dynamic forces such as earthquake and wave loading. The science of pile design has improved significantly in recent decades with the influx of high-quality data and improved understanding of the behaviour of soils and rocks.

The design of structures in earthquake-prone areas has always been a challenge for engineers. Many cities such as Shanghai, Singapore, Mexico City, Kuala Lumpur, San Francisco across the world have soft soil deposits which demand the use of pile foundations to support structural loads. Foundation elements are known to play a crucial role in the seismic response of structures. Several post-earthquake investigations following earthquakes such as the Niigata (1964), San Fernando (1971), Mexico City (1985), Loma Prieta (1989), Kobe (1995), Bhuj (2001), and Tohoku (2011) have shown damage to pile foundations, and pile-supported structures underlining the importance of the seismic design of pile foundations. Some of the observed damages in pile foundations were also due to the effects of soil liquefaction. Even overtly undamaged structures were found to have damaged piles during the Niigata (1964) and San Fernando (1971) earthquakes. With increasing demand, countries like India are developing critical infrastructure projects in regions with soft soil deposits and moderate seismicity. A common notion among engineers is that ignoring the effects of SSI in pile foundations can lead to a conservative design. A flexible base can indeed result in period lengthening and increased damping in structures. However, past experiences during events such as the 1985 Mexico City earthquake (Mendoza and Auvinet 1988), as well as theoretical studies (Mylonakis and Gazetas 2000), have shown the need for a rational design of pile foundations for the stipulated seismic

demand. Experiences from the past have led to increased attention on the analysis of soil-pile-structure interaction, falling in the broader domain of *Soil Structure Interaction* (SSI).

A pile cap or raft is an indispensable component of a pile group. A pile cap is cast over a pile group to facilitate the distribution of loads from compression or tension members onto the pile group. Although the contribution of a pile cap is ignored due to the possibility of scouring and settlement, its contact with the ground can change the vertical and lateral load transfer mechanism in the foundation system (Fioravante et al. 2008; Rollins and Sparks 2002). The concept of a combined piled raft foundation that utilises the load transfer from an embedded raft has gained acceptance as an economic foundation solution for heavily loaded structures and high rise buildings. The presence of basement floors supported by pile foundations can also change the load transfer mechanism and seismic response of buildings. Embedded pile cap has also been found to alter the dynamic impedances of pile groups as a function of the frequency of loading. Simplified analysis methods do not exist for such hybrid foundation systems. Therefore, it becomes essential to understand the dynamics of pile foundations with an embedded cap or raft. This study attempts to throw light on the response of piled raft foundations subjected to dynamic and seismic loads.

1.2 SOIL-PILE-STRUCTURE INTERACTION

1.2.1 Soil Structure Interaction-An Overview

The interdependence of the dynamic response of a structure on the dynamic response of the surrounding soil is termed *soil-structure interaction*. The presence of a deformable soil supporting a structure can alter its dynamic response in several ways. A simple representation of a single degree of freedom system with stiffness K , and damping β , on a flexible base, is using springs beneath the foundation as presented in Fig 1.1 (a) and (b). The primary effect of a flexible base is the longer fundamental period of the structure (\tilde{T}) in comparison to the fixed base period (T). The second important effect is the dissipation of energy into the soil from the structure through wave radiation and hysteretic action. In this regard, damping offered by the foundation-soil system β_o can be considered as a combination of radiation damping and hysteretic damping. The effect of SSI on the seismic response of a typical building is presented in Fig 1.1 (b). The base shear or spectral acceleration for structure considering SSI can be higher

or lower than the base shear computed for a fixed base structure, depending on the period of the structure. For buildings with long periods on the descending portion of the spectrum, the presence of a flexible base typically would result in a reduction in the base shear demand (Stewart et al. 2012). An increase in the fundamental period of a structure due to SSI need not necessarily lead to a smaller response, and hence the SSI cannot always be comprehended to play a beneficial role.

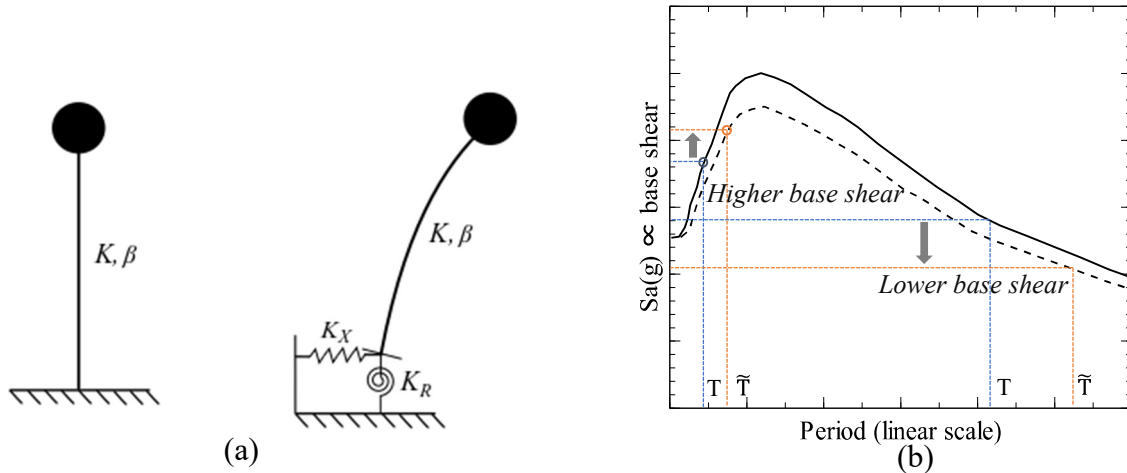


Fig. 1.1 (a) Illustration showing a SDOF system with fixed and flexible base, and (b) SSI effects on spectral acceleration (modified from Stewart et al. 2012)

Seismic soil-structure interaction (SSSI) broadly can be divided into two phenomena: a) *kinematic interaction* and b) *inertial interaction*. The inability of the foundation to match the free field motion causes the kinematic interaction. Kinematic interaction effects exist due to change in wave propagation media as a result of change in density and elasticity of the media. Foundations do not ‘follow’ the motion of soil strata, and can lead to scattering of incoming seismic waves. The kinematic response is understood to be more prominent for embedded foundations than shallow foundations. On the other hand, the mass of the superstructure transmits the inertial force to the soil causing inertial interaction. Inertial interaction is primarily dependent on the dynamic characteristics of the structure. The overall response of a structure under seismic excitation is strongly dependent on the kinematic interaction more than inertial interaction as the latter is mostly confined to structural frequencies.

A seismic soil-structure interaction problem can be solved using the direct method or the substructure method. The direct method involves modelling the soil-structure system as a single

unit and solving for the response in one step. Direct methods are applied in situation where material nonlinearity has to be rigorously modelled (Jeremic et al. 2009; Kanellopoulos and Gazetas 2019; Zhang et al. 2017a). The substructure method, on the other hand, involves splitting the system into subsystems, solving them first and then synthesizing the results to obtain the response of the total system.

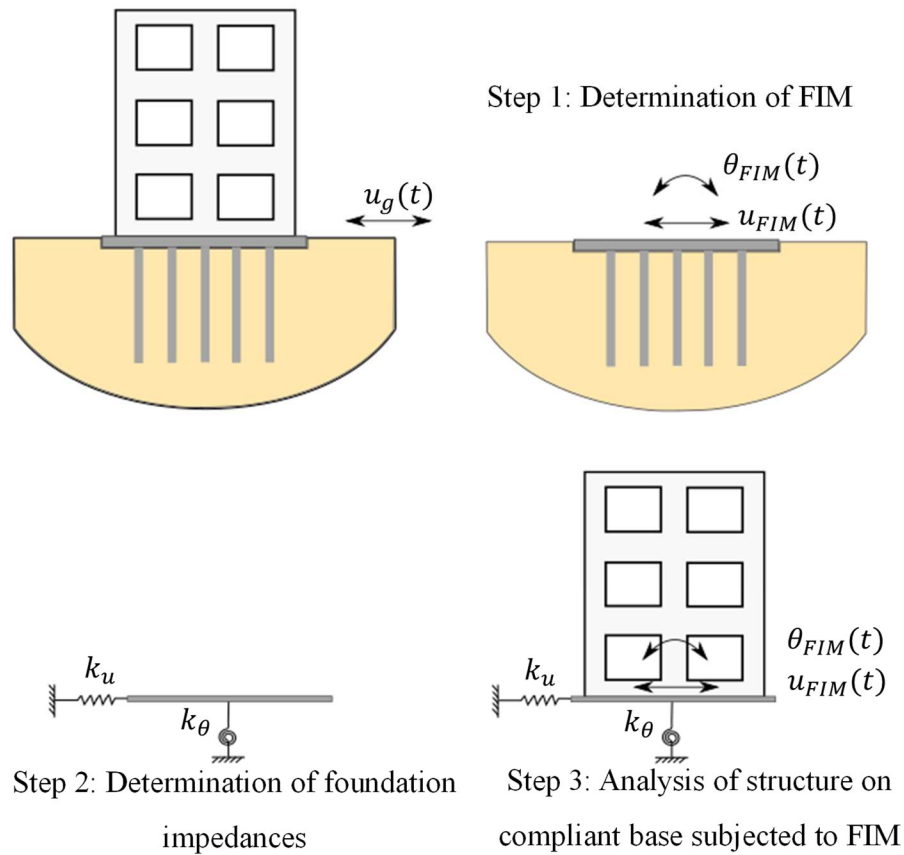


Fig. 1.2 Illustration showing the three stages of substructure method of SSI analysis

Substructuring involves splitting the soil-foundation-structure interaction problem into distinct parts as illustrated in Fig. 1.2. The three stages of analysis are:

- *Determination of the foundation input motion (FIM)*: The FIM is the motion that would occur on the foundation if the structure and foundation had no mass. The deviation of FIM from the free field ground motion is by virtue of kinematic interaction alone. FIM is often quantified in terms of transfer functions expressed as the ratio of foundation and free field motions in the frequency domain.

- *Determination of foundation impedance function:* Stiffness and damping of the foundation soil system are described by the impedance function. The impedance function takes into account the dynamic soil properties and soil layering, and are generally frequency-dependent. For rigid footings, a 6x6 impedance matrix can be defined for the three translational and three rotational degrees of freedom. For flexible foundations, an impedance matrix can be defined after discretizing the foundation geometry into finite elements (Lysmer et al. 1981a).
- *Dynamic analysis:* This step involves the dynamic analysis of the structure with a flexible base defined by the impedance function and excited by the FIM.

1.2.2 Kinematic Response of Pile Foundations

The passage of seismic waves through soil induces deformations in the soil mass, which in turn can induce stresses in embedded foundation elements such as piles. Due to the difference in stiffness, a pile would not follow the wavy movement of soil resulting in kinematic pile-soil interaction. Analogous to antennas in radio communication whose length determines the wavelength of the signal that can be received, pile foundations behave differently to seismic waves of different wavelengths. Even practically flexible piles may not be able to follow high frequency components of ground motion whereas low frequency components are mostly transmitted through the pile as FIM. Kinematic interaction in pile foundations results in a ‘filtering action’ on the free field ground motion. The key parameters influencing the kinematic response of piles include the type of soil, relative pile-soil stiffness, slenderness ratio of the pile, pile head fixity conditions, and the frequency of excitation. Kinematic bending strains induced in piles are highest at the head of a capped pile and at the location of relatively deep interfaces between layers with very different stiffnesses (Nikolaou et al. 2001). Seismically induced bending moment started being recognized by practitioners following the release of Eurocode-8, NEHRP 97, seismic guideline for harbour structures (TCLEE, 1998).

Fan et al. (1991) reported results from an extensive parametric study on the kinematic response of single and group piles. The authors classified the general shape of the kinematic displacement factor I_u defined as the ratio of pile head displacement to free field displacement, into three fairly distinct regions in the frequency range of interest for earthquake loading as reproduced in Fig 1.3. The kinematic displacement factor is nothing by the transfer function in translation.

In the case of foundations supported by pile groups, pile spacing in the direction of motion as well as axial and rotational stiffness of single pile, are understood to play significant roles in the rotational component of Foundation Input Motion (FIM) (Fan et al., 1991; Mylonakis et al., 1997). Kinematic interaction between pile and soil in general results in two prominent effects (Mylonakis et al., 1997):

- It filters out high frequency components of translational ground motion while inducing a rotational component at the pile head.
- It results in additional axial bending and shear deformation in piles.

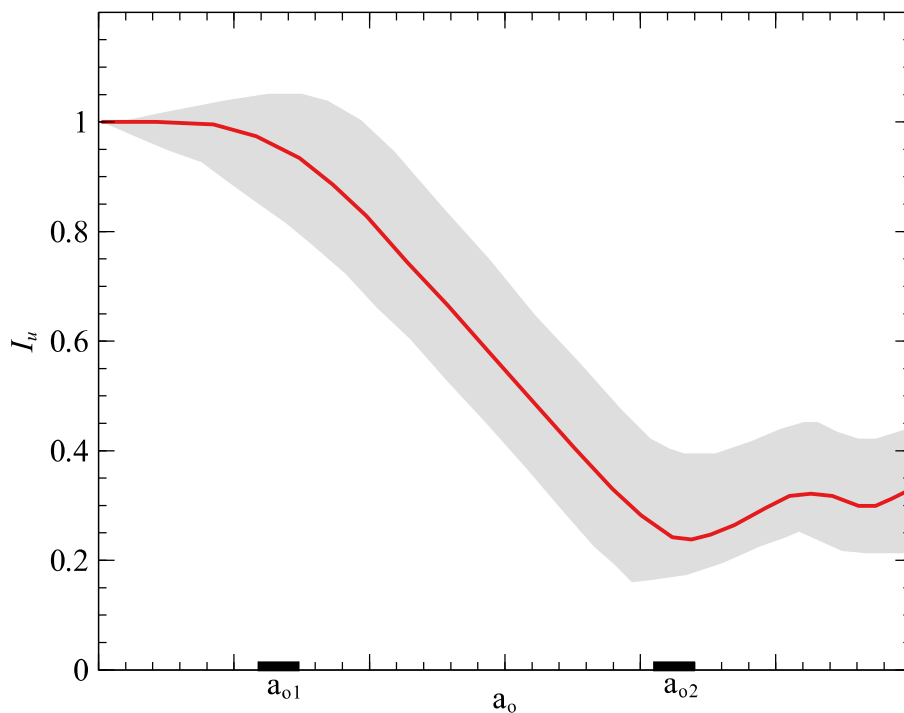


Fig. 1.3 General trend of the kinematic displacement factor of single and group piles (Modified from Fan et al. 1991)

The rotational component of motion at the pile head is significant primarily in the case of single pile foundations or footings with a very small number of piles. For large pile foundations, the induced rotation is usually irrelevant as the magnitude of rotation at pile cap level is known to decrease quadratically with pile cap width (Di Laora et al. 2017).

1.2.3 Dynamic Response of Pile Foundations

Dynamic stiffness and damping of piles or impedances are important parameters governing the inertial interaction during earthquakes. Pile impedances are also essential inputs to estimate the response of a foundation-soil system subjected to dynamic loads from the superstructure such as from vibrating machinery, wave and wind forces. Piles act as major vibration transmission paths in machine foundations. The complexity of an SSI analysis can depend on how accurately, nonlinear behaviour of pile and soil, as well as interfaces, are modelled. The stiffness of the pile in the lateral direction is very low in comparison to its vertical stiffness; hence, the lateral capacity/stiffness of the pile governs the design in most cases, where the lateral loads are dominant (Boominathan et al., 2015). Dynamic response of pile in the lateral direction due to dynamic load at pile head would be influenced mostly by the top few meters of soil below ground. The primary objective of an equipment foundation design would be to meet the stipulated performance criteria. However, most often, the intensity of the equipment excitation is not generally large enough to develop inelasticity in soil, and analysis methods which are easily applied to elastic media can be and have been employed with a fair degree of accuracy.

The impedances of a pile group are further complicated owing to the interaction between individual piles known as pile-soil-pile interaction. Unlike static interaction, dynamic group interaction is highly sensitive to frequency and requires rigorous analytical solutions or numerical methods for computation. From dynamic Winkler formulations to Finite Element based methods, several approaches are available for determining the dynamic stiffness and damping of pile groups. The pile group stiffness matrix can be determined by direct method or by the superposition principle. Data from dynamic experiments on single and group piles have shown that pile response at large amplitudes exhibit typical nonlinear behaviour (El-Marsafawi et al. 1992; Manna and Baidya 2010a; Vaziri and Han 1991). Strain dependent dynamic soil properties play an important role in the lateral dynamic response of piles, and approximate methods such as the consideration of weakened zone are essential to arrive at realistic estimates of pile stiffness.

For pile groups subjected to dynamic loads, the widely used impedance calculations methods ignore embedment effects of the pile cap. Inertial interaction in pile supported buildings subjected to seismic loads is known to be strongly influenced by the presence of surface

foundation elements like pile caps (Stewart et al. 1999). Impedance calculation considering a ground-contacting pile cap has been recommended for scenarios where cap-soil contact loss is not expected (Padrón et al. 2009; Stewart et al. 2012).

1.3 THE PILED RAFT FOUNDATION

Pile caps, often designed as solid slabs can also minimize the ill effects of one or more defective piles in a group by redistributing loads within the group. A ground-contacting pile cap is known to improve the load carrying capacity of the foundation. Although pile caps are often cast bearing with soil, the possibility of scour from the bottom surface often results in a design whereby pile cap-soil contact is ignored. There has been an increasing trend towards the design philosophy where the load is transferred to the soil from the pile cap, in parallel to the pile group, which proves economical for heavily loaded structures. Such a foundation where the total load is shared between the pile cap and the pile group is called pile raft foundation. Skyscrapers such as the Burj Khalifa, Dubai, Incheon tower, Korea, Emirates towers, Dubai, and the Messertum Tower, Frankfurt are founded on piled raft foundations (Katzenbach et al. 2000; Poulos et al. 2011; Poulos and Bunce 2008). Other structures for which piled rafts have been used are heavy storage tanks, nuclear reactor buildings, and bridge piers.

The bearing behaviour of the hybrid foundation system involves four types of interactions, namely i) pile-soil interaction, ii) pile-soil-pile interaction, iii) raft-soil interaction and iv) pile-soil-raft interaction as represented in Fig. 1.4. The complex stress field in the surrounding soil and interaction between the components make the analysis of piled rafts a demanding process. Experimental evidence (Fioravante et al. 2008; Horikoshi 1995) and numerical analyses (Alnuaim et al. 2018; Reul 2004; de Sanctis and Mandolini 2006) have shown that piled rafts do not exhibit a distinct collapse under vertical load. Even for small groups of piles, a ground-contacting pile cap can produce a ductile behaviour and a punching type failure (Viggiani et al. 2014).

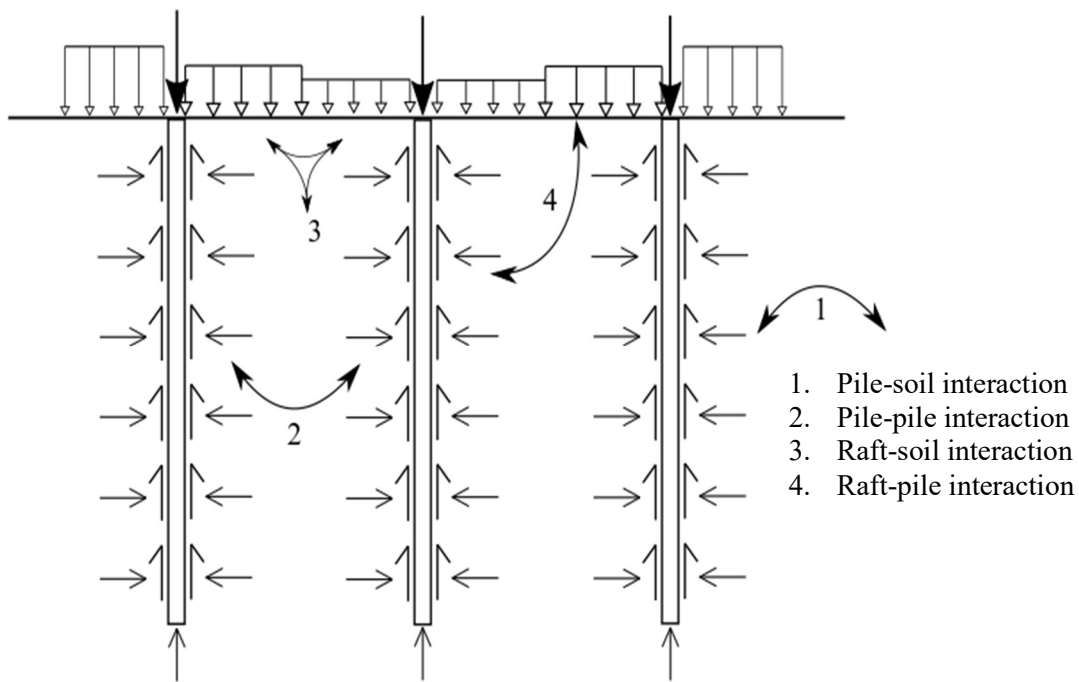


Fig. 1.4 Soil structure interaction in piled rafts

The PDR method (Poulos 2001; Poulos and Davis 1980; Randolph 1994) proposes a simple and useful method to estimate the load sharing ratio and stiffness of piled rafts. Fig 1.5 presents the tri-linear load settlement curve, which represents the PDR method. Although the theory assumes that the raft is stiff and both pile and raft show elastic behaviour until failure, it forms an elegant way to introduce the piled raft concept. In Fig. 1.5, point A represents the condition of full mobilization of pile group resistance. Beyond the point A, the tangent stiffness of the piled raft is that of the raft alone until it reaches the ultimate capacity of the piled raft at point B.

Russo and Viggiani (1998) proposed a classification of piled rafts as ‘small’ and ‘large’ piled rafts. The case when bearing capacity of the raft is insufficient to carry the total load with the required factor safety can be called small piled rafts. In such a case, the flexural stiffness of the raft is made rather high do that differential settlement is not a major problem, and the width of the raft is generally small in comparison to the length of piles. On the other hand, large piled rafts are those in which the raft offers sufficient bearing capacity so that the addition of piles are intended to reduce settlement. In such a case the width of the raft is generally greater than the length of piles.

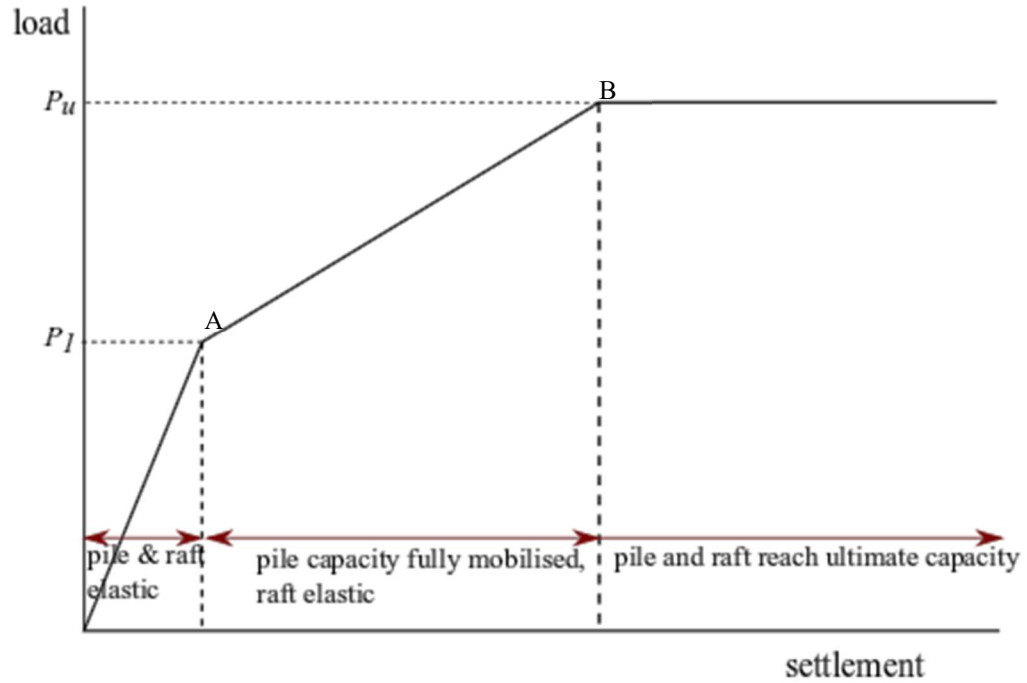


Fig. 1.5 Simplified load settlement curve of a piled raft (Modified from Poulos 2001)

In another school of thought, Randolph (1994) identified three distinct design philosophies for piled rafts as follows.

- i. The conventional approach where piles are the primary load carrying members and the raft contributes marginally to the ultimate bearing capacity
- ii. Creep piling in which sufficient number of piles are introduced to the raft to work at around 70-80% of their ultimate load capacity such that the net soil pressure under the raft is below its pre consolidation pressure of soil
- iii. Differential settlement control in which piles are strategically placed to control differential settlements and reduce the overall settlement.

The load-settlement behaviour of piled rafts is governed by the interactions between the piles and raft. An important design parameter with respect to piled rafts is the load sharing ratio (α_{pr}). The parameter also known as the piled raft coefficient, is defined as:

$$\alpha_{pr} = \sum_{i=1}^n V_{pile,i} / V_{pr} \quad (1.1)$$

where $V_{pile,i}$ represents the load carried by the i^{th} pile, and V_{pr} is the total load on the foundation. A load sharing ratio equal to zero represents a shallow foundation, while a pile group with no pile cap contact would be represented by a value of unity. The load sharing ratio is known to be a function of the total load applied. With increasing load and settlement, the share of the load carried by the raft increases. Based on numerical simulations Katzenbach et al. (1998) showed that the load sharing ratio when plotted against settlement normalized with the settlement of piled raft subjected to its permissible working load, the most practical piled raft configurations would fall in the shaded region as presented in Fig. 1.6.

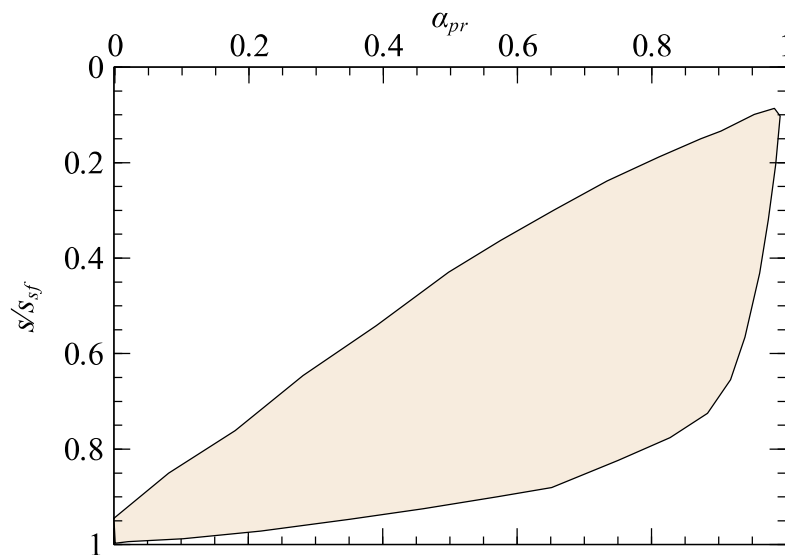


Fig. 1.6 Settlement reduction as a function of load sharing ratio (From Katzenbach et al. 1998)

In recent years, there is a clear consensus that the design of piled rafts can be optimized by arranging the piles beneath the raft at ‘strategic’ locations in order to minimize both settlement and bending moment in the raft (Cunha et al. 2001; Dinh et al. 2013; Nam et al. 2001). Studies have also shown that pile lengths in a piled raft can be optimized to minimize bending stresses in the raft as well as differential settlement (Leung et al. 2010). For large piled rafts, the optimal pile arrangement would be near the centre of the raft where maximum settlement is expected. However, post-earthquake surveys on building damages following the Mexico City earthquake of 1985, have suggested the importance of peripheral piles on the rocking resistance of buildings (Mendoza and Auvinet 1988). During seismic shaking, higher pressures usually occur

near the edge of foundations and the presence of piles near the edges play a decisive role in their seismic performance.

1.4 MOTIVATION AND RESEARCH OBJECTIVES

1.4.1 Research Questions

To meet the needs of sustainable construction, optimal foundation solutions are being considered all over the world. The piled raft foundation is an optimal solution for tall buildings and heavy structures. In parallel to the need to optimize foundations, engineers are also meet with the challenge of designing structures for the pre-determined seismic demand. Many critical infrastructure projects in seismically active regions such as the several zones along the Indo Gangetic Plain have to be built on pile foundations due to local soil conditions. In India piled rafts have been proposed for heavily loaded structures including the first nuclear power plant in a deep soil site, namely GHAVP I & II located in Gorakhpur, Haryana. Some of the challenges that engineers faced in the seismic analysis of the nuclear building were the integration of SSI, in the routine analysis methodology using finite element based structural analysis programs. The effect of a thick raft on the FIM, and pile forces could not be ascertained using available simplified methodologies for the kinematic soil-pile response. Therefore, a consensus on the seismic design strategies for pile and piled raft foundations are the need of the hour.

An embedded pile cap or an embedded basement floor can by itself transmit some of the structural loads by it bearing with soil. Static stiffness and load sharing characteristics of piled rafts have been extensively studied in the past, and methods of varying complexities exist for its computation. However, dynamic stiffness and load sharing characteristics in pile rafts subjected become relevant in the design of pile foundations subjected to dynamic loads. A comprehensive study on the dynamic response characteristics of piled rafts, using a rigorous analysis methodology is thus necessary.

The identified research questions in this regard are as follows:

- i. Does an embedded raft/basement floor alter the kinematic translational and rotational response of a pile group? Is the change in FIM on the conservative side?

- ii. During seismic shaking, how does the pile arrangement in a piled raft contribute to the rocking resistance of the structure? How are the axial forces in piles distributed during an earthquake?
- iii. How do nonlinear effects like gap formation and the disturbed zone around the pile and raft affect the seismic response?
- iv. How does an embedded raft affect the vertical, horizontal and rocking impedances of a piled raft?
- v. Is the load sharing characteristics in a piled raft frequency dependent in vertical and horizontal modes?

1.4.2 Research Objectives

The specific objectives identified for this study are

- To develop three-dimensional numerical models to study the response of pile-raft foundations subjected to kinematic and inertial loading using the substructure method.
- To study the influence of a raft on kinematic response factors of piled rafts, using the developed numerical model.
- To study the effect of an embedded raft on the dynamic impedances and load sharing characteristics of a piled raft using the developed numerical model.
- To conduct 1-g shaking table tests to compare the seismic response of a piled raft and a corresponding pile group, and verify the developed numerical models

1.5 ORGANIZATION OF THE THESIS

The thesis encapsulates details of the numerical analyses as well as experimental study and discusses the results and their practical significance. The thesis is organized into seven chapters.

Chapter 1 presents the introduction to the research topic and motivation for this study.

Chapter 2 presents a comprehensive survey of available literature on the research topic and discusses the relevant theoretical background. The research gaps identified from the survey are also discussed.

Chapter 3 presents details of the methodology adopted for numerical analysis. The essential theory and the contribution to the methodology are discussed. Verification of the developed numerical model against standard results is presented.

Chapter 4 focuses on the kinematic response characteristics of piled rafts studied using the developed numerical model. The case studies of a centrifuge shaking table test reported in literature is discussed. A parametric study focusing on the effect of a stiff raft on the kinematic response factors is presented.

Chapter 5 discusses the effect of an embedded raft on pile impedances. The case study of a compressor foundation is studied, and comprehensive numerical analyses are carried out to study the important parameters governing the dynamic interaction in piled rafts. The frequency dependence of load sharing ratio is also discussed.

Chapter 6 presents details of the 1-g shaking table test conducted to study the seismic response of a piled raft in clay. Comparative response of the piled raft against a corresponding pile group is discussed. Details of the testing program, material properties and numerical simulation of the experiment are presented.

Chapter 7 presents numerical analyses of two case studies of piled rafts. The first case study deals with the seismic response of a 2x2 piled raft-structure system. The second case study presents the kinematic response characteristics of a large piled raft designed for a nuclear building in India.

Chapter 8 summarizes the main outcomes of the work carried out and outlines recommendations for future work.

CHAPTER 2

LITERATURE REVIEW

2.1 INTRODUCTION

Pile foundations are inevitable in locations where geotechnical conditions at shallow depth are inadequate for the structural loads. In seismically active regions, it becomes increasingly important to design the foundation for additional seismic demand. The seismic response of a pile-supported foundation differs from that of a surface foundation due to its embedment in addition to wave scattering. Over the decades, researchers have attempted to solve the problem of soil-pile interaction with tools of varying complexities. This chapter presents a review of the literature on the topic of soil-pile interaction, the physical mechanism involved and methods of analysis. Following this, a review of the existing methods for design and analysis of piled raft foundations is presented. The limitations of design in the context of seismic response are reviewed. The existing research gaps in the area of seismic response of piled raft foundations are identified.

2.2 DYNAMIC SOIL-PILE INTERACTION: ANALYTICAL AND NUMERICAL METHODS

Pile foundations undergo vibrations in vertical, horizontal, torsional or rocking modes when they are exposed to external excitation such as those produced by machines, wind or earthquakes. The response of a pile to a dynamic load, or the pile stiffness and damping is caused by the interaction between soil and pile, and known to be dependent on the frequency of excitation. Based on their analysis technique, the methods can be classified as semi analytical methods, Winkler based formulations, and rigorous three-dimensional continuum-based methods.

2.2.1 Semi Analytical Methods

One of the earliest attempts to solve the problem of horizontally vibrating end bearing pile was made by Tajimi (1966) whereby a linear viscoelastic Kelvin-Voigt soil model was adopted to

model the soil stratum. A more rigorous solution was proposed by Nogami and Novák (1976) and Nogami and Novak (1977) for vertical and horizontal vibrations, respectively. The approach was based on evaluating plane strain soil reactions accounting for radiation damping in soils. Later on, Novak et al. (1978) presented closed form solutions of dynamic pile response incorporating hysteretic damping of soils. Using the developed methodology, the researchers also presented stiffness and damping constants for single piles in homogeneous and parabolic soil profiles (Novak and Aboul-Ella 1978; Novak and El Sharnouby 1983).

2.2.2 Methods based on Dynamic Winkler Foundation

The dynamic Winkler model for pile foundations can be considered as a quick alternative to complex analytical solutions. Makris and Gazetas (1992) modelled the soil using continuously distributed frequency dependent linear springs and dashpots to estimate the later stiffness of piles. For a pile on dynamic Winkler foundation subjected to lateral loads, the governing differential equation can be written as

$$E_p I_p \frac{d^4 U(z)}{dz^4} + (k_x + i\omega c_x - m\omega^2)U(z) = 0 \quad (2.1)$$

where $E_p I_p$ represents the flexural rigidity of the pile, $U(z)$ represents the displacement of pile at any point along its depth (along z axis), m is the mass per unit length of pile, and k_x and c_x represents the spring and dashpot coefficients. The spring coefficient for vertical and lateral loading has been approximated using correlations with Elastic Modulus of soil by the use of curve fitting with results from finite element formulations (Dobry et al. 1982; Makris and Gazetas 1992; Roesset and Angelides 1980). Radiation damping models such as the one dimensional model (Berger et al. 1977) and the plane strain model (Gazetas and Dobry 1984a; b) have been employed to arrive at the damping coefficient for piles. Studies using this method have found that the radiation damping is practically zero below a stratum cut off frequency. The dynamic Winkler model is robust in terms of its ability to account for soil layering and changes in pile geometry with length (Mylonakis 1995).

Another important numerical method developed for SSI problems is the cone method by Wolf et al. (1992). The method idealised a three dimensional halfspace into a truncated semi- infinite cone, thus overcoming the theoretical complexity of a three dimensional analysis. Jaya and Prasad (2004) extended the method to solve the dynamic impedances for single and group piles

embedded in layered soil stratum, which yielded good comparison with results from other analytical methods. Pal and Baidya (2018) used the cone model to successfully predict the response of the experiment using scaled down large pile group reported by Sharnouby and Novak (1984).

2.2.3 Continuum based Analytical Methods

Rigorous three dimensional continuum based methods have primarily focussed on axial and torsional vibration of piles in homogeneous and layered soil. Rajapakse and Shah (1989) developed a model based on the Green's functions for a system of buried harmonic loading configurations for a single pile embedded in an elastic medium. The response of a pile embedded in multi-layered soil was solved by Militano and Rajapakse (1999) by assembling the impedance matrix derived in closed form for a segment of pile under torsional and axial loading. Researchers such as Wu et al. (2013) and Gupta and Basu (2018) have also developed three dimensional analytical solutions for vertical vibration of end bearing single piles by assuming potential functions to decompose the displacement in soil around the pile. Luan et al. (2020) modelled the pile-soil-pile interaction considering three-dimensional stress field in soil and found a considerable difference with solutions that consider piles as one-dimensional elements. The study concludes that the classic plane strain model proposed by Novak (1974) can lead to an overestimation in soil stiffness in the low frequency range. Most studies on dynamic pile-soil interaction assume the soil to be an equivalent single-phase solid for saturated soils. Few studies have considered soil as a two-phase system, considering the compressibility of pore fluid and the interaction between the solid and fluid, making use of Biot's theory (Biot 1962). The first such study is reported in Zeng and Rajapakse (1999). Maeso et al. (2005) developed a three-dimensional BE formulation for the computation of single and group pile impedances considering two phase soil. They found that a saturated porous medium can cause an increase in the stiffness from very low frequency values in comparison to elastic drained soil. Similar observations were also made by Zhou and Wang (2009). Another novel framework for the vertical response of single pile in poroelastic soil was reported by (Zheng et al. 2015).

2.2.4 Pile-Soil-Pile Interaction

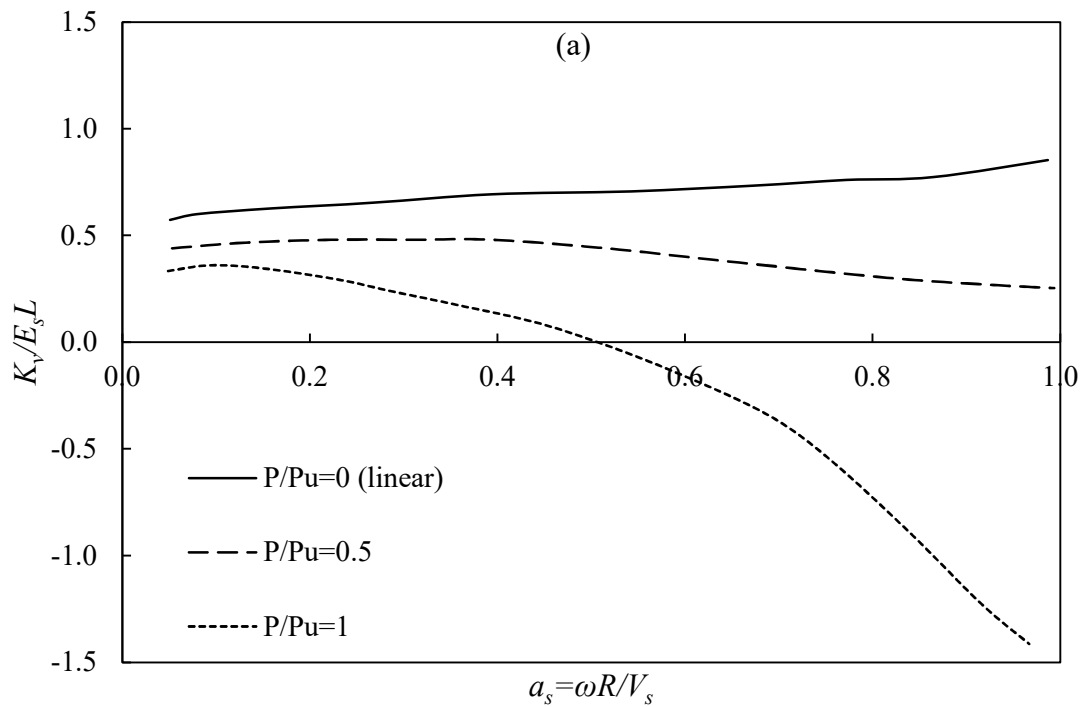
Pile-soil-pile interaction has been found to have a profound impact on the dynamic stiffness of pile groups (Kaynia 1982). Dynamic pile group behaviour is highly dependent on frequency as well as pile spacing. For close spacing, pile group stiffnesses have been found to resemble that of footings, while groups with large spacing is dominated by the interaction between the piles (Kaynia 1982). The pile spacing to diameter ratio has been found to affect both real and imaginary part of interaction factors in both vertical and lateral directions (Gazetas et al. 1991). Makris and Gazetas (1992) employed the attenuation function proposed by Gazetas and Dobry (1984b) to compute the lateral response of a ‘receiver pile’ subjected to waves generated from the transmitter pile. This *wave interference method* has also been extended to the case of layered soil by considering a different attenuation function for each layer (Mylonakis 1995). The closed form solutions obtained using dynamic Winkler spring approach was found to match closely, results from rigorous solutions and is undoubtedly a quick solution alternative for piles in layered soil.

2.2.5 Effect of Soil Nonlinearity

The soil in the vicinity of the pile shaft is known to have a major influence on the pile impedances. Novak (1980) proposed the addition of a homogeneous annular zone of weaker soil around the pile to account for nonlinear effects arising out of the degradation of shear modulus of soil. Han and Novak (1988) reported results from dynamic experiments on large scale model piles subjected to strong harmonic excitation and concluded that the consideration of a weakened zone around piles is inevitable in predicting the response at large amplitudes. However, Novak and Han (1990) found that the presence of a weak zone with non-zero mass leads to undulating impedances owing to wave reflections at the fictitious interface between the two media. To overcome this limitation, Vaziri and Han (1993) formulated a boundary zone with a parabolic variation of the medium properties. The parabolic variation in the weak zone nullified the oscillation in impedances and led to a better agreement between theoretical and field measurements. El Naggar and Novak (1995) studied the nonlinear lateral dynamic response of piles using a model employing nonlinear springs and observed that the effect of nonlinear soil behaviour is that it reduces the single and group pile stiffness as well as damping. This observation was further strengthened by Michaelides et al. (1998) who studied the vertical

dynamic response of single piles in nonlinear soil. The authors adopted a formulation that accounted for strain dependent soil shear modulus and hysteretic damping. The study yielded some very interesting results in terms of stiffness and damping coefficients of a single pile subjected to different load intensities. Fig. 2.1 presents the normalised vertical stiffness (K_v) and damping (C_v) coefficients of a single pile with $L/d=25$, $E_p/E_s=1000$, and plasticity index=30. The notations R , L , E_p , E_s , V_s , ω , P , and P_u represent the radius of the pile, length, elastic modulus of pile, elastic modulus of soil, shear wave velocity, angular velocity, applied load, and ultimate static axial load of the pile respectively.

It is interesting to note that both the coefficients decrease with an increase in load intensity. Up to a load intensity of half of the ultimate load, the deviation of stiffness and damping curves from their linear counterparts show a moderate variation which is consistent with the static response. It can also be noted that the frequencies above which a significant deviation occurs are above the practical frequency range of earthquakes. Thus it can be inferred that nonlinear behaviour becomes prominent at high dynamic load levels and intermediate to high frequency of loading.



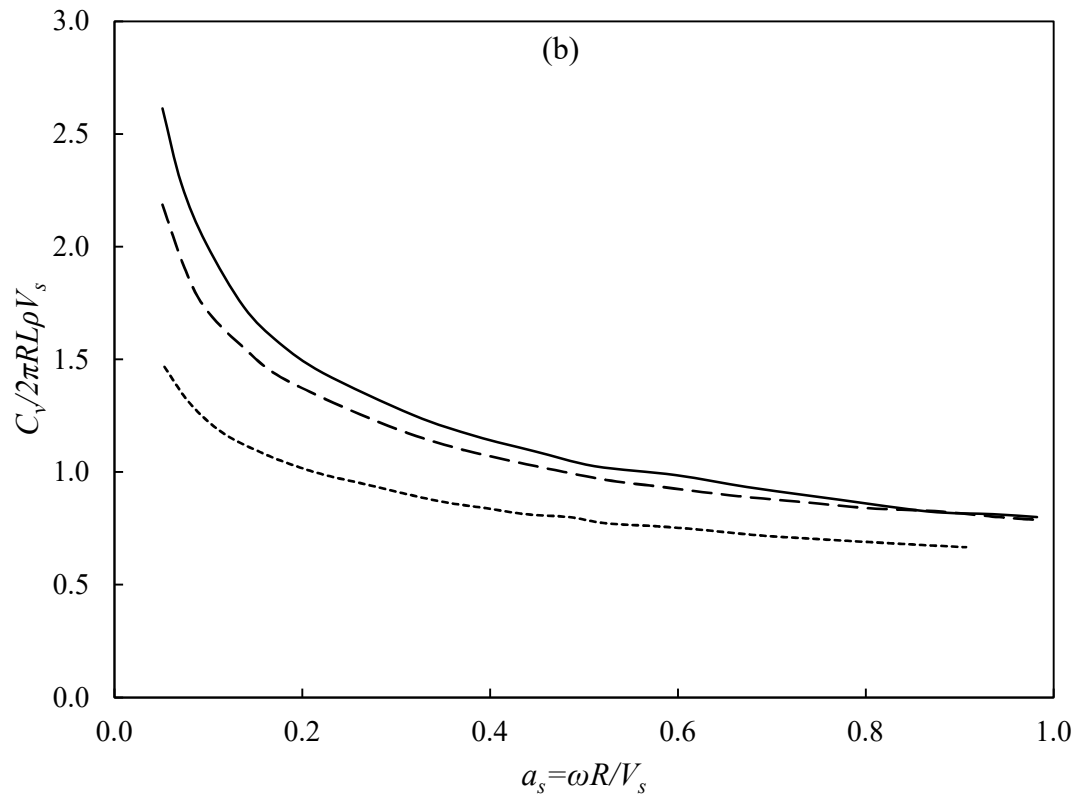


Fig. 2.1 Effect of soil nonlinearity on dynamic (a) stiffness and (b) damping of pile (Modified from Michaelides et al. 1998)

2.3 DYNAMIC SOIL-PILE INTERACTION: EXPERIMENTAL STUDIES

Analytical and numerical models are based on certain assumptions regarding material behaviour, soil-pile interaction, radiation damping etc. Physical modelling of the system can overcome this limitation. Dynamic pile soil interaction is a complicated phenomenon and experimental studies have been used to verify the applicability of different theoretical models. Some of the early experimental studies on dynamic response of piles were conducted using scaled down model pile groups at the University of Western Ontario. Novak and Grigg (1976) conducted experiments with a small group of piles subjected to dynamic vertical and lateral loads and found that the resonant amplitudes and natural frequency could be predicted well by the theoretical approach proposed by Novak (1974). El Sharnouby and Novak (1984) carried out dynamic experiments with a scaled down rectangular pile group having 102 piles. The authors also compared the experimental results with available theoretical models (Novak and El Sharnouby 1984) and found that the dynamic analytical techniques such as those proposed

by Kaynia and Kausel (1982) and Waas and Hartmann (1981) could estimate stiffness with a fair degree of accuracy for small strains. However, the prediction of damping by most methods seemed to be inaccurate unless a weak zone around the piles was considered. Dynamic tests on model single pile in clay have been reported by Boominathan and Ayothiraman (2006) and Boominathan and Ayothiraman (2007). Ayothiraman and Boominathan (2013) observed, from laboratory model tests that the depth of fixity for single pile in clay, increases under dynamic loads. An increase of the order of 1.5–2.7 times depth of fixity under static loads was observed. Nonlinear soil behavior was found to have influence in the low frequency to resonance region. The degree of nonlinearity was found to increase with in-creasing consistency of clay. Employing a similar experimental setup, Subramanian and Boominathan (2016) studied the lateral dynamic response of a model 1x2 batter pile group embedded in soft homogeneous clay. The natural frequency of batter pile group was found to be higher than vertical pile group by 34%, implying that they possess greater lateral stiffness. Vertical dynamic load tests on model piles in clayey soil was also reported by Manna and Baidya (2009). The authors reported that Novak’s complex frequency dependent analytical solution with dynamic interaction factor was able to produce reasonable estimates of the experimental results. Goit and Saitoh (2018) studied the vertical vibration of a single pile in cohesionless soil. The study revealed that for both static and dynamic conditions, the pile head stiffness for push and pull directions were distinctly different. The authors also reported that ignoring pile-soil interface nonlinearity may lead to an overestimation of pile head stiffness.

Full-scale dynamic tests form a reliable source of validation for theoretical models. Han and Novak (1988) conducted large strain dynamic experiments on full-scale piles in sand. The authors threw light on the nonlinear response of the pile-soil system under strong harmonic loads and found that good agreement can be achieved between theoretical and experimental response curves by considering a weak zone around the pile as well as pile separation. Even without a true non-linear analysis, the consideration of a weak zone, or strain corrected modulus and damping of soil around the pile was found to yield good results. Vaziri and Han (1991) compared the lateral dynamic response of a full-scale pile in frozen soil and thawed soil. The presence of a frozen soil layer was found to cause a significant reduction in the horizontal displacement and elevation in the resonant frequency. Boominathan et al. (2015) compared the lateral dynamic response of a full-scale pile from experiment with a 3D nonlinear finite element

model. Frequency response, as well as lateral dynamic stiffness evaluated using the criteria stipulated in IS 9716-1981, obtained from the FEA, was found to be in good agreement with experimental values. Results from vertical dynamic tests on single and group piles were reported by Manna and Baidya (2010) along with theoretical prediction using the Novak's continuum model. The study concluded that linear analyses could overestimate the stiffness and damping of piles due to the assumption of a perfect bond between soil and pile. Manna and Baidya (2010b) reported results from in situ lateral dynamic tests on single and group piles in layered soil. The authors observed strong nonlinearity as the excitation intensity increased, leading to a reduction in stiffness and damping for both horizontal and rocking modes. The embedment of pile cap was also studied and it was found that both stiffness and damping of the system can increase with an increase in embedment of the pile cap. Experimental studies on the vibration of vertical and batter pile groups were conducted by Bharathi et al. (2019). The authors concluded that for the same lateral loads, the batter pile groups always responded with lower displacements with the maximum reduction in the range of 40-50%.

2.4 INFLUENCE OF PILE CAP ON DYNAMIC STIFFNESS

A pile cap is an integral part of a pile group that facilitates load transfer from the superstructure. Under static loads, embedded pile caps are known to significantly increase the passive resistance of pile group under lateral loads (Rollins and Sparks 2002). While inertial interaction in pile supported buildings has been found to be strongly influenced by the presence of surface foundation elements like pile caps (Stewart et al. 1999), impedance calculation considering ground contacting pile cap has been recommended for scenarios where cap-soil contact loss is not expected (Padrón et al. 2009; Stewart et al. 2012). However, widely used impedance calculations methods for pile groups largely ignore the embedment effects of the pile cap. The case of piled raft foundations where stiffness, as well as load sharing between pile and raft, are important design parameters pose a challenge in this regard.

Investigations into dynamic raft-pile group interactions have found deviations in vertical and horizontal impedances of piled rafts, in comparison to pile groups (Fukuwa and Wen 2007; Liu and Ai 2017). Padrón et al. (2009) observed that the stiffness of a pile group with ground contacting pile cap is not necessarily greater than the case with cap soil separation, owing to constructive and destructive interference of waves generated at the pile-soil and cap-soil

interfaces. Emani and Maheshwari (2009) observed that the presence of cap-soil-pile interaction in piled rafts at higher frequencies that leads to an increase in horizontal and vertical stiffness in comparison with free standing pile groups. Nagai (2019) proposed a simplified method to predict the dynamic horizontal and rotational impedances of piled raft based on the impedances of the raft and pile group. Nakai et al. (2001) performed limited studies on the dynamic stiffness and load bearing ratio in piled rafts using the substructure method and observed that the load bearing ratio had minor changes across the frequency range studied. However, studies on dynamic load sharing considering various factors affecting soil-piled raft interaction are unavailable.

The load sharing behavior for static loading is known to vary with settlement of the piled raft foundation due to the mobilization of pile skin friction. However, the variation of load carried by piles for dynamic loads, is a function of the dynamic interaction between the components. Nakai et al. (2004) reported a relatively frequency independent load distribution from limited studies on a 2x2 pile raft model at frequencies below 12Hz. Liu and Ai (2017) observed an oscillating behaviour in the load sharing ratio with varying frequency and observed that pile-soil modulus ratio and length to diameter ratio were influencing factors.

2.5 KINEMATIC SOIL-PILE INTERACTION: ANALYTICAL AND NUMERICAL METHODS

2.5.1 Overview

Kinematic interaction results from the inability of a stiff foundation to follow the free field motion due to a propagating seismic wave. Broadly two causes for kinematic interaction in foundations can be identified. The primary cause is the *embedment effect* of the foundation. This effect becomes prominent as the depth of embedment increase. In the case of piles, the kinematic interaction can induce additional bending strains as well as alter the *foundation input motion*. The second cause of kinematic interaction is base slab averaging, in which the spatially variable ground motion, or incoherent ground motion is averaged within the footprint of a foundation (Stewart et al. 2012). Kinematic soil-pile interaction has received significant research attention since the 1970's with the advent of powerful computers. The initial development was driven by two industries: the nuclear industry and the offshore construction industry. Over time, post-earthquake examinations have revealed the importance of addressing

the phenomenon of kinematic interaction in pile foundations. With time, there has been a growing consensus regarding that kinematic soil-pile interaction analysis must precede the design of pile foundations for bridge structures, high rise buildings, heavy storage tanks etc. At present, there exist standards that prescribe seismic analysis considering kinematic interaction for important structures constructed on pile foundations. An overview of the methods of analysis and important findings from literature are presented in the following sections.

Similar to the dynamic response of pile foundations, kinematic response has been studied by researchers using methods such as semi analytical/Boundary Element Method, dynamic Winkler based methods, finite element method, and three-dimensional continuum based methods. Some of the earliest work on seismic soil-pile interaction was carried out by Margason (1977). The author put forward the assumption that pile bending can be approximated as the same as the curvature of soil for vertically propagating shear waves. This assumption though found unreliable later, was adopted by the NEHRP (1997).

2.5.2 Semi Analytical Methods

Tajimi (1969) studied the seismic response of pile foundation using a beam on elastic continuum formulation in which the soil was modelled as a Kelvin-Voigt viscoelastic stratum. Tazoh (1988) extended this method by incorporating the inertia effect of the superstructure. Blaney et al. (1976) developed a finite element formulation with the use of an efficient, consistent boundary matrix based on the work by Kausel and Roesset (1975). Development of this methodology was a significant leap in the study of kinematic pile response. The representation of pile response as a ratio between displacement at the pile head to that at the free field ground was first introduced by Blaney et al. (1976) it was carried forward and standardized by Gazetas (1984) with the introduction of the *kinematic interaction factors* defined as:

$$I_u = \frac{|u_p|}{u_{ff}} \quad (2.2)$$

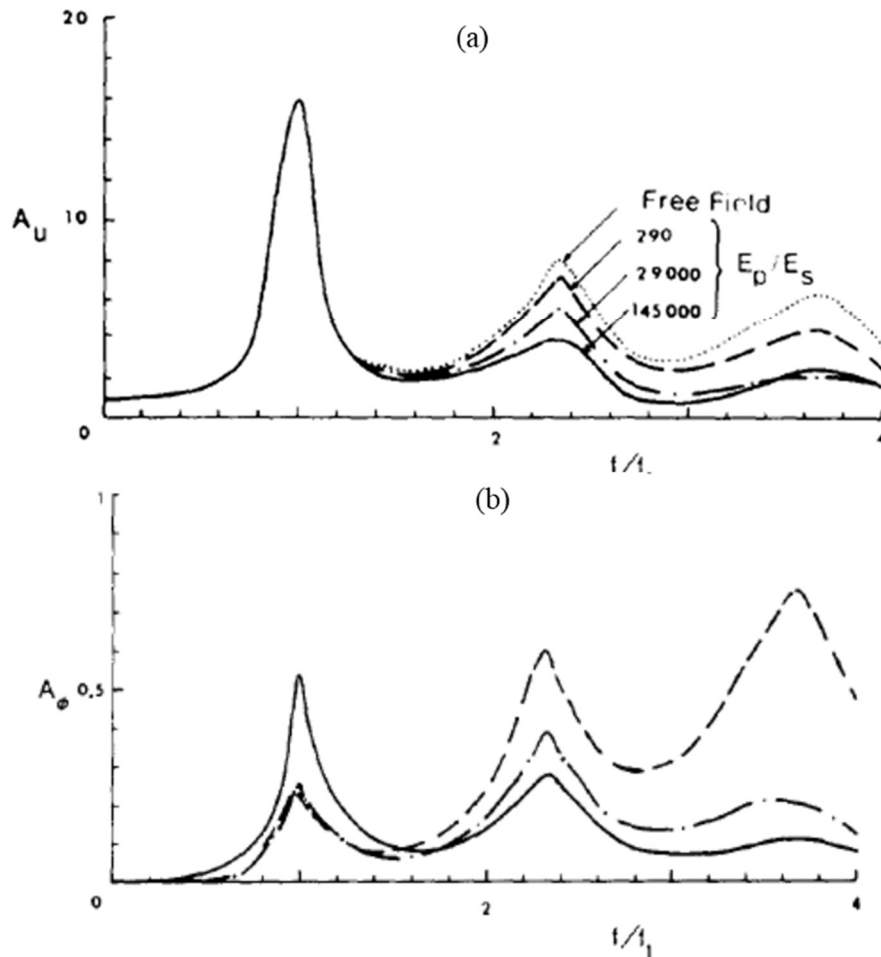
$$I_\theta = \frac{|\theta_p|d}{2u_{ff}} \quad (2.3)$$

The authors also defined kinematic amplification factors as

$$A_u = \frac{|u_p|}{u_g} \quad (2.4)$$

$$A_\theta = \frac{|\theta_p|d}{2u_g} \quad (2.5)$$

In these u_p represents the displacement at the pile head, u_{ff} represents the free field displacement, u_g represents the displacement at the bedrock level, θ_p represents the rotation at the pile head, and d is the diameter of the pile. In the absence of kinematic interaction, $I_u=1$, $I_\theta=A_\theta=0$. Fig. 2.2 (a-d) presents the kinematic interaction and kinematic amplification factors reported by Gazetas (1984) for a single pile embedded in soil model A (linear variation of Elastic modulus with depth). The factors are plotted against frequency normalised with the fundamental frequency of the stratum, f_1 . Few important observations can be made from Figures 2.2 (a,b). The first frequency of peak vibration is independent of the presence of the pile. In fact, up to a frequency of around $1.5f_1$, piles of all relative stiffness follow the ground motion.



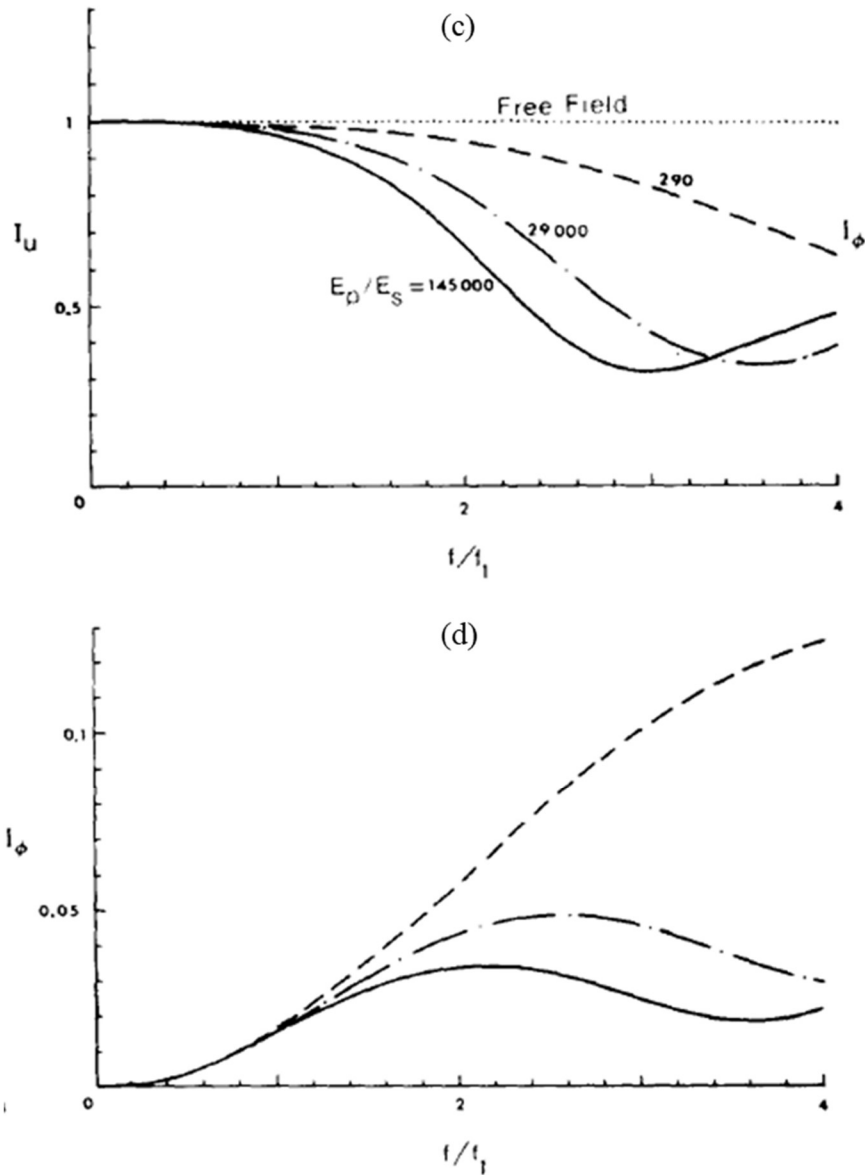


Fig. 2.2 Influence of E_p/E_s on (a,b) kinematic amplification factors and (c,d) kinematic interaction factors ($L/d=40$, $\beta_s=0.05$, $v_s=0.40$, $\rho_p/\rho_s=1.60$, soil model A)(Gazetas 1984)

As the frequency increases, piles of even less stiffness are not able to follow the ground motion. A rotational component is also developed at the head of the pile, even for purely translational ground motion. Kaynia (1982) developed a rigorous three-dimensional boundary integral type formulation for single and group piles subjected to dynamic loads. The author found that kinematic rotation in pile groups significantly reduces with the width of foundations, and hence for large pile groups, the rotational component can be ignored.

Fan et al. (1991) carried out a comprehensive analysis of the seismic response of single and group piles in various soil profiles using the same methodology developed by Kaynia (1982). A useful output from the study is the general trend of kinematic response factor in translation, I_u for single piles with two distinct transition frequencies, $a1$ and $a2$ as presented in Fig. 1.3. These frequencies were found to be affected by a) the soil profile, b) the relative rigidity of pile, c) the fixity conditions of pile head and d) length to diameter ratio of pile. It was concluded that for nonhomogeneous soil profiles single and group piles will suppress a much wider spectrum of harmonic components of the incident seismic excitation when compared to homogeneous soil profiles. The rotational component of FIM was found to be sensitive to the pile spacing ratio, pile group configuration, and pile-soil modulus ratio. Padrón (2009) developed a coupled FEM-BEM model to analyse the problem of soil-pile interaction. The author observed that the presence of a soft soil layer on top of a stiffer layer lead to a rapidly decreasing kinematic response factor in translation. Another important finding was that kinematic pile-soil-pile interaction or group interaction was almost non-existent confirming the findings of Makris and Gazetas (1992). Addressing the problem of kinematic response of pile groups, Di Laora et al. (2017) developed a simplified closed form solution for the horizontal motion and rocking of a capped pile group. The authors showed that rocking induced at the pile cap level is significant only in the case of small pile groups and slender structures.

2.5.3 Methods Based on the Dynamic Winkler Foundation

The beam-on-dynamic-Winkler-foundation (BDWF) model for modelling dynamic pile-soil has proved to be extremely versatile and has been used to study kinematic response with great advantage in computational effort. In this method, the soil-pile interaction is simulated through a set of springs and dashpots continuously distributed across the length of the pile. Similar to Eq. (2.1), the equation of motion for a pile ‘segment’ can be written as:

$$E_p I_p \frac{d^4 U_p(z)}{dz^4} + (m_p \omega^2) U_p(z) = (k_x + i \omega c_x) (U_{ff}(z) - U_p(z)) \quad (2.6)$$

The frequency dependent spring and dashpot coefficients are often determined through theoretical models (Novak et al. 1978) or from calibration with numerical solutions (Dobry et al. 1982; Kavvadas and Gazetas 1993). The BDWF has been effectively utilized by researchers (Flores-Berrones and Whitman 1982; Kavvadas and Gazetas 1993; Mylonakis 1995; Mylonakis

et al. 1997; Nikolaou et al. 2001a; Nogami et al. 1991) to study the problem of kinematic soil-pile interaction resulting in frequency domain solutions. Although the analysis is linear, moderate levels of non-linearity can be handled in this model by conducting an appropriate ground response analysis to determine strain corrected soil modulus. Several researchers attempted to quantify soil-pile interaction using the ratio of pile and soil curvature, Γ , obtained as:

$$\frac{(1/R)_p}{(1/R)_s} = \Gamma \quad (2.7)$$

where R represents curvature and subscripts p and s stand for pile and soil respectively. For harmonic excitation, it has been showed that Γ can be estimated as (Flores-Berrones and Whitman 1982; Nikolaou et al. 1995):

$$\Gamma \cong \left[1 + \frac{E_p I_p \left(\frac{\omega}{V_s} \right)^4}{k} \right]^{-1} \quad (2.8)$$

where k is the modulus of Winkler springs. Thus, the significant parameters governing the kinematic response are the flexural rigidity of pile, and stiffness of soil. A significant outcome from the studies based on BDWF is the understanding of pile bending behavior in layered soil. Dobry and O'Rourke (1983) developed a simple method based on the BDWF to determine kinematic pile bending moment at the interface between soil layers provided the confining layers are thick enough. Kavvadas and Gazetas (1993) concluded that kinematic interaction can lead to appreciable bending moments near interfaces of soil layers. Mylonakis (1995) employed a BDWF model to derive closed form solutions for the curvature ratio in homogeneous soil layer of thickness h , and showed that the ratio can achieve values greater than unity at low frequencies for certain pile slenderness ratios. Nikolaou et al. (2001) compared recorded data from instrumented building foundations during earthquakes with theoretical models and found that pile curvatures were seldom close to the soil curvatures as proposed by Margason (1977). The authors also proposed a simplified expression for kinematic bending moment at the interface of two soil layers underlain by a rigid base, based on nonlinear regression of numerical data from a comprehensive parametric study. Kinematic bending strains were found to be largest at the head of a capped pile and at locations of relatively deep layer interfaces. Another

significant finding was that pile bending due to transient excitation is only a fraction of the maximum value for harmonic excitations. Mylonakis (2001) presented a method for predicting kinematic bending moments at layer interfaces using response analysis of a mechanistic model. The author developed a theoretical function to account for strain transfer function at the layer interface. Anoyatis et al. (2013) investigated the kinematic response of a single pile in homogeneous stratum with different fixity conditions, and derived closed form solutions for bending, displacement and rotations at the pile head. An important outcome of the study was the introduction of a new dimensionless frequency parameter ($\omega/\lambda V_s$) where λ is the Winkler parameter, for normalizing the response of piles in the dynamic regime. This normalization scheme allows long piles to exhibit the same response regardless of their actual length or relative stiffness.

Phanikanth et al. (2013) developed an algorithm to analyse the seismic response of pile in liquefiable soil by the displacement-based p - y method. The method involves determining the free field displacement profile for a given ground motion and then applying the deformation profile to the pile in a pseudo static approach. Chatterjee et al. (2015) developed a force based pseudo static method based on the finite element method to analyse pile foundations under combined seismic and static loads. The methodology was found to produce conservative values of displacements and bending moments in comparison to the then existing pseudo static methods (Japanese Road Association 1996).

2.5.4 Studies using the Finite Element Method

Finite Element based models are known for their robustness in handling complex geometry and pile-soil-pile interactions. Several techniques to model pile foundations for dynamic SSI analyses using finite elements have been reported by researchers in the past. These include the use of solid elements (Alnuaim et al. 2016; Emani and Maheshwari 2009; Goit and Saitoh 2018; Liu and Zhang 2018; Nakai et al. 2004; Small and Zhang 2006), beam elements (Padrón et al. 2007; Wu and Finn 1997a), and central beam and rigid links (Jeremic et al. 2009; Martinelli et al. 2016; Mayoral and Romo 2015; Rahmani et al. 2016). The central beam and rigid link technique involves the removal of soil elements from the volume occupied by the pile, and insertion of beam elements at the center of the volume, which are connected horizontally to the soil nodes using rigid beam elements. Although the rotational degrees of freedom of the rigid

links remain unconnected at the common nodes with near field soil elements, this technique provides a direct value of forces and moments in the pile. This technique of pile modelling is capable of predicting SSI effects successfully, as demonstrated from the comparison of the response of full-scale bridge structures by Mayoral et al. (2011).

Wu and Finn (1997a, 1997b) developed a quasi three-dimensional finite element method that solves for the 3D wave equation in soil considering only the compression wave in the vertical direction and shear waves in the two horizontal directions. The absence of a full 3D formulation results in a significant reduction in computational time, and the method was validated against analytical and experimental data by Wu et al. (2015). The methodology was employed by Maiorano et al. (2009) to carry out a comprehensive parametric study on kinematic bending moments in layered soil. The authors proposed modifications to the simplified expressions proposed earlier (Mylonakis 2001; Nikolaou et al. 2001a). The methodology was also utilized by de Sanctis et al. (2010) to propose nonlinear regression based prediction equation for pile head bending moments. Di Laora and Mandolini (2011) carried out 3D Finite Element modelling of pile soil interaction in the frequency domain using the computer code ANSYS. The authors reported that the phase lag between kinematic and inertial bending moments is approximately 180° thus highlighting the rationality in summing up the maximum effects. Taking advantage of the axisymmetric geometry of a single pile in soil system, the original three dimensional problem has been simplified as two dimensional by several researchers (Di Laora and Rovithis 2015; Di Laora and de Sanctis 2013; Wilson 1965). Using such a model simplified expressions for active length and kinematic bending moment were developed by Di Laora and Rovithis (2015). Using a 3D nonlinear finite element formulation, Mucciacciaro and Sica (2018) studied the effect of soil nonlinearity on the kinematic bending moments induced in a single pile embedded in a two layer system. They found that the soil-pile strain transmissibility at the pile head and layer interface were similar for both nonlinear and linear soil modes. It was concluded that although soil nonlinearity plays a role in reducing the free field acceleration, it may cause an increase in kinematic bending moment along the whole pile length.

Di Laora and de Sanctis (2013) reported a peculiar trend in the FIM due to kinematic soil-pile interaction. The authors carried out finite element simulations on piles in two-layer systems and found that the ratio of response spectra at the top of pile and the spectra at the free field, ξ

exhibited a ‘square root’ shape. The spectral ratio, plotted against period, T forms a practical and simple way of considering SSI for design and analysis of buildings on pile foundations. It was found that there exists three critical points on the (T, ζ) plane.

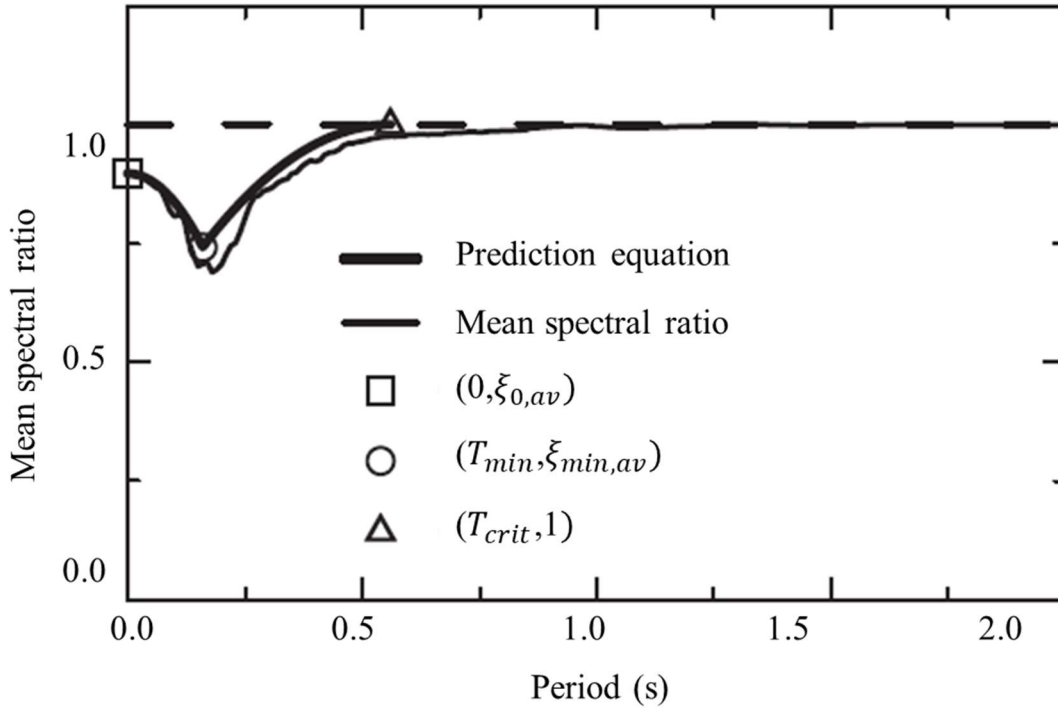


Fig. 2.3 Typical mean spectral ratios for single pile in homogeneous soil (from Di Laora and de Sanctis, 2013)

These are the spectral ratio at $T=0$, ξ_o , the point of minimum ratio defined by (T_{min}, ξ_{min}) and the point after which spectral ratio reduces to unity, $(T_{crit}, 1)$. These points, plotted on a mean spectral ratio curve for a single pile in homogeneous soil with $V_s=75$ m/s is presented in Fig.2.3. The authors suggest the following equations to obtain the ordinates and abscissa of the three points.

$$T_{min} = 12 \frac{d}{V_s} \quad (2.9)$$

$$T_{crit} = 3.5T_{min} \quad (2.10)$$

$$\xi_o = 1.71\Gamma_{t1} - 0.64 \quad (2.11)$$

$$\xi_{min} = 0.91\Gamma_{t2} \quad (2.12)$$

where Γ_{t1} and Γ_{t2} are defined as

$$\Gamma_{t1} = \left(1 + 0.15 \frac{\omega_s \lambda_p}{V_{s1}} \right)^{-1} \quad (2.13)$$

$$\Gamma_{t2} = 2.5\Gamma_{t1} - 1.5 \quad (2.14)$$

In these equations, ω_s is an average circular frequency parameter, λ_p is the Winkler parameter and V_{s1} is the shear wave velocity of the first layer (see Di Laora and de Sanctis, 2013). Iovino et al. (2019) extended the numerical model to study the kinematic response of a long pile in soil with shear modulus varying continuously with depth. A simplified Winkler free expression for the kinematic response factor was developed for practical use. It was found that for piles embedded in the stratum with continuous variation in shear modulus, the spectral ratio showed two distinguishable minima, instead of one. The effect of an embedded pile cap was also studied and it was concluded that pile cap embedment provides stronger filtering compared to the case with elevated pile caps.

Turner et al. (2017) carried out a comprehensive analysis on kinematic soil-pile interaction and proposed statistical models for predicting the transfer function and spectral ratios for free and fixed headed piles. The study considered soil nonlinearity, practical soil profiles, radiation damping, and variable frequency content of the ground motion. The authors conclude that a first order approximation of the pile group response could be estimated by reducing the transfer functions obtained from single pile prediction models by an additional 5% beyond a corner frequency (frequency beyond which a significant de-amplification of the free field motion occurs).

2.6 KINEMATIC SOIL-PILE INTERACTION: EXPERIMENTAL EVIDENCE

2.6.1 1-g Shaking Table Tests

Shaking table tests in 1-g conditions is regarded as a useful approach to understand SSI effects in pile foundations. Although the results bear the limitations of the absence of an elevated stress field, they are capable to producing quality data for validation of theoretical models. Some of the earliest studies on seismic soil-pile interaction using shaking table was carried out by Kubo (1969). He studied the seismic response of a 3x3 model pile group made of steel embedded in dry sand. Kagawa and Kraft (1981) performed shaking table tests on piles in liquefiable sand.

They observed that the natural frequency of the pile soil system kept reducing as the soil liquefied. Mizuno and Iiba (1992) conducted shaking tests with model piles embedded in a elastic medium composed of polyacrylamide and bentonite to partially address similitude issues. This was the first study where actual earthquake time history was used as base excitation, and the results highlight the influence of building frequency on the dynamic response. Liu and Chen (1991) carried out shaking table experiments with large groups of model piles in liquefiable soil. The authors studied the effect of pile installation and found that although pile driving causes local densification of soil, global liquefaction mechanism could still affect the lateral or axial load carrying capacity of the piles.

One of the most comprehensive studies on the seismic response of pile foundations in soft clay was carried out at the University of California Berkeley by Meymand (1998). The principles of scaling relationships were utilized to develop an adequate model satisfying the primary parameters governing pile response. A circular flexible container was developed and a synthetic clay mix was developed similar to San Francisco Bay mud. The author reported moderate influence of pile cap embedment on the rocking stiffness of pile groups. Tests evaluating piled rafts although inconclusive were also reported, highlighting the scope for further studies. Chau et al. (2009) carried out shaking table tests on a 1:7 scale model structure supported by a 2x2 end bearing pile group in sand. This was one of the few studies where model piles were made of concrete. The tests was also simulated using a finite element model developed in the program SAP 2000, in which gap elements were used to model the pounding between soil and pile.

A series of shaking table tests with a 15 storey model building on a 4x4 pile group in soft clay was carried out by Hokmabadi et al. (2014, 2015). The authors adopted a synthetic clay mix similar to that used by Meymand (1998). The authors found that the lateral deflection and inter-storey drift in the model building on the pile group was higher than the case of fixed base structure. This was attributed to the rocking component introduced by the pile group. The tests were also simulated using a 3D finite difference model developed in FLAC 3D with a good agreement with experimental results. Durante et al. (2016) investigated the seismic response of single and group piles in sand with various pile head fixity conditions. The model piles made of Aluminium tube sections were embedded in a two layer sand bed. It was found that bending moments from inertia loads were confined to the upper layer, while bending moments in the lower layers were induced by kinematic interaction. The period lengthening effect due to SSI

was found to be higher for an oscillator connected to a free headed pile, as compared to the case of a fixed head pile.

2.6.2 Centrifuge Model Tests

Centrifuge modelling has the advantage of simulating the realistic gravitational stress field that can replicate prototype conditions. From the late 1970's, centrifuge shaking table tests have been conducted to study a wide range of SSI problems. Most of the studied were focused on piles in liquefiable soil (Abdoun et al. 1996; Boulanger et al. 2003; Brandenberg et al. 2005; Chang et al. 2006; Finn 1987; Liu and Dobry 1995; Scott et al. 1977; Ting and Scott 1984). Caf e (1991) reported results from a centrifuge shaking table test on a model of the Struve Slough Bridge on peaty soil which had suffered significant damage during the Loma Prieta earthquake. The bridge support consisted of model piles, and the results indicated large bending moment near the pile head due to kinematic effects. A simplified finite element model was also developed by the authors and was found to simulate the experiment with a fair degree of accuracy.

Wilson (1998) and Boulanger et al. (1999) studied the seismic response of various pile models in a two layer system housed in a flexible soil container. The soil profile consisted of a top layer of Bay mud and a bottom layer of Nevada sand. A dynamic p - y model was then evaluated against the experimental results. The study was extended to evaluate the performance of a structure supported by a group of nine piles founded in soft clay (Curras et al. 1999). A dynamic beam on nonlinear Winkler foundation model was developed and a good agreement between the experiment and simulation was obtained in terms of structural responses, pile bending moments and cap rotations. This work substantiated the use of the dynamic p - y method for pile group supported structures. Banerjee and Lee (2013) studied the seismic response of a single pile with an added mass at the pile head, embedded in soft kaolin clay. The authors found that the response at the pile head was higher than the free field across a wide frequency range. This is however, counterintuitive to the theoretical models and can be attributed to the combination of inertial and kinematic effects.

2.7 SEISMIC RESPONSE OF PILED RAFT FOUNDATIONS

2.7.1 Overview

The Piled raft (PR) foundation, a composite foundation system that shares load between piles and raft, has been accepted as an economic foundation alternative to limit total and differential settlements. A conventional pile group (PG), on the other hand, is designed such that vertical loads are resisted by the skin friction and end bearing of the pile. The traditional practice in pile design is the capacity-based design approach that ignores the load sharing between raft and piles even if the raft is embedded in the ground. As discussed in Chapter 1, the mechanism of load transfer in a piled raft, on the other hand, involves raft–soil–pile and pile-soil-pile interactions which form a complicated SSI problem.

2.7.2 Numerical Modelling of Dynamic Response

Investigations into dynamic raft-pile group interactions have found deviations in vertical and horizontal impedances of piled rafts, in comparison to pile groups (Fukuwa and Wen 2007; Liu and Ai 2017). Padrón et al. (2009) observed that the stiffness of a pile group with ground contacting pile cap is not necessarily greater than the case with cap soil separation, owing to constructive and destructive interference of waves generated at the pile-soil and cap-soil interfaces. The authors presented the effect of pile cap separation on dynamic response in terms of moduli and phase differences between pile group and piled raft foundations. Emani and Maheshwari (2009) observed that the presence of cap-soil-pile interaction in piled rafts at higher frequencies leads to an increase in horizontal and vertical stiffness in comparison with free standing pile groups.

Nakai et al. (2001) performed limited studies on the dynamic stiffness and load bearing ratio in piled rafts using the substructure method and observed that the load sharing between the piles and raft had minor changes across the frequency range studied. Nakai et al. (2004) reported a relatively frequency independent load distribution from limited studies on a 2x2 piled raft model for frequencies below 12 Hz. Liu and Ai (2017) proposed an analytical method to compute the dynamic response of piled raft foundations subjected to vertical loads. They observed an oscillating behavior in the load sharing ratio with varying frequency, outlining that pile-soil relative stiffness and slenderness ratio L/d were the governing factors. Figure 2.4 shows the frequency dependent load sharing between pile and raft obtained from the study. The

problem of impedances of a capped pile was studied by de Almeida Barros et al. (2019) using a boundary element model. They found that cap diameter as well as soil anisotropy can significantly influence horizontal and rocking impedances of a capped pile.

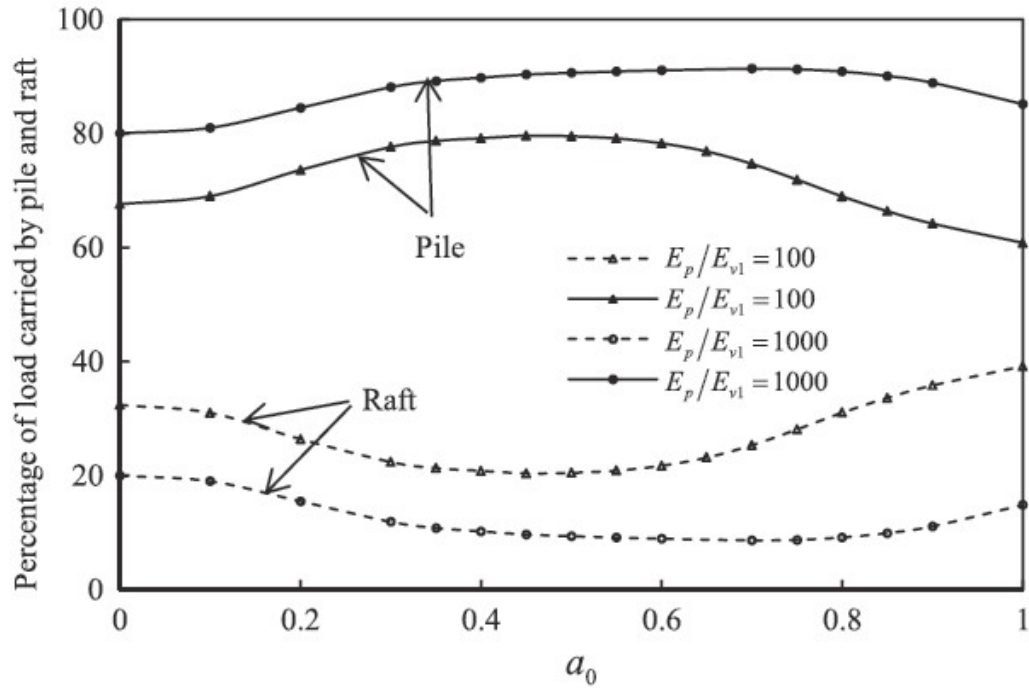


Fig. 2.4 Frequency dependent variation in the load sharing between piles and raft for $L/d=20$ (from Liu and Ai 2017)

The static vertical stiffness of piled rafts can be estimated based on the individual stiffness of raft and pile group and the interaction factor of pile group on raft, α_{rp} as originally proposed by Clancy and Randolph (1993) and Poulos (2001). Nagai (2019) extended this concept to the dynamic problem by expressing the dynamic piled raft stiffness in terms of frequency dependent pile group and raft stiffnesses, and a frequency dependent dynamic interaction factor. The author observed that this dynamic interaction factor for horizontal and rotational modes reflects a dynamic phenomenon for piled rafts with uniform pile spacing, and proposed empirical equations to predict the same. The simplified method was found to predict the dynamic horizontal and rotational impedances of piled rafts based on the impedances of the raft and pile group for the pile configurations studied.

2.7.3 Numerical Modelling of Seismic Response

Seismic soil-piled raft-structure interaction has been studied by researchers over the years using numerical tools of varying intricacy (Chandra et al. 2014; Kumar et al. 2016; Mayoral et al. 2009; Mayoral and Romo 2015; Nakai et al. 2004; Zhang et al. 2017a). The ISSMGE guideline for piled raft foundation emphasizes that the computational method should contain a realistic geometric and material model of foundation components and soil continuum (Katzenbach and Choudhury 2013). The effect of pile-raft connection, on seismic performance of an idealized building structure was studied by Nakai et al. (2004). The authors compared the performance of a pile group, piled raft, piled raft with unconnected piles as well as unpiled raft for the same superstructure. Results from the study indicate that adding piles to a raft increases base shears, mildly increases overturning moments, and decreases maximum accelerations. This observation could be attributed to kinematic rocking induced at the raft, by the pile group. Kumar et al. (2016) conducted numerical analysis using a 3D finite element model employing a Mohr Coulomb constitutive model for soil. They compared the bending moment obtained in a piled raft from a pseudo static method and dynamic analysis and observed marginal variation in the results due to the absence of SSI effects in the pseudo static method. Both Banerjee et al. (2014) and Zhang et al. (2017a) have convincingly simulated centrifuge shaking table tests on piled raft in clay systems using 3D nonlinear FE modelling employing a hyperbolic hysteretic soil model. Liu and Zhang (2019) extended the numerical model to incorporate randomness in the maximum shear modulus of surrounding clay, by using a three-dimensional random field. The authors recommend an amplification factor of 1.2 on bending moment prediction equations from a reliability based design framework.

Finite Element based sub structuring techniques have also been used to simulate full scale and centrifuge model tests involving seismic response of PR foundations. Mayoral et al. (2009) compared actual seismic response of an urban bridge support system consisting of a box foundation with piles on soft clay, with computed results using two dimensional models in the substructure based SASSI program. Mayoral and Romo (2015) investigated the seismic response of bridges with massive foundations using the SASSI 2000 program. The structure was modelled with three-dimensional beam elements and lumped masses, the foundation with 3-D brick finite elements, and the piles with three dimensional beam elements and excavated soil with rigid links, to account for pile diameter effects.

2.7.4 Physical Modelling

Physical modelling in 1-g and n-g conditions have been used by researchers in the past to study the seismic response of piled raft and the key differences with pile groups. Studies based on 1-g shaking table tests suggest that in comparison to pile groups, piled rafts generate lesser horizontal displacements and bending moment in piles (Matsumoto et al. 2004; Yuksekol et al. 2015). The behaviour of piled raft has also been observed to deviate significantly from the static response near resonant input frequency (Matsumoto et al. 2004). In the case of PR with short piles, surrounding soil has been observed to apply additional inertial loading on the foundation, and it is unlikely that dynamic or cyclic load tests at raft level will parallel its seismic response character (Banerjee 2009; Banerjee et al. 2007; Kang et al. 2012). The development of bending moment in piles has been found to be influenced more by ground movement than inertial loading from superstructure (Yamashita et al. 2012a, 2016a).

Centrifuge shaking table based studies on seismic response characteristics of PR foundations in clay have been reported by researchers such as Banerjee et al. (2014), Kang et al. (2012) and Zhang et al. (2017a). Banerjee et al. (2014) proposed regression analyses based relationships for the active slenderness ratio and maximum bending moment in terms of the stiffness, mass and acceleration ratios. He observed that the maximum bending moment was located near the pile head and increased with increase in added mass on the raft, implying a greater contribution from inertial interaction. Goh and Zhang (2017) proposed relationships for predicting the maximum pile bending moment and peak raft accelerations, from centrifuge test results supplemented by an extensive parametric study using the finite element method.

Similar studies on PR foundations have shown that the influence of raft soil interaction reduces horizontal acceleration, inclination and bending moment in piles (Hamada 2016; Horikoshi et al. 2003; Nakai et al. 2004). In the case of PR with short piles, surrounding soil has been observed to apply additional inertial loading on the foundation, and it is unlikely that dynamic or cyclic load tests at raft level will parallel its seismic response character (Banerjee et al. 2007, 2014; Kang et al. 2012). The axial stiffness and load sharing between raft and pile are key parameters in the design and analysis of piled rafts. From centrifuge model studies on micro piled rafts in clay and sand, Alnuaim et al. (2015a; b) observed that the load carried by the raft gradually increases with the applied load, and reaches a plateau. Similar behavior has been

reported from studies based on numerical modelling (Alnuaim et al. 2017; Kumar and Choudhury 2018; Lee et al. 2015). The proportion of vertical load transmitted by the raft and piles is also known to be affected by the raft flexibility, which in turn is influenced by the pile spacing and raft thickness (Alnuaim et al. 2016; Lee et al. 2010).

2.7.5 Field Observations

Lessons from previous earthquakes such as the Mexico City earthquake of 1985 have provided valuable lessons on the behaviour of pile supported structures. Since the 1950's, engineers in Mexico have been using friction piles to mitigate the problems associated with ground subsidence (Romo et al. 2000). The idea was to design friction piles with near to one safety factor such that the building settlements follow ground subsidence. However, this led to dangerously high slab-soil contact pressures during earthquakes. Post-earthquake surveys on building damages reported by Mendoza and Auvinet (1988) have found that buildings with piles near the periphery suffered lesser damage, thus highlighting the importance of peripheral piles on the rocking resistance of foundations. The geo-seismic instrumentation of a box piled raft bridge support system in Mexico City has provided valuable data following the occurrence of two earthquake events (Mendoza and Romo 1996, 1998). The instrumented box piled raft had 77 square reinforced concrete piles of dimensions 0.5 m x 0.5 m. The responses of the bridge support system to the two Michoacán Coast earthquakes of 1997 were documented by Mendoza et al. (2000). A comparison of the transfer function of motion of the foundation with respect to the free field soil showed a higher interaction in the vertical direction, compared to lateral direction (Mendoza et al. 2004). The authors attributed this observation to the large stiffness contrast between pile and soil in the vertical direction, in comparison to the horizontal direction. This trend was also observed from data recorded during the Tehuacan earthquake of 1999, where the vertical peak acceleration in the free field was reduced by a factor of 0.14 by the foundation (Romo et al. 2000). Mayoral et al. (2009) reported recorded data of the same bridge support system subjected to the 2004 Guerrero Coast earthquake. They found that a 2D substructure based simulation using the SASSI methodology was able to simulate the response with a fair degree of accuracy.

Grid form ground deep mixing walls (DMW) has been used to supplement piled rafts in liquefiable soils in Japan (Tokimatsu et al. 1996). Uchida et al. (2012) reported the performance

of a four storey parking facility supported by a piled raft with grid form DMW, subjected to the 2011 Tohoku Pacific Earthquake. A 2D substructure based dynamic analysis was carried out and it was concluded that the ground improvement was able to successfully prevent liquefaction beneath the foundation. Yamashita et al. (2012b) studied the static and seismic performance of a base isolated 12 storey residential building in Tokyo on piled raft supported by grid form DMW, after the 2011 Tohoku Earthquake. The foundation consisted of 16 piles with length of 45m and diameter of 0.8-1.2 m. During the earthquake, the peak horizontal acceleration at the first floor was found to be 30% less than that of the free field due to kinematic soil-pile interaction in addition to the base isolation effects. No significant change in foundation settlement or load sharing between pile and raft were observed after the earthquake. The load ratio briefly reduced from a value of 0.669 to 0.660 near the end of the event, and then increase to 0.667. Another case history of a seven storey building in Tokyo supported by a friction piled raft supported by DMW was reported by (Yamashita et al. 2016b). The response of the building with a footprint of 119 m x 32 m was founded on a raft supported by 70 friction piles designed as settlement reducers. From recorded data, it was found that pile head bending moments were dominated by kinematic effects rather than inertial effects. The grid form DMW was found to induce additional lateral stiffness to the raft such that most of the horizontal load was carried by the raft. This resulted in a significantly small bending moment near the pile head during ground shaking.

2.8 CODAL PROVISIONS ON SSI

Despite having been the subject of active research since the 1970s, SSI has been integrated into very few codal provisions. Most guidelines that recommend the use of SSI in the seismic analysis do not elaborate on the methods or establish procedures. This can be attributed to the lack of consensus and certitude regarding the role of SSI for varying soil, foundation, and structural characteristics.

United States

One of the first attempts to frame guidelines on SSI was made by the Applied Technology Council (ATC) in the ATC 3-06 of 1978 (ATC 1978). The code gave provisions to reduce the design base shear considering an elastic structural response. Following research that led to the

understanding that inelastic response of structures could diminish the effects of SSI, the ASCE 7-10 (ASCE 2013) introduced a cap on the base shear reduction to be no less than 70% of the original value. The ASCE 7-10 requires that piles be designed for the moment, shear, and deflections considering the interaction of the shaft and soil, with no mention of the influence of kinematic soil-pile interaction on the FIM. The FEMA 440 (ATC 2005) provided guidelines on the consideration of kinematic SSI effects in buildings with shallow embedment. The code proposed the use of the ratio of response spectra (RRS) factor to account for base slab averaging (Kim et al. 2003) as well as embedment effects.

The ASCE 4-16 (ASCE 2017), is one of the few standards that have guidelines on SSI in pile foundations. It clearly mandates that SSI effects be considered for all safety-related nuclear structures. The standard states that if the free-field ground motion is being used as FIM, the rotational component of FIM can be ignored and the results can be considered as conservative.

Europe

The Eurocode 8, EN 1998-5 (EN 1998-5 2004) recommends the consideration of SSI for structures which are either slender or have considerable $P-\delta$ effects. The standard identifies the structures and soil conditions for which SSI must be considered but does not specify any quantification of SSI effects. The standard recommends the consideration of kinematic soil-pile interaction only in critical conditions (e.g. high seismicity and soft liquefiable soil). The code also allows for treating the soil-pile interaction as an elastic problem unless the conditions warrant the use of fully nonlinear approaches.

Japan

The JSCE 15 (2007) standard suggests the use of SSI effects in the design of bridge abutments, retaining walls, underground structures, and deep foundations. The code leaves the choice of modelling of the soil-structure system and the method of analysis to the designer.

India

Indian standards such as IS 1893-3 (BIS 2014a) and IS 1893-4 (BIS 2015) mandate the use of SSI only for the design of bridges and industrial structures. The seismic codes for general buildings and liquid retaining structures (BIS 2014b, 2016) are, on the other hand, completely silent on this aspect.

Other codes such as the International Building Code (ICC 2018) and the New Zealand Standard (NZS) 1170.5 (2004) do not prescribe any guidelines for incorporating SSI. The NZS 1170.5, however, mentions a factor known as the structural performance factor which depends on SSI among other parameters. In short, codal provisions on kinematic and inertial SSI in pile foundations are restricted. The ASCE 7-10 and the ASCE 4-16 are among the few standards that provide guidelines on some aspects of soil-pile interaction. Although other codes do not specify regulations for soil-pile interaction, many of them acknowledge the need for site-specific studies for pile foundations on soft soils subjected to high-intensity earthquake loads.

2.9 SUMMARY

Based on a comprehensive summary of the literature related to soil-pile interaction, the following key observations are made:

- Dynamic response of pile foundations is dependent on the frequency of loading as well as the soil pile stiffness contrast. Pile group stiffness is particularly affected by pile-soil-pile interaction and is frequency dependent. The problem of vertical and lateral vibration of the single pile has been tackled using methods of varying rigor and complexity. Dynamic Winkler based formulations when calibrated using finite element models can surprisingly produce reliable estimates of pile head stiffness. Soil non linearity has been found to have a significant impact on the dynamic stiffness of piles at loads of higher intensity. The bending moments induced from inertia loads are mostly confined near the pile head. The influence of an embedded pile cap, as in the case of piled raft cannot be assumed to be conservative. Comprehensive studies on the alteration in stiffness as well as load sharing characteristics in vibrating piled rafts are scarce.
- Kinematic soil-pile interaction can alter the input motion transmitted to the structure. Analytical and numerical tools of varying complexity have been adopted to study the problem over the decades. Kinematic interaction can result in pile bending moments near the pile head as well as at layer interfaces. Although soil nonlinearity can alter the kinematic response, approximate considerations such as using soil stiffness from an equivalent linear method, have been found to yield fairly good results. Closed form

solutions proposed to predict kinematic bending moments, by various researchers have promising prospects in practical design. Pile-soil-pile interaction or group effects have been found to be negligible by several researchers. Pile induced filtering of ground motion, if addressed properly can lead to higher efficiency in seismic design. Spectral reduction ratio forms a practical design parameter than can aid the practical design of structures on pile groups. However, very few studies have evaluated the effect of embedded pile cap or basement floor on the kinematic response of pile groups.

- Seismic response of piled raft foundations has been studied using complex physical modelling as well as rigorous numerical modelling. Most studies, however, did not separate kinematic and inertial effects. Substructure based numerical models have been successfully used by researchers to simulate the responses of piled raft-structure systems under seismic loading. Limited studies have also shown that the presence of ground-contacting raft can alter that vertical impedances and load sharing characteristics. There is also a scarcity of field data from instrumented structures on piled rafts under earthquake loading.

CHAPTER 3

SOIL-STRUCTURE INTERACTION: NUMERICAL MODELLING IN THE FREQUENCY DOMAIN

3.1 INTRODUCTION

The phenomenon of soil structure interaction involves interaction between three linked systems, namely the structure, foundation, and the underlying geological stratum. For near-surface SSI problems, the geological medium is often idealized as a semi-infinite body with a planar surface. The response of the soil stratum that is not influenced by the structural response or wave scattering around the foundation is termed free field response. Body wave travelling in an unbounded elastic medium, when encountered by an interface results in a reflected and transmitted wave. A foundation which is practically stiffer than the soil medium around it, when struck by a wavefront of body waves, scatters the waves around it. The inability of an embedded foundation to ‘follow’ the response of the soil medium leads to a response that is different from the free-field response, resulting in kinematic interaction. The higher the stiffness contrast between the foundation and soil, the higher is the kinematic interaction between the two systems. However, the interaction and transfer of energy are two-sided. An ideal vibrating elastic structure system dissipates energy back into the soil medium through the foundation, by means of base shear, moment and torsion at the foundation-soil interface, in what is termed inertial interaction. The interdependence between the responses of both structure and foundation results in soil-structure interaction. The classic example of a vibrating footing at the surface of an elastic halfspace involves dispersion of energy into the infinite medium due to the effect of propagating waves. The footing response is thus damped due to the presence of radiation damping. In addition, kinematic and inertial interaction effects are both frequency-dependent. In order to propose simplified solutions for practical seismic design of foundation-structure systems, it becomes necessary to study the kinematic interaction and foundation impedance problems separately.

Structural members can undergo inelastic deformations depending on the strains induced. Soil medium is seldom elastic in nature, and strains developed in the region adjacent to the

foundation or the ‘near field zone’, results in a change of its dynamic characteristics. Foundations in motion can slide and even get detached from the soil around it. In buildings founded near the surface, ignoring the effects of gapping and uplift can reduce energy dissipation and increase structural response (Bolisetti et al. 2018). Rise in pore pressure in submerged soils can also trigger liquefaction which can result in a drastic reduction of soil stiffness. Rigorous modelling of soil-structure interaction will, therefore, need to consider realistic free-field site response, wave scattering, frequency-dependent foundation stiffness’s, nonlinear soil, and structural behaviour, and interface nonlinearity. In this chapter, the SSI analysis methodology adopted for numerical analysis, its implementation, and verification using standard results are presented.

3.2 METHODS OF ANALYSIS FOR SSI PROBLEMS

The complex phenomenon of soil-structure interaction can be tackled by simplifying it by means of reasonable assumptions. Assumptions such as elastic behaviour of soil, horizontal soil layers, rigid foundations, welded foundation-soil contact etc. have been used by researchers to arrive at closed form solutions for simple foundation geometries (Reissner 1936, Bycroft 1956, Luco and Westmann 1972, Kausel et al. 1975, Nogami and Novak 1977, Velestos and Prasad 1989). Analytical methods have the limitation of simple foundation geometries and linear analysis (Dobry and Gazetas 1988; Mylonakis and Gazetas 1999; Novak et al. 1984; Shadlou and Bhattacharya 2014). Many practical problems such as irregularly shaped foundation mats, embedment effect of pile caps, or even nonlinear soil behaviour, do not have readily available analytical solutions. Numerical solutions of the equations of motion have been attempted using transform methods as well as numerical integration codes. For example, the Laplace transform has been used to solve the equations of motion for laterally vibrating piles (Makris and Gazetas 1992, 1993), and the Fourier transform has been employed for a wide variety of SSI problems (Gupta and Trifunac 1991; Gutierrez and Chopra 1978; Roesset and Kausel 1976). Since the inception of the Fast Fourier Transform algorithm (Cooley and Tukey 1965) and the advent of computing tools that can handle large finite element meshes, transforming the equations of motion into the frequency domain has proven to be an efficient way to solve the governing differential equations. An essential parameter in the analyses in the frequency domain is the frequency increment or the frequency points at which the dynamic stiffness’s, amplification

factors etc. are computed. It is common to do the computations at a limited number of frequency points and interpolate the results in between. On the other hand, time-domain methods involve a step by step integration of the equations of motion. This facilitates the use of nonlinear stress-strain relationships for materials. However, practical issues with the use of time-domain methods include the generation of the system damping matrix, numerical stability, and the need for artificial boundaries.

Numerical methods for SSI problems include the finite element method (FEM), Finite Difference Method (FDM), Boundary element method (BEM), and hybrid methods that combine the FEM and analytical solutions. However, all of these methods have certain assumptions and simplifications and seldom problem-free. For example, the accuracy of the solution using the FEM depends on how the artificial boundary is defined, as the soil medium, in reality, is unbounded. Finite element based methods have been employed in several past studies to extract foundation impedances incorporating soil nonlinearity (Gazetas et al. 2013; Goit and Saitoh 2018; Kanellopoulos and Gazetas 2019; Yamashita et al. 2018). The FEM and FDM have the advantage of their compatibility with advanced constitutive models (Amorosi et al. 2017; Coleman et al. 2016; Zhang et al. 2017c). Modelling of the soil domain and structure using finite elements can lead to large models requiring tremendous computational effort. The use of boundary elements and hybrid techniques in the frequency domain can lead to a considerable saving in computational cost. However, these methods rely on iterative procedures to account for strain dependent dynamic soil properties. Therefore, it becomes necessary to use the right tool for SSI analyses considering the problem at hand.

Broadly, SSI methods can be classified as *direct methods* and *substructure methods*. In the direct method of analysis, the entire soil-foundation medium is modelled as one unit and analyzed in a single step. Most of the direct methods work in the time domain, wherein the governing differential equation is solved by time marching algorithms. This allows for advanced nonlinear constitutive models to be used for soil, structure, and interface elements, making the method suitable for accurate modelling of a wide range of practical problems. The unbounded soil domain is often modelled by locating the artificial boundary at a sufficient distance so that the soil's internal damping absorbs the reflected waves before they reach the boundary. The use of an absorbing or transmitting boundary is also common in the direct method. The substructure method, on the other hand, is based on the concept of splitting the

problem into parts and then solving each part separately using the most amenable technique after introducing suitable simplifications. For example, the soil may be analyzed as a halfspace, to generate impedances for the substructure. The impedances can then be used as a boundary condition, in the dynamic analysis of the structure under an excitation. The substructure approach for SSI includes the following steps (i) evaluation of free-field soil motion and corresponding soil properties (ii) evaluation of foundation input motion considering kinematic interaction (iii) evaluation of linear or nonlinear foundation springs and dashpots to represent stiffness and damping of the soil-foundation interface (iv) seismic response analysis of the combined structure-spring/dashpot system. Substructure based methods are often solved in the frequency domain, employing the method of superposition. The solution in the frequency domain restricts the material modelling to visco-elastic, and therefore approximations like the equivalent linear method are often used to account for material nonlinearity. The substructuring based methods are computationally faster than direct methods by a factor of over 10 (Bochert et al. 2015).

3.3 A HYBRID FEM-BEM TECHNIQUE FOR SSI PROBLEMS: THE SASSI METHODOLOGY

3.3.1 Overview

Coupled FEM-BEM formulations are known for their computational efficiency and have been employed by several researchers to study SSI problems with complex geometry (Liingard et al. 2007; Spyrakos and Xu 2004; Vasilev et al. 2015). The fundamental idea is to model the near field accurately while modelling the far-field using analytical solutions that are computationally faster. The FEM-BEM based ACS SASSI program (Ghiocel Predictive Technologies 2014) couples a three-dimensional finite element model of the foundation and near field soil with far-field soil modelled by the Thin Layer Method (Kausel 1981), and is adopted in this study. The program is an improved version of the original SASSI code (Lysmer et al. 1981a) developed at the University of California Berkeley, in the late 1970s. The methodology has become an industry standard and is widely used in the nuclear industry.

Based on how the interaction at the soil and structure interface is modelled, the methods of substructuring can be classified as the rigid boundary method, the Flexible Boundary methods, the Flexible Volume method, and the Substructure Subtraction method. The Flexible Volume

Substructuring Method (FVSM) reduces the dynamic stiffness of the structure by the corresponding properties of the excavated soil volume, which is retained within the horizontally layered halfspace and is the most accurate among the substructuring schemes (Tabatabaie 2013). The computational steps involved in an SSI analysis using the SASSI methodology are:

- i. The solution of the Site Response Problem: This step involves the computation of free field response at the interaction nodes of the free field substructure model.
- ii. Solving the impedance problem: This step involves the calculation of the complex impedance matrix $[X_{ff}]$ corresponding to the group of interaction nodes in the free field soil medium (represented by the subscript).
- iii. Forming the load vector: For seismic problems, the load vector is formed using the solution from steps 1 and 2. For foundation vibration problems, the process is similar to that in the finite element method.
- iv. Forming the complex stiffness matrix: The complex stiffness matrix is formed according to the partitioning of the system. The partitioning for the FVSM is discussed in section 3.3.2.
- v. The solution of the equation of motion: The solutions at the discrete frequency points are determined first, and transfer functions of responses are computed. Response to transient ground motion or external loads are then calculated by interpolation schemes and inverse Fourier Transforms.

3.3.2 The Flexible Volume Substructuring Method

The Flexible Volume Substructuring Method (FVSM) involves dividing the soil-foundation-structure system into three subsystems viz. free field site, the excavated soil volume substructure, and the structure subsystem of which the foundation replaces the excavated soil volume. The equation of motion of the subsystems can be expressed as

$$[M]\{\ddot{U}\} + [K]\{U\} = \{Q\} \quad (3.1)$$

where $[M]$, and $[K]$ are the total mass and stiffness matrices respectively, $\{U\}$ is the nodal displacement vector, and $\{Q\}$ is the load vector. For harmonic excitation, the load vector and displacement vector can be written as

$$\{\hat{Q}\} = \{Q\}e^{i\omega t} \quad (3.2)$$

$$\{\hat{U}\} = \{U\}e^{i\omega t} \quad (3.3)$$

where $\{Q\}$ and $\{U\}$ are the load and displacement vectors at a given frequency, ω . A matrix $[C]$ can be defined such that

$$[C] = [K] - \omega^2[M] \quad (3.4)$$

The equation of motion for each frequency can now be expressed as

$$[C]\{U\} = \{Q\} \quad (3.5)$$

The partitioning of the soil foundation-structure system for the FVSM method is presented in Fig. 3.1. As per the FVSM partitioning, the free field site and the excavated soil volume both interact at the periphery as well as within its volume.

The equation of motion can now be expressed as:

$$\begin{bmatrix} X_{ii} - C_{ii}^2 + C_{ii}^3 & X_{iw} - C_{iw}^2 & C_{is}^3 \\ X_{wi} - C_{wi}^2 & X_{ww} - C_{ww}^2 & 0 \\ C_{si}^3 & 0 & C_{ss}^3 \end{bmatrix} \begin{Bmatrix} u_i \\ u_w \\ u_s \end{Bmatrix} = \begin{Bmatrix} X_{ii}u'_i + X_{iw}u'_w \\ X_{ww}u'_w + X_{wi}u'_i \\ 0 \end{Bmatrix} \quad (3.6)$$

$$\begin{bmatrix} X_{ii} - C_{ii}^2 + C_{ii}^3 & X_{iw} - C_{iw}^2 & C_{is}^3 \\ X_{wi} - C_{wi}^2 & X_{ww} - C_{ww}^2 & 0 \\ C_{si}^3 & 0 & C_{ss}^3 \end{bmatrix} \begin{Bmatrix} u_i \\ u_w \\ u_s \end{Bmatrix} = \begin{Bmatrix} X_{ii}u'_i + X_{iw}u'_w \\ X_{ww}u'_w + X_{wi}u'_i \\ 0 \end{Bmatrix} \quad (3.7)$$

where C and X represent the complex frequency dependent dynamic stiffness matrix, the impedance matrix, the force vector, and the displacement vector respectively. The indices 2 and 3 represent the excavated soil volume and the structure respectively, and subscripts i , w and s represent nodes at the boundary between soil and structure, within excavated soil and on the structure respectively. The displacements u'_i , and u'_w represent the free field motion for the interaction nodes, obtained from the site response problem.

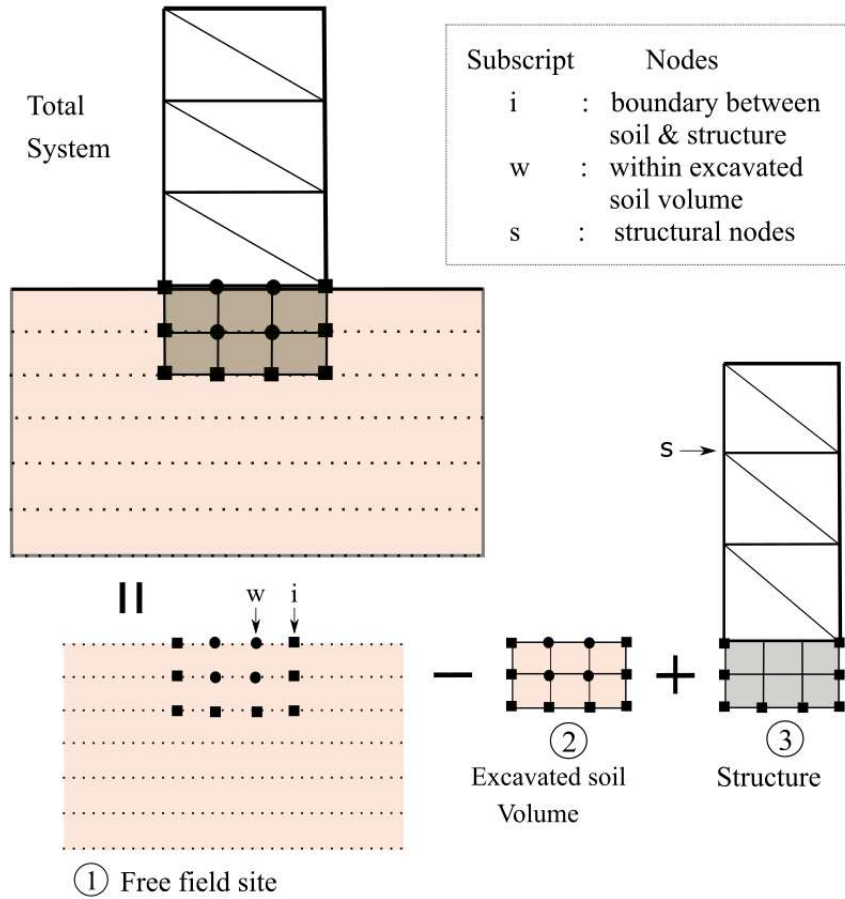


Fig. 3.1 Substructuring in flexible volume method (Modified from Ostadan and Deng, 2012)

The analysis model primarily consists of two separate FE meshes, one for the excavated soil, and second, containing the foundation and near field soil elements. A node numbering scheme that connects the two meshes at the boundary is adopted. On the other hand, for foundation vibration problems, the load vector comprises of external forces represented by P , at the corresponding degrees of freedom as in Equation 3.8.

$$\begin{bmatrix} X_{ii} - C_{ii}^2 + C_{ii}^3 & X_{iw} - C_{iw}^2 & C_{is}^3 \\ X_{wi} - C_{wi}^2 & X_{ww} - C_{ww}^2 & 0 \\ C_{si}^3 & 0 & C_{ss}^3 \end{bmatrix} \begin{Bmatrix} u_i \\ u_w \\ u_s \end{Bmatrix} = \begin{Bmatrix} P_i \\ 0 \\ P_s \end{Bmatrix} \quad (3.8)$$

The 3D finite element library in the ACS SASSI program consists of the brick element (8 nodes), beam element, thin shell element (4 nodes) and thick shell element (4 nodes), spring

elements (2 nodes) and general mass/stiffness matrix elements. Excavated soil is always modelled using brick elements for 3D analysis. As linear interpolation functions are used for the 3D elements, the size of elements can influence the accuracy of the analysis. For dynamic problems, the accuracy of the analysis also depends on the method used to compute mass matrix in the elements. For brick elements that have a combination of half consistent mass matrix with half lump mass matrix, the maximum element size less one-fifth of the shortest wavelength forms the optimal meshing criteria (Lysmer, J., & Kuhlemeyer 1969; Ostadan and Deng 2012).

3.3.3 The Site Response Problem

The site response analysis for the horizontally layered site model consists of the Eigenvalue Problem for the system in the frequency domain formulated by Waas (1972). The formulation is based on the Thin Layer Method whereby the physical layers of the soil medium are subdivided into layers, similar to finite elements, such that the thickness is small in comparison to the characteristic wavelength of the propagating wave (Kausel 1981; Kausel and Roësset 1981; Waas 1972). The maximum thickness of soil layers is set such that it does not exceed one-fifth of the wavelength at the highest frequency of analysis. The equation of motion of a layered soil system to incident SV and P wave motion can be expressed as (Chen 1980):

$$([A]k^2 + [B]k + [G] - \omega^2[M])\{V\} = \begin{Bmatrix} 0 \\ P_b \end{Bmatrix} \quad (3.9)$$

where k is the wavenumber, ω is the frequency, P_b is the load vector depending on the nature of the wave field, and matrices A , B , G and M are symmetric matrices assembled from the layer submatrices defined using material properties and thickness of the layers. The detailed formulations for Rayleigh, SH, and Love waves, used in the site response problem, can be found in Chen (1980). The solution of the Eigen equations are performed using a numerical technique proposed by Waas (1972). The mode shapes and associated wave numbers are then used to compute the transmitting boundary condition in the lateral direction. At the base, a semi-infinite halfspace is modelled using a combination of extra soil layers and a viscous boundary. The fundamental mode Rayleigh wave in an elastic halfspace is known to decay rapidly with depth. After a depth of around one and a half wavelength, its amplitude is known to vanish. The n extra soil layers are therefore assigned varying thicknesses depending on the frequency of analysis (Lysmer et al. 1981b). The simulation of halfspace is illustrated in Fig 3.2.

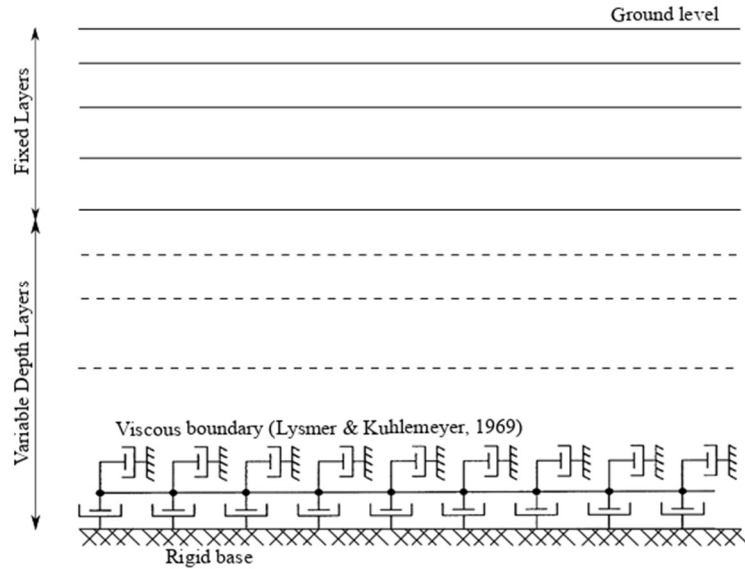


Fig. 3.2 Halfspace simulation using additional layers and viscous boundary (From Lysmer et al. (1981a))

3.3.4 Impedance Analysis

The frequency-dependent impedance matrix $\begin{bmatrix} X_{ii} & X_{iw} \\ X_{wi} & X_{ww} \end{bmatrix}$ is obtained in the impedance analysis stage. An axisymmetric model is set up for the problem of a rigid circular massless disc in cylindrical elements enclosed by a transmitting boundary (Lysmer et al. 1981a). The radius of the soil column is fixed such that it represents an interacting node and the area around it. The radius of the column, r_o is best fixed at 0.9 times the largest size of the FE mesh for accuracy (Kim et al. 2016). A cylindrical coordinate system is used exclusively for this model, and Fourier harmonics are used to expand the element displacement field in the tangential direction. The vertical and horizontal displacements at any node at a radius r from the axis of the model are then calculated and used to assemble the compliance matrix. The axisymmetric problem is set up to derive the force-displacement responses for all degrees of freedom of every node below the ground surface to construct the compliance matrix in the FVSM methodology. For 3D problems, the compliance matrix is of order $3i \times 3i$, where i is the number of interaction nodes. The impedance matrix is then obtained by inverting the compliance matrix. The inversion process forms the most computationally expensive step in the analysis, making the number of interaction nodes the prime factor that decides the computational cost of analysis.

3.3.5 Algorithm for Meshing and Node numbering

The finite element mesh groups for the FVSM methodology consists of excavated soil mesh and a structural mesh. Both these groups have independent node numbering, however, with common nodes at the boundary (PredictiveTechnologies 2014). The structural mesh includes the superstructure, foundation as well as explicitly defined near field soil elements. Near-field soil elements are essential to simulate pile-soil-pile interaction or raft-soil-pile interactions in the case of piled rafts. It is to be noted that the nodes of excavated soil mesh are interaction nodes in the analysis. Complex geometry such as that in a pile group can lead to an increase in the number of nodes. To reduce the computational cost, it is possible to make the excavated soil mesh as regular (with orthogonal joints) and as coarse as possible without violating the element size criteria (Ghiocel 2019).

For the analyses presented in this thesis, the finite element meshes were created using the SAP2000 program (Computers and Structures Inc., 2009). A Matlab code was developed to identify and renumber nodes at the boundaries of the excavated soil and structural meshes. The algorithm duplicates the finite element mesh below ground level to form the excavated soil and structural meshes. It then identifies peripheral nodes, then changes the node numbering of the structural mesh such that the peripheral nodes are common to both excavated soil and structural meshes.

The code also acts as a central data processor feeding soil property data, finite element data, input motion details, and other details to generate the input file for the SSI analysis. The algorithm flow chart is presented in Fig 3.3.

Fig. 3.4 (a) shows a typical FVSM model for a 2x2 pile group model with a pile spacing of 5 times the pile diameter. The excavated soil finite element mesh is presented in Fig. 3.4 (b). A breakup of the structure finite element mesh (consisting of foundation and near field soil) is presented in Fig. 3.4 (c) and (d). The near field soil elements were defined, as shown in Fig. 3.4 (c) such that the pile-soil-pile interaction is captured. The pile group modelling using the central beam and rigid link method is presented in Fig 3.4 (d).

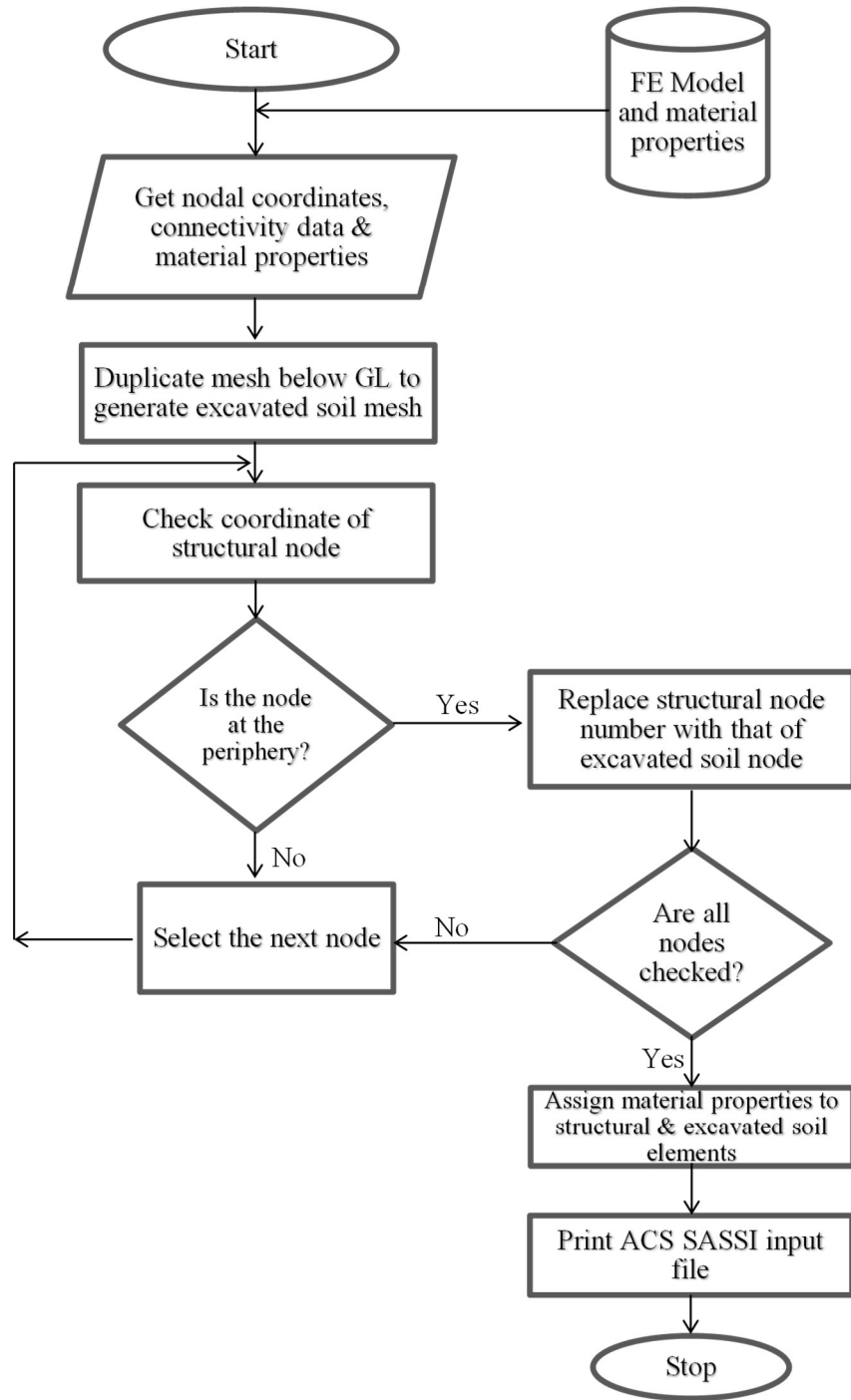


Fig. 3.3 Algorithm to generate FVSM model from FE data

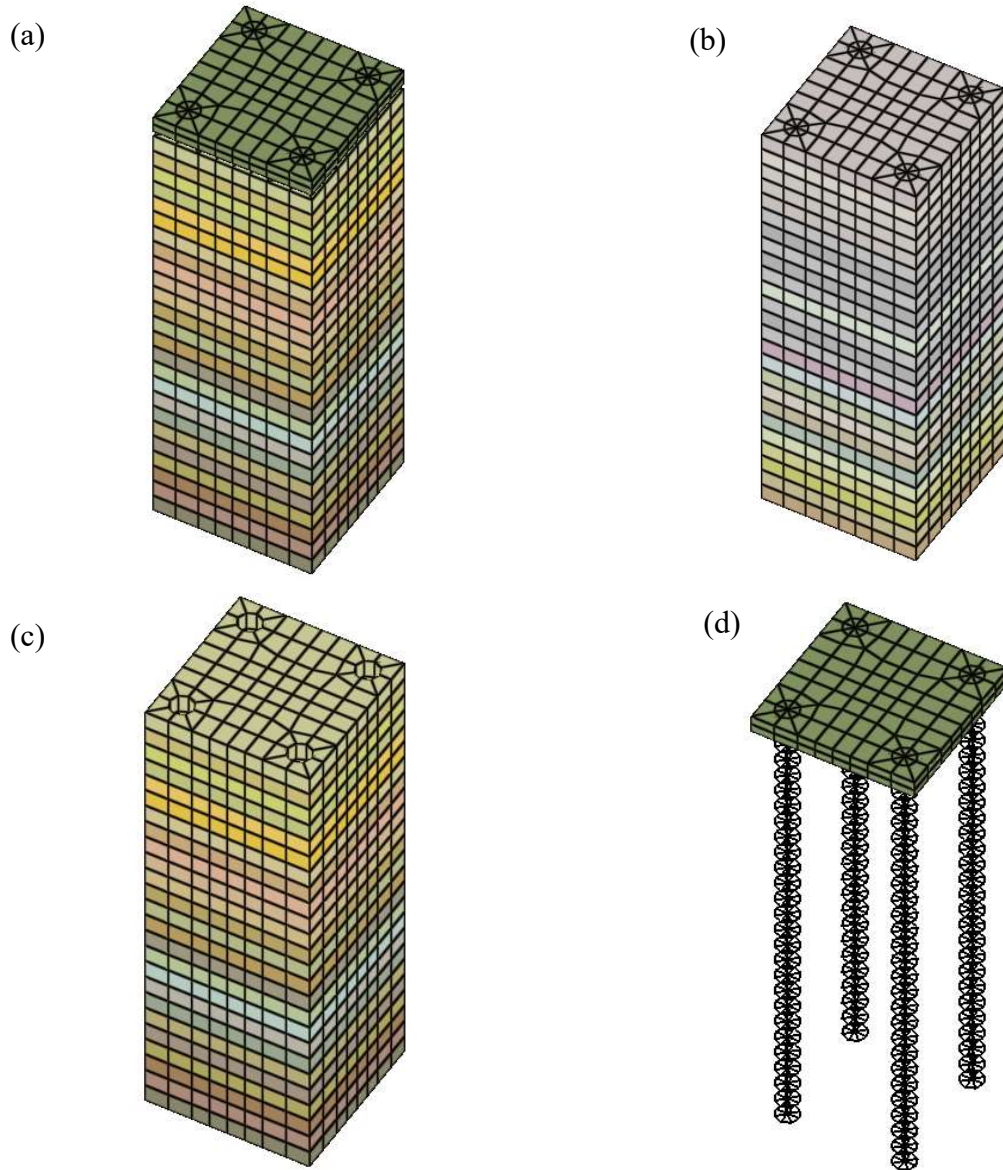


Fig. 3.4 Images of the (a) total FE mesh of a 2x2 pile group, (b) the excavated soil mesh (c) the near field soil mesh and (d) the foundation mesh

3.3.6 Modelling Piled Rafts

A piled raft foundation subjected to a propagating wave field poses a complex SSI problem. Computational models used for the analysis of such foundation systems need to realistically model the geometry and material behaviour of both foundation and soil (Katzenbach and Choudhury 2013). Seismic response of foundation structure systems involves a combination of lateral and rocking movement resulting in both pile-soil-pile and raft-soil-pile interactions.

Researchers in the past have reported several techniques to model pile foundations for dynamic SSI analyses using finite elements. These include the use of solid elements (Alnuaim et al. 2016; Emani and Maheshwari 2009; Goit and Saitoh 2018; Liu and Zhang 2018; Nakai et al. 2004; Small and Zhang 2006), beam elements (Padrón et al. 2007; Wu and Finn 1997a), and central beam and rigid links (Jeremic et al. 2009; Martinelli et al. 2016; Mayoral and Romo 2015; Rahmani et al. 2016). The central beam and rigid link technique involves the removal of soil elements from the volume occupied by the pile, and insertion of beam elements at the centre of the volume, which are connected horizontally to the soil nodes using rigid beam elements. Although the rotational degrees of freedom of the rigid links remain unconnected at the common nodes with near field soil elements, this technique provides a direct value of forces and moments in a pile. An illustration showing this modelling technique is presented in Fig. 3.5.

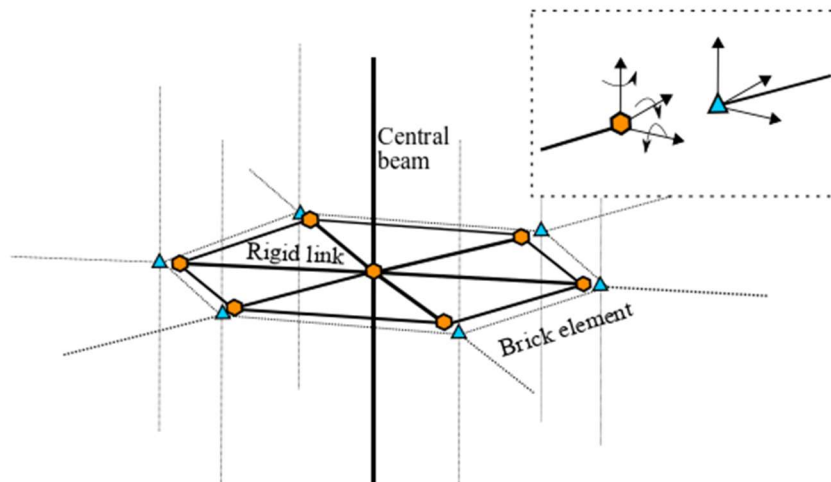


Fig. 3.5 Illustration of the central beam and rigid link method for pile modelling

Previous studies (Mayoral et al. 2011) have shown that this technique of pile modelling can perform reasonably well in simulating the seismic response of bridge support systems. Pile foundation models described in this thesis employ both the central beam and rigid link model as well as the brick element model. The raft or pile cap can be modelled using brick elements (Banerjee et al. 2014; Zhang et al. 2017a) or shell elements. However, if the pile is modelled using beam elements, a connection with a minimum of two brick element nodes are required for effective transfer of moments. Therefore, in cases where piles are modelled using beam

elements, the pile beams are ‘inserted’ into the raft bricks with a connection with three or more raft nodes. The near field soil modelled using brick elements are explicitly added around the piles for two specific reasons. Firstly, these elements enable accurate simulation of pile-soil-pile and raft-soil-pile interactions. Another use of near field soil elements is to incorporate secondary nonlinearity in the SSI analysis. The shear modulus and damping properties of near field soil can be updated based on the strain, induced during motion, using an equivalent linear iterative scheme. Soil near the foundation can be subjected to high strain levels, and accounting for the modified properties becomes crucial in simulating real-world problems.

3.3.7 Verification with Standard Results

Dynamic stiffness of single group piles

The accuracy of the FE model was checked for the case of a 2x2 pile group under vertical vibration against the rigorous solution by Kaynia (1982). The impedance functions for 2x2 pile groups with length to diameter ratio, $l/d=15$, pile-soil modulus ratio $E_p/E_s=1000$, and spacing to diameter ratio (s/d) varying from 2 to 10, reported by Kaynia (1982) were considered. Three-dimensional single pile and pile group models were generated with the piles modelled by the central beam and rigid links. The near field soil between piles was modelled using volume elements to rigorously model pile-soil-pile interaction effects. Rigid massless pile cap was modelled using brick elements. Harmonic vertical loads were applied at the pile cap level, and the complex displacement at the centre of the pile cap was used to calculate the impedance. For comparison, the complex impedance obtained are presented in the form given by Kaynia (1982) as

$$K(a_o) = k(a_o) + ia_o c(a_o) \quad (3.10)$$

where a_o is the dimensionless frequency defined as

$$a_o = \frac{\omega d}{V_s} \quad (3.11)$$

The stiffness and damping coefficients for the pile group are normalized with the static, or near-zero frequency stiffness of the corresponding single pile. The impedance functions from the present study are plotted along with the results by Kaynia (1982) in Fig. 3.6 (a) and (b).

The simulation is found to capture pile-soil-pile interaction well, and the results are found to closely follow the reference curves.

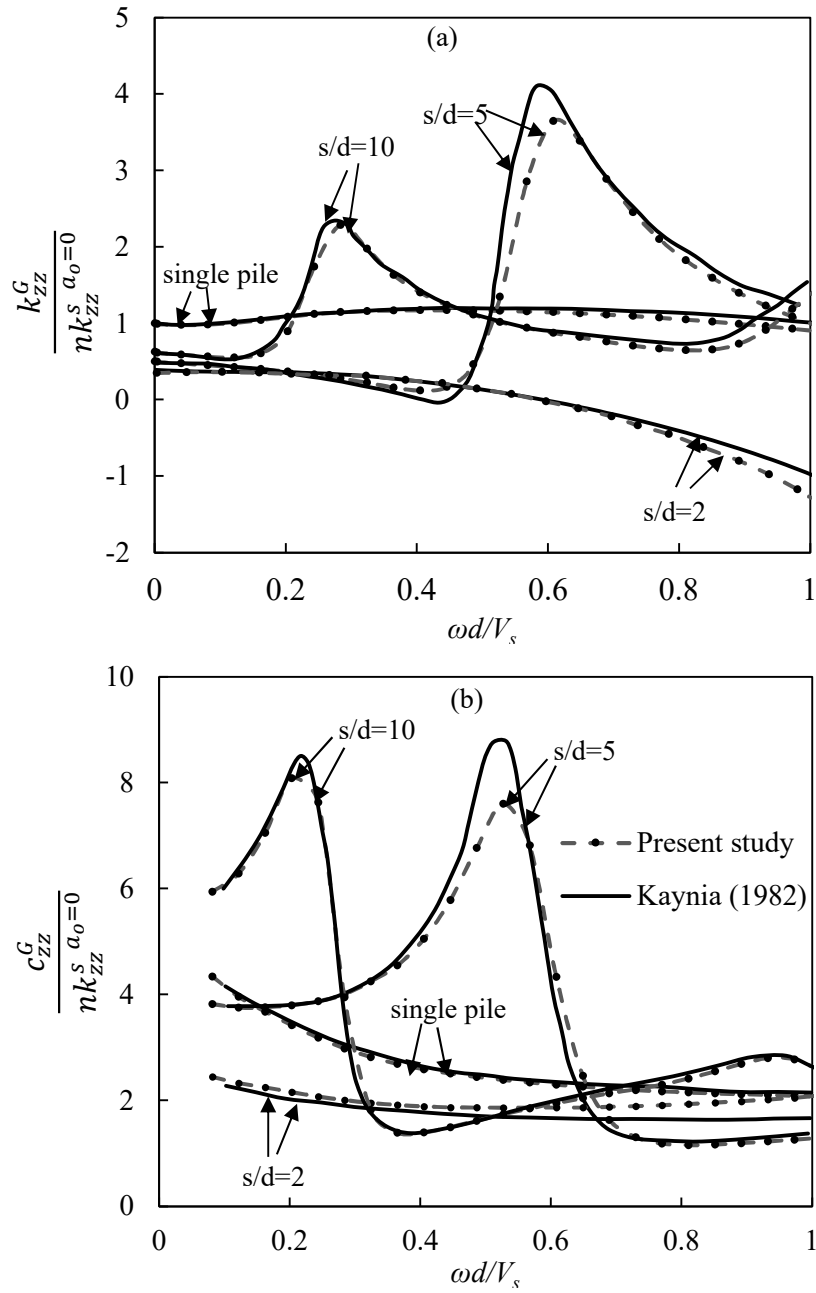


Fig. 3.6 Normalized (a) stiffness and (b) damping coefficients for single and 2x2 pile group in vertical vibration

Kinematic response of single and group piles

The methodology was also evaluated for the kinematic response of single and group piles. The results presented by Fan et al. (1991) using the three-dimensional boundary value problem developed by Kaynia and Kausel (1982) is used as the reference problem in this study. The cases of single pile and 2x2 pile group with $l/d=15$ embedded in elastic halfspace are considered. The piles were modelled using the beam and rigid link technique, and the near field soil was modelled using brick elements. A seismic response analysis for vertically propagating s waves is performed keeping the ground surface as control point. This ensures that the transfer functions obtained from the analysis are directly in the classic form defined as in Eq. 3.12 and Eq. 3.13.

$$I_u = \frac{u_p}{u_{ff}} \quad (3.12)$$

$$I_\varphi = \frac{\theta d}{u_{ff}} \quad (3.13)$$

In these equations, u_p represents the displacement at the pile head, u_{ff} represents the free field displacement, θ represents the rotation at the pile head, and d represents the pile diameter. The comparison of kinematic interaction factor in displacement and rotation for single free headed pile in homogeneous soil obtained from the simulation and those reported by Fan et al. (1991) are presented in Fig. 3.7 (a) and (b) respectively. The simulation is found to replicate the trend of I_u and I_φ accurately. The simulation is found to underestimate the peak rotational kinematic response by up to 11% in the case of comparatively stiff soil ($E_p/E_s=1000$).

The methodology was also evaluated for fixed headed pile groups embedded in elastic halfspace with elastic modulus ratio of 1000. Three models with spacing to diameter (s/d) ratio of 3, 5, and 10 were analyzed. Pile group models were developed with near field soil elements explicitly defined between the piles. The finite element mesh of the pile group with $s/d=5$ is presented in Fig. 3.4. The pile cap was modelled using stiff brick elements to ensure fixity at the pile heads. The comparison of kinematic response factors obtained from the analysis and those reported by Fan et al. (1991) are presented in Fig. 3.8 (a) and (b). The developed models were found to capture the translational response with good accuracy. Apart from the underestimation in

maximum rotation for the case of $s/d=3$, the simulation was found to reproduce the rotational kinematic response factor with a fair degree of accuracy.

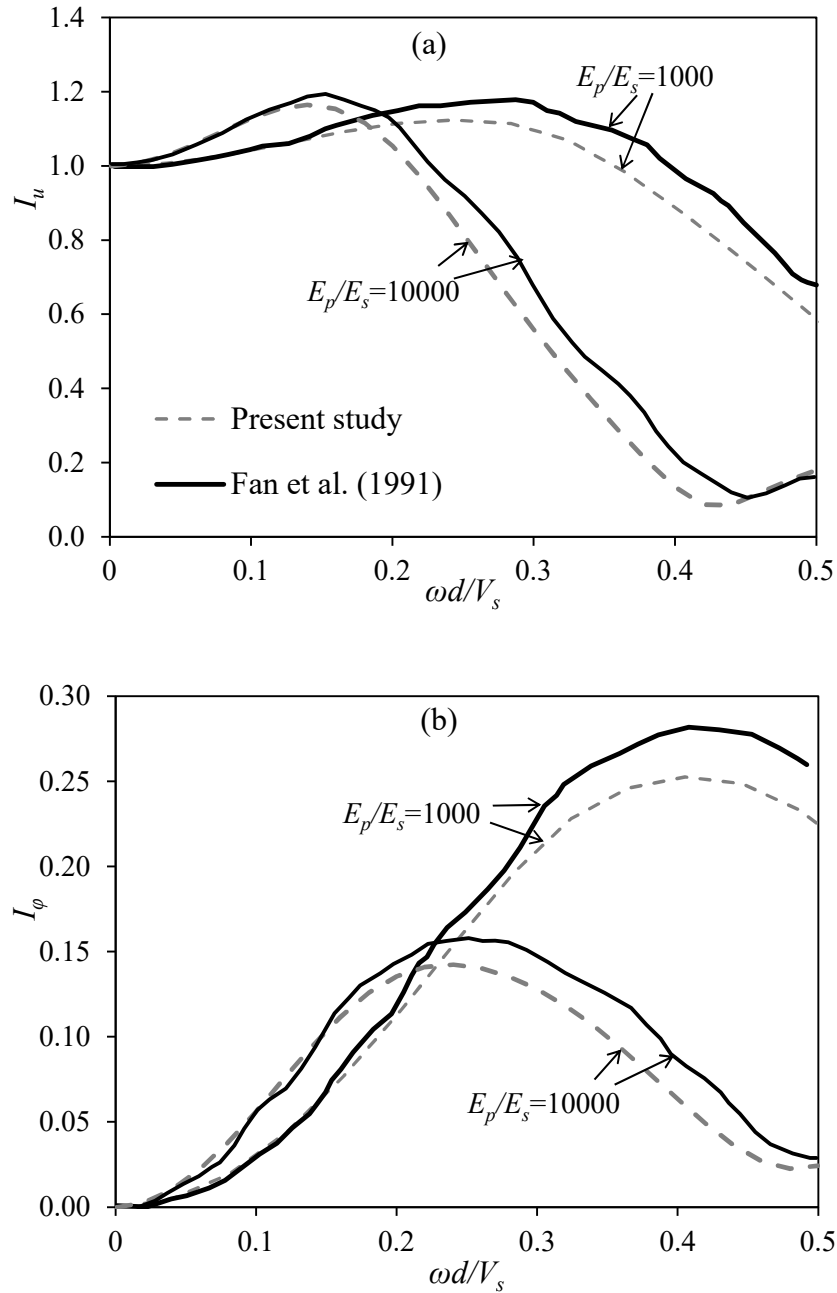


Fig. 3.7 Kinematic response factors for single free headed piles in homogeneous soil; comparison of results with Fan et al. (1991)

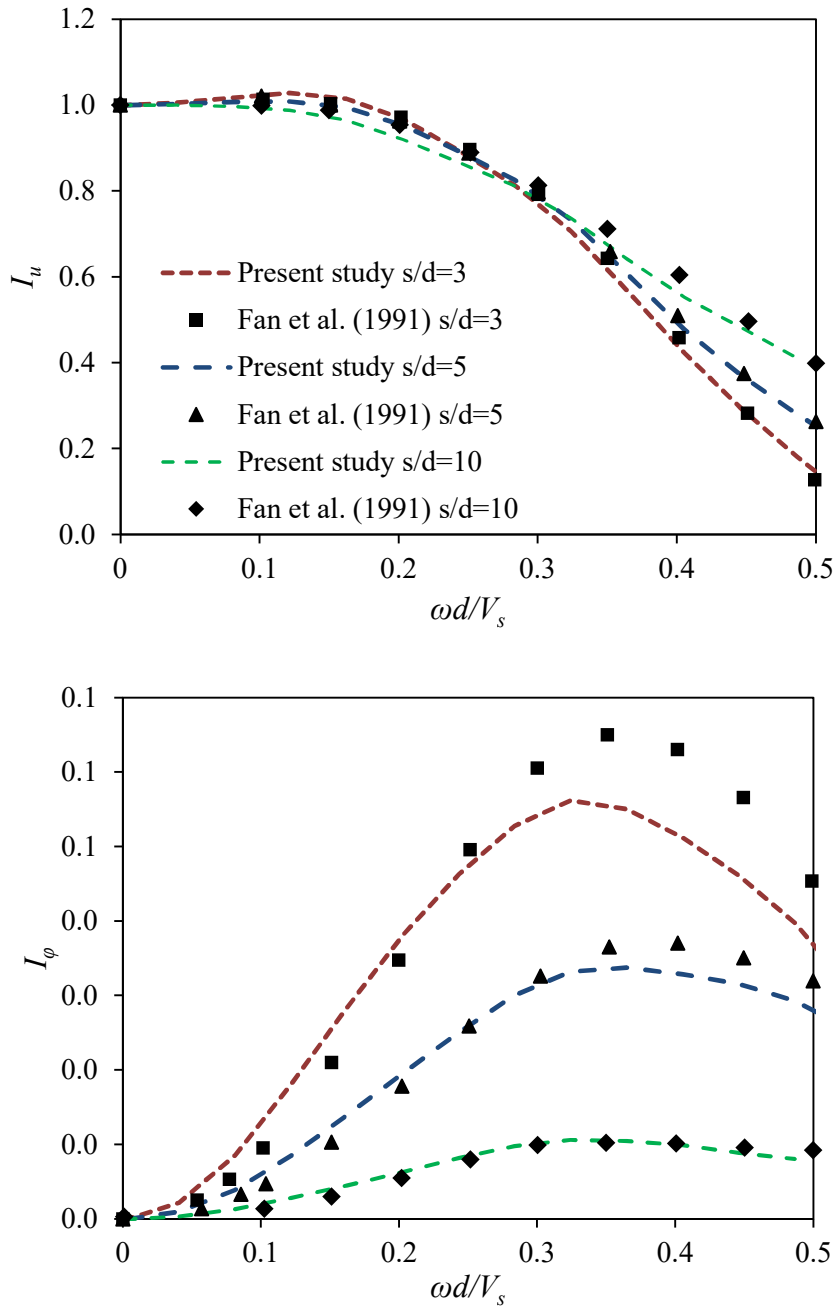


Fig. 3.8 Kinematic response factors for a fixed head 2x2 pile group in homogeneous soil; comparison of results with Fan et al. (1991)

3.4 CONCLUDING REMARKS

Numerical tools of varying complexity have been used by researchers in the past to analyse the problem of soil-pile interaction. Solutions in the frequency domain are computationally

efficient and reliable for low strain problems where the material properties can be assumed to be linear. However, for high strain problems where soil behaviour is seldom linear, time-domain methods with appropriate constitutive models are suitable. However, a combination of the substructuring method, along with the equivalent linear method to account for soil nonlinearity can be adopted to analyse the SSI in the frequency domain with a reasonable degree of accuracy.

The finite element-based three-dimensional soil structure interaction methodology that follows the FVSM technique using the ACS SASSI program is evaluated for application in soil-pile interaction problems. A framework is developed for meshing generation and model development using the Matlab program. The methodology is then evaluated against standard results available from literature for impedance functions as well as kinematic response factors of single and group piles. The method of modelling piles using central beam and rigid links along with near field soil elements is adopted in this study. The methodology is found to reproduce the vertical impedances of a 2x2 pile group, reported by Kaynia (1982) with a reasonable degree of accuracy. Three-dimensional models were also developed to evaluate the kinematic response of single and group piles subjected to vertically propagating s waves, as presented in Fan et al. (1991). Results from the present study are found to simulate the kinematic translational response with a high degree of accuracy. Although an underestimation in the maximum rotational response for closely spaced piles ($s/d=3$) is noted, the methodology is found to simulate the rotational response for larger spacings reliably. The adopted methodology is considered adequate to rigorously simulate pile-soil-pile interactions as in the case of piled rafts.

CHAPTER 4

KINEMATIC RESPONSE OF PILED RAFT FOUNDATIONS

4.1 INTRODUCTION

Pile foundations, owing to their stiffness, are reluctant to follow the movement of soil during seismic shaking, leading to reduced displacement and acceleration transferred to the superstructure. This phenomenon, known as kinematic interaction, induces additional forces and moments in a pile. Evidence from past earthquakes has clearly underscored the importance of kinematic bending moments in the structural design of piles. Large bending moment induced pile failures have been observed near the pile cap as well as at depths where the effects of inertial are likely to vanish (Koyamada et al. 2006; Nikolaou et al. 2001b). Kinematic interaction results in two major effects in a pile-supported structure. These are the modification of foundation input motion and bending moment in piles.

The foundation input motion at the head of a pile foundation is commonly specified with respect to the free field ground motion as transfer functions. The transfer functions, commonly referred to as kinematic response factors in translation and rotation, are defined as follows:

$$I_u = \frac{u_p}{u_{ff}} \quad (4.1)$$

$$I_\theta = \frac{\theta_p d}{u_{ff}} \quad (4.2)$$

where u_p represents the displacement at the pile head, u_{ff} represents the free field displacement, θ_p represents the rotation at the pile head, and d is the diameter of the pile. Due to the presence of a pile cap, group effects come into play in the kinematic response of pile groups. The kinematic interaction between a group of piles connected at the pile cap can result in an additional rotational component of the Foundation Input Motion (Di Laora et al. 2017). It is also known that a pile foundation can filter out high frequency components of the free field motion. Di Laora and de Sanctis (2013) studied the response of piles to transient ground motion

and reported that the ratio of spectral accelerations resemble a square root shape with a characteristic critical point after which the filtering effect becomes negligible.

Piles may also experience significant curvature due to strains developed in soil due to vertically propagating of shear waves in soil. Several of researchers have proposed empirical equations to predict the kinematic bending moments induced in a pile embedded in homogeneous soil profile (Banerjee et al. 2014; Dobry and O'Rourke 1983) as well as two-layered profile (Di Laora et al. 2012; Maria et al. 2009; Nikolaou et al. 2001b; Sica et al. 2011). In the presence of a restraining pile cap, kinematic forces tend to dominate over inertial forces. The kinematic pile head moments become significant for large diameter piles (Di Laora and Mandolini 2011b; Di Laora and Rovithis 2015). Only a few codes such as the Eurocode 8 (EN 1998-5 2004) recommends the consideration of kinematic bending moments under certain geotechnical conditions.

A shallow foundation member such as an embedded raft, in addition to piles such as a raft, can influence the kinematic response of pile groups (Stewart et al. 2012). Padrón (2009) studied the influence of an embedded raft on the kinematic response of 2x2 and 3x3 pile groups employing a coupled FEM-BEM methodology and found that for amply spaced pile groups ($s/d=5$), the FIM of piled raft closely matches that of the corresponding shallow footing. The results presented by Padrón (2009) albeit limited, form one of the few references on the behaviour of piled rafts to vertically propagating SV waves. The transition from pile behaviour to shallow footing behaviour and the factors that govern them needs to be investigated in detail. Iovino et al. (2019) conducted a finite element-based analysis on single piles with embedded pile cap, and found that an increasing pile cap embedment leads to a lower kinematic response factor in translation. Similar observations for single piles were also reported by Rovithis et al. (2019). This provided the initial motivation for the work presented in this chapter. The chapter focusses on the effect of an embedded raft on the kinematic response factors. Three different pile groups with varying geometry and soil profiles were chosen for a comprehensive numerical analysis. The methodology described in Chapter 3 is evaluated against a centrifuge shaking table test reported by Banerjee (2009). The model is then adopted to carry out a parametric study to study the effect of pile spacing on the kinematic response of a 2x2 piled raft. A detailed study is then conducted for two other piled raft foundations with varying geometry and soil properties. The frequency response is discussed in terms of kinematic response factors, and transient response

is discussed in terms of spectral ratios. In the present study, the abbreviations *PG* is used to denote a pile group where the physical contact between raft and soil is not considered, and *PR* to denote a piled raft.

4.2 CASE STUDY OF A PILED RAFT IN CLAY

4.2.1 Foundation and Soil Properties

Banerjee (2009) reported the seismic response of a 2x2 piled raft in kaolin clay studied by conducting a series of centrifuge shaking table tests.

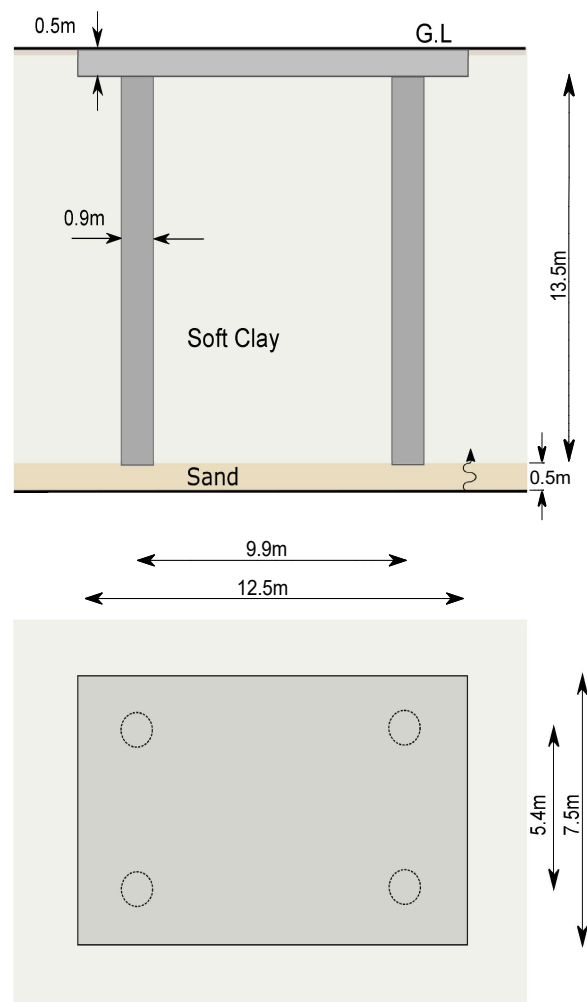


Fig. 4.1 Schematic diagram of the PR-clay system

This model is adopted in the present study to evaluate the kinematic response characteristics of piled rafts in terms of frequency response and transient response. The experimental data is also

used to evaluate the performance of two pile modelling techniques. The PR foundation has a raft dimension of 12.5 m x 7.5 m x 0.5 m along with four piles with a diameter of 0.9 m and length of 13 m as presented in Fig. 4.1. The dimensions of the pile-raft system correspond to the prototype scale of the centrifuge test model at 50 g level. The piles were bolted into the raft to model the fixed pile head condition. The piled raft system was subjected to a vertical load of 605 tonnes applied using stacked steel plates. The piles were made of hollow steel pipe sections with concrete in-fill.

The clay used in the tests was Malaysian Kaolin clay prepared by slurry consolidation, which had a bulk unit weight of 16 kN/m³. The variation of G_{max} with depth, as well as modulus degradation and damping ratio curves used in the SSI analysis were adopted as reported in Banerjee (2009). Material properties used in the analysis are listed in Table 4.1.

Table 4.1 Material properties used in the piled raft model

Property	Raft	Pile
Material	Steel	Concrete in-fill hollow steel pipe sections
Unit weight (kN/m ³)	77.0	25.2
Young's Modulus (GPa)	200.0	94.5
Poisson's ratio	0.25	0.20

Foundation elements were assigned linear elastic material properties considering the low strain levels involved in the experiments. The elastic modulus and flexural rigidity of piles were estimated as per the prototype properties and dimensions reported by Banerjee et al. (2014).

4.2.2 Finite Element Model of the Foundation-Soil System

A three-dimensional finite element model that includes structural elements and near field soil elements was developed for the FVSM based analysis. Near field soil elements were explicitly modelled to capture pile-soil-pile and raft-soil-pile interactions. The raft was modelled using 8 noded brick elements. The load applied at the top of raft by placing steel plates, was simplified as distributed load on the upper face of the raft. Piles can be modelled using several techniques in the finite element method such as using regular beam elements Wu and Finn (1997), solid

brick elements Nakai et al. (2004), by introducing special inter pile elements Ostadan (1983), or using a central beam with rigid links as discussed in Chapter 3. Although, the modelling of piles using solid elements is popular owing to the inclusion of volume effects, bending moment extraction requires indirect calculation from strain or from very flexible embedded beam elements. Nakai et al. (2004) suggested that simplifying pile as beam elements underestimates impedance functions and over estimates foundation input motions. The use of brick elements, and the inter pile elements to model pile for the same piled raft clay system were assessed by Varghese et al. (2019) and Boominathan et al. (2018) respectively. Although these studies were limited to a single ground motion, a reasonable match with experimental results was observed. Another technique of modelling piles is by the use of a central beam and rigid links whereby the volume occupied by pile is left open and the beam element, with flexural rigidity of the actual pile is inserted into the cavity. A web of short rigid beam elements connects the pile beam to the adjacent soil elements to facilitate load transfer. The major advantage of this approach is that the actual geometry of the pile soil system is modelled and pile deformations in axial bending and shearing modes are accurately transferred to the surrounding soil Jeremic et al. (2009). Mayoral et al. (2011) modelled piles using this technique to simulate seismic response of a bridge support system in the SASSI program. In the present study, applicability of two modelling techniques, viz. pile as beam element and pile as central beam and rigid links, were evaluated for the PR system.

The pile-as-beam model, which is referred to as Model 1 in the present study, takes into account the flexural rigidity of pile but does not simulate volume effect of piles, which plays an important role in group interaction effects, particularly for closely spaced piles. Another drawback of the model is the inability to simulate pile soil slip using interface elements. In spite of these drawbacks, certain situations necessitate the use of beam elements for piles, such as large pile groups, where other modelling techniques result in tremendous computational cost. The second technique evaluated in this study, namely Model 2, is the one in which pile is modelled as central beams with radial rigid links. One disadvantage of this model is that the rotational degrees of freedom of the rigid links remain unconnected as the solid brick element nodes have only translational degrees of freedom. The number of interaction nodes remains the same as the case of pile modelled using brick elements.

The finite element meshes of Model 1 and Model 2 are presented in Fig. 4.2 (a) and 4.2 (b), respectively. Figure 4.2 (c) presents Model 2 with the adjacent soil elements hidden, for clarity. Model 1 used in the present study, has 460 number of interaction nodes in comparison to 2960 for Model 2. Run time in a 16GB RAM workstation, for the SSSI analysis was 2 minutes for Model 1 compared to 4 hours for Model 2, using a fast solver enhanced analysis. The significant difference in run time makes a comparison of simulation results meaningful.

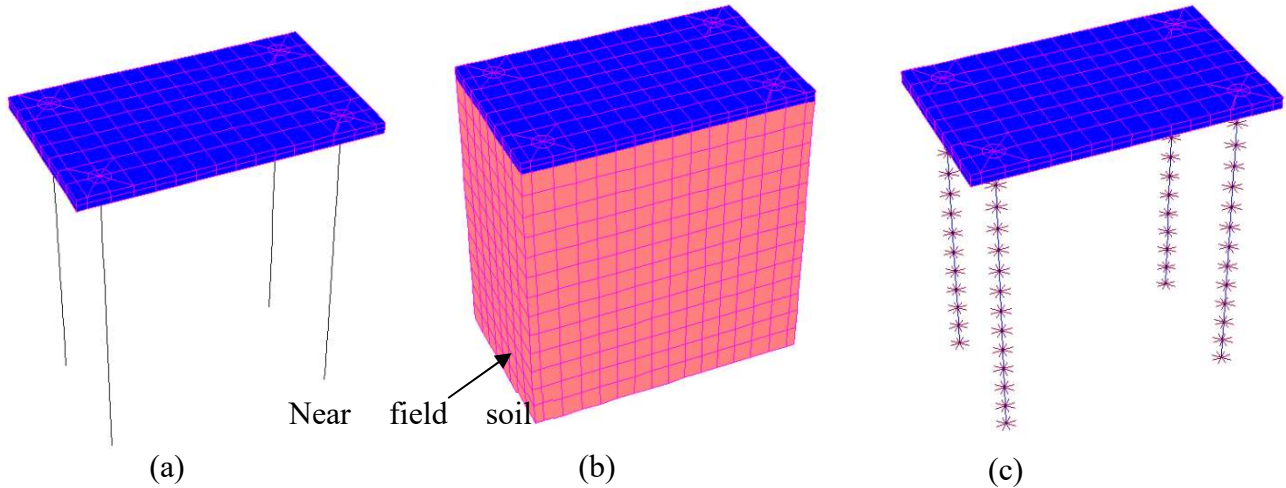


Fig. 4.2 (a) Finite element mesh of Model 1 (b) Model 2 showing structural elements with near field soil elements (c) Model 2 without near field soil elements

The soil is modelled using equivalent linear approach incorporating the variation of shear modulus and damping ratios with the shear strain induced due to the propagation of shear waves. The equivalent linear analysis was performed for various input motions using the in-built module in the ACS SASSI program, to obtain strain dependent shear modulus and damping ratios at various soil layers.

4.2.3 Simulation of the Experiment

To evaluate the developed numerical model, three input motions used in the centrifuge test, reported in Banerjee (2014) were used. The time histories of acceleration were synthetically developed using the typical response spectra of Sumatran earthquakes measured at the rock sites in Singapore. The input motions with peak accelerations of 0.017 g, 0.05 g and 0.16 g, will be referred to as ‘Earthquake-1’, ‘Earthquake-2’ and ‘Earthquake-3’ respectively in the present study. Time history and Fourier spectra of the three input motions are presented in Fig 4.3 (a),

(b), and (c) respectively. It can be noted that all the three input motions have longer period, typical for far field seismic events.

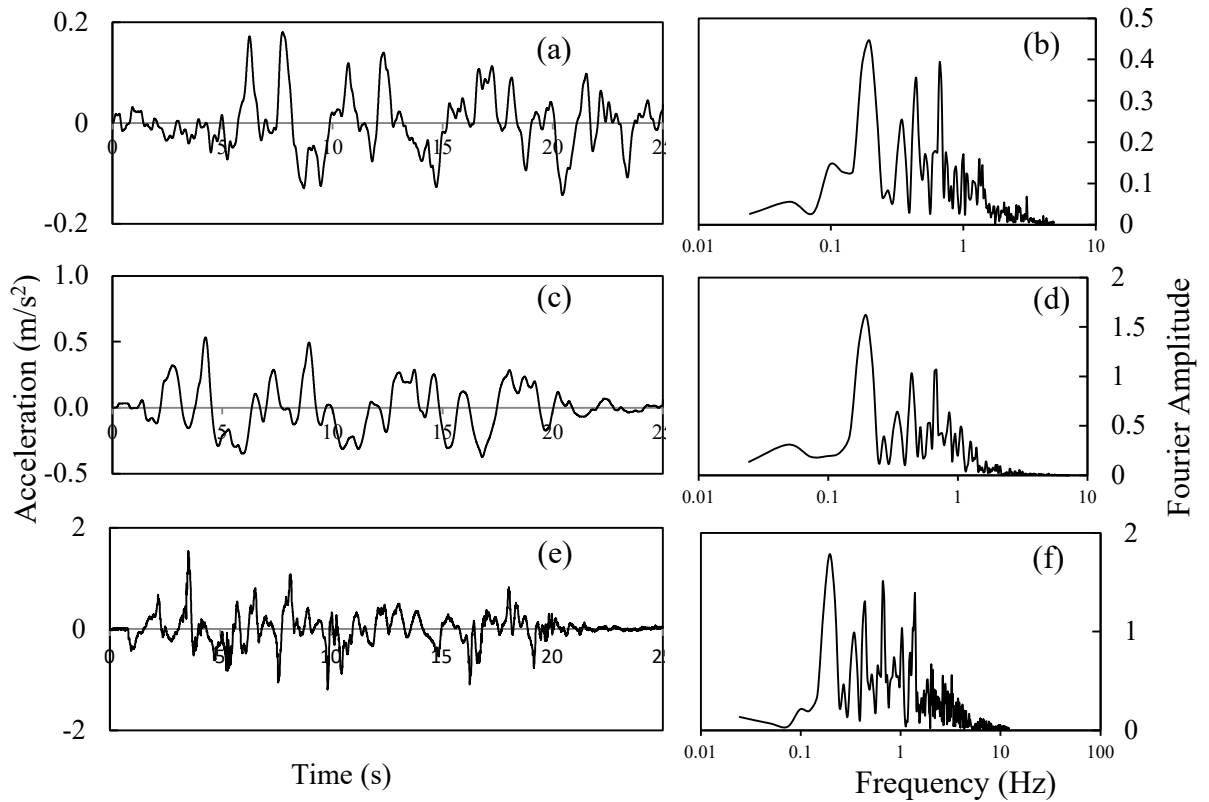
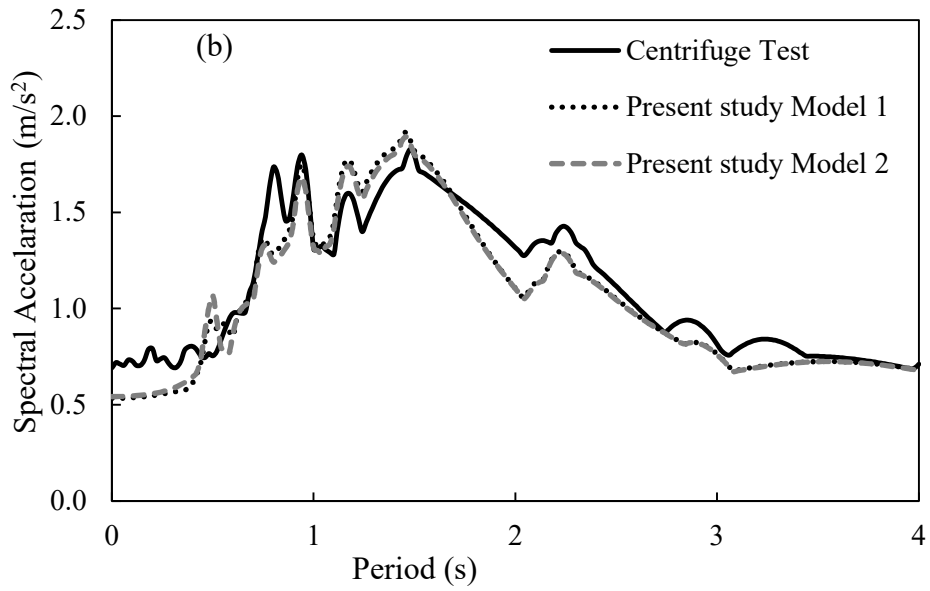
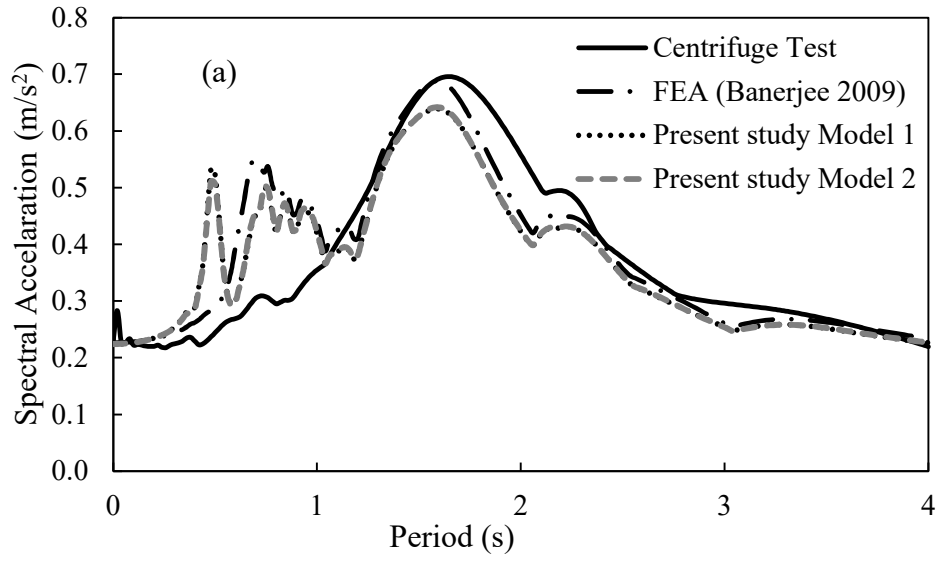


Fig. 4.3 Time histories & Fourier spectra of (a) Earthquake-1, (b) Earthquake-2, and (c) Earthquake-3

The SSSI analysis was performed for over 40 frequencies in each case based on the frequency content of input signals and a free vibration analysis. The radius of central soil column that in the POINT module of the ACS SASSI program was set to 0.9 times the average mesh size following the suggestions by Kim et al. (2016). Input motion, in the form of vertically propagating s-waves was applied at the bottom most layer as in the experiment. The response spectra at the top of raft, obtained from the analysis are presented, along with experimental results in Fig. 4.4 (a), (b) and (c) for Earthquake-1, Earthquake-2 and Earthquake-3 respectively. The simulation was found to reproduce most of the predominant peaks in the spectra. A reduction in peak spectral ordinate of the order of 8% and 50% respectively for Earthquake -1 and Earthquake -3 input motion is observed. Results from the present study are



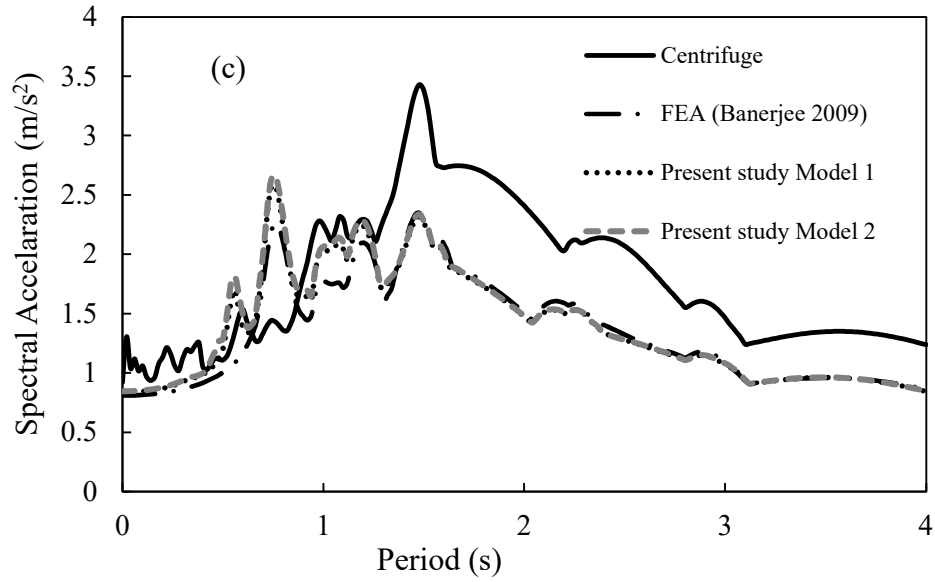
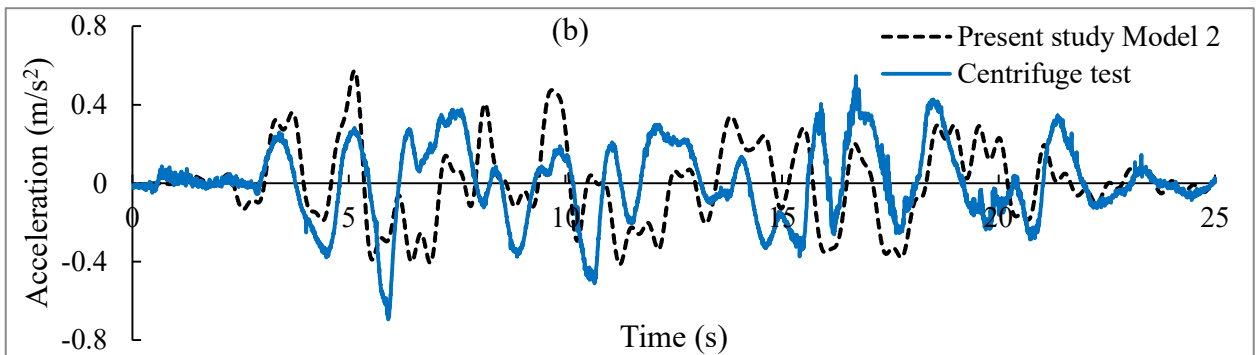
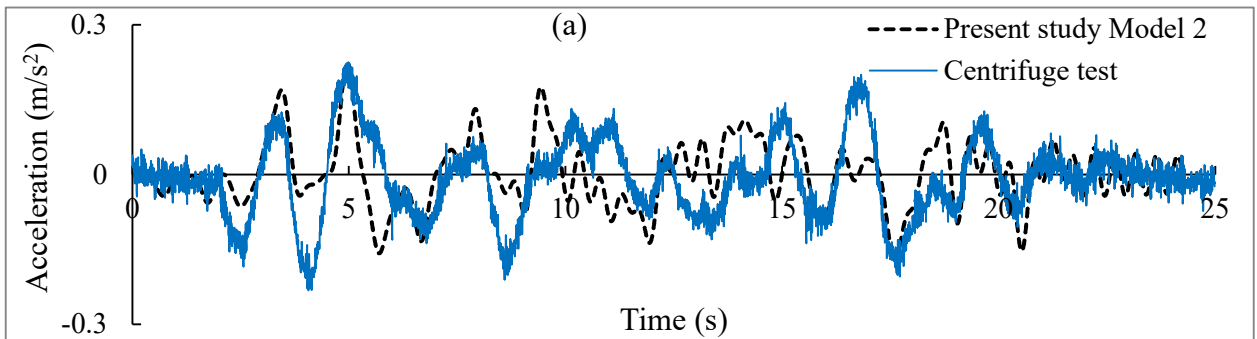


Fig. 4.4 Response spectra comparison at the top of raft for (a) Earthquake-1, (b) Earthquake-2, and (c) Earthquake-3 input motion



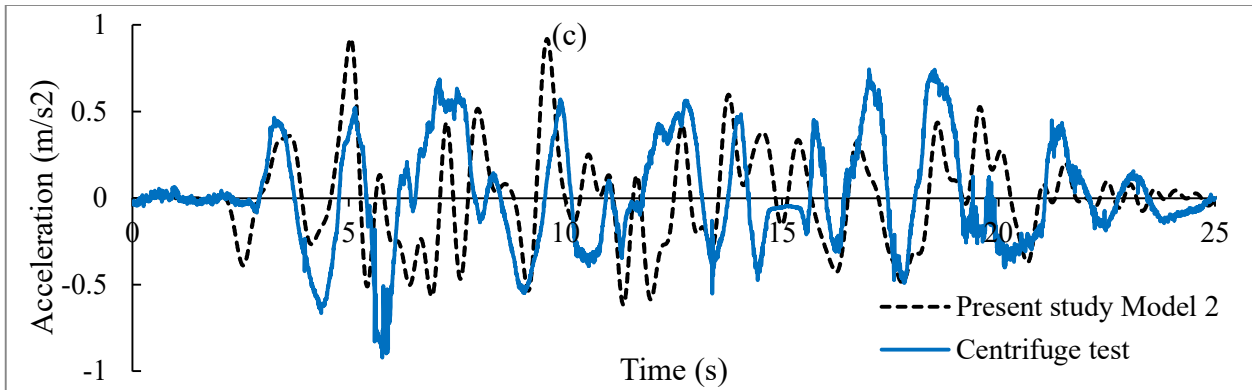


Fig. 4.5 Comparison of time histories at the top of raft for (a) Earthquake-1, (b) Earthquake-2, and (c) Earthquake-3 input motion

observed to be in agreement with nonlinear Finite Element Analysis (FEA) with a hyperbolic–hysteretic soil model, reported by Banerjee (2009). Both the models developed in the present study produce similar spectra with minor differences at higher frequencies. Low period peaks at 0.5s for Earthquake -1 and 0.75s for Earthquake -3, were observed to be amplified by the simulation in comparison to FEA results. The FEA result for Earthquake -3 input motion is also observed to show a similar reduction in the peak spectral ordinate. The time histories at the top of raft obtained from the simulation using Model 2, and Centrifuge test reported by Banerjee (2009), are presented in Fig 4.5 (a), (b), and (c) for comparison. The simulation is found to locate the instance of peak acceleration with a fair degree of accuracy.

Maximum bending moment envelopes were also obtained from the time histories of bending moment obtained at the nodes of the beam elements constituting a pile in the model. A comparison of maximum bending moment envelopes obtained from the two models, with experimental results is presented in Figure 4.6 (a), (b), and (c). The bending moment envelopes computed from the analysis of Model 2 matches reasonably well with those measured during centrifuge tests. In comparison, Model 1 exhibits greater amplification in maximum moment, especially during the application of large earthquakes. It is to be noted that the case of Earthquake-3 involved greater strains and hence greater nonlinearity. Effects like gap formation and settlements are not considered in the present analysis and hence an over estimation in bending moment by equivalent linear approach is not unusual. In the numerical analyses described in the following sections, modelling technique used in Model 2 is adopted.

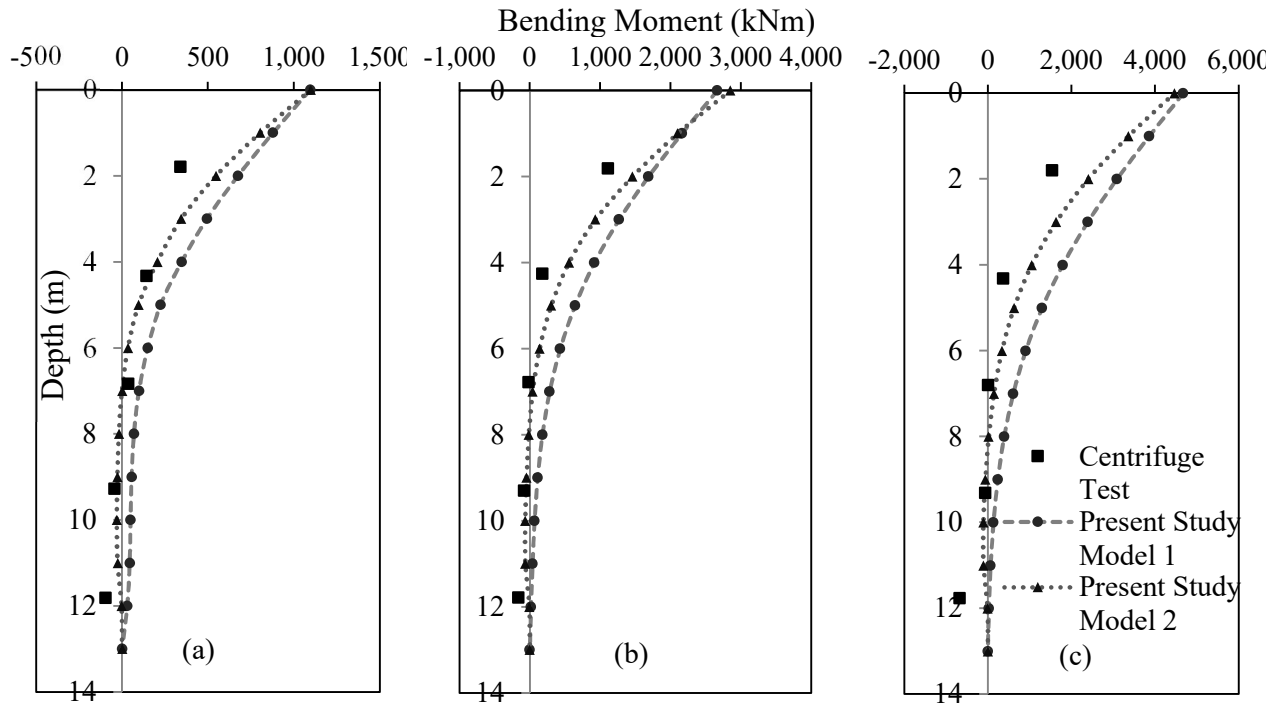


Fig. 4.6 Maximum bending moment envelope in pile vs depth for (a) Earthquake -1, (b) Earthquake -2, and (c) Earthquake -3 input motion

4.2.4 Effect of Pile Spacing on Kinematic Response Factors

The model developed in the previous section is used further to study the effect of pile spacing on the kinematic response characteristics. The piled raft-clay system discussed in the previous section is adopted as shown in Fig. 4.7 with the pile being assigned an elastic modulus of 32 GPa, Poisson's ratio of 0.15 and a unit weight of 25 kN/m³. The raft was modelled to behave rigidly by satisfying the relative stiffness criterion suggested by Simone (1966). The clay layer of 13.5 m, having similar dynamic properties as in the centrifuge test model, is assumed to overlay a 3 m thick sand stratum with V_s of 400 m/s, followed by rock with V_s of 1500 m/s. Thus, the pile is fixed at the head and unrestrained at its tip. The average modulus degradation and damping curves for the sands reported by Seed and Idriss (1970) was adopted for the sand layer, while those proposed by Schnabel (1972) was adopted for the rock layer.

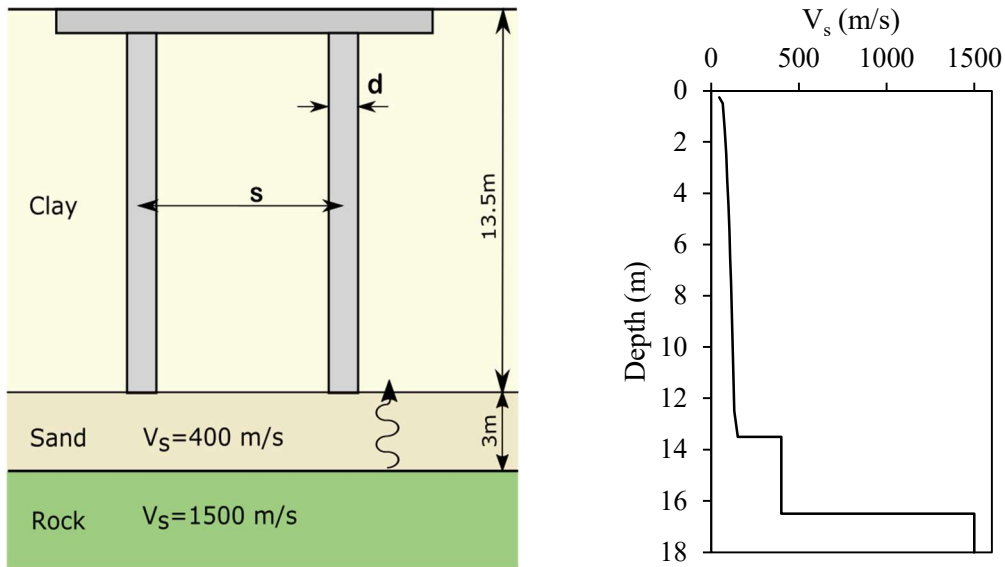


Fig. 4.7 (a) Schematic diagram showing the piled raft soil system and (b) the shear wave velocity profile

In the case of foundations supported by pile groups, pile spacing in the direction of motion as well as axial and rotational stiffness of single pile, are understood to be controlling factors in the rotational component of the foundation input motion (Fan et al. 1991; Di Laora et al. 2017). A parametric study was conducted to study the effect of pile layout, on the translational and rocking response of the piled rafts and pile groups, subjected to vertically propagating s-waves. Three dimensional models were created for pile groups with the same pile configuration as in the piled rafts. For pile group models, the piles are connected to each other at their heads with rigid links to simulate fixed head condition and eliminating any effect of an embedded pile cap. Location of piles in the direction of motion, rather than that in the transverse direction, is known to affect rotation at the pile cap level for pile groups. Models with pile spaced at s/d ratios of 4, 6, 8, and 10, while maintaining the same raft dimensions were used in the study. A series of analyses with the input motion defined at the ground level was performed and displacement transfer functions in translation and rocking at the centre of raft were extracted. It was observed that transfer functions at the edge of raft were very similar to the ones at the centre node, owing to the high flexural rigidity of the raft material. Hence only the values extracted at centre of raft are discussed in this study. The transfer functions presented in this study, in translation and rotation are defined in Eq. (4.1) and Eq. (4.2) respectively. Fig. 4.8 presents kinematic response

factor in translation for different spacing ratios, obtained at the centre of raft, plotted against dimensionless frequency. It is observed that the translational response of the four pile configurations fall in a narrow band, up to an a_o value of 0.4.

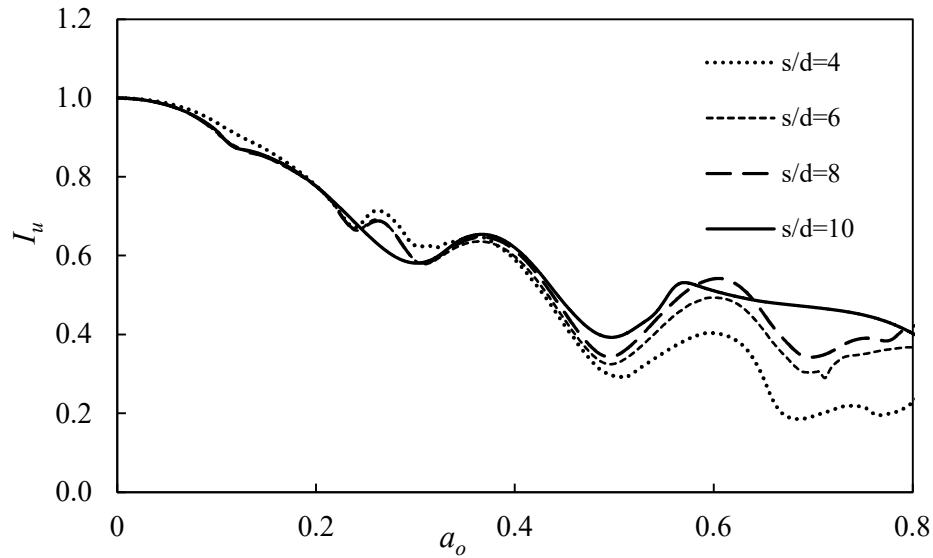


Fig. 4.8 Kinematic response factor in translation, for PR obtained at top of raft for different pile spacing

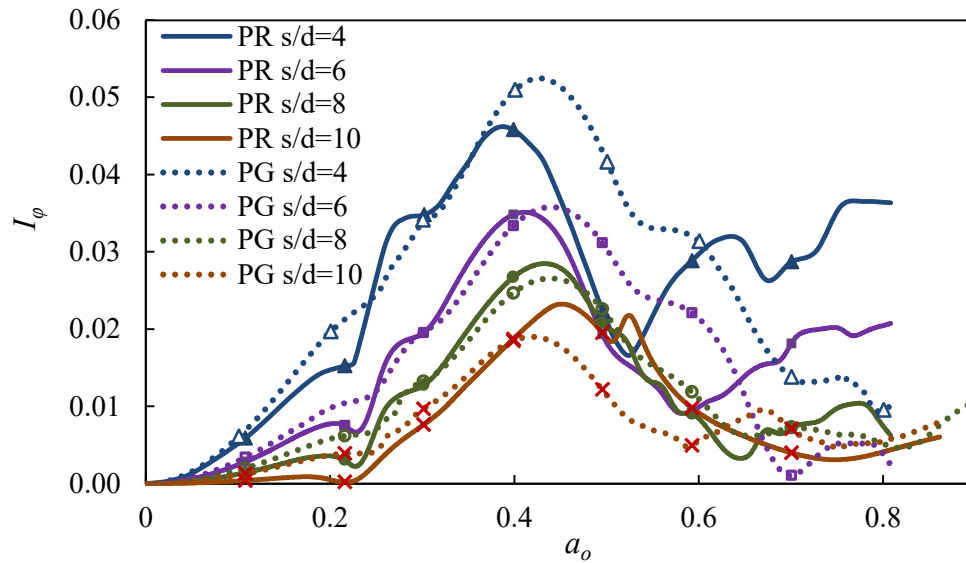


Fig. 4.9 Comparison of transfer functions in rotation for piled rafts and the corresponding pile groups, for different pile spacing

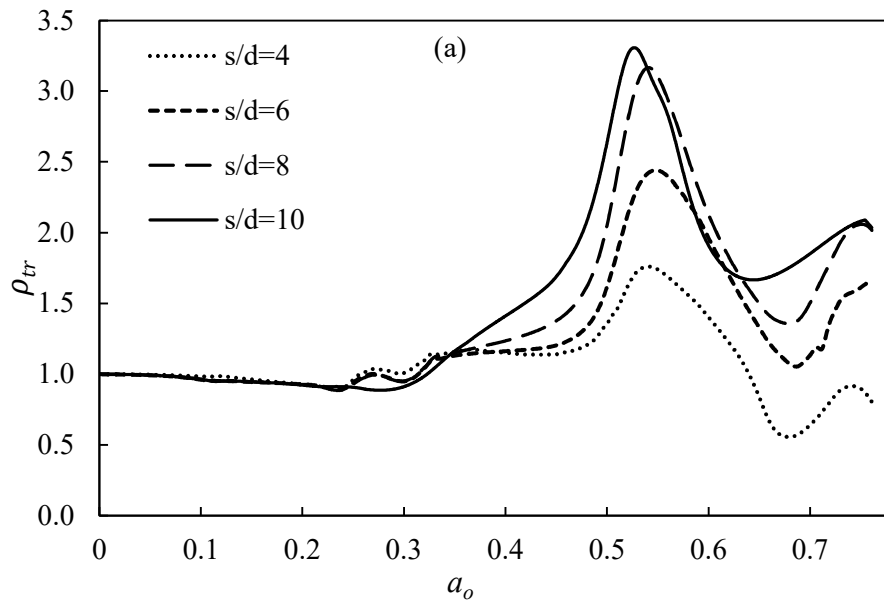
The rocking response shows significant dependence on pile configuration, decreasing with increasing spacing between piles as seen in Fig. 4.9. The peak rotational transfer function value for spacing ratio 4 is about two times the peak value for spacing ratio 10. It should be noted that axial forces generated in piles separated farther apart can create greater resisting moment to counter rocking of the raft. In comparison to pile groups, piled rafts exhibit a notable decrease in I_ϕ in the range of a_o between 0.4 and 0.6 (Fig. 4.9). The presence of raft is also observed to amplify rotations at higher frequencies, with the amount of amplification decreasing with an increase in spacing.

The effect of raft on the kinematic response of the corresponding pile group can be studied by considering the ratio of amplitudes of motion of piled raft and pile group, ρ_{tr} and ρ_{rot} as defined in Eq. (4.3) and Eq. (4.4). These ratios thus form multipliers for kinematic response factors of pile groups, to obtain the factors for piled rafts.

$$\rho_{tr} = \frac{u_{PR}}{u_{pg}} \quad (4.3)$$

$$\rho_{rot} = \frac{\phi_{PR}}{\phi_{PG}} \quad (4.4)$$

Variation of response factor ratios ρ_{tr} and ρ_{rot} for different pile spacing is presented in Fig. 4.10 (a) and 4.10 (b) respectively.



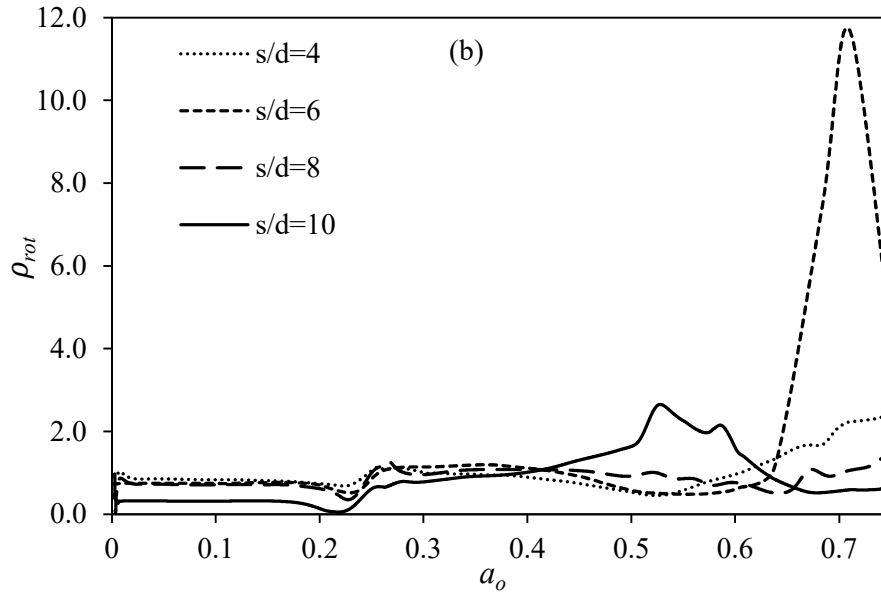


Fig. 4.10 Kinematic interaction factor ratio in (a) translation and (b) rotation

It is interesting to note that the presence of a raft does not alter kinematic translation at the top of a pile group in the low frequency region, up to an a_o value of 0.35. The presence of raft is found to produce significant increase in translational foundation motion, in the dimensionless frequency range of 0.5 to 0.6. The presence of raft is found to have prominent influence on rotation only after an a_o value of 0.6.

4.3 INFLUENCE OF RAFT EMBEDMENT ON KINEMATIC RESPONSE

Estimating the FIM forms an important step in the substructure-based SSI analysis. Available analytical formulations (Di Laora et al. 2017; Mylonakis 2001) however, do not consider the influence of foundation soil contact on the kinematic response. Limited studies by Padrón (2009) have shown that for amply spaced pile groups with foundation embedment, the kinematic response characteristics approaches that of the shallow footing. In the following sections, two different piled raft systems, in homogeneous and layered soil are considered. Corresponding pile groups are also modelled to demarcate the effect of foundation embedment on kinematic response. The models are subjected to nine earthquake time histories with varying frequency content, to study the transient response. The results are categorized into frequency response and transient response for clarity. The effect of foundation embedment is evaluated

by plotting transfer functions from the frequency response, and spectral reduction ratio, soil pressure, and bending moments from the transient response analysis.

4.3.1 Case Study of a Rectangular Piled Raft System

In order to study the effect of foundation embedment on the kinematic response of rectangular piled rafts, the hypothetical example of a pile raft considered by Poulos et al. (1999) is adopted. The piled raft with piles of diameter 0.5 m and length 10 m is assumed to be embedded in a homogeneous soil stratum of 20 m thickness overlying a hard stratum as shown in Fig. 4.11. The spacing to diameter ratio in the x-direction is 4 for the 5x3 configuration and 8 for the 3x3 configuration. The pile is assigned an elastic modulus of 30 GPa, and a Poisson's ratio of 0.2. In the present study, the raft is made to behave as rigid by assigning stiffness satisfying the criteria by Simone (1966), to avoid the effects of raft flexibility. This assumption is however, in several practical cases inherently satisfied by the superstructure foundation system due to the presence of structural columns. A second model with a 3x3 pile configuration, with the same raft dimension is also developed keeping the raft dimensions unchanged. The raft was assigned near zero mass to avoid any effects of inertial interaction.

The effect of soil stiffness was studied by varying the pile-soil modulus ratio defined as E_p/E_s where E_p is the elastic modulus of pile, and E_s is the elastic modulus of soil. Three different homogeneous soil profiles with modulus ratio of 1500, 1000, and 500 and a layered profile with exponential variation in shear modulus, are considered in this study. The exponential variation in the shear stiffness of soil is defined in the following form (Vrettos 1991):

$$E_s(z) = E_{s\infty} [b + (1 - b) \left(1 - e^{-\frac{qz}{d}}\right)] \quad (4.5)$$

where b is the ratio of Elastic Moduli of soil at the surface and at infinite depth ($E_{s\infty}$), z is the depth, d is diameter of pile, and q is a dimensionless inhomogeneity factor controlling the rate of increase or decrease of stiffness. The variation of shear wave velocity with depth assuming a constant unit weight of 17.5 kN/m³ is presented in Fig 4.12. To calculate dimensionless frequency for the exponential soil profile, the weighted average shear wave velocity value of 140 m/s was used.

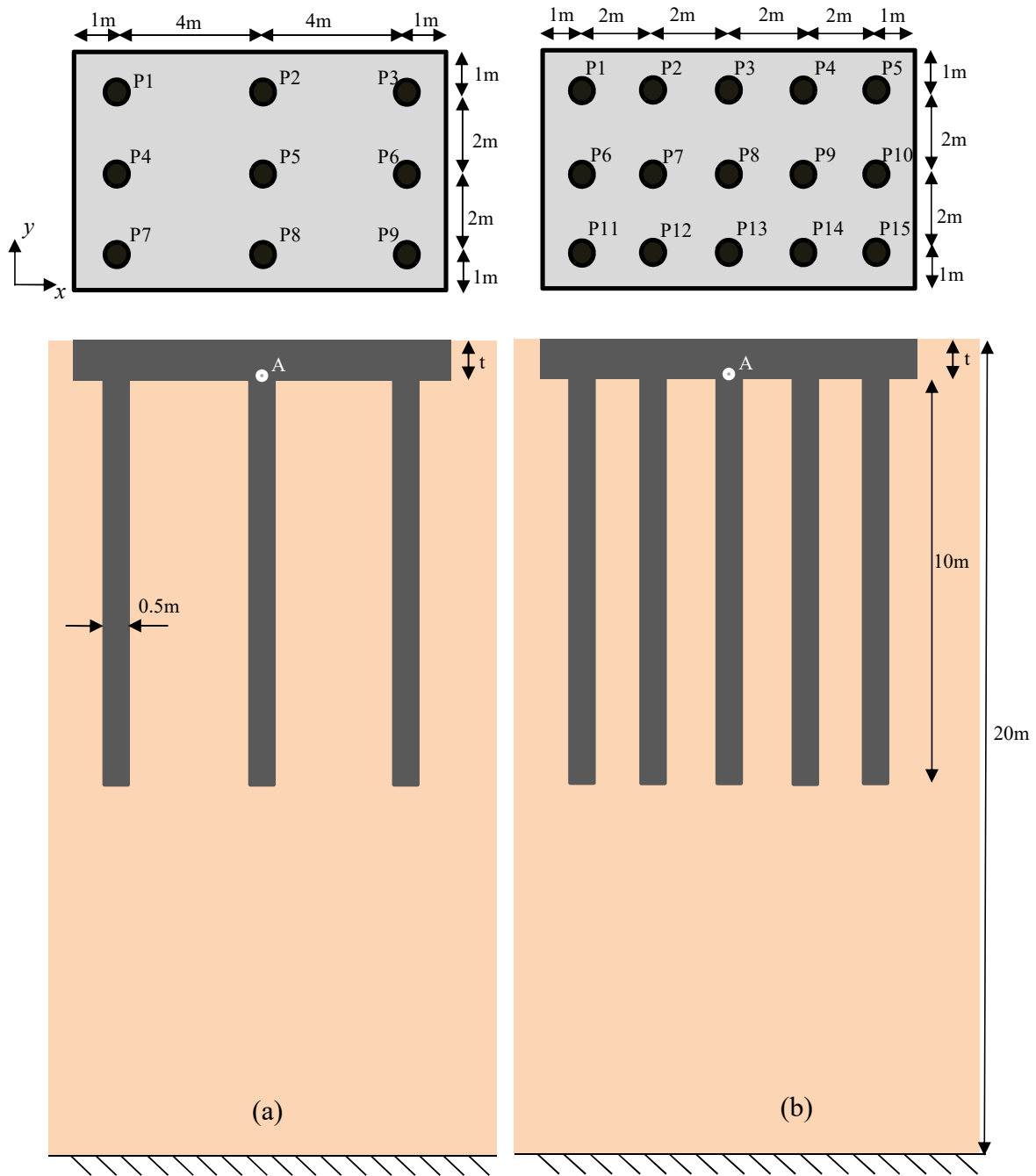


Fig. 4.11 Schematic diagram showing the piled rafts with (a) 3x3 and (b) 5x3 pile configurations

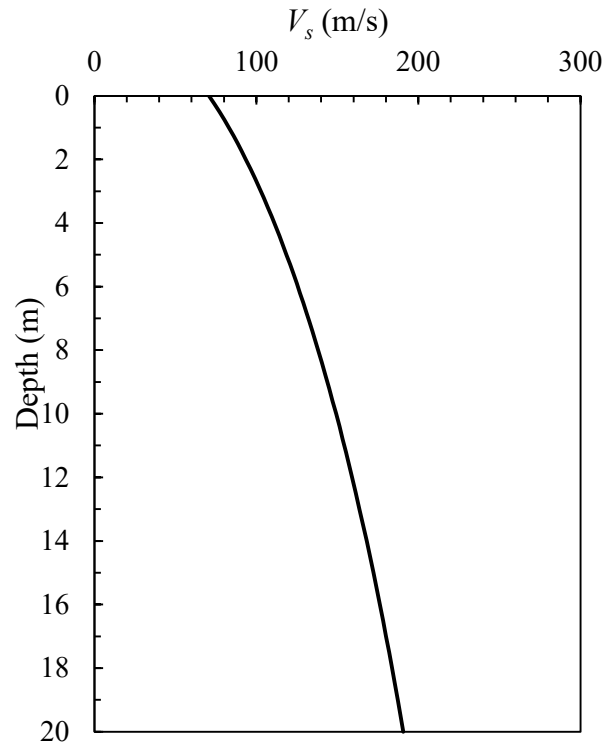


Fig. 4.12 Variation of V_s with depth for exponential soil profile

The various cases considered in the study are summarized in Table 4.2. Since detailed comparisons with pile groups are also included in the study, the pile diameter was identified as a suitable factor to represent raft thickness. The finite element models were developed using the method described in Chapter 3. For nodes along the symmetry plane, the translational degrees of freedom perpendicular to the plane were restrained. The FE mesh of the 3x3 piled raft case with raft thickness equal to two times the diameter is shown in Fig. 4.13. Near field soil elements were explicitly defined to capture raft-soil-pile and pile-soil-pile interaction.

4.3.2 Frequency Response

The response of the soil foundation system is evaluated for vertically propagating shear waves. The analyses were carried out for a total of 34 frequencies covering a frequency range of 0.01 Hz to 22 Hz. The control point for input motion was defined at the ground level to extract the transfer functions in displacement and rotation with respect to free field motion. Response to harmonic loads, or transfer functions are evaluated based on the response at the bottom of the raft represented by point A in Fig. 4.11.

Table 4.2 Details of the foundation systems analysed

Case	Foundation	Raft Thickness	Soil profiles
1	3x3 Piled raft	$t=1d, 2d, 3d, 4d, 5d$	Homogeneous with $E_p/E_s=1500$, $E_p/E_s=1000$, and $E_p/E_s=500$; Exponential profile
2	3x3 Pile group		
3	Single pile (fixed head)		
4	5x3 Piled raft	$t=1d, 2d, 3d, 4d, 5d$	Homogeneous with $E_p/E_s=1000$, and $E_p/E_s=500$; Exponential profile
5	5x3 Pile group		
6	Single pile (fixed head)		

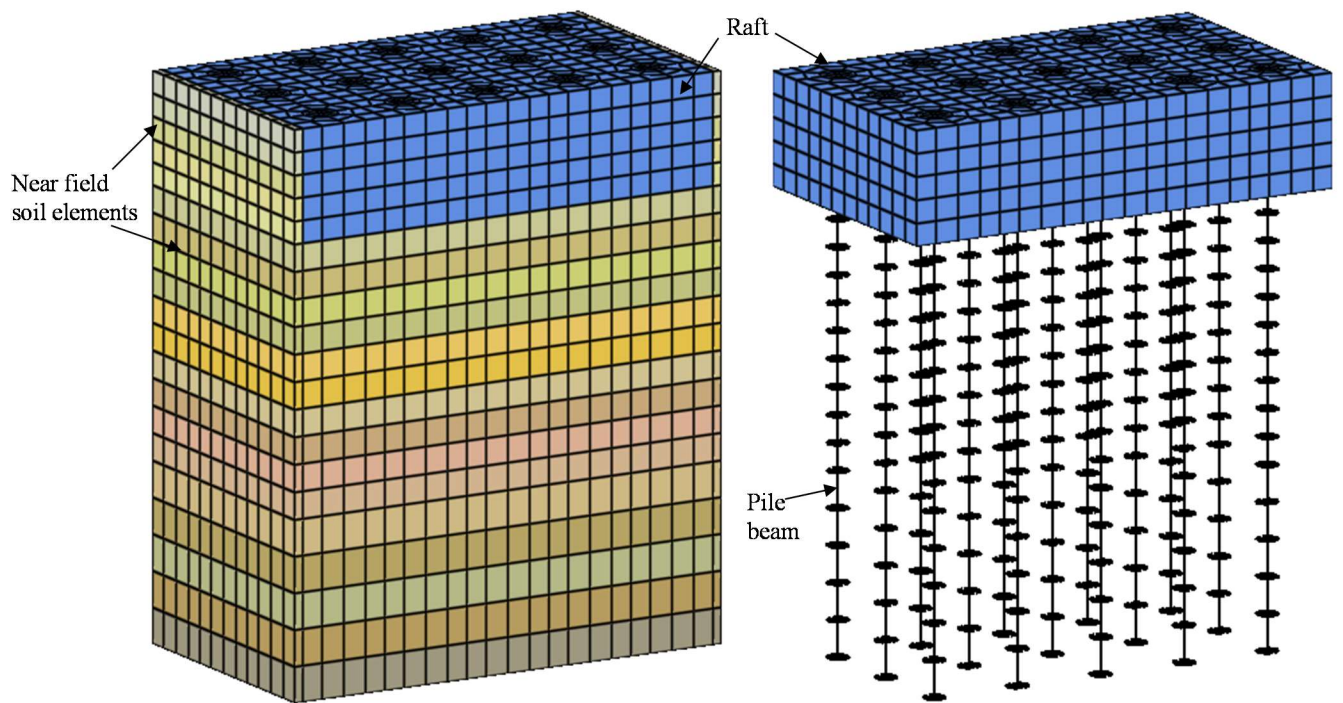
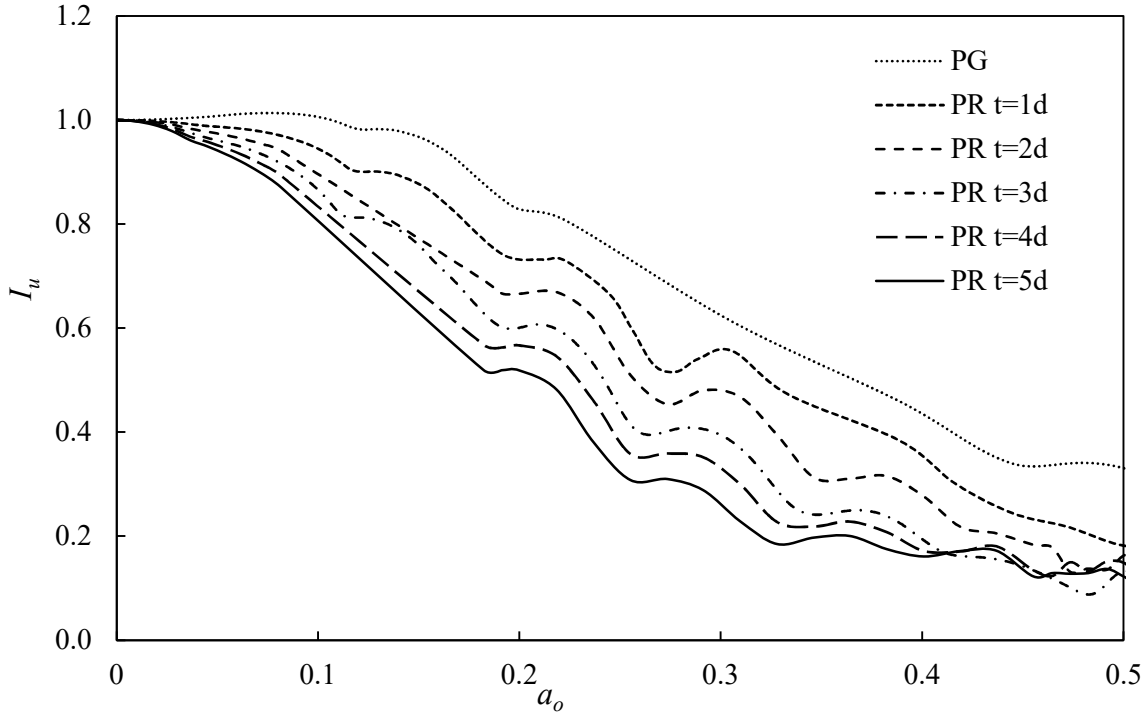


Fig. 4.13 Finite element mesh of the 5x3 piled raft ($t=5d$) (a) with near field soil elements and (b) without near field elements

3x3 Piled Raft

The kinematic response factor in translation for the 3x3 piled rafts with varying raft thickness in soil with modulus ratio of 1000, is presented in Fig 4.14 (a). It was found increasing raft thickness results in a decreasing translational response in the dimensionless frequency of 0.025 to 0.5, which forms the frequency range of importance for earthquake engineering. The embedment of raft by a thickness of one pile diameter was found to cause a reduction of up to 20% in the translational response. As the embedment is increased to five times pile diameter, the translational response is reduced by a factor of 0.4.

The significant reduction in translational response in the dimensionless frequency range of 0.1 to 0.4 is also associated with an increase in rotation, as shown in Fig. 4.14 (b). For the model with $t=5d$, the maximum rotational response is 1.88 times that of the pile group. However, this effect is prominent only for raft thicknesses greater than 3d. Although, rocking in pile groups is a function of the pile layout and pile spacing, the presence of an embedded raft is found to cause a significant increase in rocking at dimensionless frequencies ranging from 0.2 to 0.3.



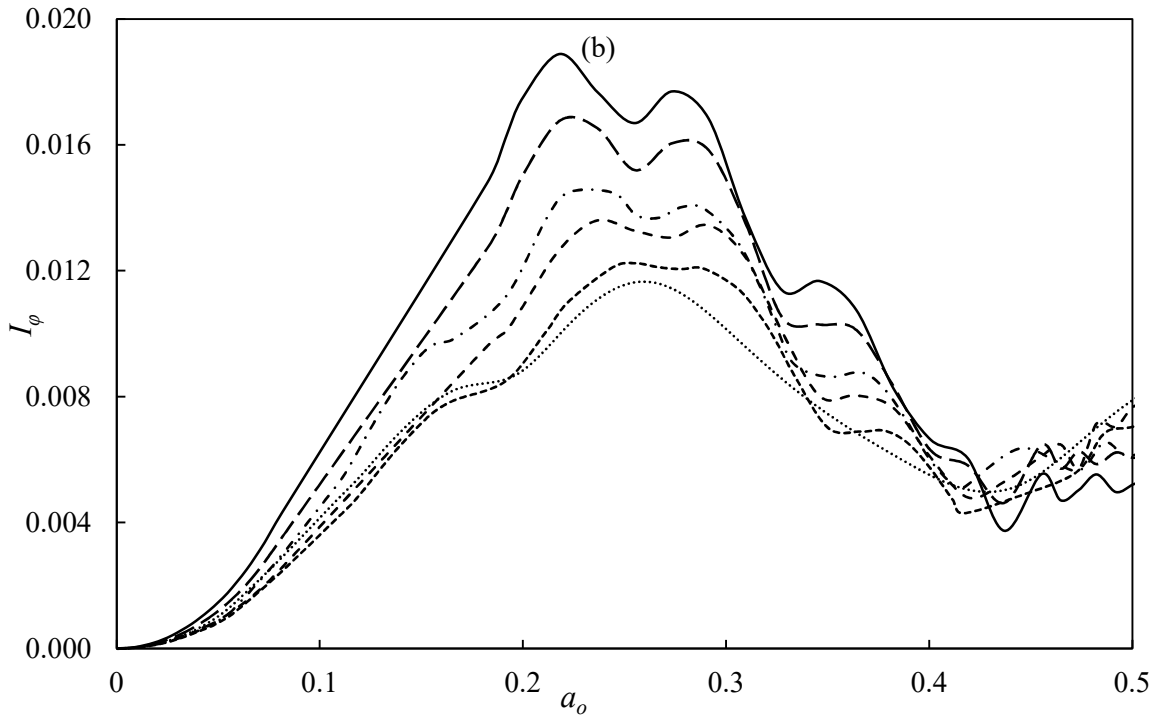
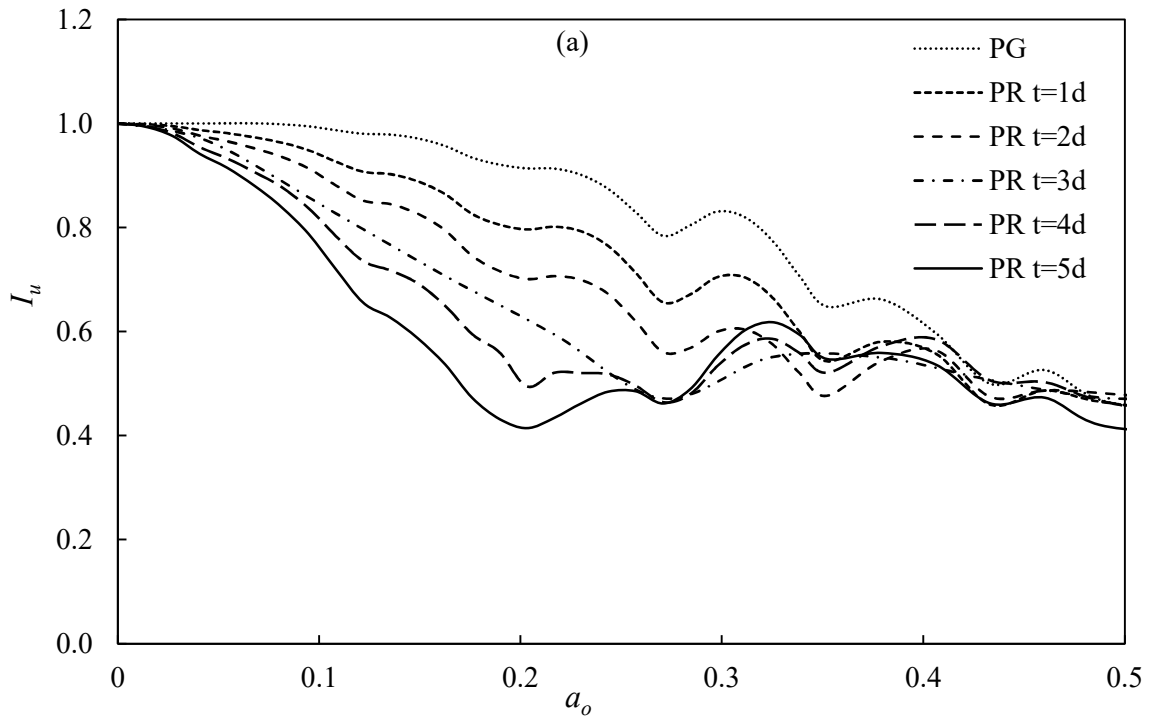


Fig. 4.14 Kinematic response factor in (a) translation and (b) rotation for the 3x3 piled raft in homogeneous soil with $E_p/E_s=1500$



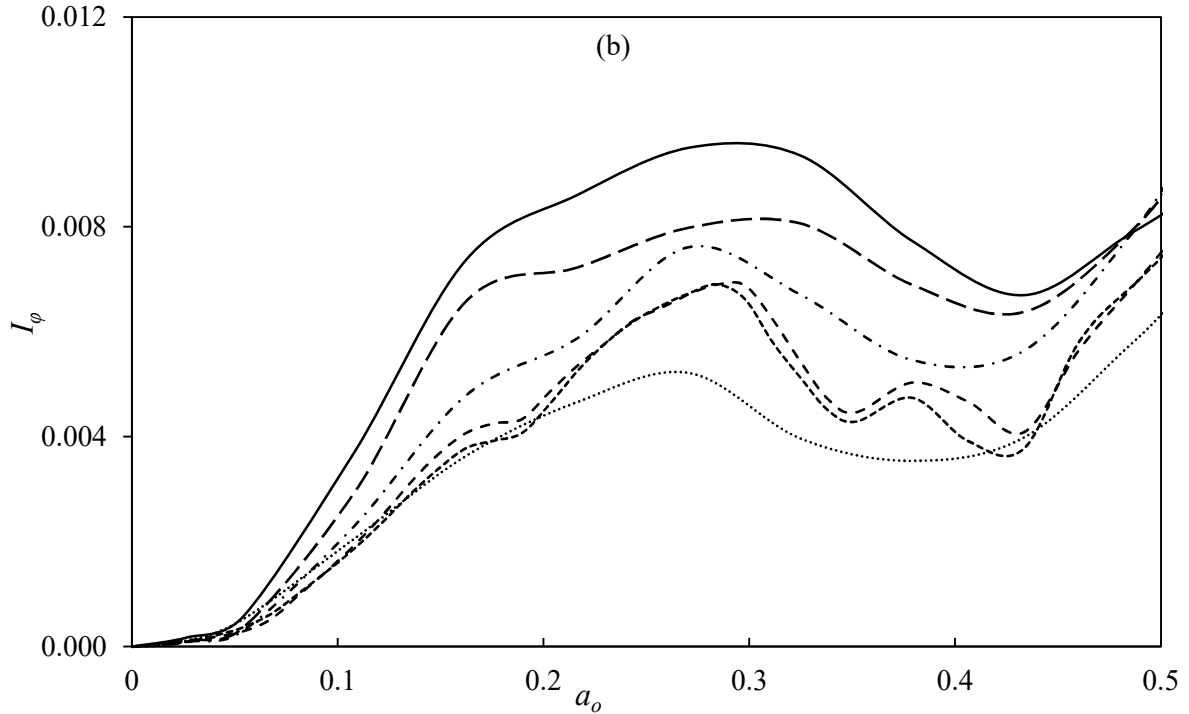
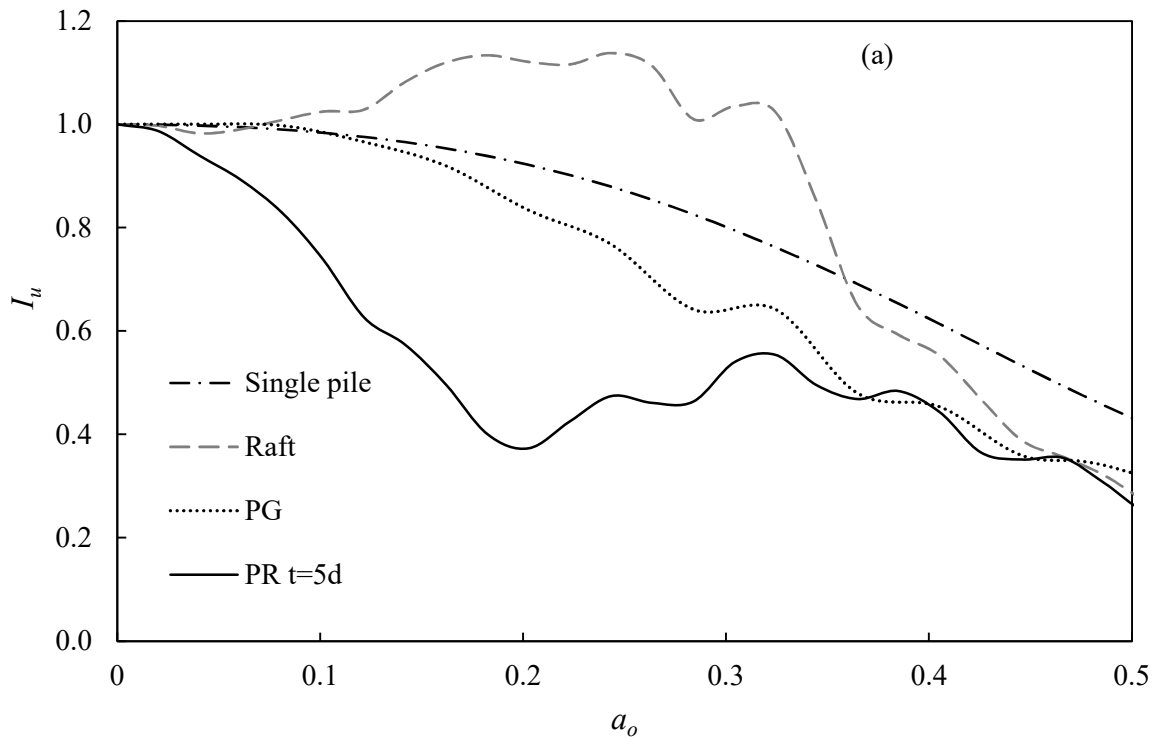


Fig. 4.15 Kinematic response factor in (a) translation and (b) rotation for the 3x3 piled raft in homogeneous soil with $E_p/E_s=500$

The kinematic response factors in translation and rotation for pile draft models in homogeneous soil profile with $E_p/E_s = 500$ is presented in Fig. 4.15 (a) and (b) respectively. The threshold dimensionless frequency after which raft embedment causes an alteration in kinematic response is found to be 0.025, which corresponds to a frequency of around 1 Hz. At higher frequencies the effect of embedment is found to be prominent. For example, at $a_o=0.2$, the translational response of the piled raft with $t=5d$ is 0.45 times that of the pile group. The effect of embedment on rocking response is however, considerable only for thicknesses greater than $3d$ and at dimensionless frequencies greater than 0.1.

A comparison of kinematic interaction factors of piled raft, pile group, fixed head single pile and raft models for the case of homogeneous soil stratum with $E_p/E_s=1000$ is presented in Fig. 4.16 (a) and (b). The raft model consisted of a 10 m x 6 m raft with an embedment of 2.5 m corresponding to five times diameter. For the purpose of comparison, the transfer functions were calculated using the response obtained at the centre of the bottom face of the raft. The single pile model was created using the central beam and rigid link method with near field soil elements extending radially to three times the pile diameter.

Fig 4.16 (a) shows the significant filtering action brought about by the introduction of an embedded raft, in comparison with the corresponding fixed head single pile. From the comparison of the rocking response of the different foundation types as shown in Fig. 4.16 (b) it can be seen that the raft foundation model exhibits higher rocking than all other models across the frequency range studied. Previous studies (Luco and Wong 1987; Day 1977) have shown that increasing embedment of shallow footings leads to an increase in rotational response across frequencies of practical interest. The increase in rotational response of piled raft models with increasing embedment observed in this study, could be attributed to the additional rocking induced by the raft. The kinematic response factors for the four foundation types in the soil profile with exponential variation in stiffness, is presented in Fig. 4.17 (a) and (b). The filtering effect in translational response due to embedment of raft in piled raft models is found to be prominent up to a dimensionless frequency of 0.23, which corresponds to 10Hz in this case.



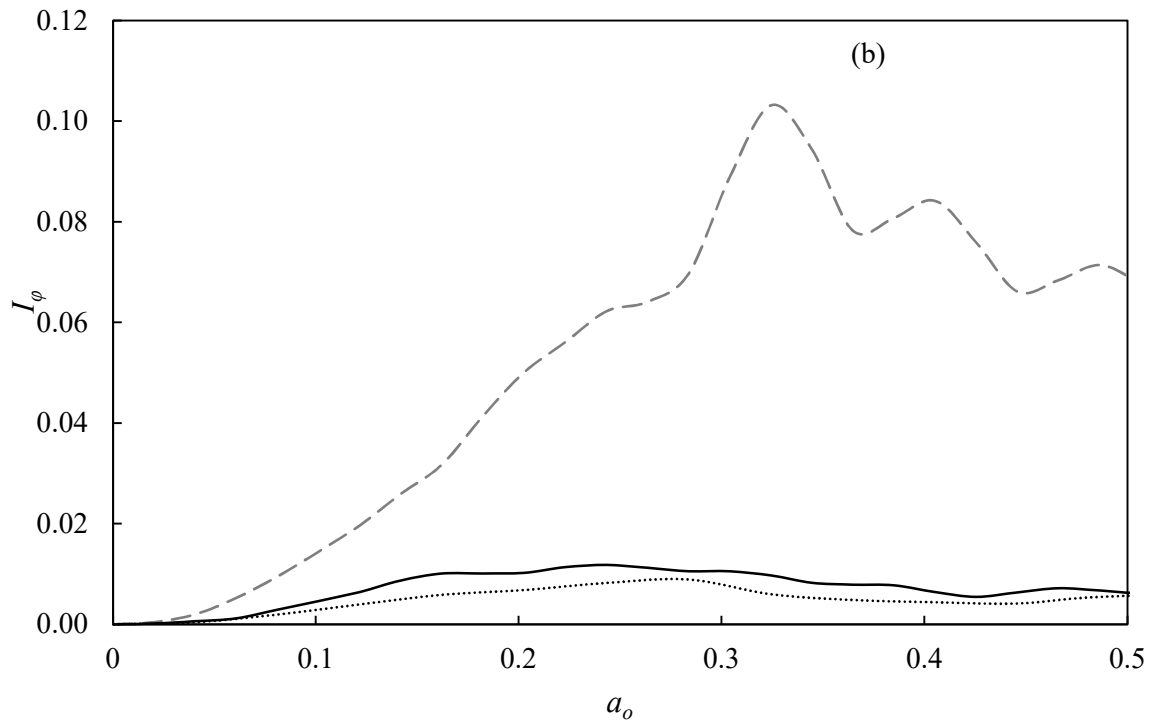
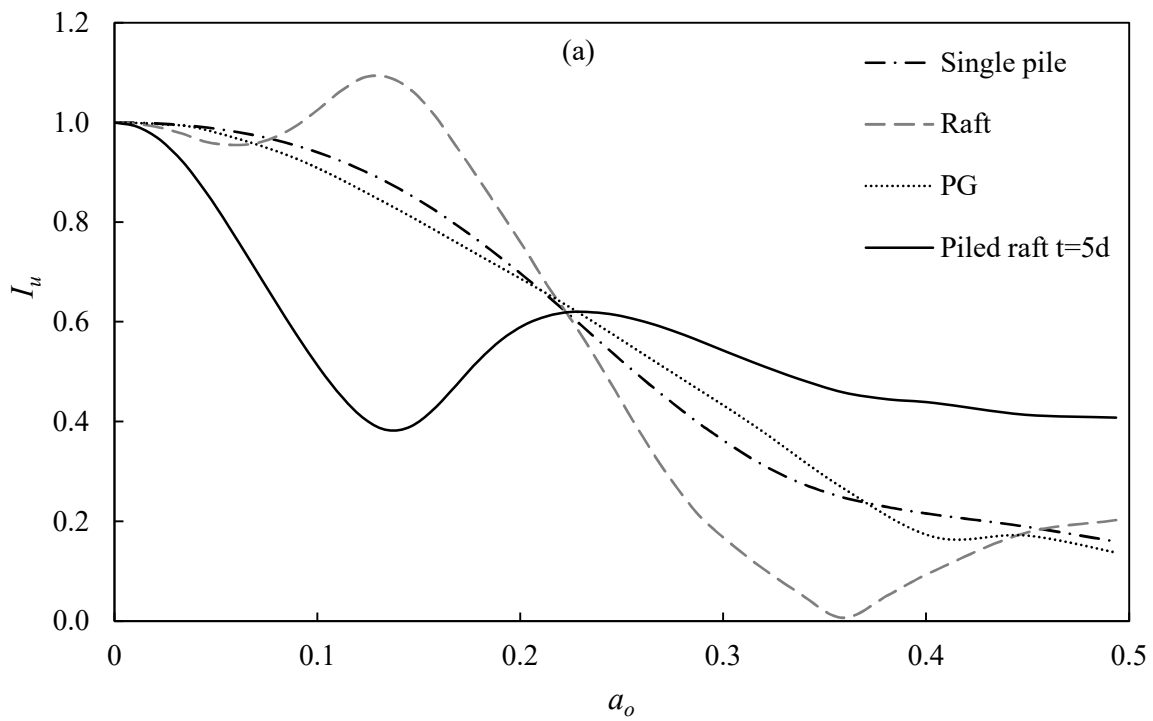


Fig. 4.16 Comparison of kinematic response factor in (a) translation and (b) rotation for 3x3 piled raft and corresponding fixed head single pile, raft, and pile group models in homogeneous soil with $E_p/E_s=1000$



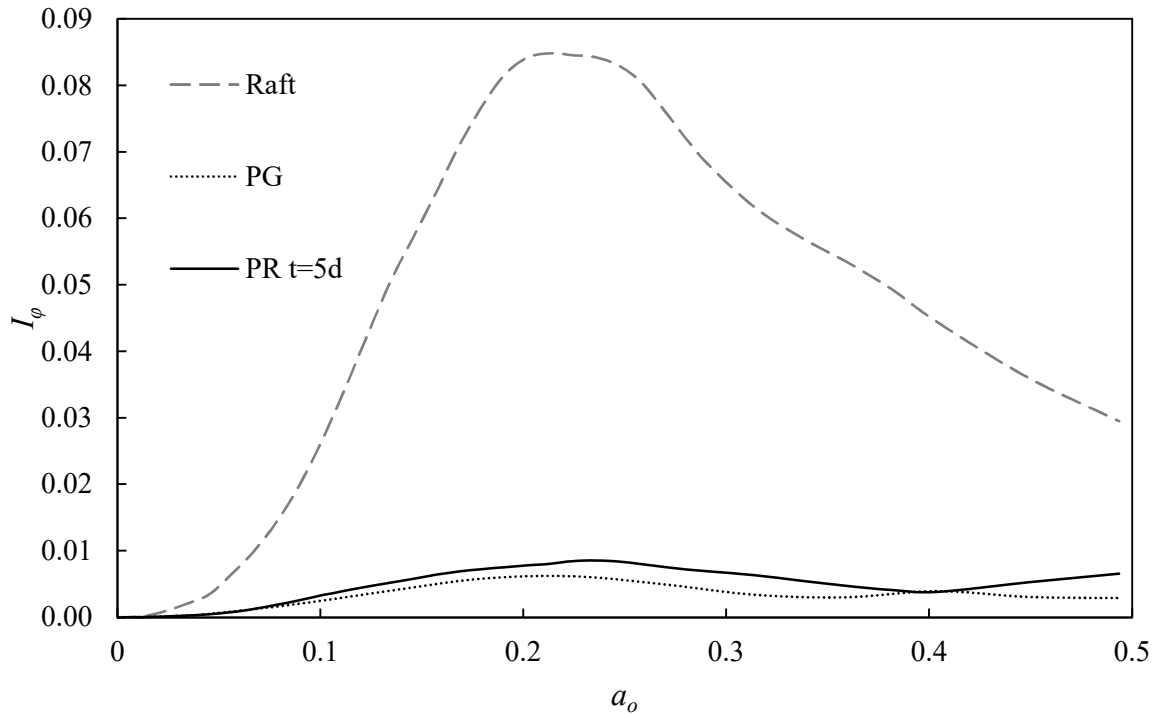


Fig. 4.17 Comparison of kinematic response factor in (a) translation and (b) rotation for 3x3 piled raft and corresponding fixed head single pile, raft, and pile group models in layered soil profile with exponential variation in stiffness

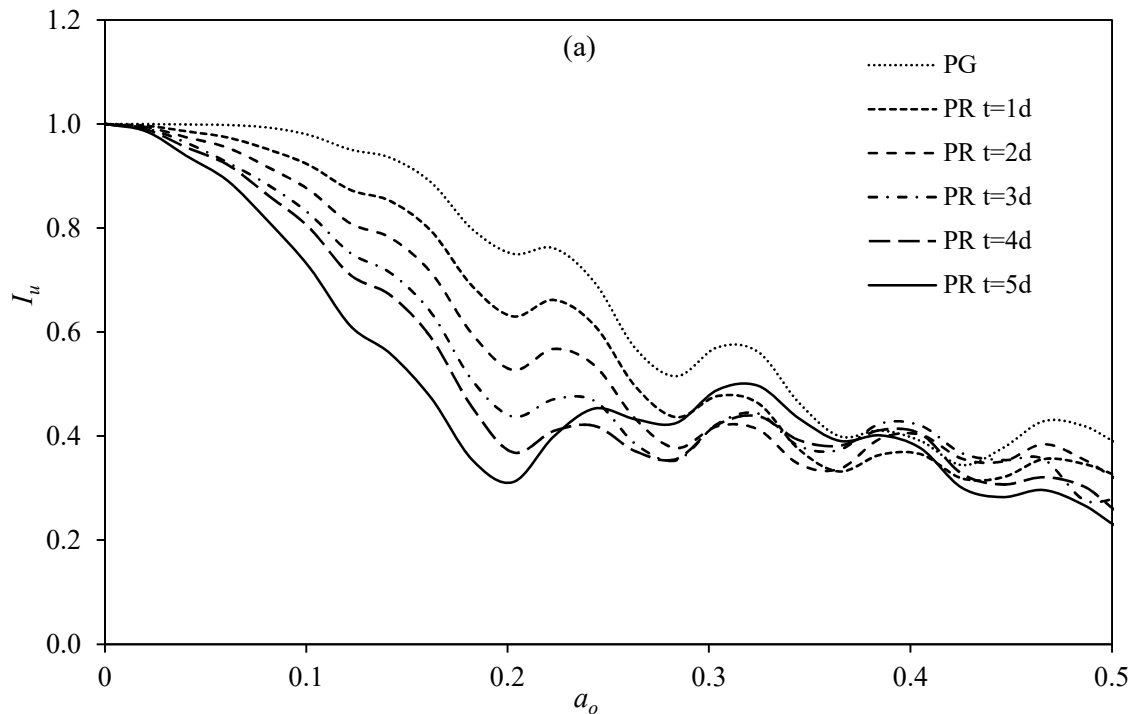
It is also observed that the kinematic response factor in translation for the pile group, closely follows the curve of the fixed head single pile. Another observation is that beyond the frequency threshold of $a_o=0.23$, the piled raft translates at a higher amplitude in comparison with the pile group.

5x3 Piled Raft

Another set of analyses were carried out for the piled raft models with 5x3 pile configuration. Studies based on analytical methods (Di Laora et al. 2017) have shown that the rotational component of acceleration diminishes strongly with increasing the number of piles and pile spacing. Five different models were created with the raft thickness varying from zero (pile group) to 5 times the pile diameter. The kinematic response factors for 5x3 piled rafts embedded in homogeneous soil stratum with $E_p/E_s=1000$ is presented in Fig 4.18 (a) and (b). As in the case of 3x3 piled raft, considerable decrease in the kinematic translation is found in the frequency range of interest to earthquake engineering ($a_o<0.4$). The most prominent dip in

translation was found at an a_o value of 0.2 where the response of piled raft with raft thickness equal to five times pile diameter is 0.42 times that of the pile group.

For the case of homogeneous soil stratum with $E_p/E_s = 500$, the effect of raft embedment on translational response has a similar trend with the case of 3x3 pile configuration, as shown in Fig. 4.19 (a). However, the additional rotational response due to higher raft embedment ($t=4d$, $t=5d$), observed in models with 3x3 pile configurations, is suppressed by the presence of the two additional rows of piles as shown in Fig. 4.19 (b). For example, an embedded raft with a thickness of $5d$ increased the rocking response was by 2.1 times for the 3x3 PR case, whereas the increase was only 1.2 times for the 5x3 PR case. The trend is also observed for the case of exponential soil profile, as shown in Fig. 4.20 (a) and (b). For the exponential profile, the rotational response is practically indistinguishable for piled rafts with varying raft embedment depths. However, a clear trend of increasing filtering of translational response with increasing raft embedment is observed up to a dimensionless frequency of 0.23, which corresponds to a frequency of 10 Hz.



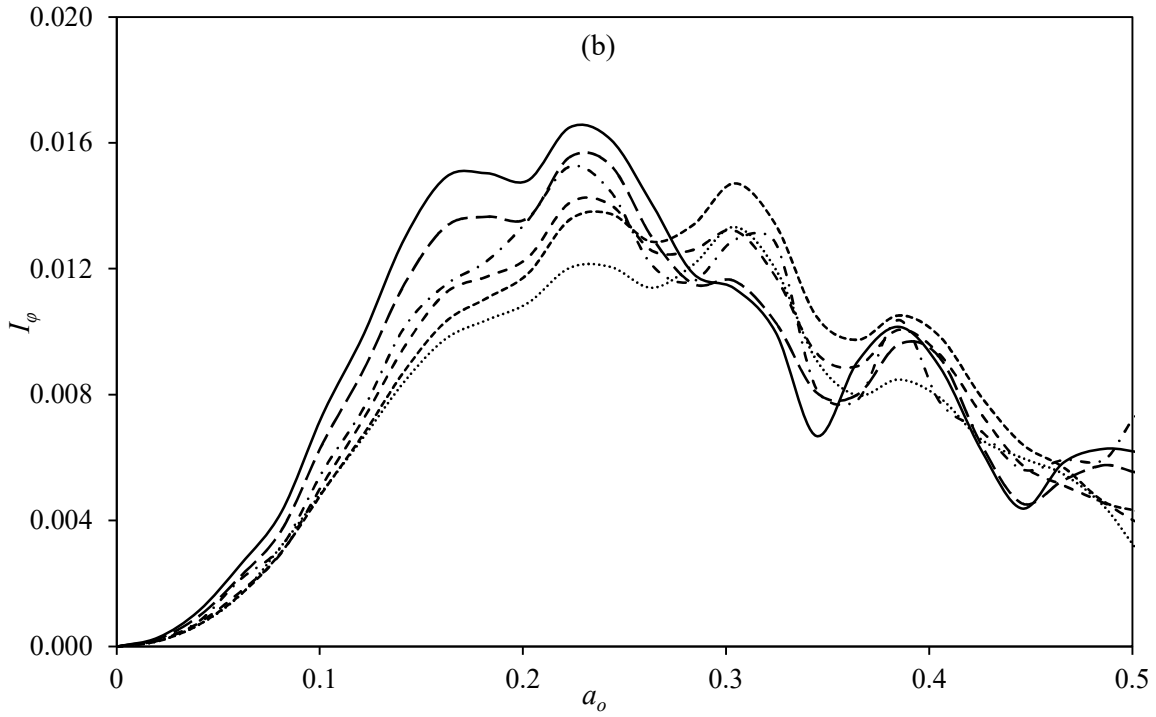
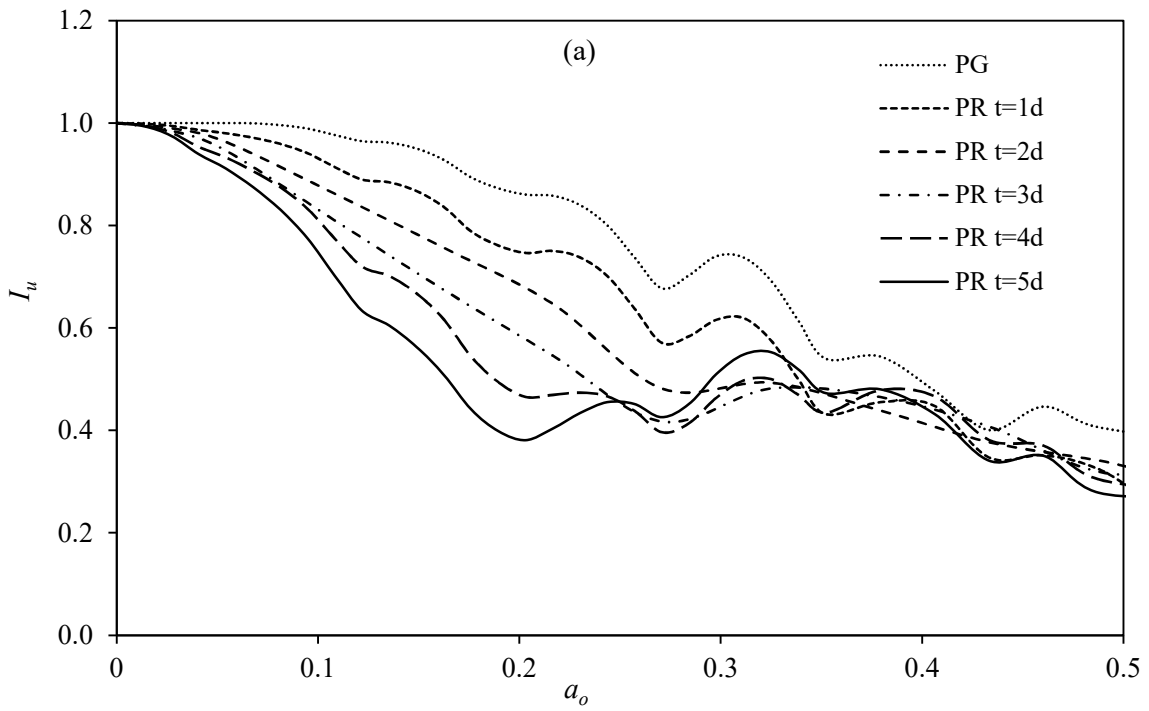


Fig. 4.18 Kinematic response factor in (a) translation and (b) rotation for the 5x3 piled raft in homogeneous soil with $E_p/E_s=1000$



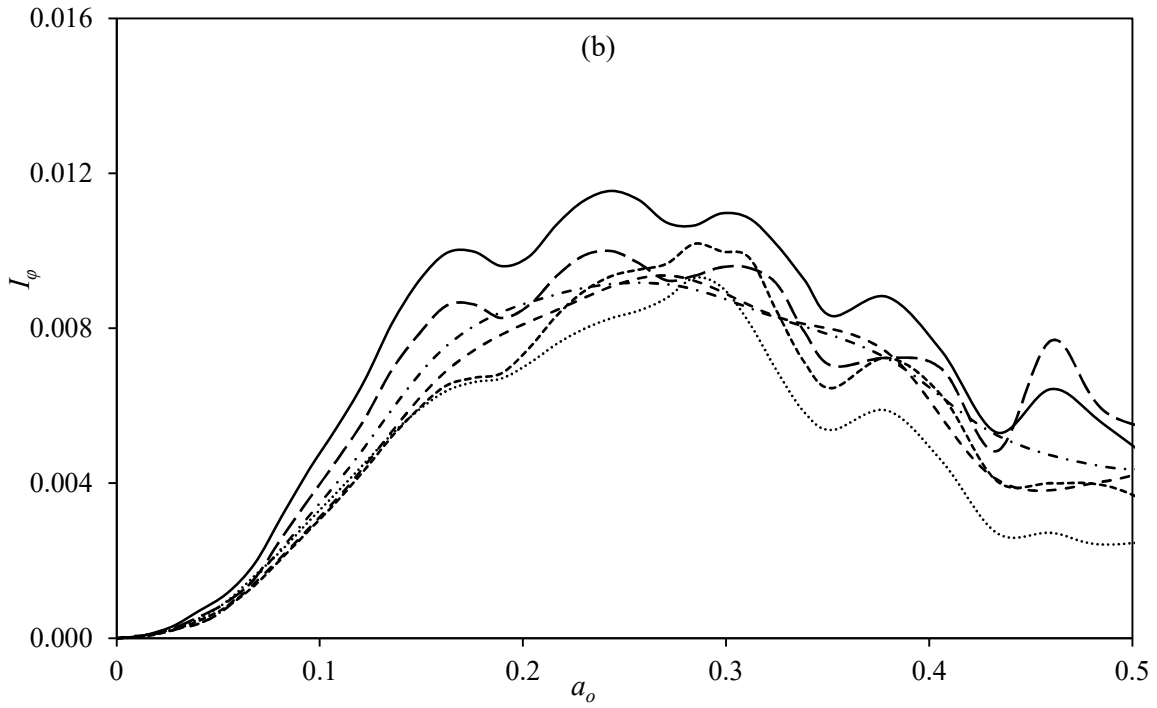
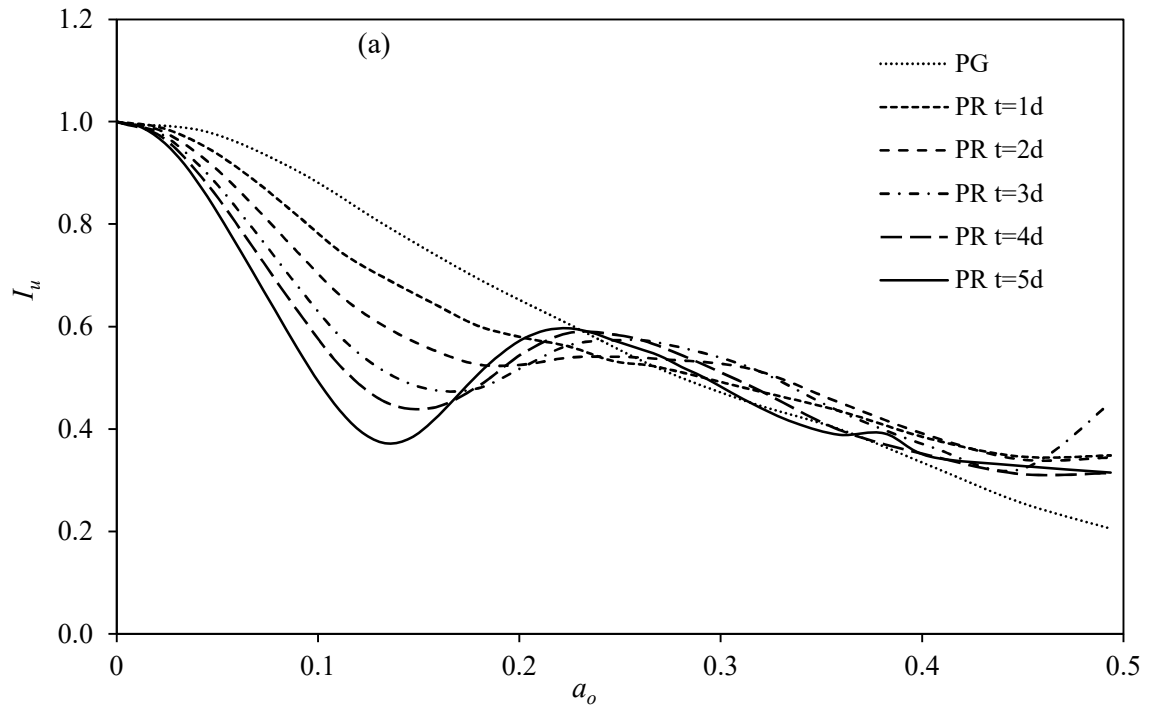


Fig. 4.19 Kinematic response factor in (a) translation and (b) rotation for the 5x3 piled raft in homogeneous soil with $E_p/E_s=500$



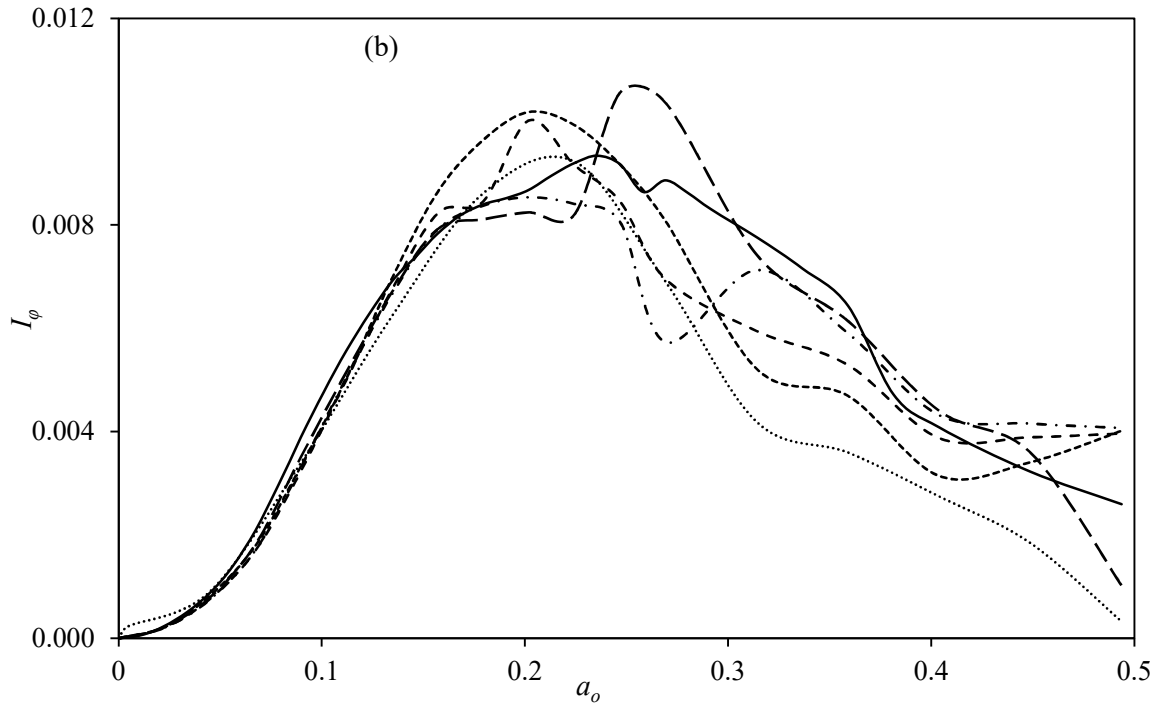


Fig. 4.20 Kinematic response factor in (a) translation and (b) rotation for the 5x3 piled raft in layered soil profile with exponential variation in stiffness

4.3.3 Transient Response

Previous studies (Di Laora et al. 2013, Iovino et al. 2019) have shown that pile induced filtering of translational ground motion can be quantified using the ratio of response spectra at the pile head and free field. Acceleration spectral ratio provides an advantage of practical applicability as the foundation input motion for pile supported structures can be estimated from the free field response spectrum. Semi empirical formulae have been proposed to estimate the threshold frequencies and spectral ratio at these thresholds, for single piles. In this study the effect of raft embedment on the spectral ratios is studied by carrying out a comprehensive parametric study using the 3D models described in section 4.3.1. The response of piled raft foundations to transient ground motion was studied by rigorous SSI analysis using recorded ground motions with varying frequency content. In the frequency domain, transient response is calculated by multiplying the Fourier spectra of the input motion with the transfer functions of structural response. Interpolation schemes are employed to interpolate the transfer functions between the frequencies of analysis. In this study, the interpolation scheme originally adopted in the 1982

SASSI program was employed. The interpolation accuracy was checked by ensuring that spurious peaks do not exist in the transfer function plots.

Eight recorded acceleration time histories with varying frequency content were chosen for the study. The peak acceleration of the time histories varies from 0.015g to 0.147g. Details of the accelerograms used are presented in Table 4.3. Frequency content of earthquake motion can be quantified using the predominant frequency and mean frequency parameters. Predominant frequency refers to the frequency corresponding to maximum spectral acceleration. Mean frequency can be defined as (Rathje et al. 1998):

$$f_m = \frac{\sum_i C_i^2 \cdot f_i}{\sum_i C_i^2} \quad \text{for } 0.25 \text{ Hz} \leq f_i \leq 20 \text{ Hz} \quad (4.6)$$

where C_i is the Fourier amplitude and f_i is the discrete Fourier transform frequencies. The variation in frequency content across the eight acceleration time histories is presented in Fig. 4.21.

Table 4.3 Details of the input ground motions

Earthquake	Year	Recording Station	PHA (g)	M _w	Epicentral Distance (km)
Central Mexico	2017	UNAM	0.054	7.1	116.4
Norcia	2016	Colforito	0.125	6.2	43.8
Ferndale	2014	Ferndale Fire Station	0.062	6.8	73.2
Amberley, NZ	2016	Greta Valley	0.140	7.8	25.7
Niigata, Japan	2004	IBR002	0.015	6.6	170.0
Landers	1992	Amboy	0.146	7.4	73.9
Christchurch, New Zealand	2011	McQueen's Valley	0.147	6.3	15.0
Valparaiso	2017	Curacavi	0.059	6.9	87.7

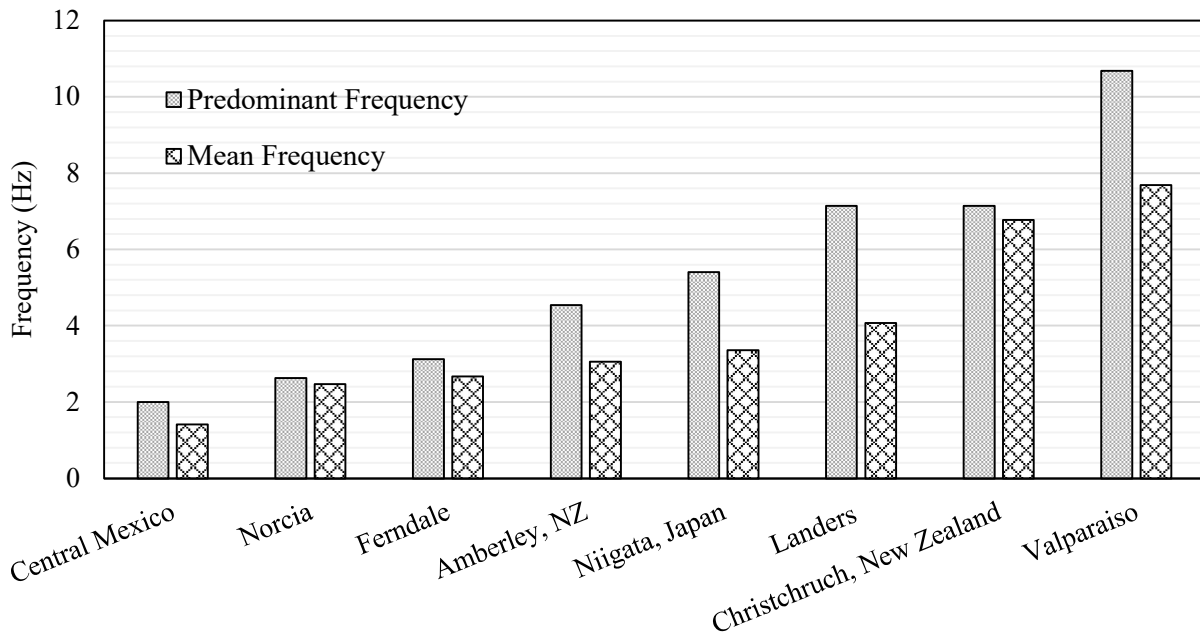
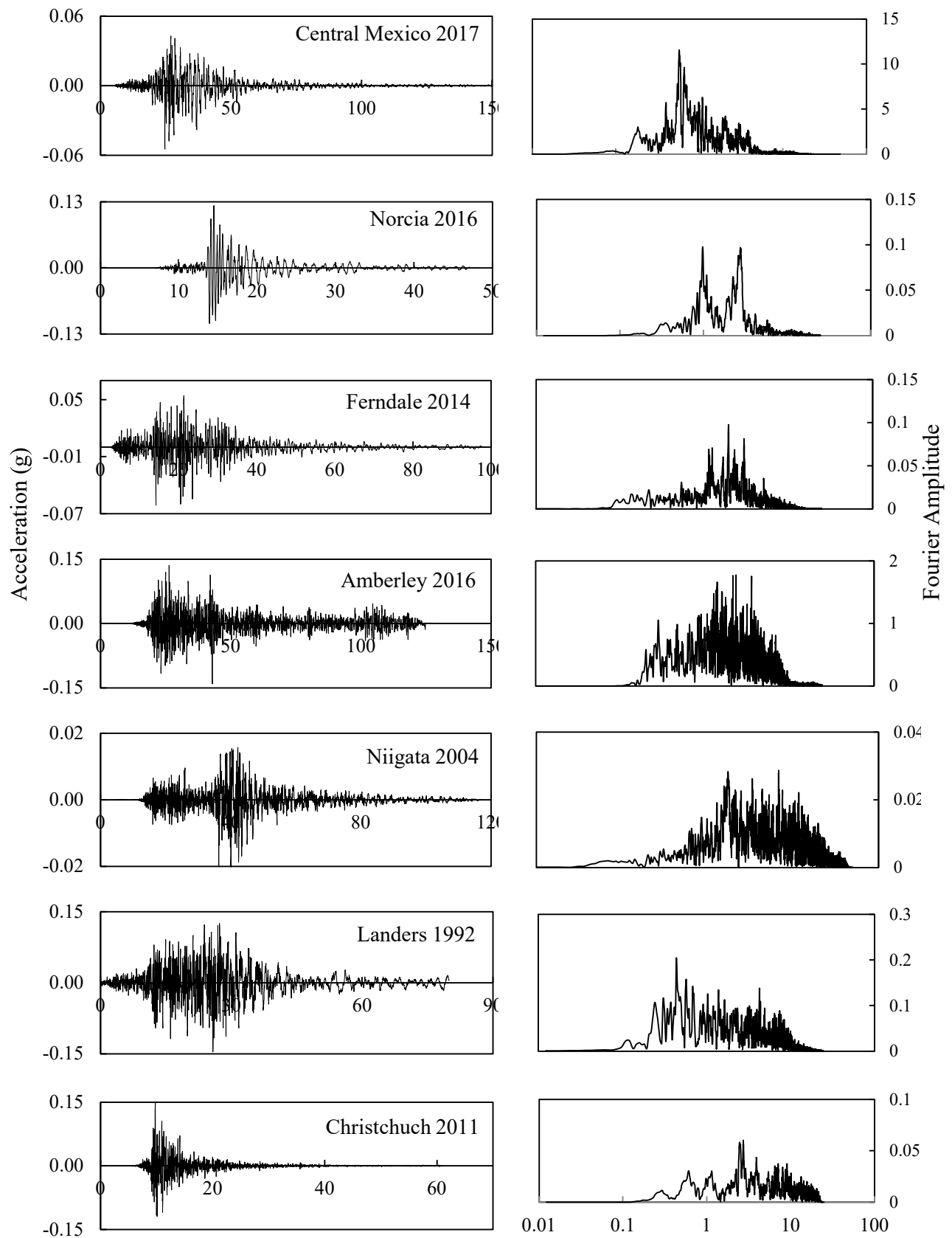


Fig. 4.21 Variation of frequency content in the selected input ground motions

Acceleration time histories considered in the parametric analysis and their Fourier spectra are presented in Fig. 4.22. The selected input motions have mean frequencies varying from 1.4s to 7.7s. The various pile foundation models described in Table 4.2 were subjected to the eight time input motions. The input motion was defined at the ground level and the acceleration response at the centre of the pile cap was extracted. The time histories of response obtained from the pile group and piled raft models in soil profile with exponential modulus variation subjected to the Norcia 2016 and Valparaiso 2017 ground motions are presented in Fig 4.23 (a) and (b) respectively. The reduction in peak acceleration can be clearly seen in the time histories. The pile induced reduction in peak acceleration in Fig. 4.23 (a) was found to be 3% and 18% respectively for the PG and PR models.

On other hand, for the high frequency content ground Valparaiso ground motion the corresponding values are 38% and 46% as seen in Fig. 4.24 (a). The response spectra obtained at the top of PG and PR models are presented in Fig. 4.23 (b) and Fig. 4.24 (b) for Central Mexico 2017 and Valparaiso 2017 ground motions respectively.



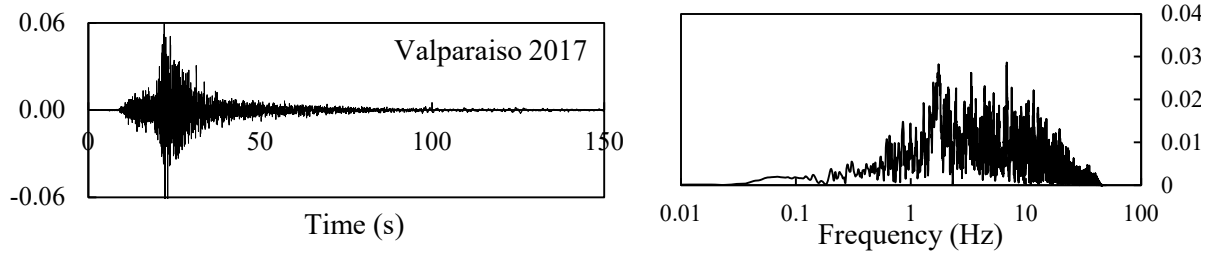
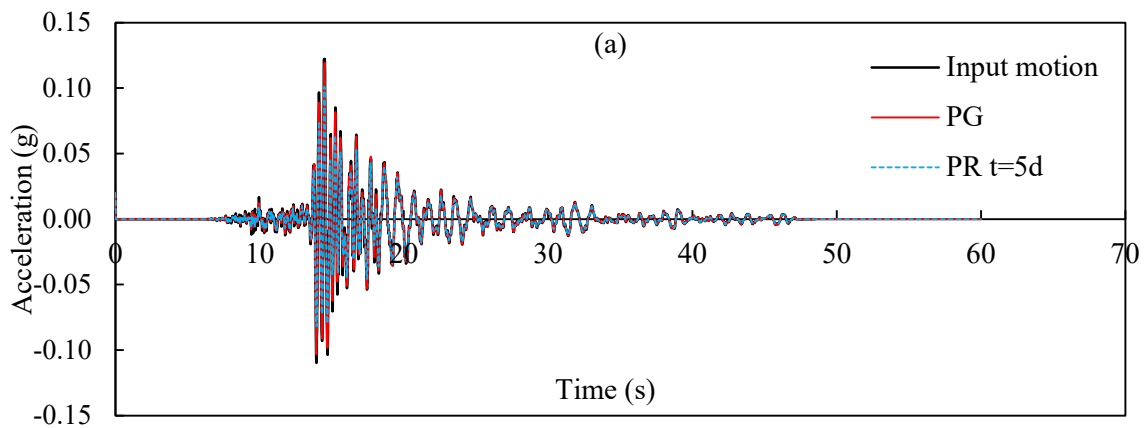


Fig. 4.22 Acceleration time histories and corresponding Fourier spectra considered in the study

Following Di Laora and de Sanctis (2013), the spectral ratio, ξ is defined as

$$\xi = \frac{S_{a,p}}{S_{a,f}} \quad (4.7)$$

where $S_{a,p}$ is the spectral ordinate at the top of pile foundation and $S_{a,f}$ is the spectral ordinate at the free field level. The spectral ratio function for pile foundations follow a square root shape as seen in Fig. 4.23 (c) and Fig. 4.24 (c). It can be seen that the filtering caused by an embedded raft, is high and moderate for Valparaiso and Norcia ground motions respectively. It should be noted that the spectral ratio function for pile groups and piled rafts follow a square root shape similar to that observed for single piles.



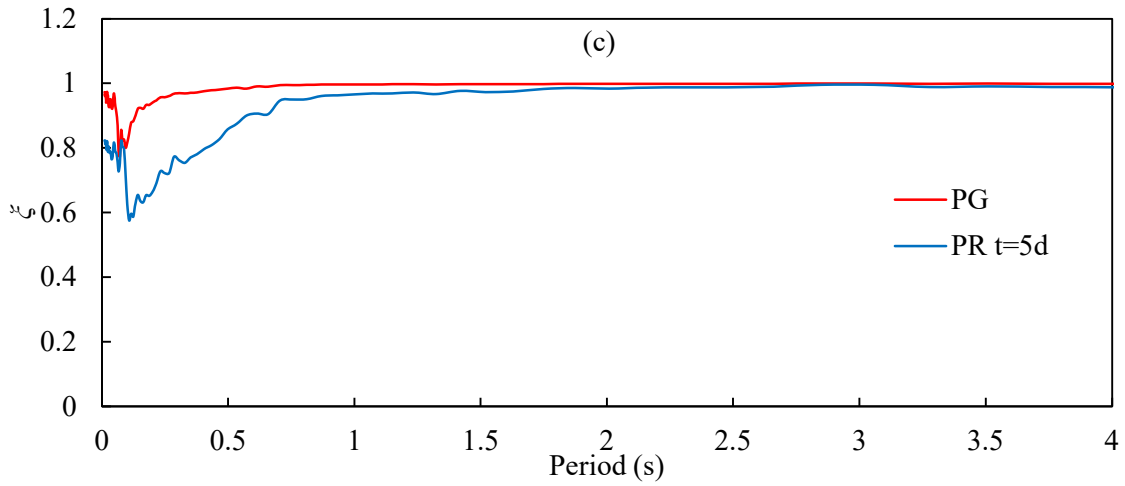
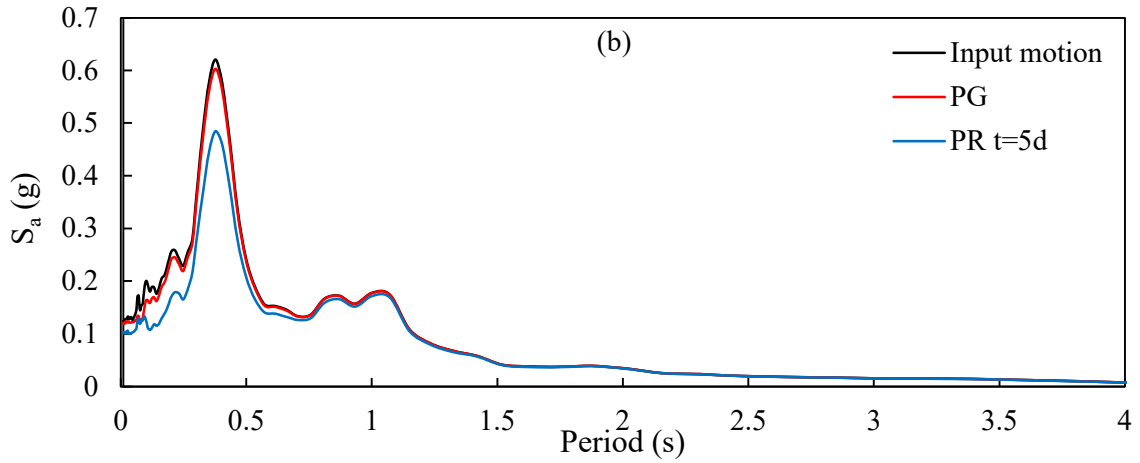
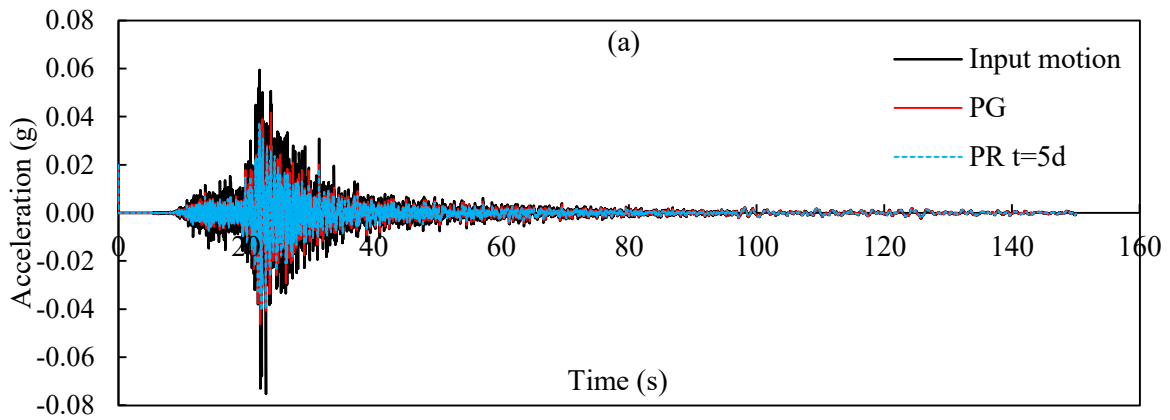


Fig. 4.23 (a) Time history of responses, (b) response spectra at the raft level and (c) spectral ratio for models with 3x3 pile configuration in exponential soil profile subjected to the Norcia 2016 ground motion



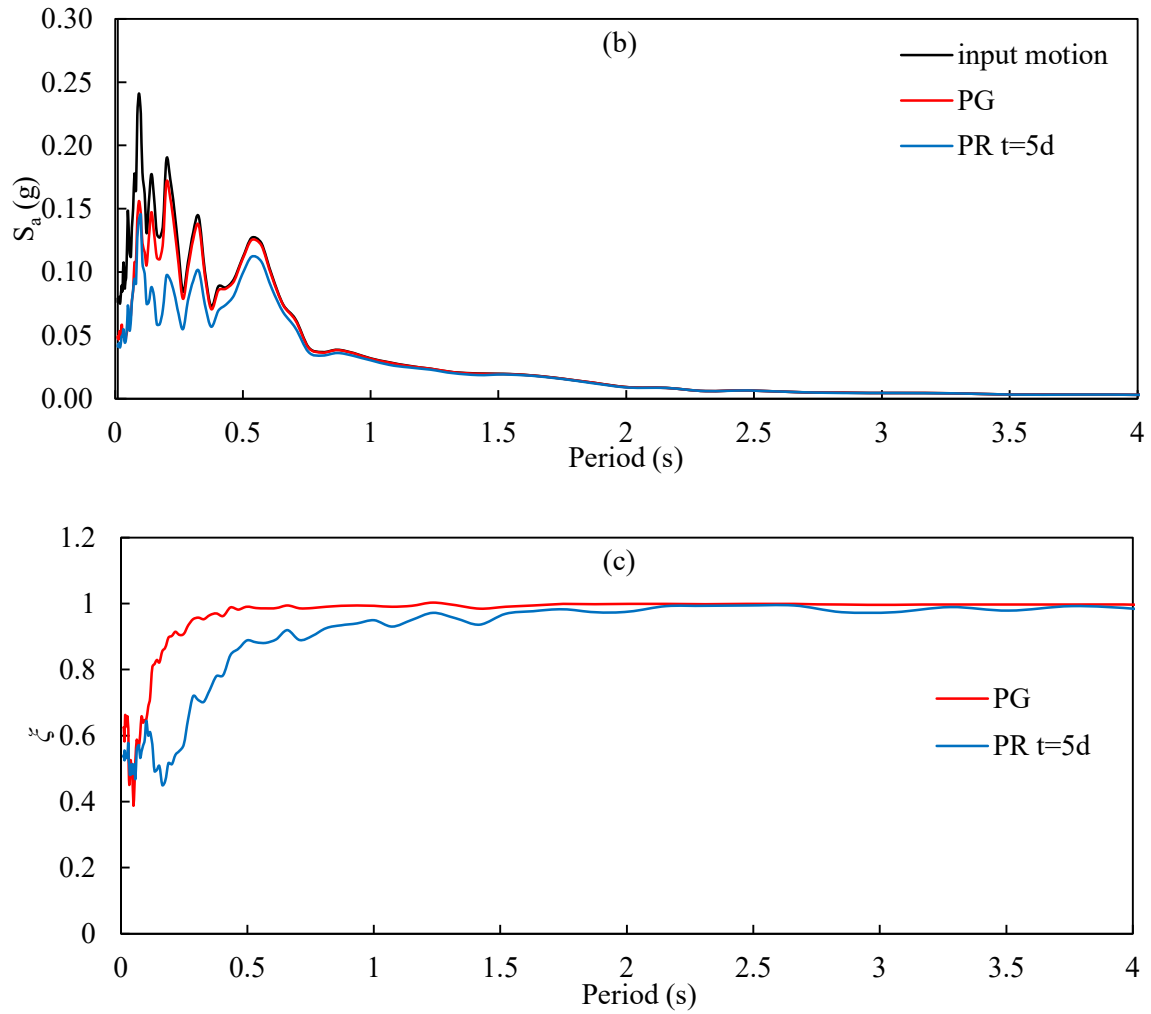


Fig. 4.24 (a) Time history of responses, (b) response spectra at the raft level and (c) spectral ratio for models with 3x3 pile configuration in exponential soil profile subjected to the Central Mexico 2017 ground motion

It is also possible to average the results from all the input ground motions and define a mean spectral ratio as

$$\bar{\xi} = \frac{\text{Average response spectrum of pile head motion}}{\text{Average response spectrum of the free field motion}} \quad (4.8)$$

The various parameters that define the spectral ratio function can be identified with the help of a typical mean spectral ratio plot for a 3x3 pile group models in homogeneous soil with $E_p/E_s=1000$, presented in Fig. 4.25. The spectral acceleration ratio at zero period, ξ_0 essentially represents the ratio of peak acceleration. This parameter is a purely kinematic interaction factor and is known to be strongly affected by the frequency content of the input ground motion (Di Laora and de Sanctis 2013).

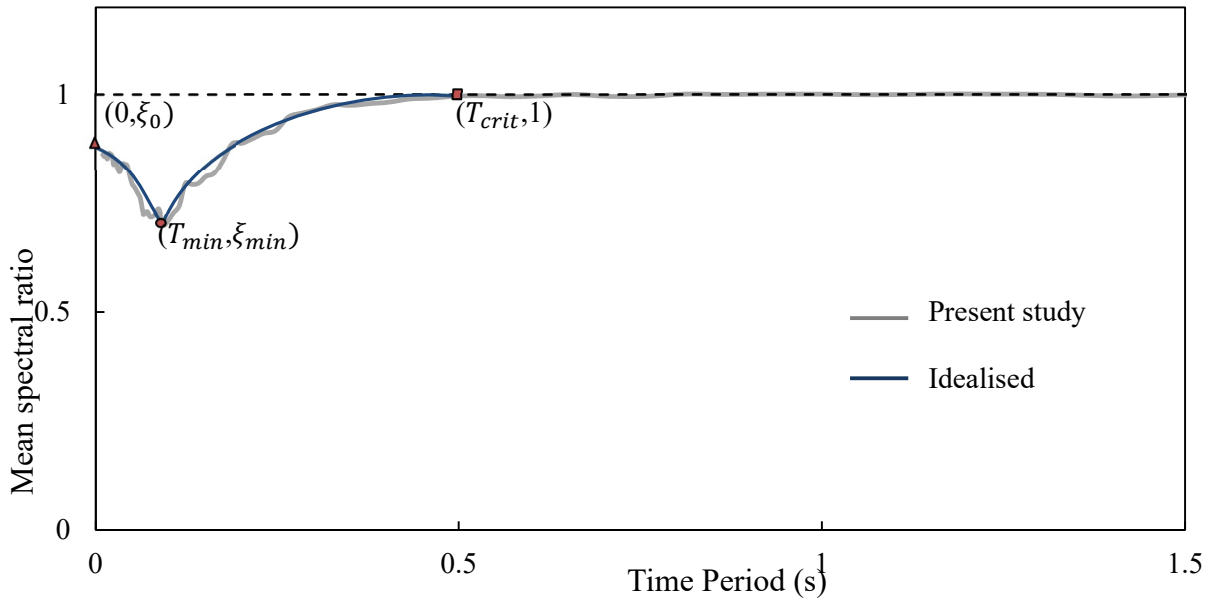


Fig. 4.25 Mean spectral ratio curve (grey line) plotted with idealised curve (blue line) for 3x3 pile group models in homogeneous soil stratum with $E_p/E_s=1000$

The point at which the function reaches a minimum is defined by (T_{min}, ξ_{min}) . The parameter ξ_{min} is also a function of the frequency content of the input ground motion as observed from Fig. 4.23 (c) and Fig. 4.24 (c). The structural period after which the spectral ratio is nearly coincident with unity is defined as the critical period, T_{crit} and this point is defined by $(T_{crit}, 1)$.

The expressions proposed by Di Laora and de Sanctis (2013) for the parameters have been presented in Equations 2.9 to 2.14 and are not repeated for brevity. The characteristic periods, T_{min} and T_{crit} were found to be dependent on the soil shear wave velocity rather than frequency content of the ground motion. The following equations were proposed to predict the spectral ratio curve for a fixed headed single pile.

$$\xi(T) = \xi_o - (\xi_o - \xi_{min}) \left(\frac{T}{T_{min}} \right)^2 \quad T \leq T_{min} \quad (4.9)$$

$$\xi(T) = 1 - (1 - \xi_{min}) \left(\frac{T_{crit} - T}{T_{crit} - T_{min}} \right)^2 \quad T_{min} \leq T \leq T_{crit} \quad (4.10)$$

$$\xi(T) = 1 \quad T > T_{crit} \quad (4.11)$$

The spectral ratio obtained from the present analysis for single piles were compared against the prediction equations. Typical results obtained from the present study and from equations 4.9 to 4.11 for the Norcia 2016, Landers 1992, and Valparaiso 2017 ground motions are presented in Fig. 4.26 (a)-(c). The threshold structural periods from Eq. 2.9 and 2.10 were found to be in agreement with the results from the present study. The prediction of ξ_o and ξ_{min} were found to be satisfactory for Norcia 2016 and Valparaiso 2017 ground motions. However, the prediction underestimated the ordinates for the Landers 1992 input motion.

The spectral ratio for the 3x3 piled raft with varying raft embedment is presented in Fig. 4.27 (a) and (b). A key finding from the comparison is that all the critical points in the spectral ratio are influenced by increasing foundation embedment. The ordinates, ξ_o and ξ_{min} were found to be reduce with increasing embedment of raft. The critical period T_{crit} was found to be shifted to higher periods with increasing embedment. For piled rafts with embedment of 5 pile diameters, the critical period was five to six times the threshold T_{min} . This forms a significant deviation from the behaviour of single and group piles that follow the relationship in Eq. 2.10. However, period T_{min} was not found to be influenced by embedment effects. The mean spectral ratio for single pile, pile group and piled rafts obtained by averaging the results from all eight input ground motions as per Eq. 4.8, is presented in Fig. 4.28 and Fig. 4.29 for homogeneous soil layer ($E_p/E_s=1000$) and exponential soil profile respectively. A reduction in ξ_o which also translates into a reduction in peak acceleration of the FIM was found to be 20% when the embedment increased from $1d$ to $5d$.

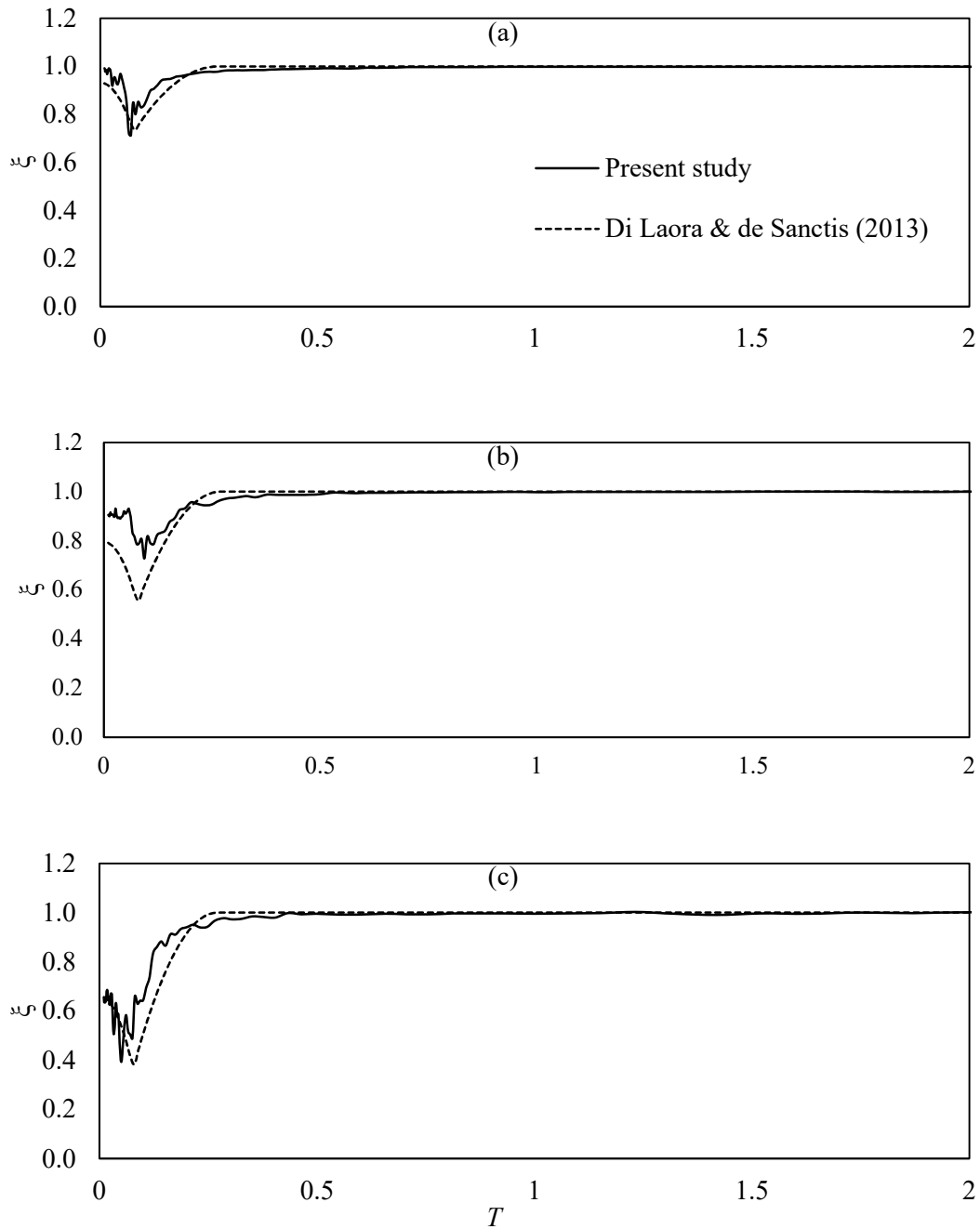


Fig. 4.26 Spectral ratio for single pile for (a) Norcia 2016, (b) Landers 1992, and (c) Valparaiso 2017 ground motions

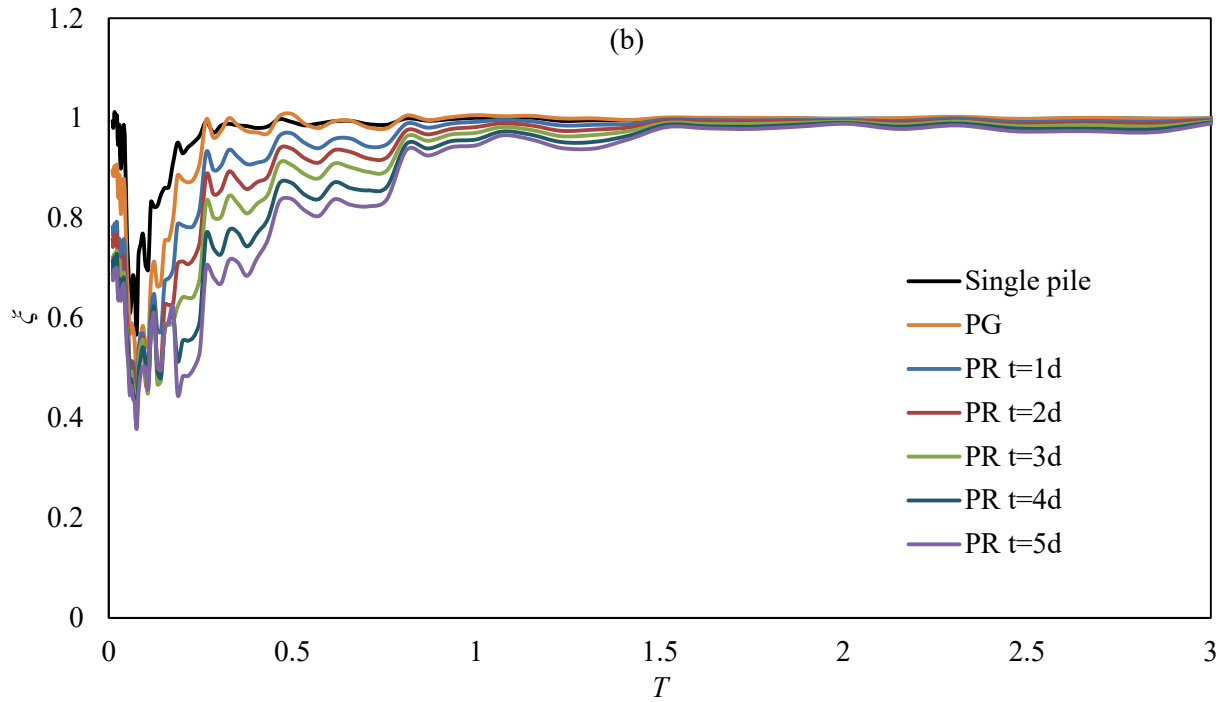
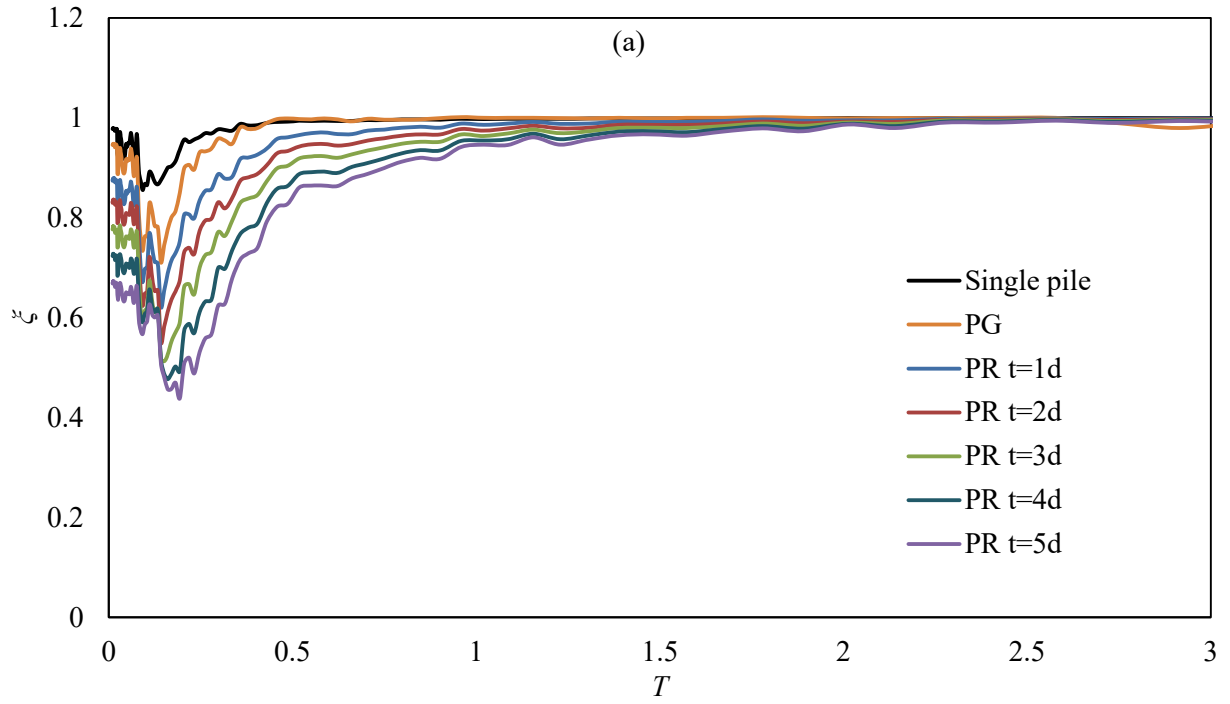


Fig. 4.27 Variation in spectral ratio for 3x3 piled rafts in homogeneous soil layer with $E_p/E_s=1000$, obtained for (a) Amberley 2016 and (b) Christchurch 2011 ground motions

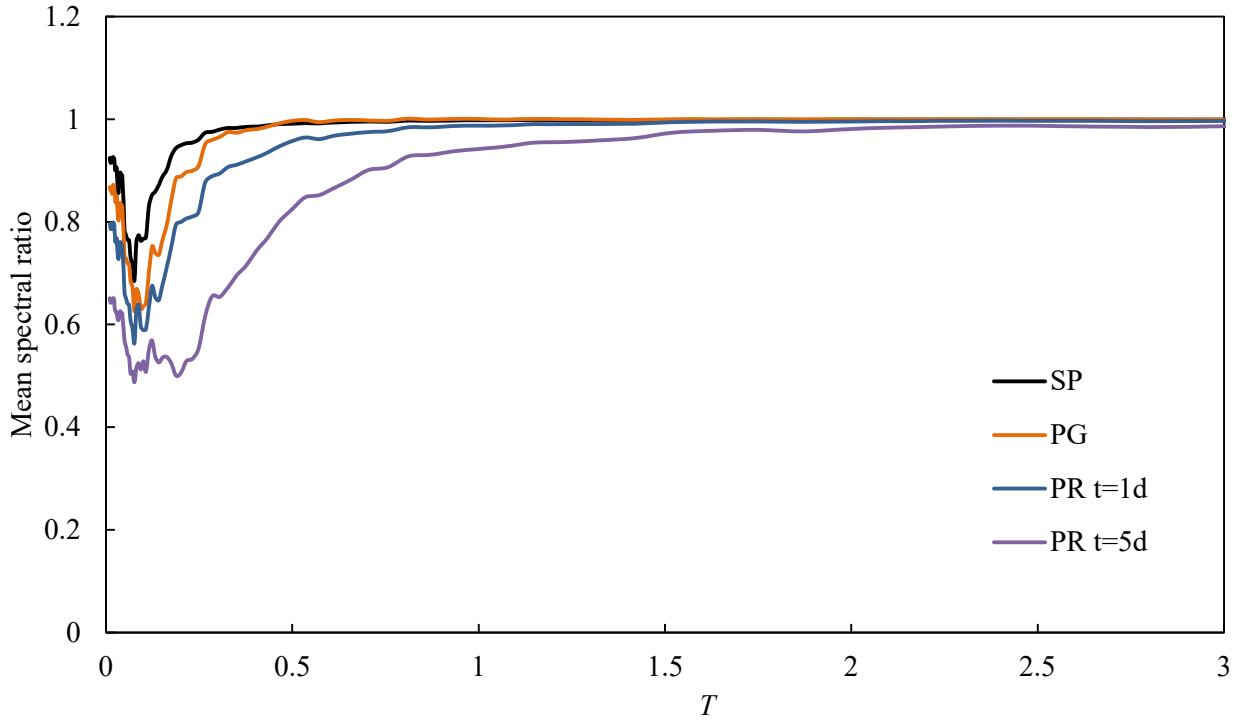


Fig. 4.28 Mean spectral ratio for 3x3 piled rafts in homogeneous soil layer with $E_p/E_s=1000$

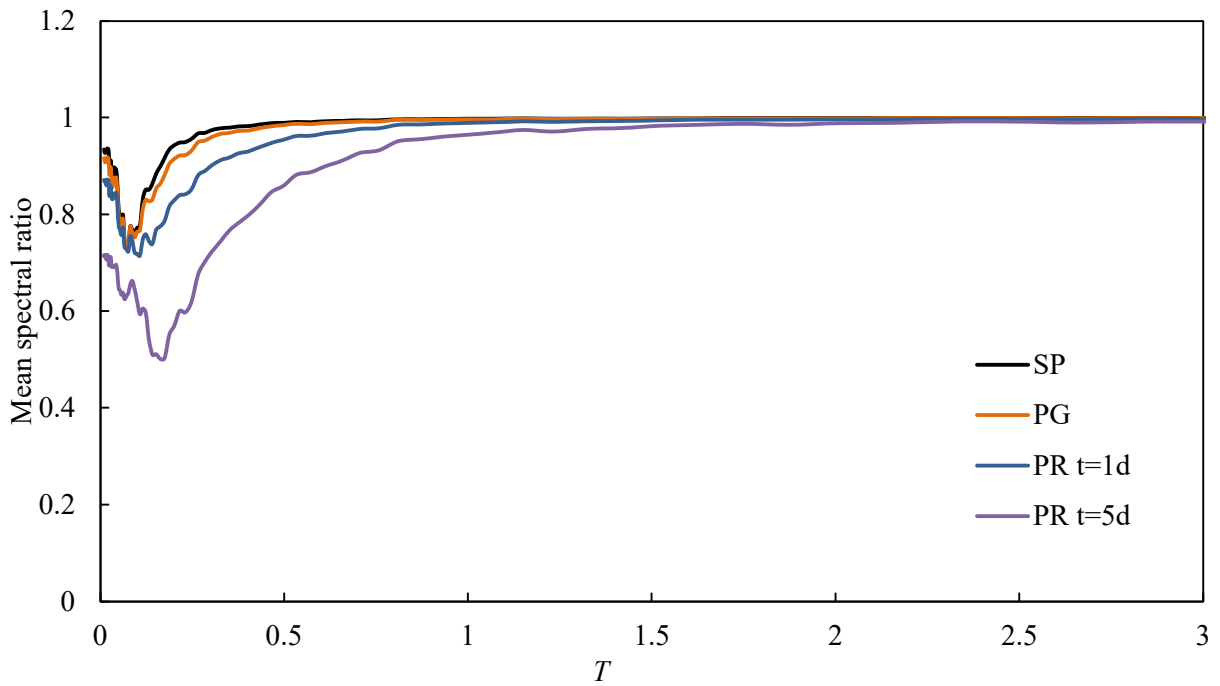
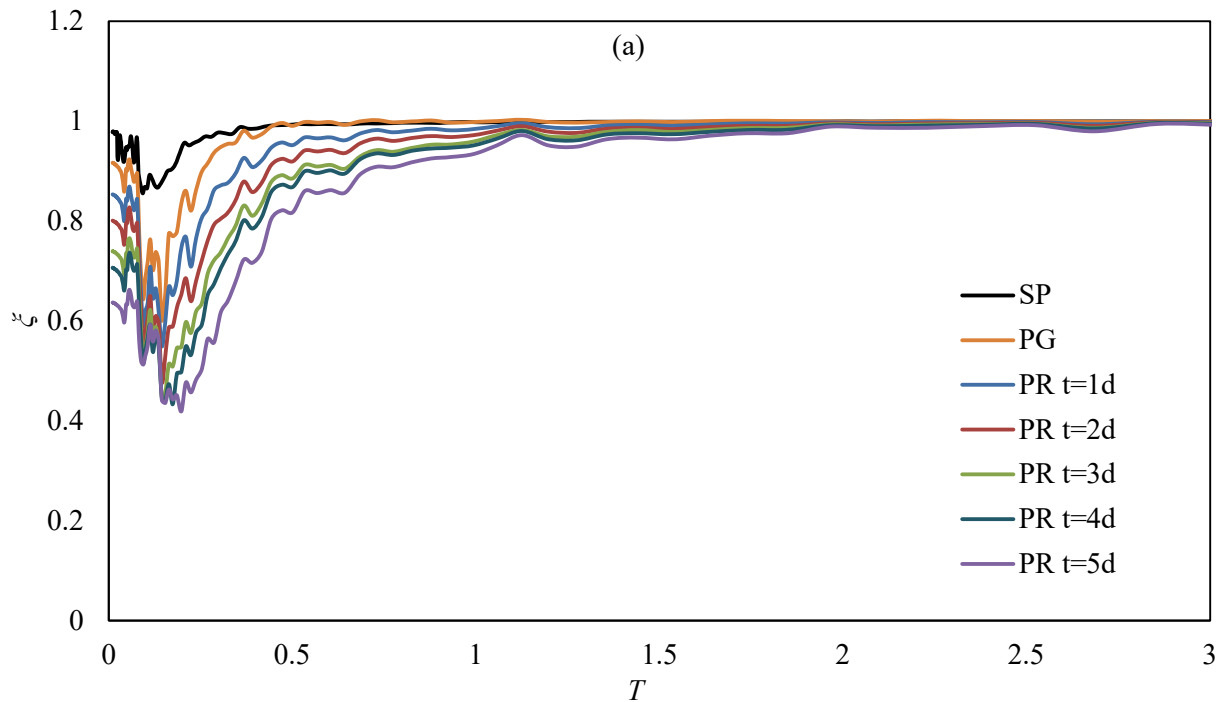


Fig. 4.29 Mean spectral ratio for 3x3 piled rafts in layered soil with exponential stiffness profile

The spectral ratios were also evaluated for piled rafts with 5x3 pile configuration. Fig. 4.30 (a) and (b) presents the variation of spectral ratio with embedment for 5x3 piled rafts in homogeneous profile with $E_p/E_s=1000$ for the Amberley 2016 and Christchurch 2011 ground motions. A reduction of peak acceleration in tune of 23-30% can be seen when the embedment increases from zero to $5d$. The mean spectral ratios for pile foundations in homogeneous and exponential soil profiles is presented in Fig. 4.31 and Fig. 4.32 respectively. It is interesting to note from Fig. 4.29 and Fig. 4.32 that the 3x3 and 5x3 configurations of pile group or piled raft do not exhibit a considerable difference in the mean spectral ratio. This should be read together with findings from section 4.3.2, where it was found that the translational response is not significantly affected by an increase in the number of piles in the direction of motion. The results also provide confidence in using the single pile spectral ratio as a first estimate for pile groups with minimal or no cap embedment. This is particularly true in the case of exponentially varying stiffness profile. For an embedment depth of $1d$, the critical period T_{crit} was found to be significantly higher than T_{min} (in the order of 13 to 18 times) unlike the case of single pile and pile group.



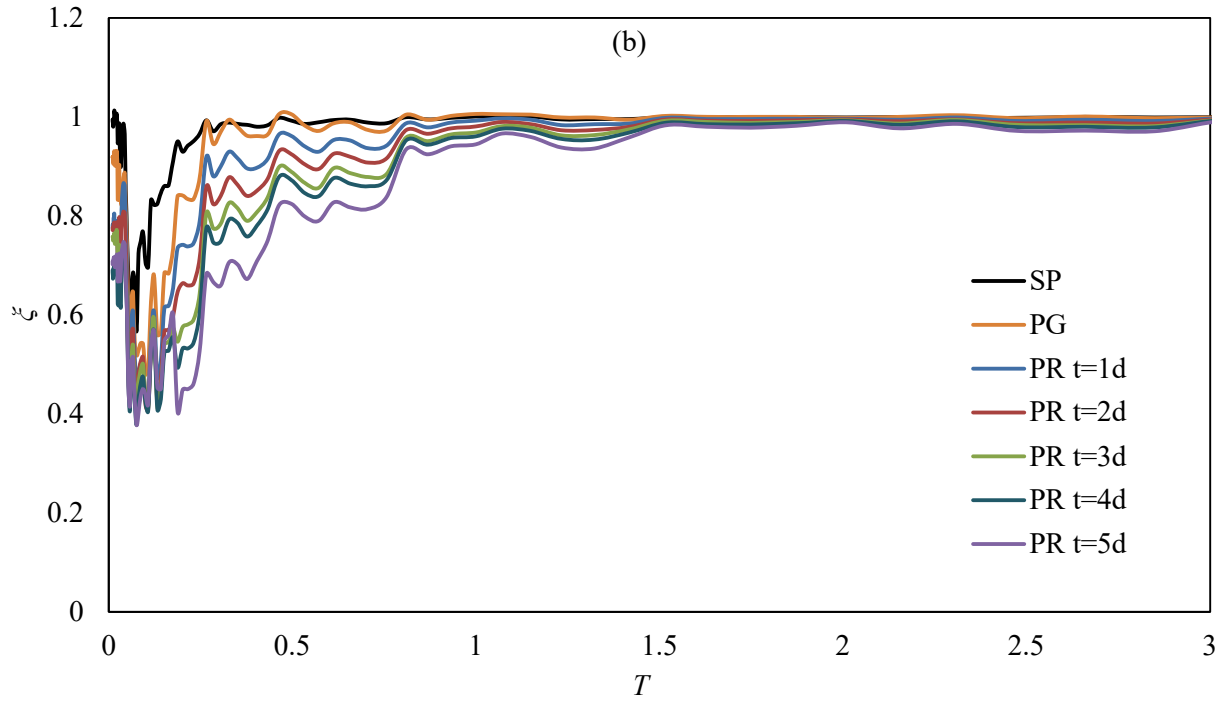


Fig. 4.30 Variation in spectral ratio for 5x3 piled rafts in homogeneous soil layer with $E_p/E_s=1000$, obtained for (a) Amberley 2016 and (b) Christchurch 2011 ground motions

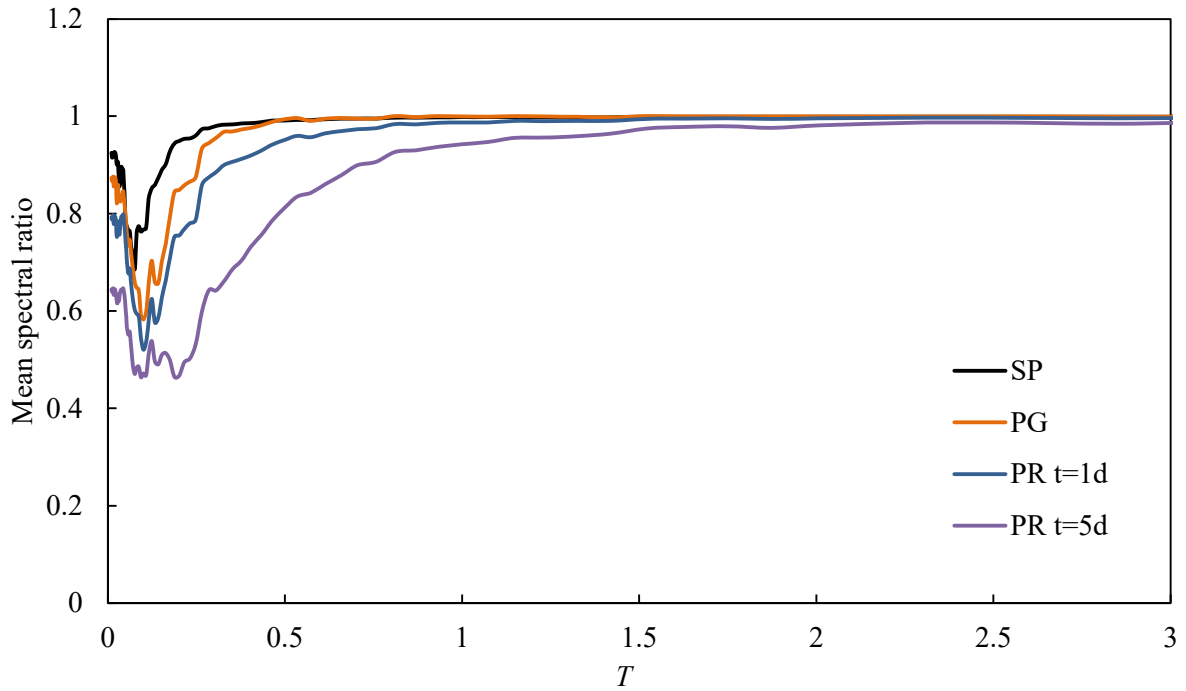


Fig. 4.31 Mean spectral ratio for 5x3 piled rafts in homogeneous soil layer with $E_p/E_s=1000$

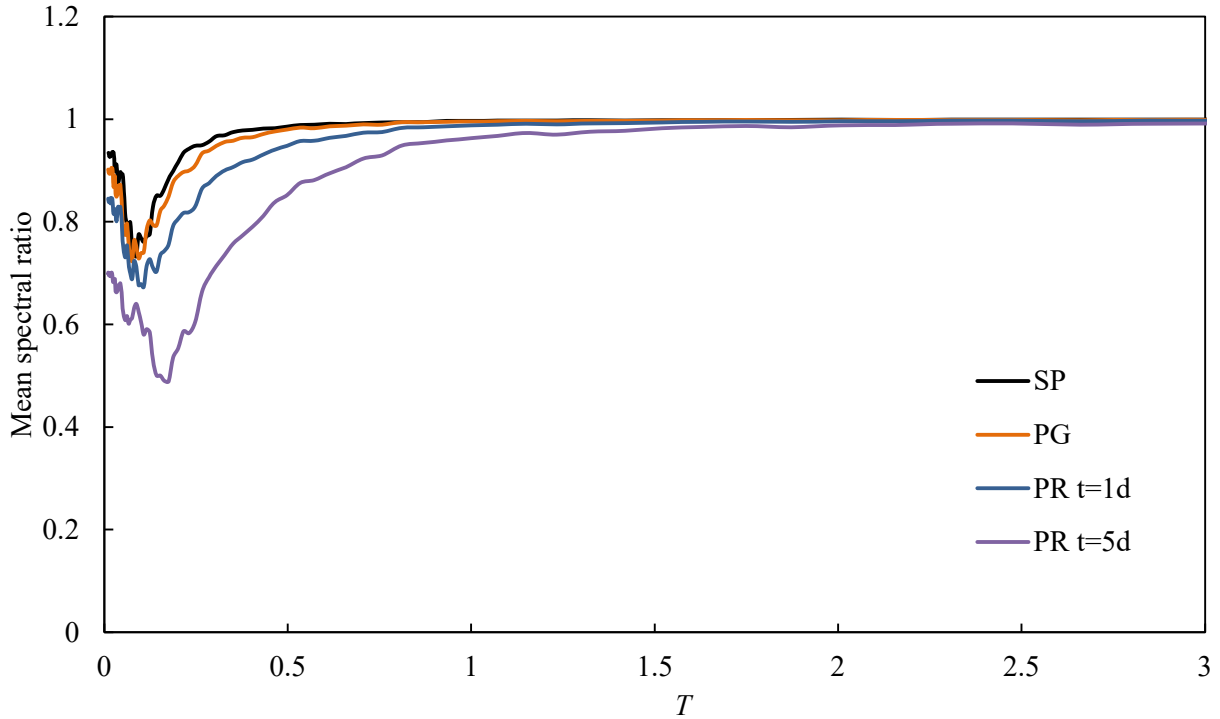


Fig. 4.32 Mean spectral ratio for 5x3 piled rafts in layered soil with exponential stiffness profile

Kinematic bending moment forms an important seismic design consideration for pile foundations. For piles in homogeneous soils, the maximum kinematic bending strains are expected at the pile head (Nikolaou et al. 2001a; de Sanctis et al. 2010). The effect of foundation embedment on the kinematic bending moment was studied using the case of the 5x3 piled raft in homogeneous layer with $E_p/E_s=1000$. The bending moment time histories in the corner pile, P1 and the centre pile, P8 as identified from Fig. 4.11 were extracted from the post processing module of the ACS SASSI program. The maximum bending moment profile was then constructed by plotting the moment profile against normalized depth (h/l) corresponding to the instance of maximum bending moment. The maximum bending moment profiles for the centre pile P8 of the piled raft and pile group, for three ground motions with low, intermediate and high frequency content are compared in Fig. 4.33. The bending moment profile of both the piled raft and the pile group follow the same trend across pile depth. The noticeable difference is at the pile head where piled raft induces a higher moment in comparison with the pile group. The pile head moment in the piled raft was found to be 1.3 to 1.6 times that of the pile group.

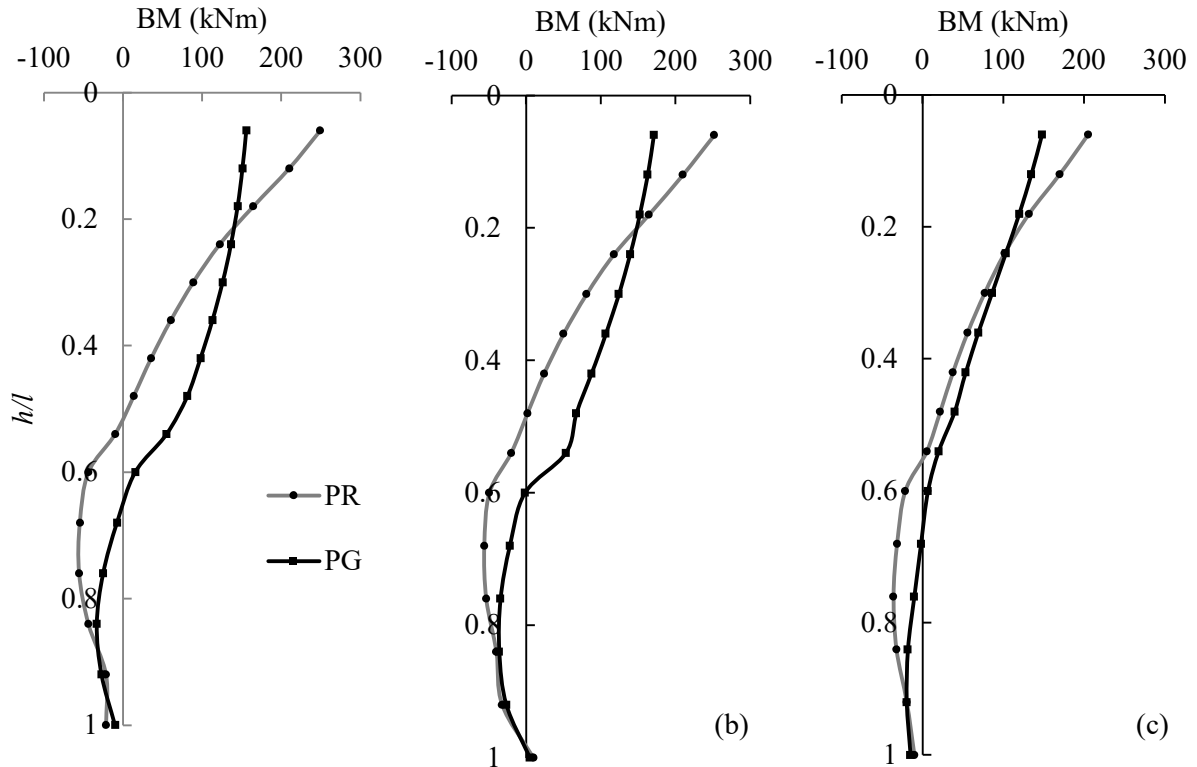


Fig. 4.33 Maximum bending moment profile of pile P8 for (a) Norcia 2016, (b) Amberley 2016 and (c) Christchurch 2011 input motion

The comparison of maximum bending moment profiles of the corner pile (P1) is presented in Fig 4.34. The difference in the bending moment profiles of centre and corner piles were found to be minimal. This is indicative of the minimal pile-soil-pile interaction for kinematic loading. The embedment of raft was found to increase the pile head moment by 1.3 to 1.7 times. However, the difference between piled raft and pile group was found to narrow down as the frequency content of the input motion was increased.

4.4 CONCLUDING REMARKS

The influence of raft embedment on the kinematic response of piled rafts was studied using two case studies. The first case study considered a piled raft-clay system adopted in a centrifuge shaking table test reported by Banerjee (2009). A simulation of the centrifuge experiment was carried out using a 3D model created using the FVSM technique. Results in terms of response spectra and bending moment profiles from two different pile modelling techniques were compared with those from the experiment.

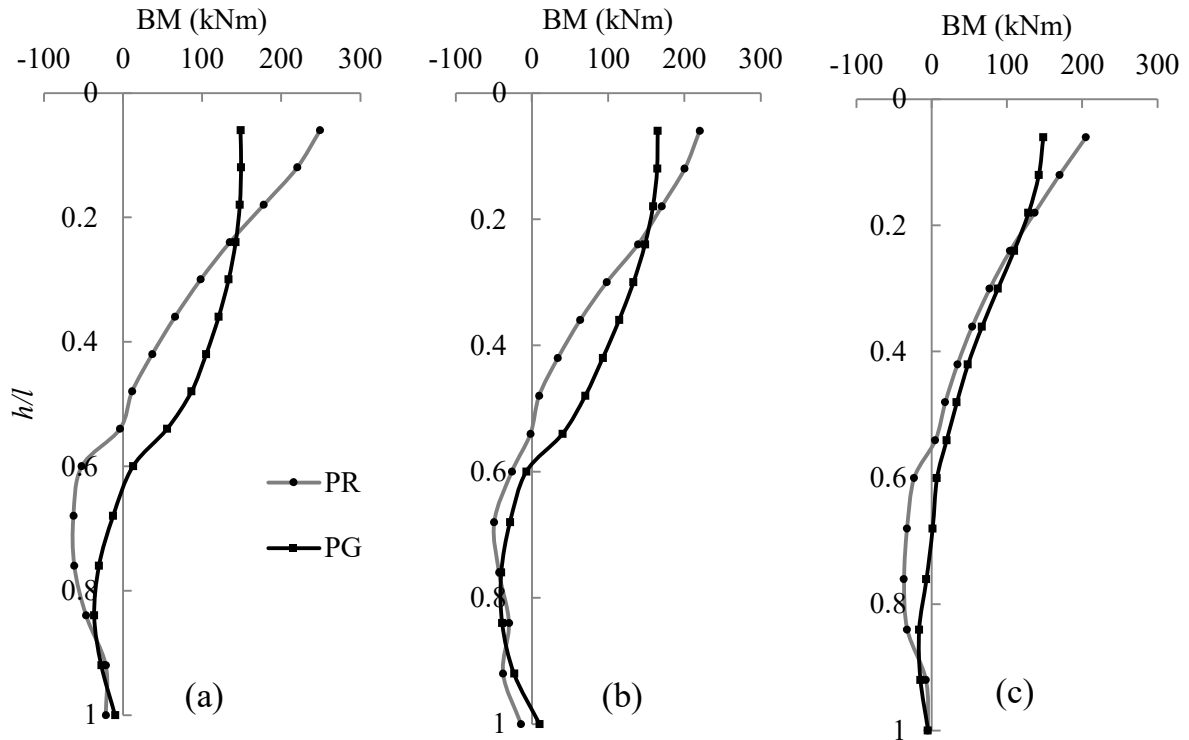


Fig. 4.34 Maximum bending moment profile of pile P1 for (a) Norcia 2016, (b) Amberley 2016 and (c) Christchurch 2011 input motion

The model with pile modelled using volume elements is found to reproduce bending moments in piles to a greater degree of accuracy. The model developed also simulates the centrifuge experiment with a similar degree of match as a nonlinear FE-based analysis reported in the literature. The model was extended to study the role of pile layout on the kinematic response characteristics. From a kinematic response study, it is noted that the kinematic response factors for translational and rotation exhibit similarity with those of a pile group at dimensionless frequency values below 0.4.

The influence of raft embedment on the kinematic response characteristics was then studied comprehensively considering a hypothetical case study reported by Poulos et al. (1999). Two piled raft models with 3x3 and 5x3 pile configurations embedded in homogenous and layered soil profiles were modelled. Transfer functions in translation and rotation were obtained for raft embedment varying from zero to five times the pile diameter. It was found increasing raft thickness results in a decreasing translational response in the dimensionless frequency of 0.025 to 0.5, which forms the frequency range of importance for earthquake engineering. The decrease

in translation was found to be associated with an increase in rocking response. Although, rocking in pile groups is a function of the pile layout and pile spacing, the presence of an embedded raft is found to cause a significant increase in rocking at dimensionless frequencies ranging from 0.2 to 0.3. The results are intuitive considering previous studies that have shown that shallow foundations exhibit higher rocking with increasing embedment depth. A clear trend of increasing filtering of translational response with increasing raft embedment is observed up to a dimensionless frequency of 0.23, which corresponds to a frequency of 10 Hz.

Kinematic response to transient ground motion was then studied by evaluating the spectral ratio considering eight different earthquake motions with varying frequency content. The spectral ratio provides an advantage of practical applicability as the foundation input motion for pile supported structures. Embedment of the raft was found to influence all of the critical parameters that define the spectral ratio curve. The most significant effect was the decrease in peak acceleration, as well as shifting of the critical period T_{crit} . Available predictions equations for single piles were evaluated using results from the present study and were found to be fairly accurate. Results from the study suggest that the single pile spectral ratio can be used as a first estimate for pile groups with minimal or no cap embedment, particularly in the case of exponentially varying soil stiffness profile. However, raft embedment in the order of five pile diameters can result in a significant deviation in this regard. A comparison of the maximum bending moment profiles in piled raft and pile group models showed that a raft embedment of $5d$ can cause an increase in the pile head bending moment by 1.3 to 1.6 times.

CHAPTER 5

DYNAMIC STIFFNESS CHARACTERISTICS OF PILED RAFT FOUNDATIONS

5.1 INTRODUCTION

Pile foundations are commonly adopted to support critical structures in regions with incompetent shallow soil strata. Scenarios where dynamic loads act on the foundation from the superstructure require soil structure interaction (SSI) analysis, which involves estimation of the frequency dependent foundation stiffness as well as dynamic interaction factors. Pile supported structures have been commonly used to support structures such as vibrating machinery and hammers, bridge piers, wind turbines, power plant structures. At large displacements, soil pile interaction also results in soil nonlinearity, pile slippage and pile separation (Burr et al. 1997; El-Marsafawi et al. 1992; Manna and Baidya 2010b; Vaziri and Han 1991).

A pile cap is an integral part of a pile group that facilitates load transfer from the superstructure. Under static loads, the lateral capacity of the combined system is known to be significantly increased by the passive resistance of the pile cap (Rollins and Sparks 2002). While inertial interaction in pile supported buildings has been found to be strongly influenced by the presence of surface foundation elements like pile caps (Stewart et al. 1999), impedance calculation considering ground contacting pile cap has been recommended for scenarios where cap-soil contact loss is not expected (Padrón et al. 2009; Stewart et al. 2012). However, widely used impedance calculations methods for pile groups largely ignore the embedment effects of the pile cap. The case of piled raft foundations where stiffnesses as well as load sharing between pile and raft are important design parameters, pose a challenge in this regard.

Investigations into dynamic raft-pile group interactions have found deviations in vertical and horizontal impedances of piled rafts, in comparison to pile groups (Fukuwa and Wen 2007; Liu and Ai 2017). Padrón et al. (2009) observed that the stiffness of a pile group with ground contacting pile cap is not necessarily greater than the case with cap soil separation, owing to constructive and destructive interference of waves generated at the pile-soil and cap-soil interfaces. Emani and Maheshwari (2009) observed that the presence of cap-soil-pile

interaction in piled rafts at higher frequencies leads to an increase in horizontal and vertical stiffness in comparison with free standing pile groups. The problem of impedances of a capped pile was studied by de Almeida Barros et al. (2019) using a boundary element model. They found that cap diameter as well as soil anisotropy can significantly influence horizontal and rocking impedances of a capped pile. Nagai (2019) proposed a simplified method to predict the dynamic horizontal and rotational impedances of piled rafts based on the impedances of the raft and pile group.

This chapter presents results from numerical analyses carried out to study dynamic stiffness characteristics of piled raft foundations. The case study of a compressor unit foundation in Hazira, India, comprising of a 2x2 pile group with an embedded raft, is adopted. A dynamic lateral load test conducted on a full-scale test pile at the site is presented. A Soil Structure Interaction (SSI) analysis methodology comprising the finite element (FE) based substructure method is employed to rigorously capture the pile-soil-pile, raft-soil-pile and raft-soil interactions under dynamic loads. Data from a full-scale dynamic load test on a single pile is used to evaluate the numerical modelling procedure. Parametric SSI analyses are then carried out to study the effect of an embedded pile cap on the dynamic interaction factors and load sharing ratio in pile rafts in both vertical and lateral modes of vibration. Various models such as the hypothetical capped pile model to 2x2 piled rafts were analysed using the substructuring based FE method. The primary emphasis, is given to the following aspects

- To study the effect of an embedded raft on the stiffness and damping coefficients for varying soil-pile relative stiffness's
- To examine the dynamic interaction factor in vertical and horizontal mode, for piled rafts with uniform and non-uniform pile spacing
- To evaluate load sharing characteristics in piled rafts under dynamic vertical and horizontal loads.

5.2 DYNAMIC STIFFNESS OF PILED RAFT FOUNDATIONS

5.2.1 Case Study of a Compressor foundation

Pile foundations are commonly used to support machinery in power generation and petrochemical plants, in scenarios where competent soil stratum is absent at shallow depths (Ali et al. 2017; Han 2008; Han et al. 1999). The case study of a pile-supported compressor unit designed for a chemical plant situated in Hazira, India is used as a reference problem in this study. The compressor, gear, motor, and piping systems were designed to be placed on a baseplate of size 8.7 m x 3.8 m, which in turn is supported by a foundation comprising of four bored cast in situ piles of 500 mm diameter. A layout of the compressor unit is presented in Fig. 5.1. The operating speed of the compressor is around 10000 rpm, while the total equipment weight on the foundation is 51.1 tonnes. The maximum allowable velocity at the foundation level for the operating machinery was 2.5 mm/s. The soil profile at the site consists of layers of silty clay and silty sand with relatively hard stratum occurring at a depth of 15 to 20 m. Results from SPT and seismic cross hole tests carried out in boreholes at the location are presented in Fig. 5.2. The top 10 m comprised of layers of silty clay with SPT values ranging from 5 to 10. Hard sandy stratum with SPT N values of over 44 and shear moduli greater than 433 MPa was observed beyond a depth of 15 m. Table 5.1 summarizes the soil layer characteristics at the site. The axial capacity in compression for a bored cast in situ pile with diameter of 500 mm and length of 18 m was estimated to be 700 kN, and a 2x2 pile group was adopted for the foundation. The piles were cast with M35 grade concrete, conforming to IS 456 2000 (BIS 2000).

Dynamic analysis of the machine-foundation-soil system requires computation of foundation impedances. Even though traditional foundation design ignores the pile cap-soil contact, Padrón et al. (2009) have shown that effect of a ground contacting pile cap on the dynamic response at high frequencies need not be on the conservative side. In cases where the piled raft design philosophy is followed, the load sharing between raft and piles during steady-state vibration at higher frequencies needs to be ascertained.

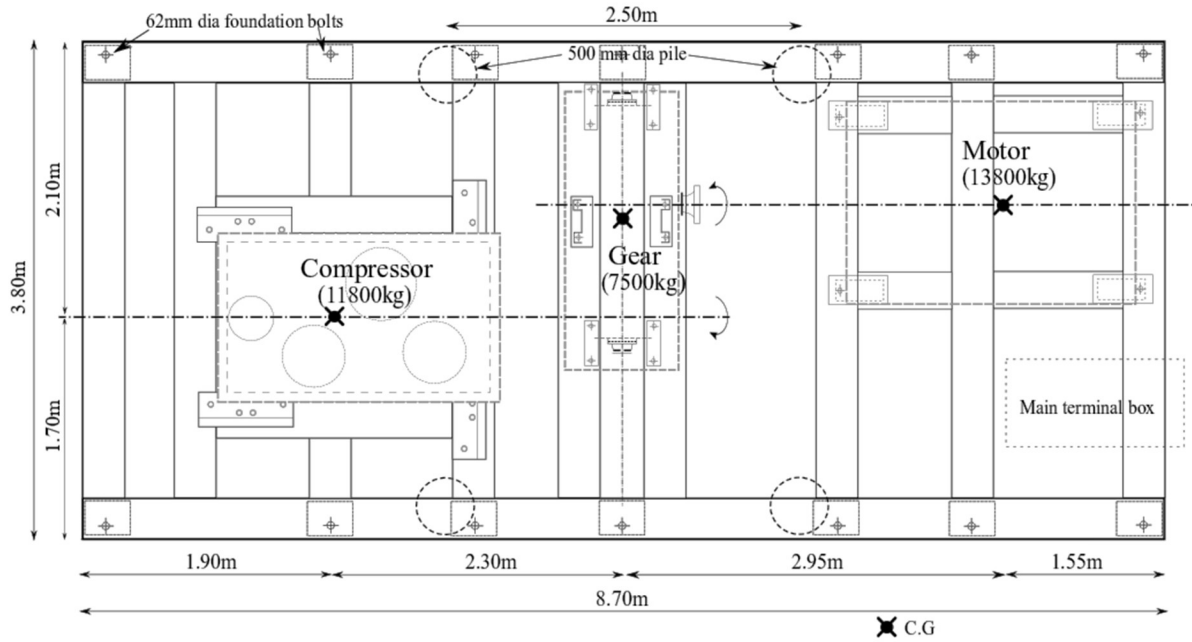


Fig. 5.1 Layout of the compressor unit and base pad

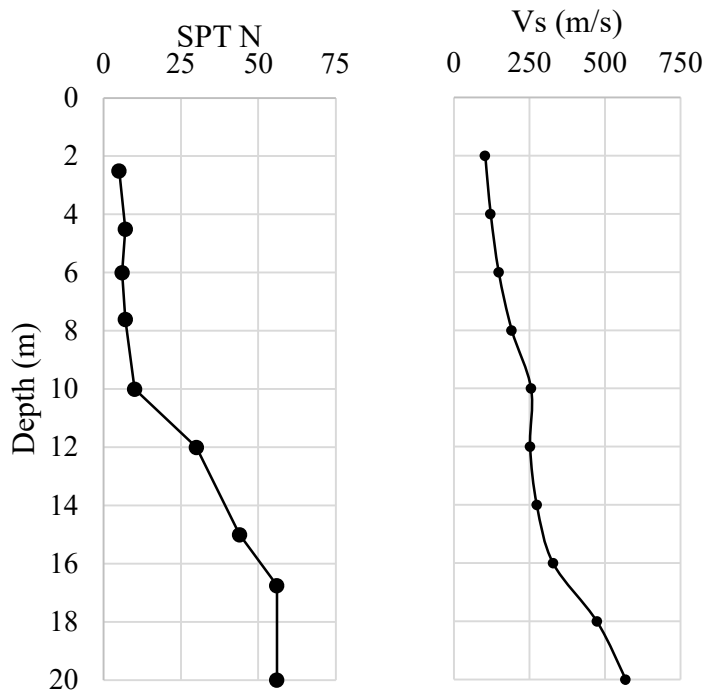


Fig. 5.2 Soil layering along with shear wave velocity and SPT N profile at the site

A field test program consisting of lateral free and forced vibration tests on a single test pile at the site in Hazira, India was carried out. The bored cast in situ type pile with a diameter of 0.5 m and length of 18 m was cast with M35 grade concrete, conforming to IS 456 2000. The length to diameter ratio (l/d) of the pile was 36. To facilitate fixing of the oscillator, a pile cap of dimensions 0.75 m x 0.75 m x 0.75 m was cast on top of the pile. Fig. 5.3 presents the experimental setup. The pile cap was not in contact with the ground. The flexural reinforcement of the pile consisted of ten T16 bars and its helical reinforcement consisted of T8 bars. Following the criteria suggested by Dobry et al. (1982) and Poulos and Hull (1989), the pile can be considered to be flexible for the soil profile at the site.

Table 5.1 Soil properties at the site

Depth (m)	Description	Unit Weight (kN/m ³)	Liquid limit (%)	Plasticity index (%)	Water content (%)	Average SPT N
0.0-2.5	Dark brown silt	16.7	72	36	30	5
2.5-5.0	Black silty clay	17.0	53	27	27	7
5.0-9.5	Black silts with seams of fine sand	17.5	-	-	43	8
9.5-11.5	Black silty clay with seams of fine sand	17.5	38	22	38	10
11.5-14.0	Silty sand	18.0	-	-	27	30
14.0-16.0	Blackish silty sand	18.0	-	-	20	44
16.0-18.0	Clay with sand	19.0	47	27	21	56
18.0-20.0	Brownish silty sand	19.8	-	-	-	60

The pile was subjected to a free vibration test as well as a series of forced vibration tests. Conforming to IS 9716:1981 (BIS 1981), the free vibration tests were performed by the application of a lateral load followed by sudden release. The reaction load was provided by a second pile of the same dimensions constructed at a distance of 3m from the test pile. The lateral load was applied by rotating a pulling screw, and the load was released using a clutch arrangement. Two tests were conducted on the same pile. The free vibration response was then recorded using two uniaxial accelerometers attached to the pile cap at the pile cut off level. Data from the accelerometers was amplified and recorded using a data acquisition system connected to a computer.

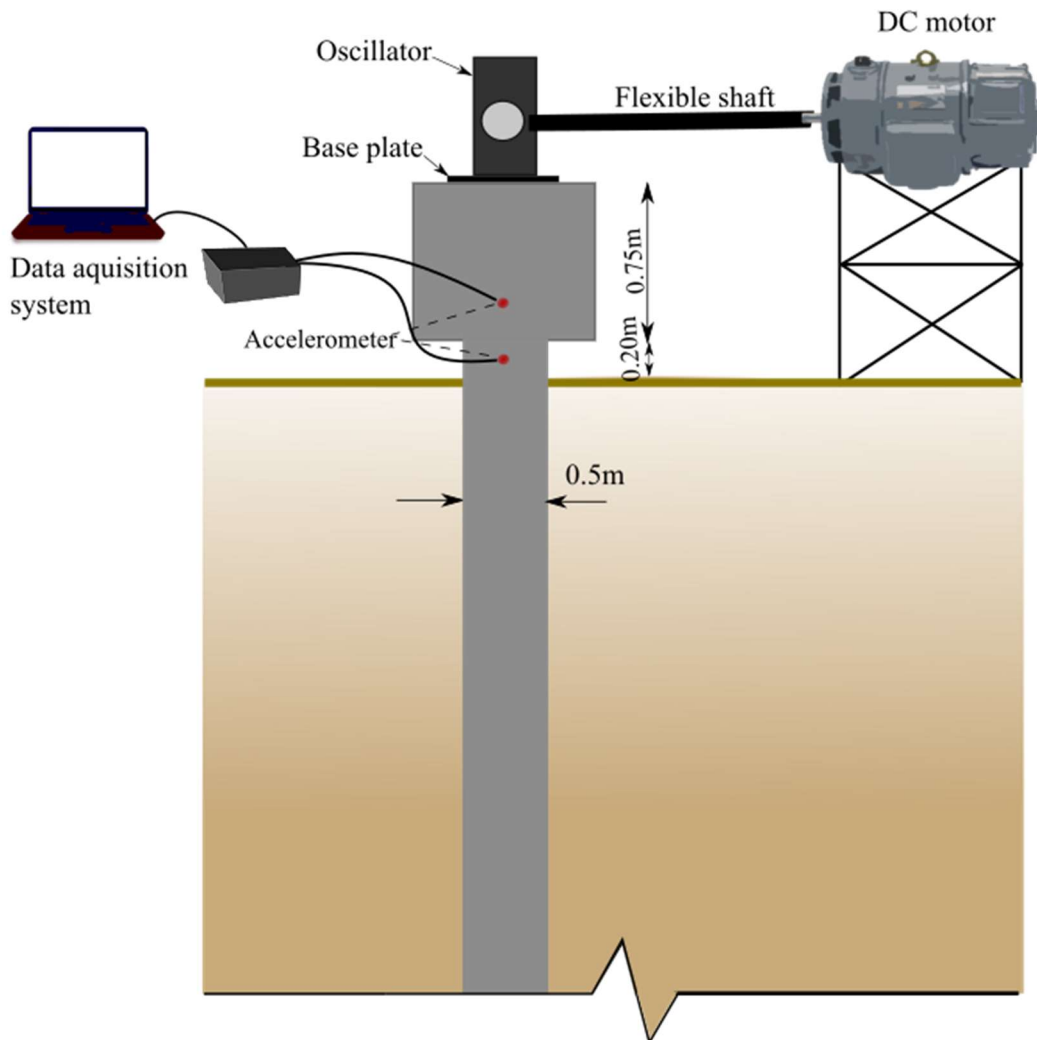


Fig. 5.3 An illustration of the experimental setup

A Lazan eccentric mass oscillator was then attached to the pile cap. This type of oscillator has been used extensively in previous studies to drive soil-pile-mass systems (Ayothiraman et al. 2012; Boominathan et al. 2002, 2015; Boominathan and Ayothiraman 2006; Elkasabgy and El Naggar 2013; Gle and Woods 1984; Han and Novak 1988; Manna and Baidya 2010b; a). The oscillator assembly together with the mild steel base plate weighed 113 kg in total. The oscillator was driven by a DC motor via a flexible shaft. A photograph showing the pile and oscillator assembly is presented in Fig. 5.4.

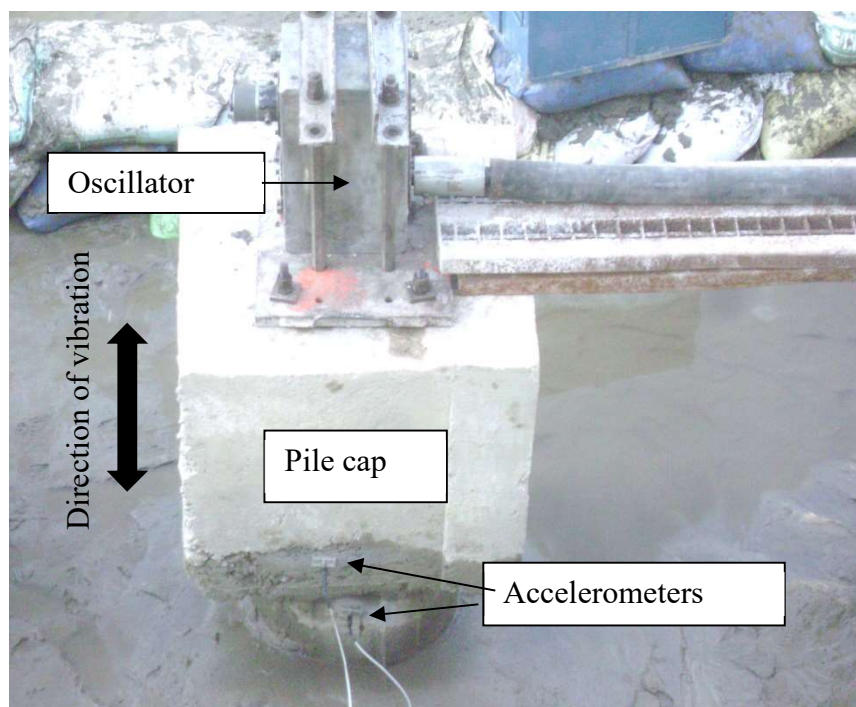


Fig. 5.4 Photograph showing the pile and oscillator assembly

The force exerted by the oscillator was controlled by adjusting the phase angle between the two unbalanced masses mounted on counter rotating shafts. The oscillator was operated in the frequency range of 9 to 30 Hz for which the amplitude of force varied from 0.5 to 7.4 kN. The exiting force-frequency relationship for the oscillator is presented in Table 5.2. A speed control unit was used to control the speed of the DC motor, and a tachometer was used to measure the rotational speed of the shaft.

Table 5.2 Magnitude of quadratic excitation force from the oscillator

Angle of eccentricity of masses (degrees)	32.8	49.2	65.6	82
Excitation force (N)	$4.75f^2$	$7.12f^2$	$9.49f^2$	$11.86f^2$

f is the frequency in Hz

A 3D finite element model was developed to simulate the free and forced vibration response of the single pile in layered soil. The cube shaped pile cap was modelled using eight noded solid elements and was not in contact with the adjacent soil elements as in the field. The oscillator and its base pad are considered as point loads on the pile cap. The soil properties described in Table 5.1 were assigned to the soil layers. The pile material behaviour was assumed to be linear elastic with a Young's modulus value of 29 GPa, Poisson's ratio of 0.2 and a unit weight of 25 kN/m³. The meshing of the geometry was carried out, restricting the maximum height of elements below one-fifth of the maximum wavelength considered in the analysis (Kim et al. 2016; Lysmer et al. 1981b). A cutaway section of the FE model showing the pile, pile cap and near field soil elements is presented in Fig. 5.5

The free vibration response of the pile was simulated by applying an impulse at the center of the vertical face of the pile cap. An impulse of 15Ns was applied to produce a maximum displacement comparable to the displacement observed during the field test. A comparison of the free vibration response from the experiment and simulation is presented in Fig. 5.6. The experimental and estimated values of damped natural frequency for horizontal mode are presented in Table 5.3. The simulation is observed to produce a reasonable estimate of the natural frequency of the pile soil system.

The simulation of the forced vibration response was also carried out using the same model. The dynamic vertical forces calculated based on the eccentricity and frequency were distributed on the nodes on the top of the pile cap. Convergence in the equivalent linear technique was observed within 4 iterations for all the analyses. The displacement response at the node corresponding to the accelerometer location at the pile (refer Fig 5.4) was then extracted in the post processing stage of the analysis.

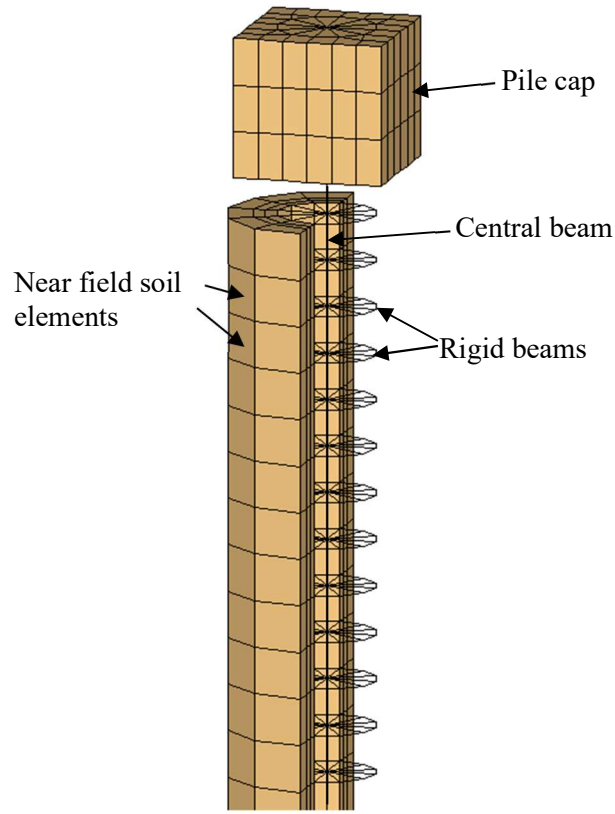


Fig. 5.5 FE model of the single pile-soil system considered in the experiment

Table 5.3 Damped natural frequency of the pile-soil system

	Experiment	Simulation	Error (%)
Natural frequency (Hz)	20.00	18.18	9.10
Damping ratio (average)	0.127	0.120	5.5

A comparison of the frequency response curve obtained from experiment and corresponding simulations is presented in Fig. 5.7. The response of the pile soil system was evidently nonlinear with resonant frequency decreasing with increasing amplitude of exciting force.

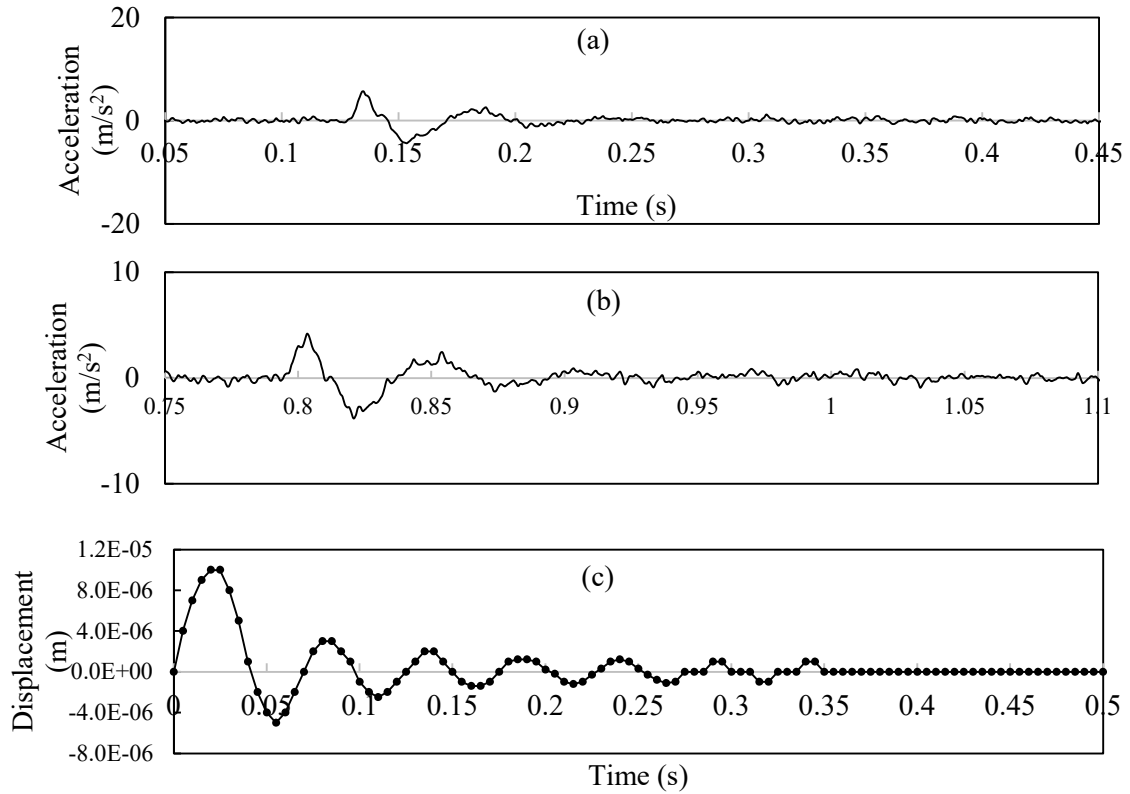


Fig. 5.6 Free vibration response from (a)-(b) experiments and (c) simulation

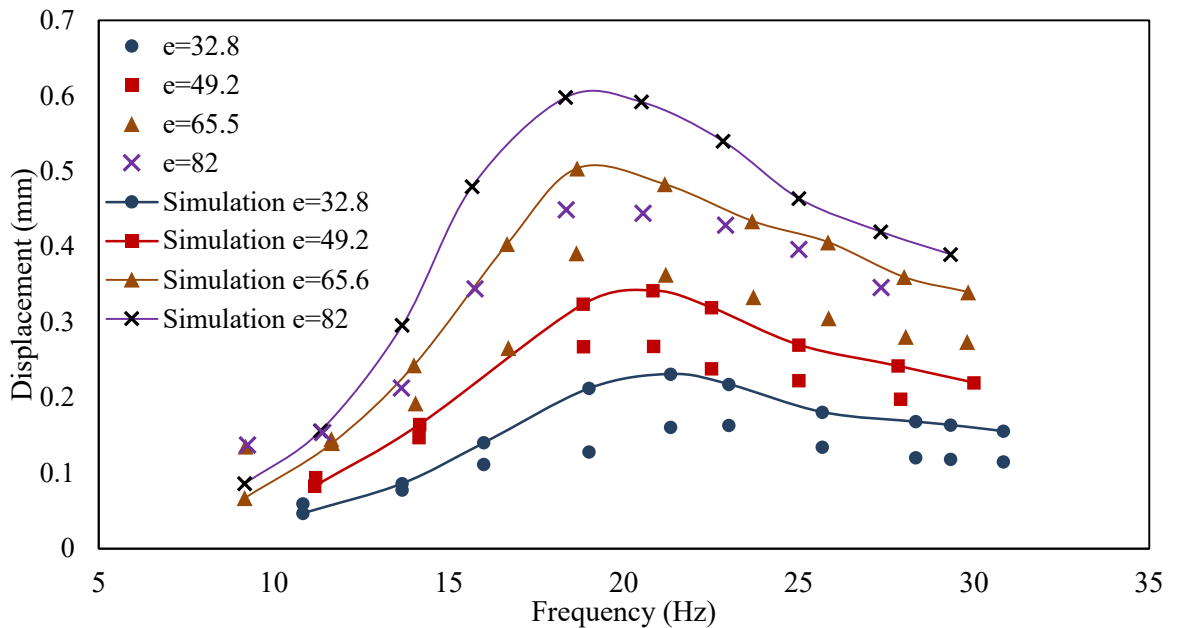


Fig 5.7 Frequency response curve of the pile in horizontal vibration, for varying eccentricity of oscillator mass

The resonant frequency observed from forced vibration tests was found to be slightly higher than the natural frequency observed from free vibration tests at lower excitation intensities, and lower at higher intensities. Similar observations have been reported in the past by several authors (Biswas and Manna 2018; Elkasabgy and El Naggar 2018; Han and Novak 1988). The simulation was found to capture the variation in resonant frequencies. However, the maximum error in the displacement amplitude was found to be around 33% at higher eccentricities of 65.6 and 82 degrees. The amplified response from the simulation can be attributed to the assumed modulus degradation and damping curve for soil layers as well as the inherent limitations with the equivalent linear approach. Previous studies on the dynamic response of elastic piles in poroelastic media have shown that the presence of saturated pervious soils can influence the lateral dynamic stiffness of piles (Liu and Ai 2017; Maeso et al. 2005; Wen et al. 2015; Xu et al. 2010; Zheng et al. 2015; Zhou and Wang 2009). The effects of saturated soil, as well as nonlinear pile-soil interface behaviour, is not considered in the model used. However, notwithstanding the limitations, the adopted methodology is found to provide a reasonable approximation of the dynamic pile response.

The SSI methodology discussed in the previous sections was extended to study the factors influencing dynamic stiffness and load sharing behaviour of piled rafts. Two different groups of piled rafts were considered in this study as presented in Fig. 5.8 (a). A hypothetical system consisting of a single pile connected to a rigid massless circular raft, referred to as capped pile, is first considered to investigate the influence of the ground contacting cap on the impedances and load transfer mechanism in a combined pile-cap system. The second group of models include piled rafts with 2x2 pile configuration corresponding to the machine foundation as presented in Fig. 5.8 (b). Pile layout in a piled raft can be represented in terms of a dimensionless area ratio, A_r defined as

$$A_r = \frac{A_g}{A} \quad (5.1)$$

where A_g represents the area circumscribed by the pile group, and A represents the total area of raft. In both the foundation groups, the area ratio was varied in order to assess the contribution of the raft on the dynamic response. The SSI analyses were carried out for the actual layered soil profile at the site, as well as for homogeneous profiles with modulus ratio, E_p/E_s of 100,

500 and 1000. In all the models developed, the piles were modelled using the beam and rigid link method. Table 5.4 presents details of the piled raft models considered in this study

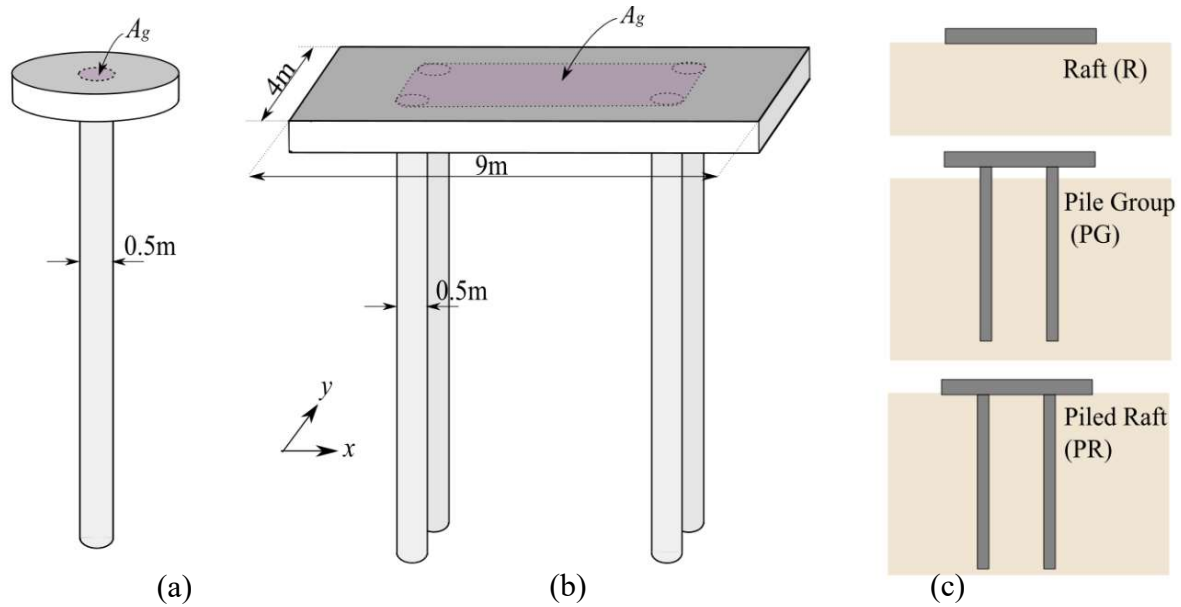


Fig. 5.8 Illustrations showing (a) capped pile, (b) the 2x2 PR foundation and (c) the three foundation types analyzed

Table 5.4 Details of the piled raft foundations analysed

Case	Foundation	Area ratio (A_r)	Soil profiles
1		0.04	
2	Capped pile	0.06	Layered*; Homogeneous with $E_p/E_s = 100$, $E_p/E_s = 500$, and $E_p/E_s = 1000$
3		0.11	
4		0.25	
5		0.25	
6	2x2 piled raft	0.50	Layered*; Homogeneous with $E_p/E_s = 100$, $E_p/E_s = 500$, and $E_p/E_s = 1000$
7		0.75	

*Soil profile described in Table 4.1 and Fig. 4.2

The complex dynamic stiffness of foundation systems is represented in the conventional form as in Eq. 5.2. The real term is indicative of stiffness while the imaginary term represents damping in the system.

$$K(a_o) = k(a_o) + ia_o c(a_o) \quad (5.2)$$

where a_o is the dimensionless frequency defined as

$$a_o = \frac{\omega d}{V_s} \quad (5.3)$$

The coefficients K_x and C_x are calculated using the response of the foundation soil system to a unit vertical harmonic load using the expression

$$F_z = (K_z + i\omega C_z)(U_{real} + iU_{comp}) \quad (5.4)$$

where F_x is the applied load, and U_{real} and U_{comp} are the components of complex displacement. Thus to evaluate foundation stiffnesses, a unit harmonic load is applied on the foundation nodes in the desired direction and the resulting complex displacement is extracted.

5.2.2 Capped Pile Model: Vertical and horizontal Vibrations

The capped pile problem is largely theoretical and is aimed at quantifying the change in stiffness and radiation damping due to the presence of a ground contacting rigid circular cap. Figures 5.9 (a,b) show the frequency dependent vertical stiffness and damping coefficients of the capped pile models in the layered soil profile. The change in vertical stiffness and damping terms with the introduction of the circular cap i.e. the ratio of capped pile coefficients to the corresponding single pile coefficients, for varying A_r is presented in Figures 5.10 (a) to (h). A noteworthy trend is observed for models with A_r of 0.06 and 0.04. For these models, the stiffness coefficient is observed to follow a decreasing trend with increasing frequency. The increase in damping coefficient with decreasing area ratio is indicative of the enhanced radiation damping from the additional area of the raft. The alteration in impedance functions due to an embedded raft is found to become significant as the pile soil stiffness contrast reduces. For example, at a

frequency of 20 Hz, the energy radiated from the foundation, represented by the damping coefficient, is twice that of a single pile when the area ratio is 0.04.

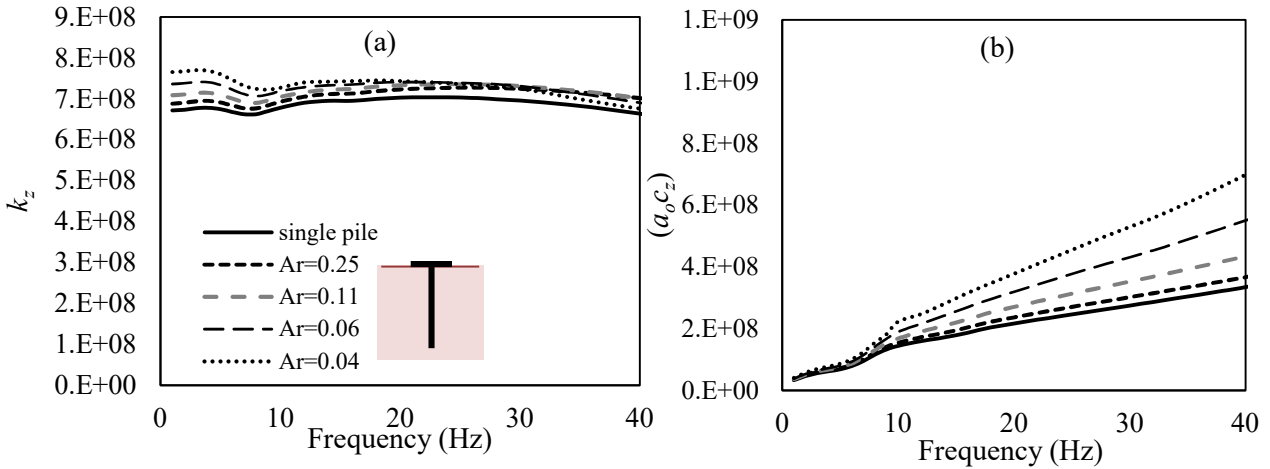
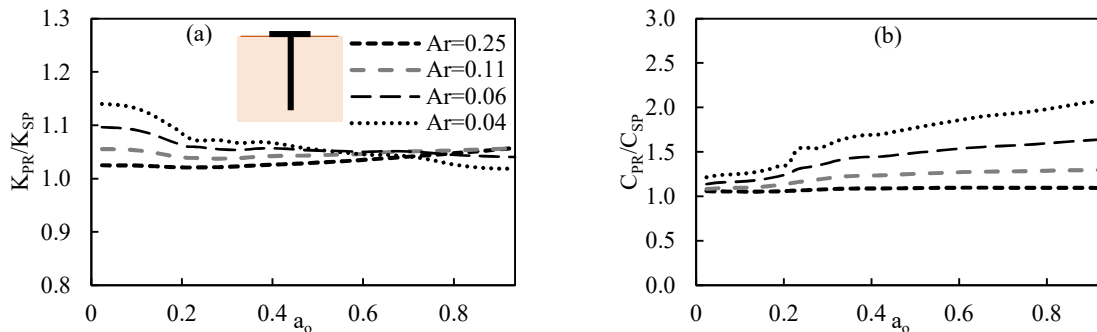


Fig. 5.9 Variation of (a) vertical stiffness and (b) damping coefficients of capped piles with area ratio

The horizontal stiffness and damping coefficients normalized to the corresponding single pile coefficients for the four soil profiles are presented in Fig. 5.11 (a) to (h). The pile cap is found to impart a significant influence on the horizontal stiffness and damping coefficients. As the area ratio increases, a clear trend of decreasing stiffness coefficient and increasing damping coefficient becomes evident. At a frequency of $a_o=0.5$, the damping coefficient of capped pile with area ratio of 0.04 is found to be 4.3 to 10.6 times that of the corresponding free headed single pile.



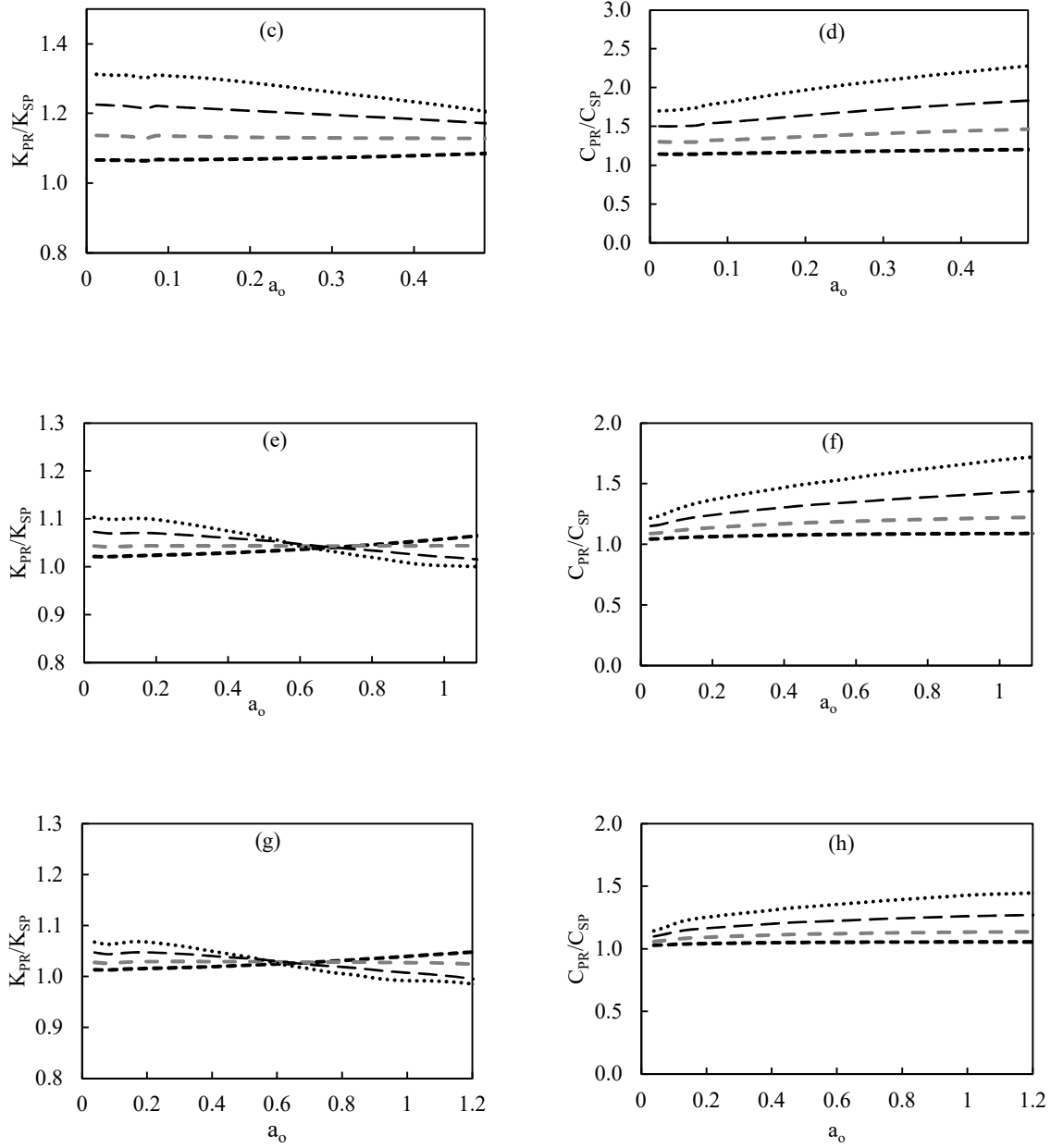


Fig. 5.10 Vertical stiffness and damping coefficients of capped piles normalized with corresponding single pile coefficients for (a)-(b) layered, (c)-(d) homogeneous; $E_p/E_s = 100$, (e)-(f) homogeneous; $E_p/E_s = 500$, and (g)-(h) homogeneous; $E_p/E_s = 1000$ soil profiles

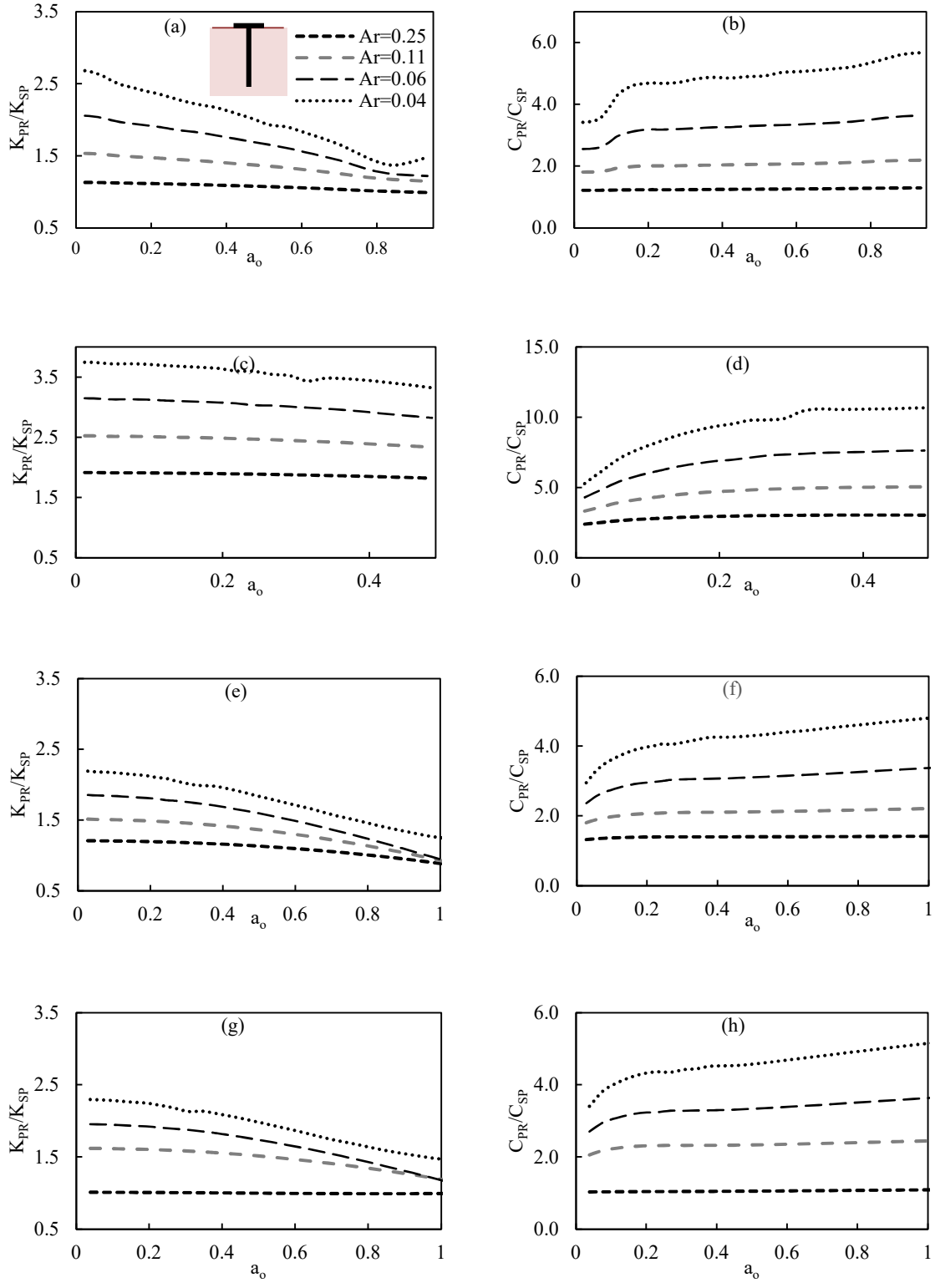


Fig. 5.11 Horizontal stiffness and damping coefficients of capped piles normalized with corresponding single pile coefficients for (a)-(b) layered, (c)-(d) homogeneous; $E_p/E_s = 100$, (e)-(f) homogeneous; $E_p/E_s = 500$, and (g)-(h) homogeneous; $E_p/E_s = 1000$ soil profiles

5.2.3 Piled raft: vertical and horizontal vibration

Piled rafts with 2x2 pile configuration, with three different area ratios, were developed for dynamic response in vertical and horizontal modes. The dimensions of the raft in all the models were restricted to a length of 9 m, breadth of 4 m, and a thickness of 0.6 m. The centre to centre spacing of the pile group in the transverse direction was maintained at 3 m, while three different longitudinal spacings of 2.08 m, 4.64 m and 7.20 m were adopted to represent area ratios of 0.25, 0.50 and 0.75. Figure 5.8 (b) presents an illustration of the 2x2 piled raft models developed. Additional models with the raft (R) and pile group (PG) were also analyzed as presented in Fig 5.8 (c). The pile group models were developed with the same pile layout as in the piled raft models. In the PR and PG models, the piles were modelled by the central beam and rigid links along with near field soil elements. In the FEM-BEM formulation, near field soil elements are essential in capturing raft-soil-pile and pile-soil-pile interactions. Images of the FE model of the piled raft with $A_r=0.25$ are presented in Figures 5.12 (a) and 5.12 (b).

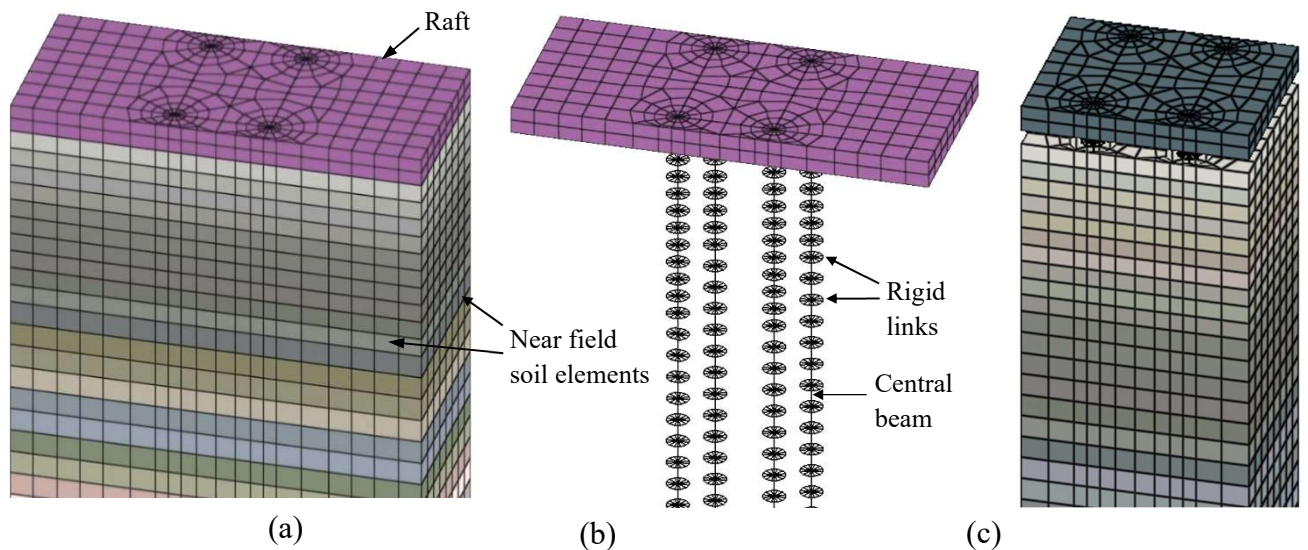


Fig. 5.12 (a) FE mesh of the PR model with $A_r=0.25$ (b) the PR model shown without near field soil elements and (c) the corresponding PG model

Fig. 5.12 (c) shows the corresponding pile group model with the same pile layout, for which the rigid massless raft was not in contact with soil elements. In the piled raft models, the raft was modelled as rigid and massless with only the bottom surface in contact with soil, to isolate

the effects of inertia and side contact. Rigid behaviour of the raft was ensured by following the criteria suggested by Meyerhof (1953) and Ulrich et al. (1988).

The notions k_R , k_{PG} , and k_{PR} will be used to denote stiffness of raft, pile group and piled raft respectively. The static vertical stiffness of piled rafts can be estimated based on the individual stiffnesses of raft and pile group and the interaction factor of pile group on raft, α_{rp} as (Clancy and Randolph 1993; Poulos 2001) :

$$k_{PR} = \frac{[[k_P + k_R(1 - 2\alpha_{rp})]]}{\left[1 - \left(\frac{k_R}{k_P}\right)\alpha_{rp}^2\right]} \quad (5.5)$$

This concept can be extended to the dynamic problem by expressing the piled raft stiffness in terms of frequency dependent pile group and raft stiffnesses, and a frequency dependent interaction factor, α_d as

$$k_{PR} = \frac{[[k_{PG}(f) + k_R(f)(1 - 2\alpha_d(f))]]}{\left[1 - \left(\frac{k_R(f)}{k_{PG}(f)}\right)\alpha_d^2(f)\right]} \quad (5.6)$$

The dynamic interaction factor, can be expressed as

$$\alpha_d = \frac{k_{PG}}{k_{PR}} \left[1 \pm \sqrt{\left(1 - \frac{k_{PR}}{k_R}\right)\left(1 - \frac{k_{PR}}{k_{PG}}\right)} \right] \quad (5.7)$$

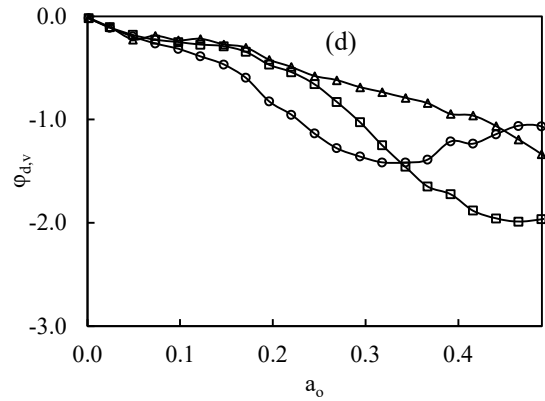
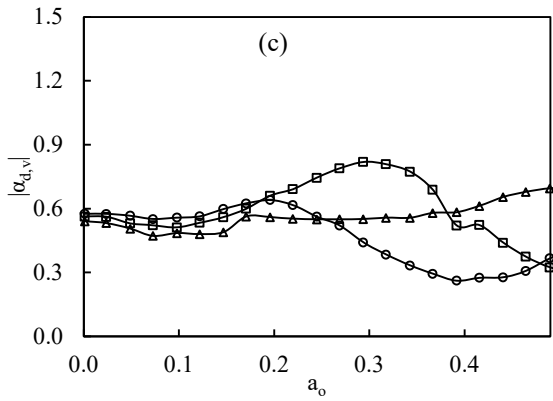
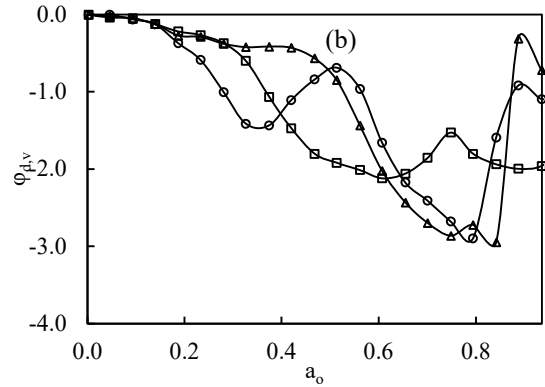
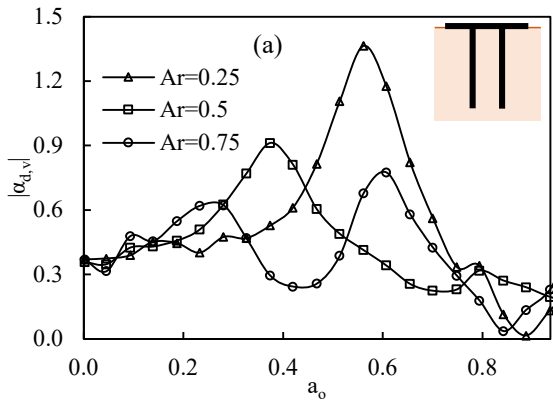
For a dynamic vertical or horizontal load represented by Eq. 5.8, the interaction factor can be expressed as in Eq. 5.9.

$$F = F_o \exp(i\omega t) \quad (5.8)$$

$$\alpha_{d,i} = |\alpha_{d,i}| \exp(i\varphi_{d,i}) \quad (5.9)$$

where i is the mode of vibration. The amplitude and phase angle (in radians) of the vertical dynamic interaction factor for various piled raft configurations and soil profiles is presented in Fig. 5.13 (a-h). The frequency is normalized with shear wave velocity, V_s , and the diameter of pile, d . The amplitude and phase were found to deviate from the static values after a certain threshold dimensionless frequency that varies from 0.045 to 0.075 depending on the soil profile. The amplitude $|\alpha_{d,v}|$ was found to exhibit characteristic peaks beyond the threshold frequency. The phase angle remains low at low frequencies suggesting that the piled raft and the pile group

vibrate with the same phase. The phase angle $\varphi_{d,v}$ exhibits an increasing trend with dimensionless frequency after a notable inflection point that varies from 0.1 to 0.22. These characteristics are similar to the response of a dynamic system. However, the trend becomes less obvious as the pile spacing in x direction increases, as evident from the wavy nature of amplitude and phase for the case with $A_r=0.75$.



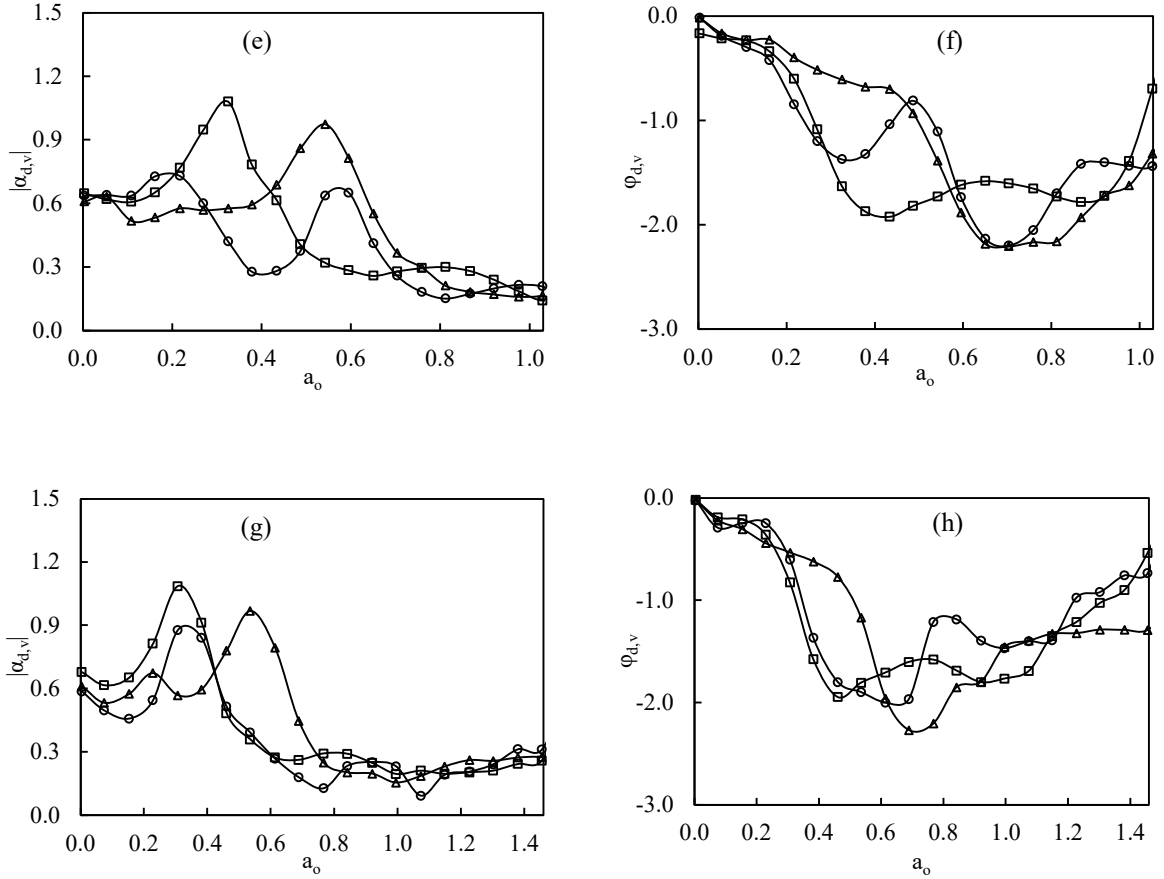


Fig. 5.13 Amplitude and phase of the dynamic interaction factor for piled rafts in (a)-(b) layered, (c)-(d) homogeneous; $E_p/E_s = 100$, (e)-(f) homogeneous; $E_p/E_s = 500$, and (g)-(h) homogeneous; $E_p/E_s = 1000$ soil profiles

Nagai (2019) observed that this dynamic interaction factor for horizontal and rotational modes reflects a dynamic phenomenon for piled rafts with uniform pile spacing, and can also be estimated using empirical equations. The magnitude and phase of the dynamic interaction factor in horizontal mode can be expressed as given by Nagai (2019):

$$|\alpha_d(a)| = \frac{\xi \cdot a_i^2}{\sqrt{(\eta \cdot a_i \cdot a)^2 + (a_i^2 - a^2)^2}} \cdot \exp(-\zeta \cdot a) \quad (5.10)$$

$$\varphi_d(a) = -\tan^{-1} \left(\frac{\eta \cdot a_i \cdot a + \delta}{a_i^2 - a^2} \right) \quad (5.11)$$

where $a (=f.s/V_{s,LA})$ is the frequency normalized with pile spacing (s) and Lysmer's analog shear wave velocity ($V_{s,LA}$), a_i and ζ are constants with values of 0.56 and 0.66 respectively. The coefficients ξ , η , and δ are determined from the static interaction factors as

$$\xi = |\alpha_d(0)| \quad (5.12)$$

$$\eta = \frac{\xi}{|\alpha_d(a_i)|} \cdot \exp(-\zeta \cdot a_i) \quad (5.13)$$

$$\delta = -a_i^2 \tan\{\varphi_d(0)\} \quad (5.14)$$

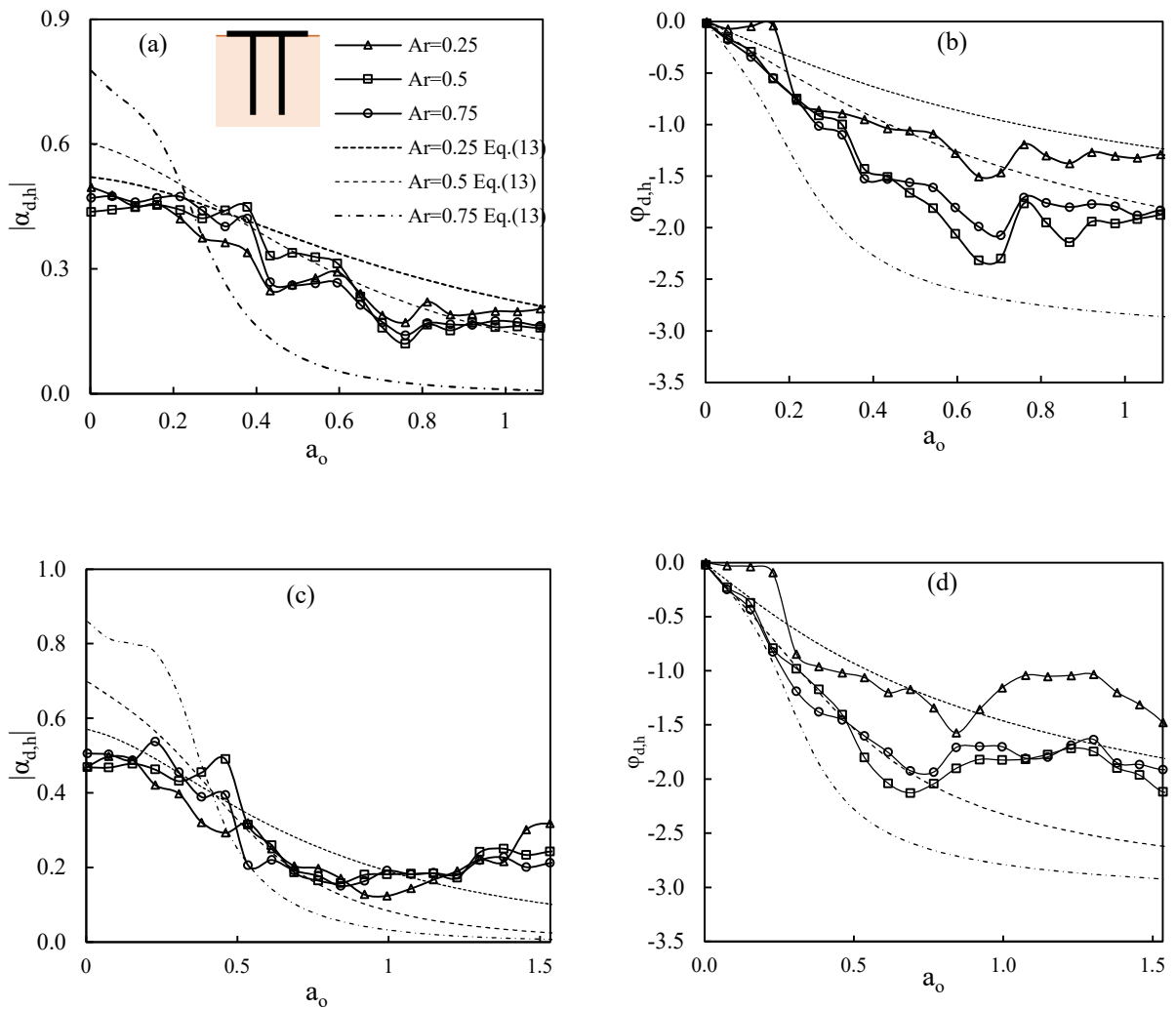


Fig. 5.14 Amplitude and phase of the horizontal dynamic interaction factor for piled rafts in homogeneous soil profile with (a)-(b) $E_p/E_s = 500$, (c)-(d) $E_p/E_s = 1000$

The dynamic interaction factor obtained from the analyses is presented along with comparison using Eq. 5.10 and Eq. 5.11 for two different homogeneous soil profiles in Fig. 5.14. For the piled raft models considered in this study, the pile spacings are non-uniform. The prediction is found to produce a noteworthy scatter in the estimate of the interaction factor, for $A_r=0.25$ as shown in Figures 5.15 (a,b).

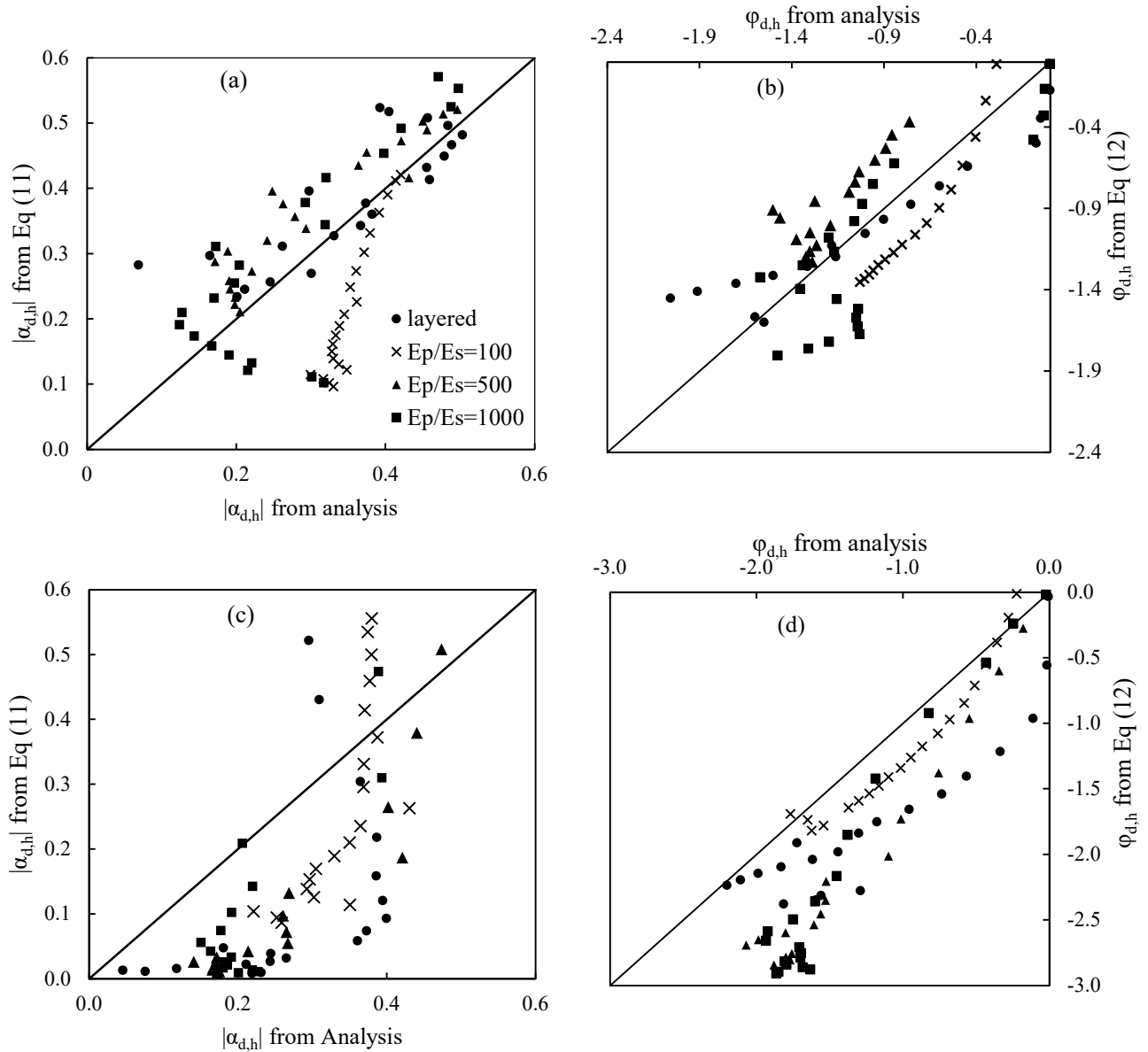


Fig. 5.15 Comparison of amplitude and phase of dynamic interaction factor for piled rafts from the analysis and prediction equations for (a)-(b) $A_r=0.25$ and (c)-(d) $A_r=0.75$

The comparison between predicted and calculated values of interaction factor for $A_r=0.75$ where the spacing in the x direction is 2.4 times the spacing in y direction exhibits a larger error as presented in Fig. 5.15 (c,d). The reason for the scatter can be attributed to the fact that the piled raft models considered in the study by Nagai (2019) were square piled rafts with area ratio of unity, unlike the models considered in the present study.

5.3 DYNAMIC LOAD SHARING IN PILED RAFTS

Load sharing between the raft and pile group for static loading is a well-studied aspect of piled raft design (Clancy and Randolph 1993; Kumar and Choudhury 2018; Mandolini et al. 2005; de Sanctis and Russo 2008). The load ratio represents the load carried by piles, and can be expressed as:

$$LR = \frac{\text{Load carried by piles}}{\text{Total load on piled raft}} \quad (5.15)$$

The load sharing behaviour for static loading is known to vary with settlement of the piled raft foundation due to the mobilization of pile skin friction. However the variation of load carried by piles for dynamic loads, is a function of the dynamic interaction between the components. Nakai et al. (2004) reported a relatively frequency independent load distribution from limited studies on a 2x2 piled raft model for frequencies below 12 Hz. Liu and Ai (2017) observed an oscillating behaviour in the load sharing ratio with varying frequency, outlining that pile-soil relative stiffness and slenderness ratio L/d were the governing factors.

5.3.1 Capped Pile: Vertical and Horizontal Vibration

The load ratio in vertical vibration for the capped pile models is presented in Fig. 5.16 (a)-(d) for the layered and homogeneous soil profiles. The load ratio is found to be mostly frequency-independent for the range of frequencies analysed. The maximum deviation from near zero frequency values of load ratio is 6.5% for the case of homogeneous soil profile with $E_p/E_s=1000$. However, the load sharing behaviour is a function of the soil-pile stiffness ratio, with the load carried by the pile decreasing with increasing soil stiffness.

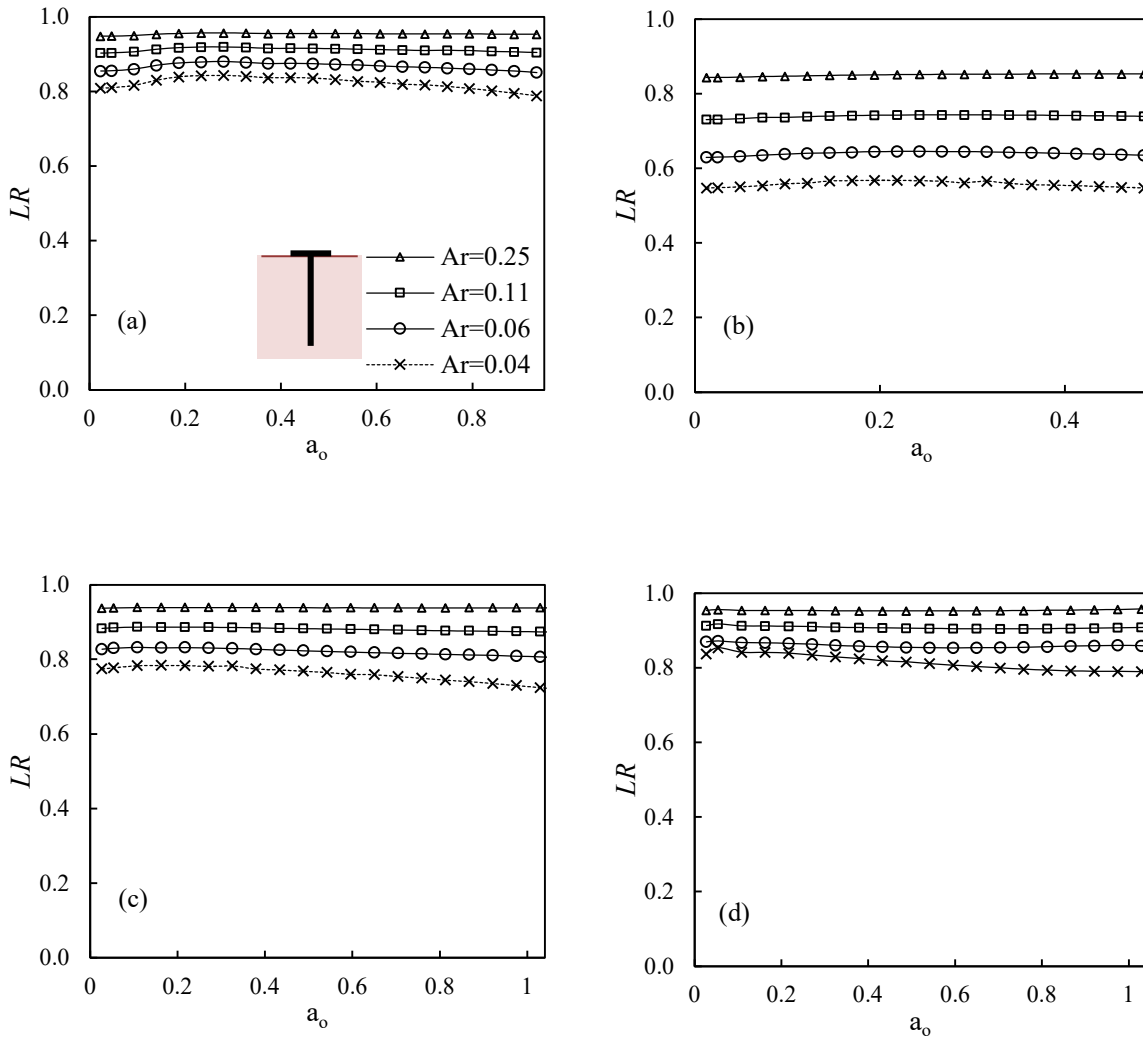


Fig. 5.16 Vertical load ratio for capped pile models in (a) layered, (b) homogeneous; $E_p/E_s = 100$, (c) homogeneous; $E_p/E_s = 500$, and (d) homogeneous; $E_p/E_s = 1000$ soil profiles

The load ratio in horizontal mode of vibration for the various soil profiles is presented in Fig. 5.17 (a-d). Apart from the case of stiff homogeneous soil stratum ($E_p/E_s = 100$), the load ratio in horizontal mode exhibits a mildly increasing trend with increasing frequency. A maximum increase in load ratio of 30%, from the near-zero frequency value, is found for the model with $Ar=0.04$. It should be noted that for frequencies of concern for seismic design, the load ratio in both vertical and horizontal modes are practically frequency independent.

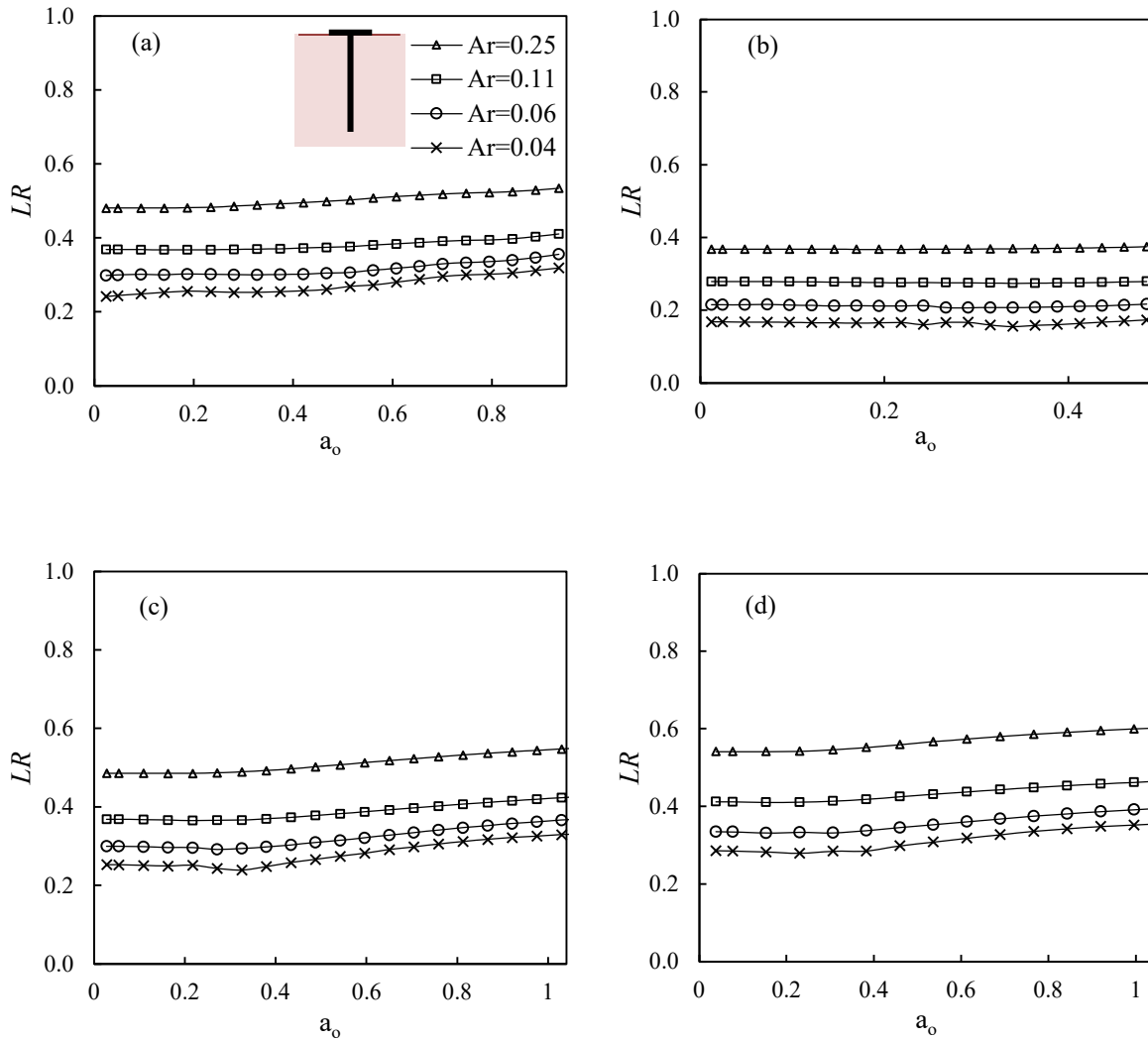


Fig. 5.17 Horizontal load ratio for capped pile models in (a) layered, (b) homogeneous; $E_p/E_s=100$, (c) homogeneous; $E_p/E_s=500$, and (d) homogeneous; $E_p/E_s=1000$ soil profiles

5.3.2 Piled raft: Vertical and Horizontal Vibration

The load ratio in vertical vibration, for piled raft models exhibits a clear dependence on frequency as well as pile-soil modulus ratio as seen in Fig. 5.18 (a)-(d). The influence of area ratio is however observed to be minimal. For the case of piled raft in layered soil profile, the load carried by piles follow a decreasing trend with frequency beyond an a_o value of 0.3, with a maximum variation of 35% in comparison with near zero frequency values. The dependence of LR on frequency is minimal for the case of homogeneous profile with $E_p/E_s=100$. As shown in Figs. 5.18 (c,d) for homogeneous soil profiles with higher pile soil stiffness contrast, the load

carried by piles is found to increase after a threshold value of a_0 that varies from 0.7 to 0.8. An increase of up to 35% is noted for the case with $E_p/E_s = 1000$.

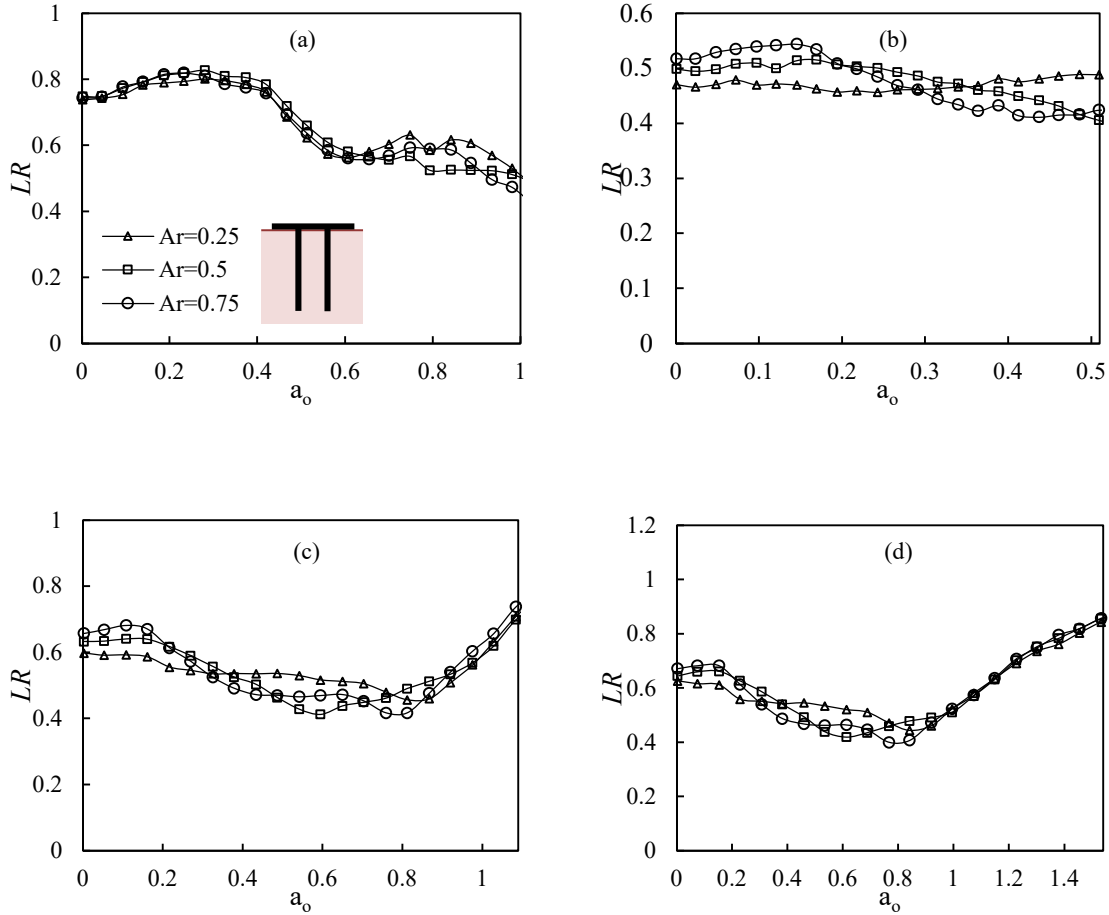


Fig. 5.18 Load ratio in vertical vibration for 2x2 PR in (a) layered, (b) homogeneous; $E_p/E_s = 100$, (c) homogeneous; $E_p/E_s = 500$, and (d) homogeneous; $E_p/E_s = 1000$

Padrón et al. (2009) presented the effect of pile cap separation on dynamic response in terms of moduli and phase differences between PG and PR foundations. The phase difference parameter can be represented as

$$\Delta\theta = \text{phase}(PR) - \text{phase}(PG) \quad (5.16)$$

where the phase is defined as

$$\text{phase}(\text{impedance function}) = \arctan\left(\frac{-k}{a_0 c}\right) + \frac{\pi}{2} \quad (5.17)$$

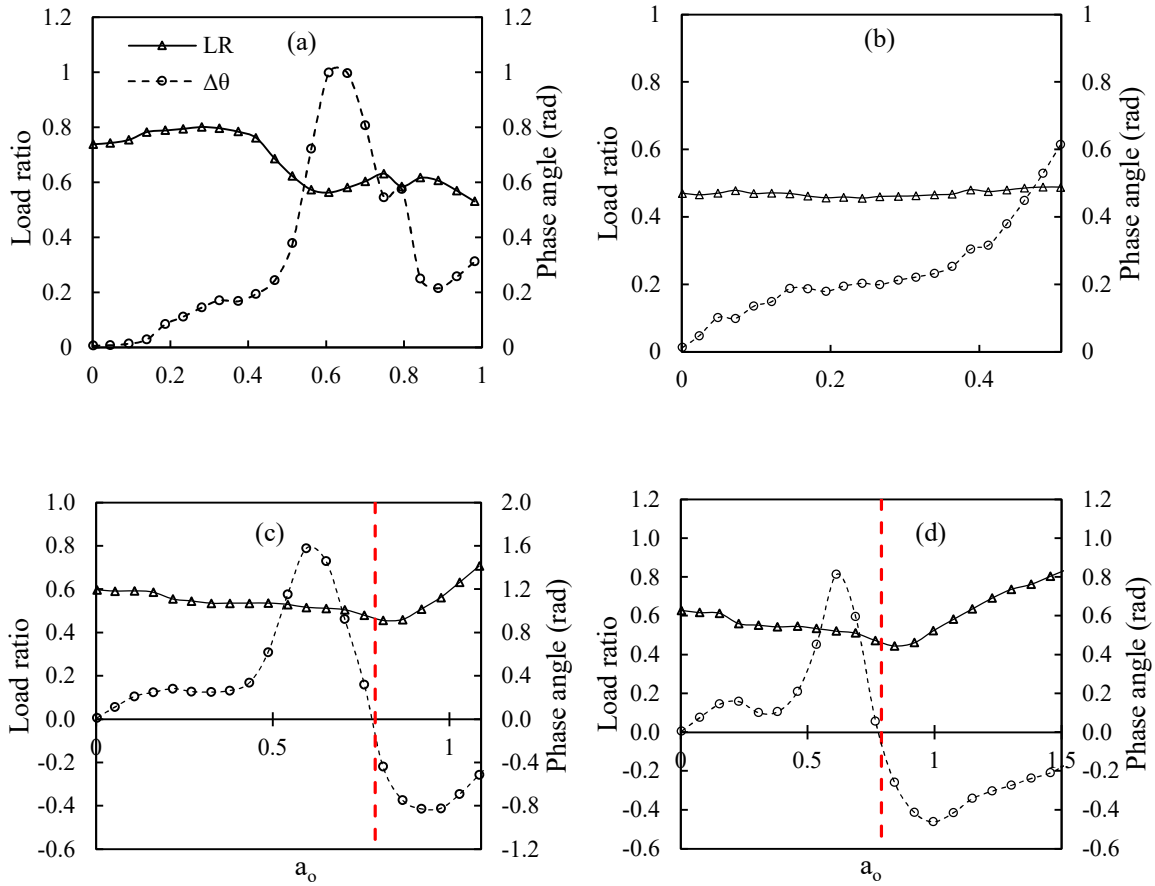


Fig. 5.19 Load ratio in vertical vibration for 2x2 PR with $Ar=0.25$ plotted with phase difference $\Delta\theta$ for (a) layered, (b) homogeneous ($E_p/E_s=100$), (c) homogeneous ($E_p/E_s=500$), and (d) homogeneous ($E_p/E_s=1000$) soil profiles

The parameter $\Delta\theta$ is plotted along with load sharing in vertical direction for various soil profiles in Fig 5.19. It can be noticed that the frequency corresponding to an increase in load sharing also corresponds to the frequency at which the phase difference dips below zero. Intuitively, this represents a situation when the vibration of the pile group is ahead of the vibration of the piled raft.

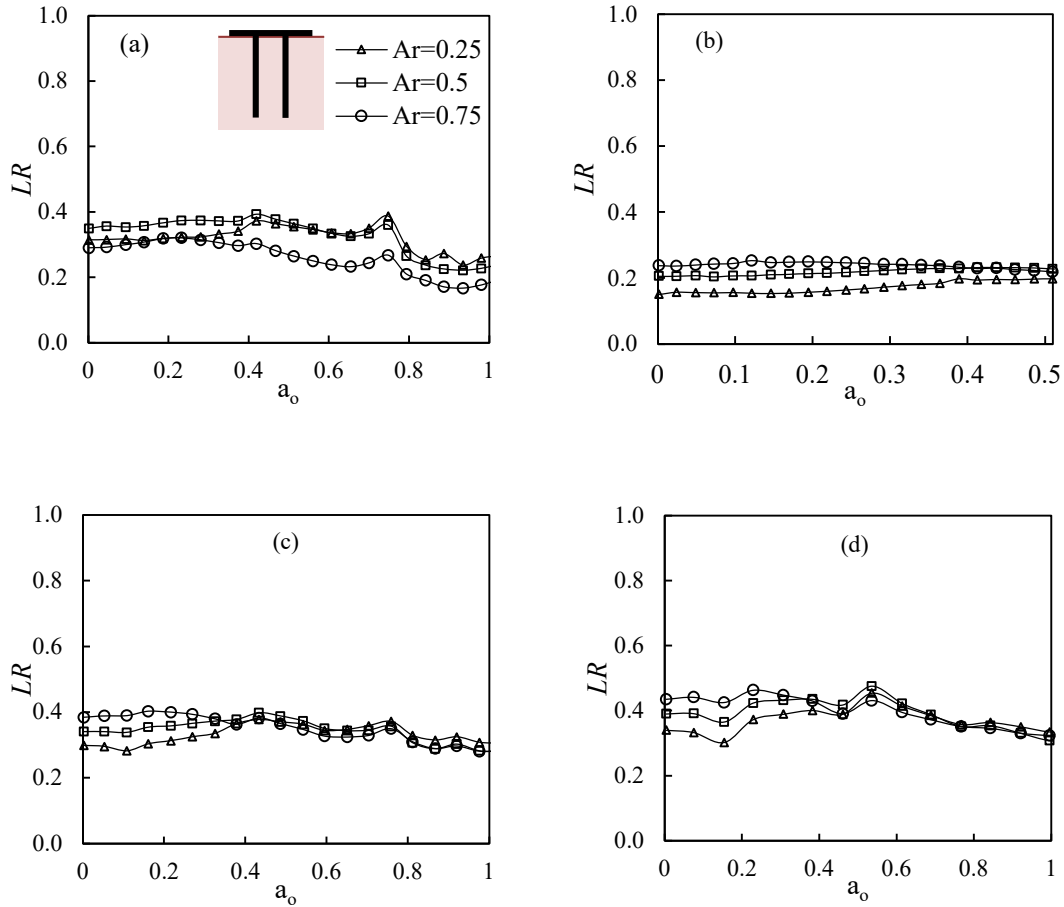


Fig. 5.20 Load ratio in horizontal vibration for 2x2 PR in (a) Layered, (b) $E_p/E_s = 100$, (c) $E_p/E_s = 500$, and (d) $E_p/E_s = 1000$

The load ratio for the 2x2 PR in horizontal mode of vibration is presented in Fig. 5.20. Load sharing in the lateral mode is found to be relatively less dependent on frequency. The dynamic load sharing can be practically assumed to be the same as the static value up to an a_o value of 0.5. The upper limit of variation with frequency is found to be 41% and 26% for the case of layered and homogeneous soil profiles respectively. The load ratio determined from static analysis can be adopted for practically homogeneous soil profiles. The influence of area ratio is evident at lower frequencies owing to static distribution of loads. However, at frequencies close to and beyond $a_o=0.5$, the influence of area ratio is observed to diminish for piled rafts in homogeneous soil profiles.

5.4 CONCLUDING REMARKS

The influence of embedded rafts on the vertical and horizontal dynamic response of piled rafts is studied using numerical analyses. The case of a piled raft foundation supporting dynamic loads from a compressor system is presented. Three-dimensional FEM-BEM based numerical models were developed to study two foundation groups, namely capped pile and piled rafts. Vertical and lateral dynamic response characteristics of the capped pile and piled raft systems were then studied for four different soil profiles.

The measured dynamic response of the full-scale pile showed moderate nonlinearity. The resonant frequency was observed to decrease below natural frequency observed from free vibration tests, with increasing force intensity. The 3D model was found to simulate the free vibration response with a fair degree of accuracy. Simulation of the forced vibration response was found to follow the experimental results for lower force intensity. Displacement amplitudes at higher force levels could be simulated with a maximum error of 33%.

The presence of a circular ground-contacting cap on a single pile was found to have a significant influence on the stiffness and damping coefficients. For models with low area ratio, a clear trend of decreasing stiffness coefficient and increasing damping coefficient, with increasing frequency is noted for both vertical and horizontal vibration modes. The alteration in impedance functions due to an embedded raft is found to become prominent when the pile-soil stiffness ratio, E_p/E_s was reduced from 1000 to 100. The piled raft dynamic interaction for vertical vibration exhibits characteristics of a dynamic system. Amplitude and phase of the dynamic interaction factor were found to be strongly influenced by both pile-soil modulus ratio and area ratio of the piled raft. Available prediction equations for horizontal dynamic interaction factor were found to produce large deviations in predicted amplitude and phase for piled rafts with non-uniform pile spacing.

The ratio of the load carried by the pile in a capped pile was found to be primarily dependent on the relative pile-soil stiffness than the frequency of vibration, in the vertical mode of vibration. However, for 2x2 piled rafts, the load ratio was found to be influenced by both frequency and pile spacing in the vertical mode of vibration. When compared to static loading, a decrease of up to 40% in the load carried by piles was observed for dynamic loading in stiff soil profiles. However, as the pile-soil stiffness contrast increased, the load ratio was found to

increase at higher frequencies. Design of the piled raft for high-frequency dynamic loads thus has to consider the deviation from static load sharing at high frequencies. Load ratio in the horizontal mode of vibration was found to be mildly affected by the frequency of loading, for both capped pile and piled raft models. In the case of piled rafts, deviation from static load ratio occurs beyond a dimensionless frequency value of 0.5 and is more prominent for the case of the layered soil profile. For the frequencies range typical of seismic loads, the load ratio from the static analysis can be adopted for practical design.

CHAPTER 6

1-G SHAKING TABLE EXPERIMENT ON MODEL PILED RAFT IN CLAY

6.1 INTRODUCTION

Physical modelling in controlled conditions is known to give valuable insights into the complex physics of soil-pile interaction. Model studies are capable of simulating phenomena in conditions that cannot be achieved in the prototype scale. Scale model tests have been the source of calibration benchmarks for theoretical models on soil-pile interaction (Anoyatis 2013; Goit and Saitoh 2018; Roy et al. 2018). The key difference between shaking table tests in 1-g and n-g conditions lies in the simulation of the stress field in the soil. This becomes critical for tests with cohesionless soils in which the stress-strain behaviour is dependent on the confining pressure. This limitation does not apply in the case of cohesive soils, in which the undrained stress-strain behaviour is not dependent on the confining pressure. However, a number of researchers (Chau et al. 2009; Durante et al. 2016; Hamayoon et al. 2016; Pitilakis et al. 2008) have studied seismic soil-pile response in cohesionless soils, to arrive at qualitative results on the mechanics governing dynamic pile behaviour. 1-g shaking table tests are generally conducted using much larger shear boxes than in centrifuge tests. This provides a greater convenience with regard to instrumentation, control and observation.

This chapter focuses on the experimental program conducted to study the seismic response of a piled raft in clay. The problem has been investigated through a 1-g shaking table test with instrumented piled raft and pile group models in clay. The experiment was carried out at the 3 m x 3 m shaking table facility at the Department of Civil Engineering, IIT Madras. The aim of the test was to study the effect of an embedded pile cap or raft, on the kinematic response of a 2x2 pile group in homogeneous clay. The two scaled down foundation models were installed in the same clay bed, and were subjected to the same base excitation for the purpose of comparison. The effect of an embedded raft on the kinematic response of a 2x2 pile group was evaluated by comparing the transfer functions of the response of a piled raft and pile group. This chapter elaborates the methodology of physical modelling and the results obtained.

6.2 SCALE MODEL SIMILITUDE IN 1-G ENVIRONMENT

Several theories of scale model similitude that relate the behaviour of the model and prototype have been postulated by researchers for a variety of applications. Methods for scale modelling applications can, in general, be categorized as dimensional analysis, similitude theory, and the method of governing equations (Kline 2012). In addition, Geotechnical engineers have also developed constitutive similarity to model nonlinear behaviour of soils (Roscoe 1968). The dimensional analysis involves reducing a parameter to its simplest form in terms of natural units, and developing scale factors for each of them. Dimensional analysis involving the Buckingham Pi Theorem has been employed by several researchers to arrive at similitude relations for soil-pile structure interaction (Gohl 1991; Kana et al. 1986; Meymand 1998). Moncarz and Krawinkler (1981) have shown that, the Cauchy condition whereby the ratio of model to prototype specific stiffness (ratio of modulus of elasticity to density) equals the geometric scaling factor, is necessary for replicating the restoring forces, inertial forces, and gravitational forces that are critical in earthquake engineering applications. Scale modelling techniques can meet the similitude requirements to the prototype with varying degrees that are often categorized as ‘true’, ‘adequate’, and ‘distorted’ (Moncarz and Krawinkler 1981). A true model satisfies all the similitude requirements whereas an adequate model allows for secondary influences to deviate. Researchers have employed adequate models for soil-pile interaction studies, in which the primary parameters such as pile geometry, and flexural rigidity were satisfied whereas secondary parameters such as mass per unit length were allowed to deviate (Meymand 1998; Moss et al. 2010).

The phenomenon of soil-pile interaction too complicated to be expressed in a single governing differential equation. It is also not feasible to attain true similarity by applying the dimensional analysis or similitude theory. Researchers in the past have adopted the principle of modelling accurately the primary forces in the system and suppressing the secondary effects that do not contribute significantly to the system response. A 1-g test on a clay-pile system provides certain intrinsic controlling conditions to establish many of the scaling parameters viz. the acceleration in model and prototype remaining the same, the model soil density remaining the same as the prototype density, and the undrained stress strain response of saturated clay is being independent of confining pressure. The dimensional analysis framework to arrive at dynamic similarity where both model and prototype experience homologous forces is not repeated here

for brevity. The scaling relations for primary variables governing clay pile interaction in terms of the geometric scale factor, λ is presented in Table 6.1.

Table 6.1 Scaling relations for primary variables

Length	λ	Mass density	1	Acceleration	1
Force	λ^3	Stress	λ	Strain	1
Stiffness	λ^2	Modulus	λ	EI	λ^5
Time	$\lambda^{1/2}$	Frequency	$\lambda^{-1/2}$	Shear wave velocity	$\lambda^{1/2}$

6.3 MODEL SOIL

6.3.1 Synthetic Clay

Clay bed for shaking table tests are usually reconstituted natural clays or synthetic clay mixes. The goal is to prepare a homogeneous clay bed with the least possible air voids or impurities. Reconstituted soil is often used in centrifuge testing where consolidation can be achieved by the centrifuge spin-up. In 1-g conditions consolidation can be deemed impractical due to the sheer size of the container. Another challenge with using reconstituted soils in 1-g testing is to satisfy the scale modelling criteria. Therefore, the clay needs to be workable for the purpose of mixing and placing in the laminar box, and it needs to satisfy the shear strength and shear wave velocity criteria at the time of shaking table testing. The use of natural clay was ruled out considering the difficulty in achieving homogeneity and satisfying similitude criteria. Previous researchers have tackled this situation by preparing synthetic clay mixes that gain strength with time by virtue of added chemicals agents such as Fly ash or lime (Meymand 1998; Tabatabaiefar 2012).

In this study, a synthetic clay mix proportion was adopted keeping in mind the twin requirements of scale modelling as well as workability during placing. Extensive studies with model clay have been reported from the University of California, Berkeley (Arango-Greiffenstein 1971; Bray 1991; Clough and Seed 1963; Meymand 1998; Sultan and Seed 1967). The primary ingredients in the “Berkeley recipe” were Kaolinite and Bentonite in the proportion of 3:1. Clough and Seed (1963) used this proportion with a water content of 200% as the mix was found to arrest the consolidation process over the testing time, as well as exhibit considerable thixotropy. Meymand (1998) used Class C fly ash in the mix as an admixture with

the aim of improving the shear stiffness without a considerable influence on the undrained shear strength. The clay mix composed of 67.5% Kaolinite, 22.5% Bentonite, and 10% class C fly ash with 100% water content, adopted by Meymand (1998) was used as a reference in this study. Developing a new synthetic clay mix for a particular prototype soil was deemed out of the scope of the current research. Studies by Hokmabadi (2014) and Tabatabaiefar (2012) have shown that similar dynamic soil properties can be achieved by adding a calculated proportion of class F fly ash together with lime. Hokmabadi (2014) adopted a class F fly ash and lime mix in the ratio 4:1 which constituted 20% by weight of the dry synthetic clay. Following these studies, a mix of Kaolinite, Bentonite, Fly Ash and Lime powder in a proportion of 60:40:16:4 was adopted for this study.

To check the suitability of this mix proportion, locally available ingredients were evaluated. Kaolinite sourced from Chennai was found to have a Liquid Limit of 32 and a Plastic Limit of 17. Na-Bentonite powder available under the SuperPlus brand name was found to have a Liquid Limit of 323 and a Plastic Limit of 32. A 4:1 mix of Class F Fly Ash from the North Chennai Thermal Power Station, and Lime powder was chosen as the admixture. The Class F Fly Ash from this source is reported to have CaO content in the range of 1.2 to 3.3 %, and SiO₂ content in the range of 58.8 to 59.3% (Dhandapani et al. 2018; Kumar and Ramamurthy 2017). The mix of Kaolinite, Bentonite, and Fly Ash in 60:20:20 was found to possess a Liquid Limit of 92, and Plasticity Index of 74. The soil classification according to ASTM D2487-17 would be CH. Following trials with different water contents, it was found that a water content of 80% provided adequate workability for mixing and placing. To determine the time dependent variation in strength and stiffness of the soil mix, vane shear and bender element tests were carried out at different time intervals. The vane shear tests were carried out as per the ASTM D4648 standard. The time varying undrained shear strength of the clay mix from vane shear tests are presented in Fig. 6.1.

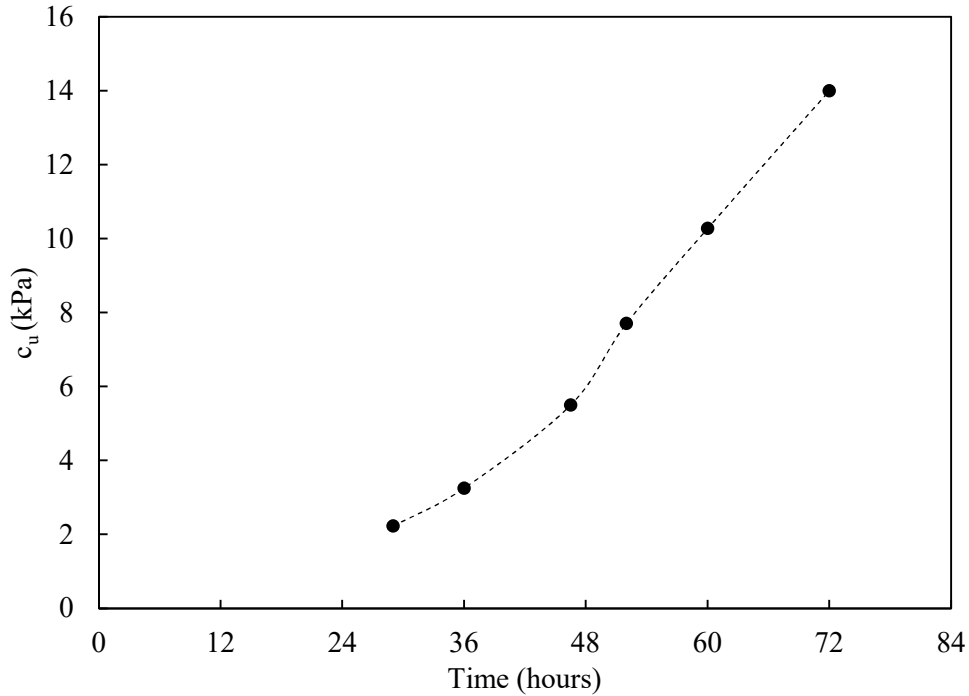
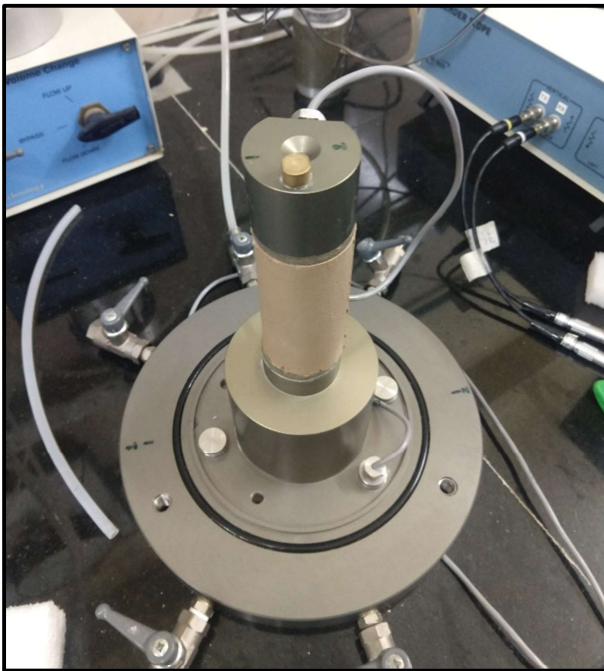


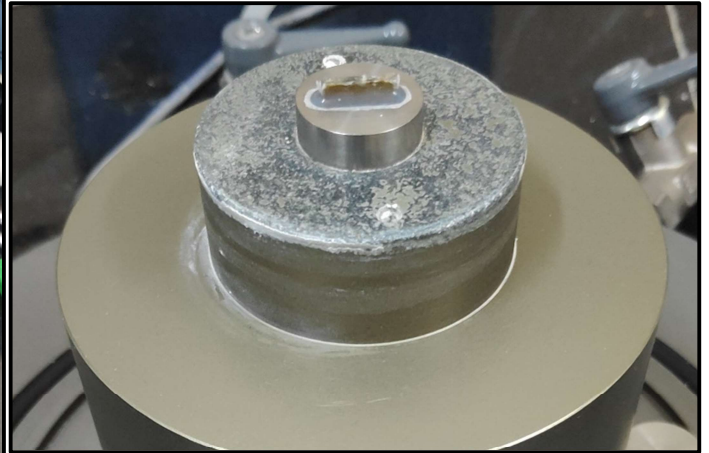
Fig. 6.1 Variation of undrained shear strength with time

6.3.2 Shear Wave Velocity of Synthetic Clay

To determine the variation of shear wave velocity of the clay mix with time, bender element tests were carried out using specimens with diameter of 50 mm and length of 100 mm. The tests were carried out using a bender element apparatus (VJ Tech make). Two piezoelectric bender probes which can transmit and receive shear waves were used to measure the travel time of shear waves through the specimen. The bender probes had a protruding depth of 2mm each. Fig 6.2 shows photographs of the Bender element and the test setup. To replicate conditions in the shaking table test, the specimens were not consolidated or subjected to cell pressure. In this study, sinusoidal shear waves with a frequency of 1 kHz were found to generate the most interpretable waveform. The signal was generated from the bender element placed at the top of the sample and the bender element placed at the bottom was used to capture the arriving wave. The difference in the time of arrival of the first wave was recorded to determine the shear wave velocity, V_s of the soil. A typical plot of the transmitted and received signals are presented in Fig 6.3. The time dependent variation in shear wave velocity for the clay mix, is presented in Fig 6.4. The properties of clay mix after 36 hours of curing is presented in Table 6.2.



(a)



(b)

Fig. 6.2 Photographs showing (a) the bender element apparatus with specimen, and (b) a close up of the bender element

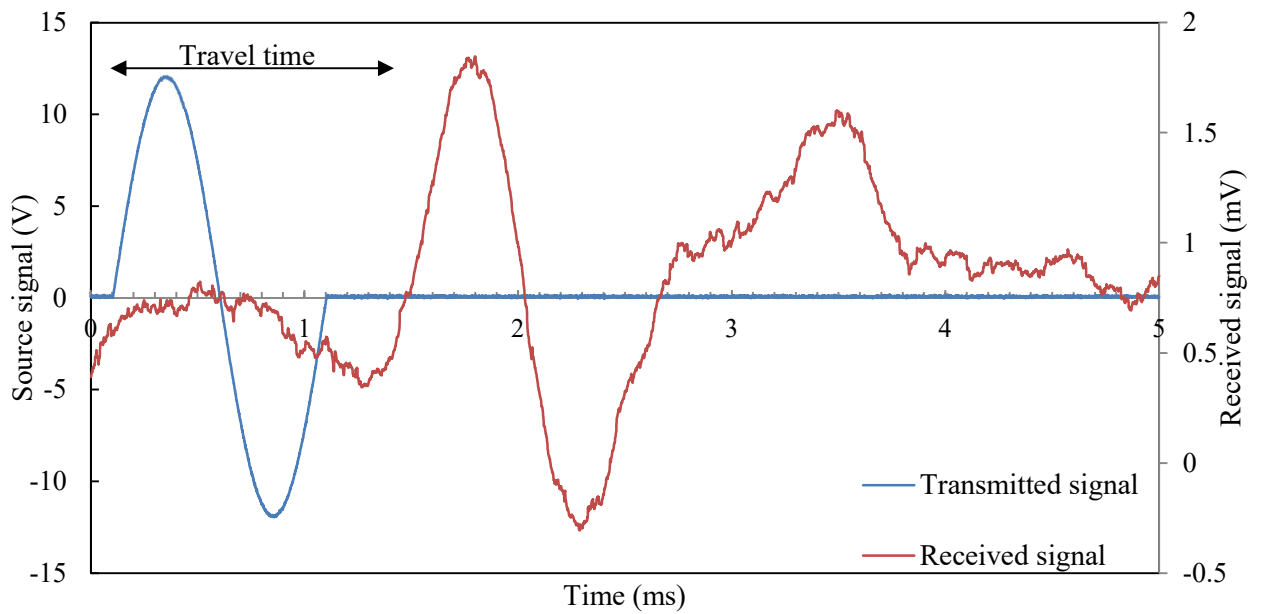


Fig. 6.3 A Plot of the transmitted and received signals recorded

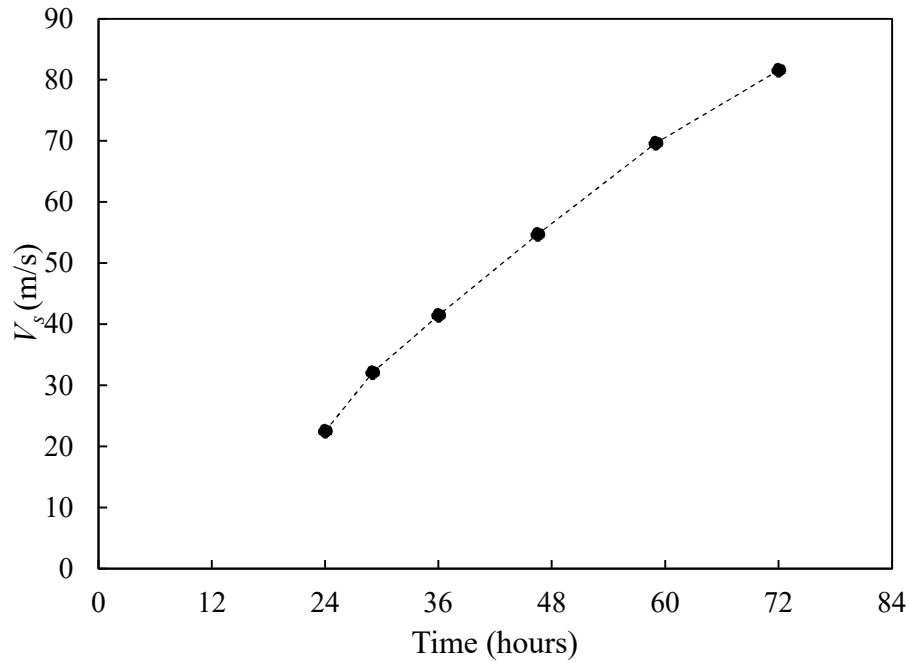


Fig. 6.4 Variation of shear wave velocity with time

Table 6.2 Properties of the clay mix after 36 hours of curing

Property	Value
Mass Density (kg/m^3)	1517
Undrained shear strength (kPa)	3.25
Low strain shear modulus, G_{max} (Mpa)	2.57
Shear wave velocity, V_s (m/s)	40.2

From the time varying shear strength and shear wave velocity plots, it was found that at 36 hours of curing, the clay mix achieves an average shear strength of 3.25 kPa, and a shear wave velocity of 40 m/s. These properties correspond to a prototype shear strength of 97.5 kPa and shear wave velocity of approximately 220 m/s. Considering workability for mixing and placing operation, as well as strength and stiffness gained after 36 hours, the clay mix with 80% water content was chosen as the model soil in this study.

6.3.3 Strain Dependent Shear Modulus and Damping

The high strain dynamic properties of the soil specimens were determined using the electro mechanical fully automated cyclic triaxial apparatus (Make: VJ Tech) as shown in Fig. 6.5. A specimen of size about 50 mm diameter and 100 mm height was placed on the apparatus after 36 hours of curing. The samples were subjected to strain controlled cyclic loading in undrained conditions, as per ASTM D3999. Multistage testing was carried out on two specimens covering strain levels of 0.01%, 0.03%, 0.05%, 0.08%, 0.1%, 0.3%, 0.5%, 1% and 2%. A schematic diagram of the multistage testing is presented in Fig. 6.6. The frequency of loading was maintained at 1 Hz. A time interval of 30 minutes was given between the loading cycles to enable equilibration of pore pressure. The tests were completed in a duration of around 2.5 hours each, such that significant change in soil properties do not happen during the testing.

The hysteresis loops for 1% strain level is presented in Fig. 6.7 (a). It is evident from Kokusho (2017) that the modulus of the soil can be calculated for the cycles between 5 and 10 cycles. In this study the secant modulus from the 5th cycle was adopted. The hysteresis loop corresponding to the 5th loop from 0.3% axial loading is presented in Fig. 6.7 (b). The secant elastic modulus E_{sec} , is determined as shown in Fig. 6.7 (b), and can be used to calculate secant shear modulus G_{sec} using the following equation:

$$G_{sec} = \frac{E_{sec}}{2(1 + \mu)} \quad (6.1)$$

where μ is the Poison's ratio which is taken as 0.5 for the undrained tests. Shear strain (γ) was derived from axial strain (ε) using the formula

$$\gamma = \varepsilon (1 + \mu) \quad (6.2)$$

The equivalent viscous damping ratio was calculated using the equation

$$Damping\ ratio = \frac{1}{4\pi} \frac{W_d}{W_s} \quad (6.3)$$

where W_d and the work done, and W_s is the stored energy calculated as shown in Fig 6.7 (b).



Fig. 6.5 Photograph of the Cyclic Triaxial Test Setup

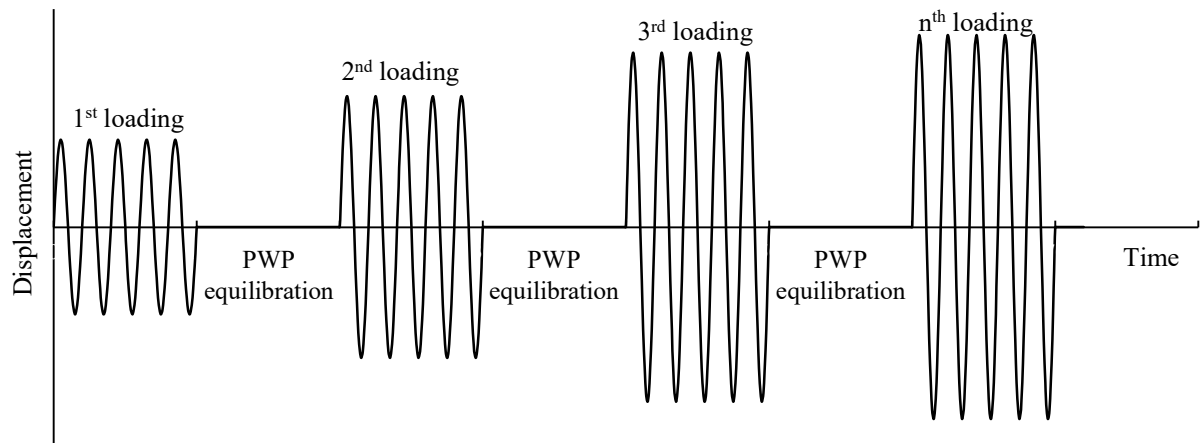


Fig. 6.6 Schematic diagram showing the multistage testing process

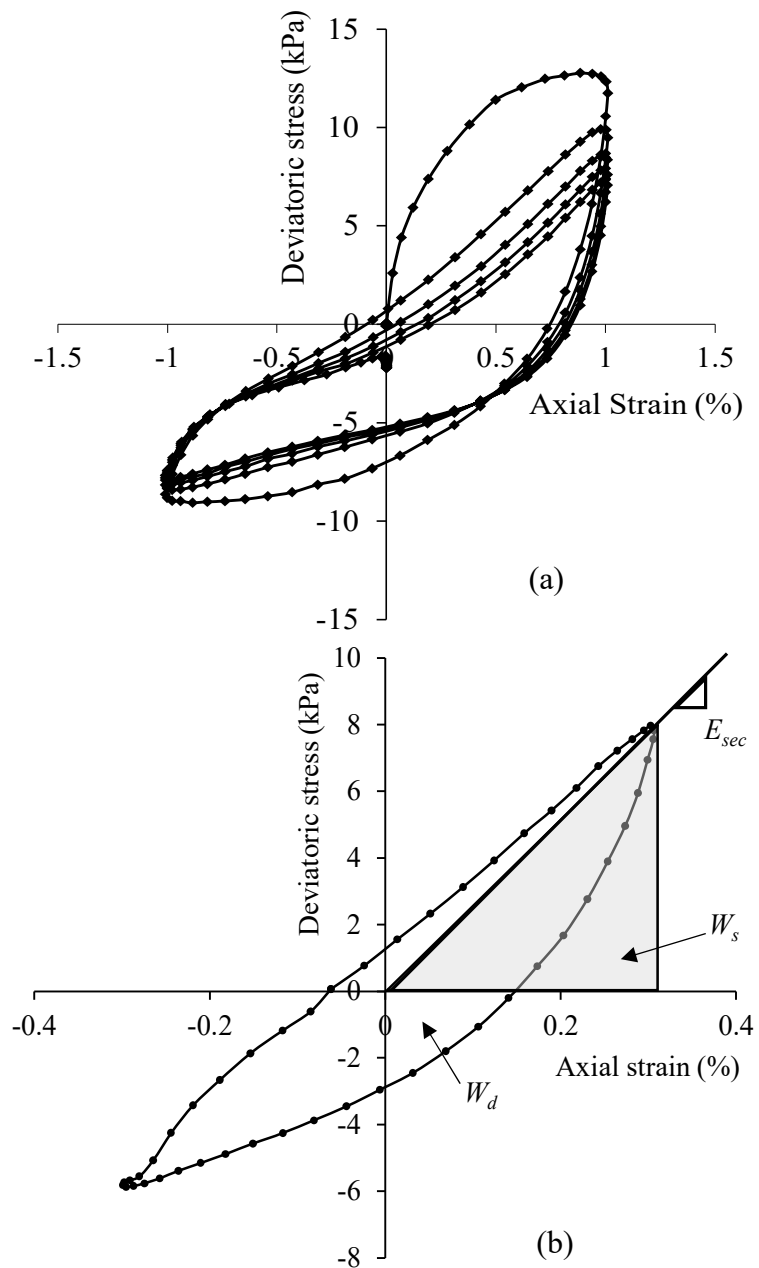


Fig. 6.7 (a) Hysteresis loops for 1% strain and (b) 5th cycle loop for 0.3% axial strain

The strain dependent modulus degradation and damping ratio computed from the experimental results are presented in Fig. 6.8 (a) and (b) respectively.

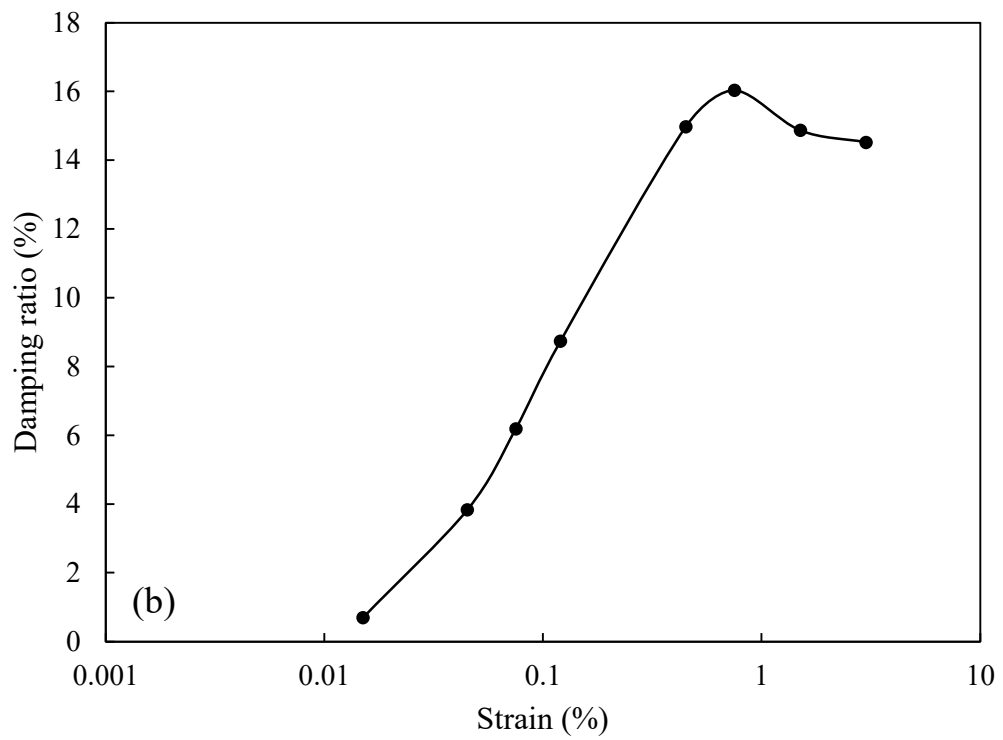
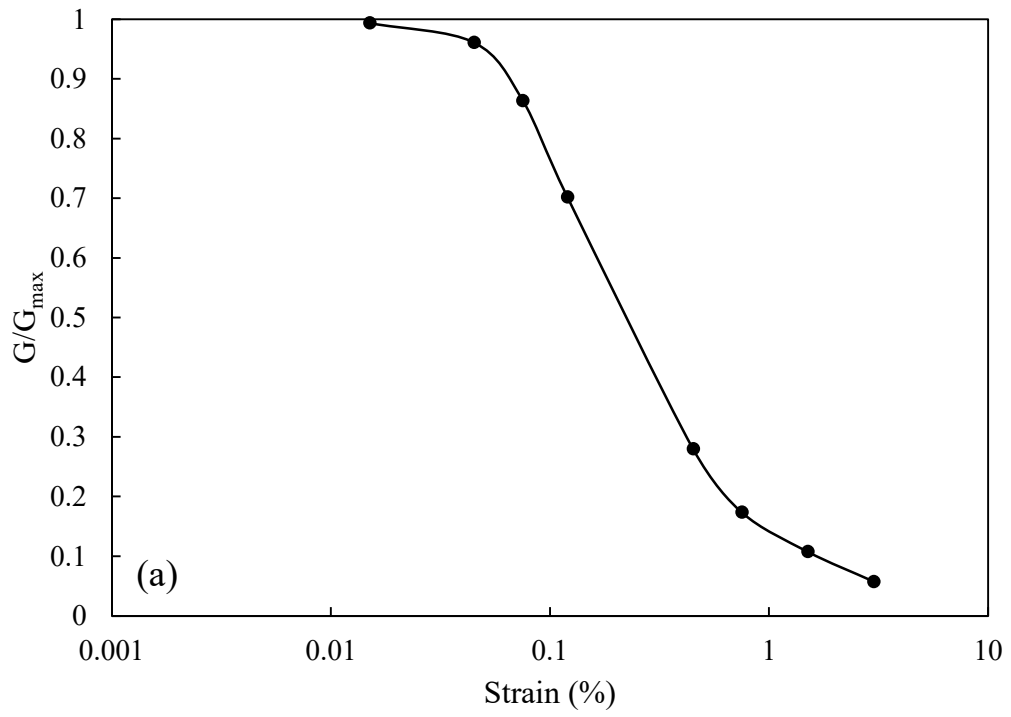


Fig. 6.8 (a) Modulus reduction and (b) Damping ratio curve obtain from cyclic triaxial tests

6.4 MODEL PILED RAFT AND PILE GROUP

A model pile design should ideally satisfy the principal factors governing pile-soil response. The most critical factors influencing pile response are flexural rigidity, length to diameter ratio, moment-curvature mechanism, ductility of material and yield behaviour, fundamental period of vibration, and relative pile-soil stiffness. When geometric similarity is strictly adhered to, pile slenderness, pile to pile spacing, group interaction, and contact surface area would be inherently preserved in the model. The governing equation for a laterally loaded pile can be expressed as

$$EI \frac{d^4 y}{dz^4} = -ky \quad (6.4)$$

where y is the horizontal deflection of the pile, z is the depth and k is a coefficient proportional to the shear modulus of soil, G . From equation 6.4, Durante (2015) showed that the dimensionless parameter (ϕ) to be used for modelling can be described by

$$\phi = \frac{Gd^4}{EI} \quad (6.5)$$

In this study the prototype pile is a circular concrete pile with diameter of 750 mm, length of 18 m, and Young's modulus of 3.16 GPa. Considering the size of the laminar box, and the foundation models, it was decided to adopt a geometric scale factor of 30 in this study. In this regard, the model pile should have a diameter of 25 mm and a length of 600 mm. To satisfy the similitude for frequency of vibration of the pile, the mass per unit length should ideally be scaled by a factor of $1/\lambda^2$ from the prototype. With conventional materials, this criterion could not be satisfied once the primary scaling requirements are satisfied. This is however not expected to significantly affect the vibration characteristics of the entire system.

Previous researchers (Durante 2015; Hokmabadi 2014; Meymand 1998) have used various materials like Aluminum, HDPE, steel for model piles in 1-g testing. Materials like Aluminum, PVC, Acrylic glass etc. were considered as prospective materials for the model pile. Aluminum tube sections however would not satisfy the flexural rigidity similitude for the clay-pile system. The parallel plate test following the ASTM D-2412-11 standard was conducted on three tube specimens each made of PVC and Acrylic glass. Tube specimens with length of 150 ± 3 mm were placed between steel plates as shown in Fig. 6.9 (a). A photograph of the specimens is presented in Fig. 6.9 (b). The specimens were loaded at a rate of 0.5 mm/min and the

displacement was recorded. A plot of the force-displacement for the PVC specimen response is presented in Fig 6.9 (c).

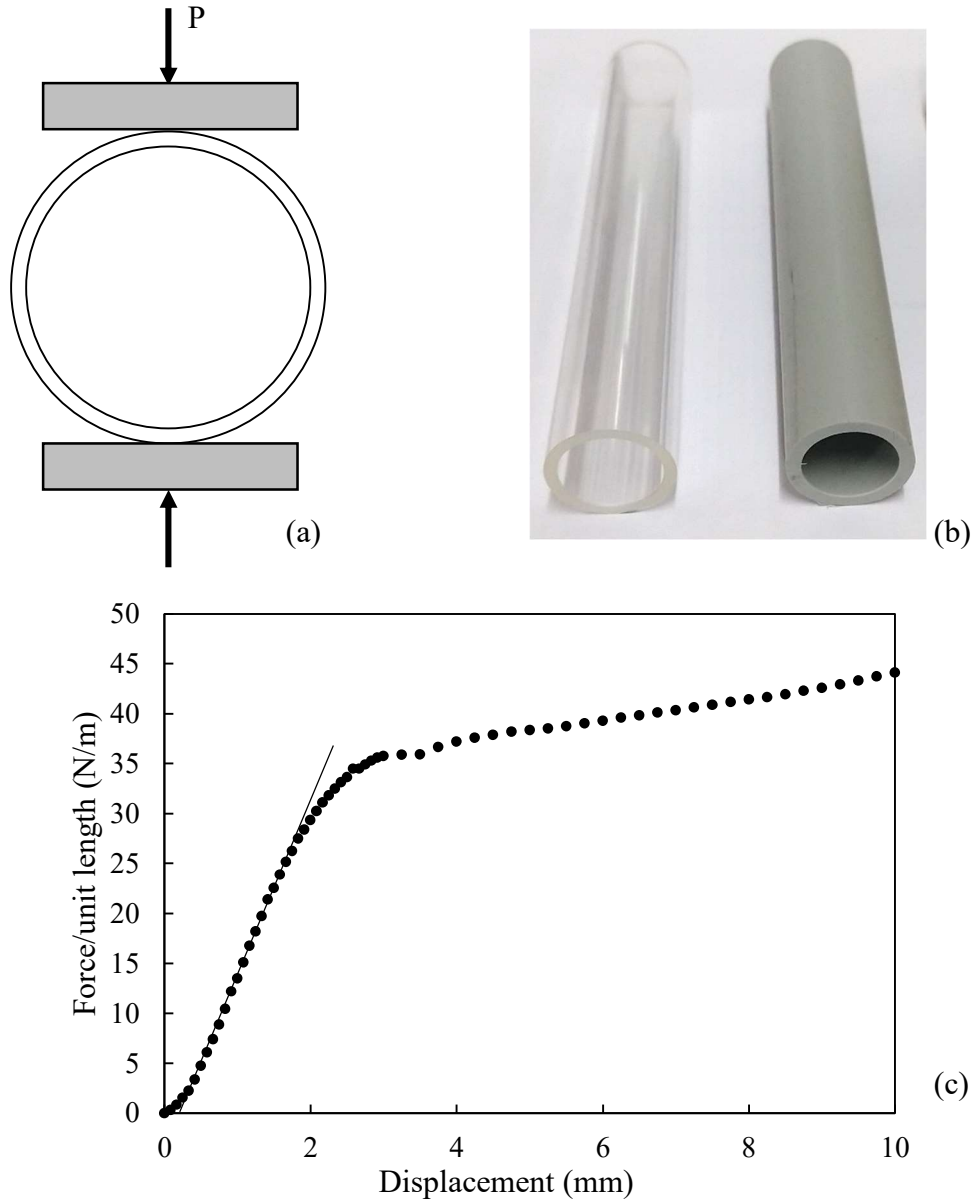


Fig. 6.9 (a) Schematic diagram of the parallel plate test and (b) photographs of the specimens made of Acrylic glass (left) and PVC (right) and (c) Typical load-deflection curve obtained for a PVC specimen

The flexural rigidity was then calculated using the equation:

$$EI = 0.149r^3(F/\Delta y) \tag{6.6}$$

where F is the force per unit length and Δy represents the deflection. The PVC pipe with outer diameter of 600 mm and thickness of 2.36 mm which provides a flexural rigidity close to the target value, was selected as the model pile for this study. Characteristics of the model pile are summarized in Table 6.3.

Table 6.3 Characteristics of the model pile

Property	Value
Outer diameter (mm)	25.00
Wall thickness (mm)	2.36
Young's modulus (GPa)	2.66
Mass per unit length (kg/m)	0.039

The pile group (PG) and piled raft (PR) models were designed with the same pile spacing of 5 times the diameter of pile. Kinematic response is ideally evaluated for massless foundations. The desirable scale model would therefore have a comparable mass for both the pile group and piled raft. A square Aluminum plate of dimensions 224 mm x 224 mm x 18 mm with a mass of 2.45 kg was used as the pile cap for the model pile group. In order to isolate inertial effects from the response of the pile foundation, it is desirable to have the least possible mass at the raft level. Considering the thickness of the raft in the piled raft model, a solid raft would not be feasible for a comparative study due to the influence of inertia forces from the additional mass. In this regard, a raft model with an Aluminum plate at the base and stainless-steel plates of thickness 3 mm as side walls was fabricated. The embedment of the raft was fixed at 100 mm which corresponds to four times the pile diameter. The total mass of the model raft was 3.65 kg. An illustration showing the piled raft model is presented in Fig. 6.10. The side walls of the opposite sides were supported by steel struts to minimize buckling of the plates. Photographs showing the raft and pile cap are presented in Fig. 6.11. The two foundation models along with the locations for bending strain measurement are presented in Fig. 6.12.

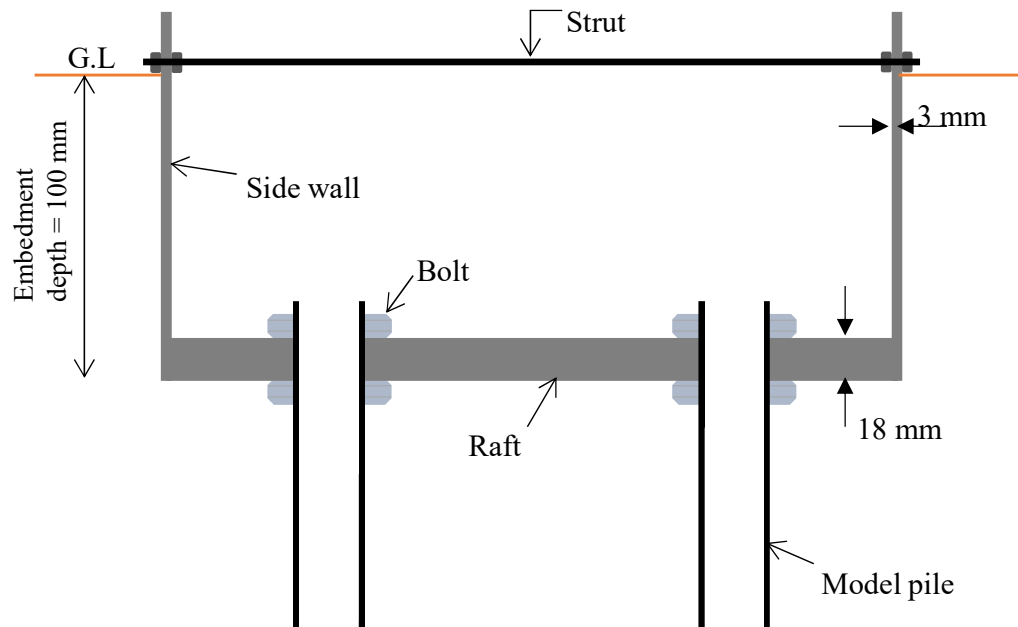


Fig. 6.10 An illustration of the model piled raft



Fig. 6.11 Photographs showing the raft (left) and the pile cap (right)

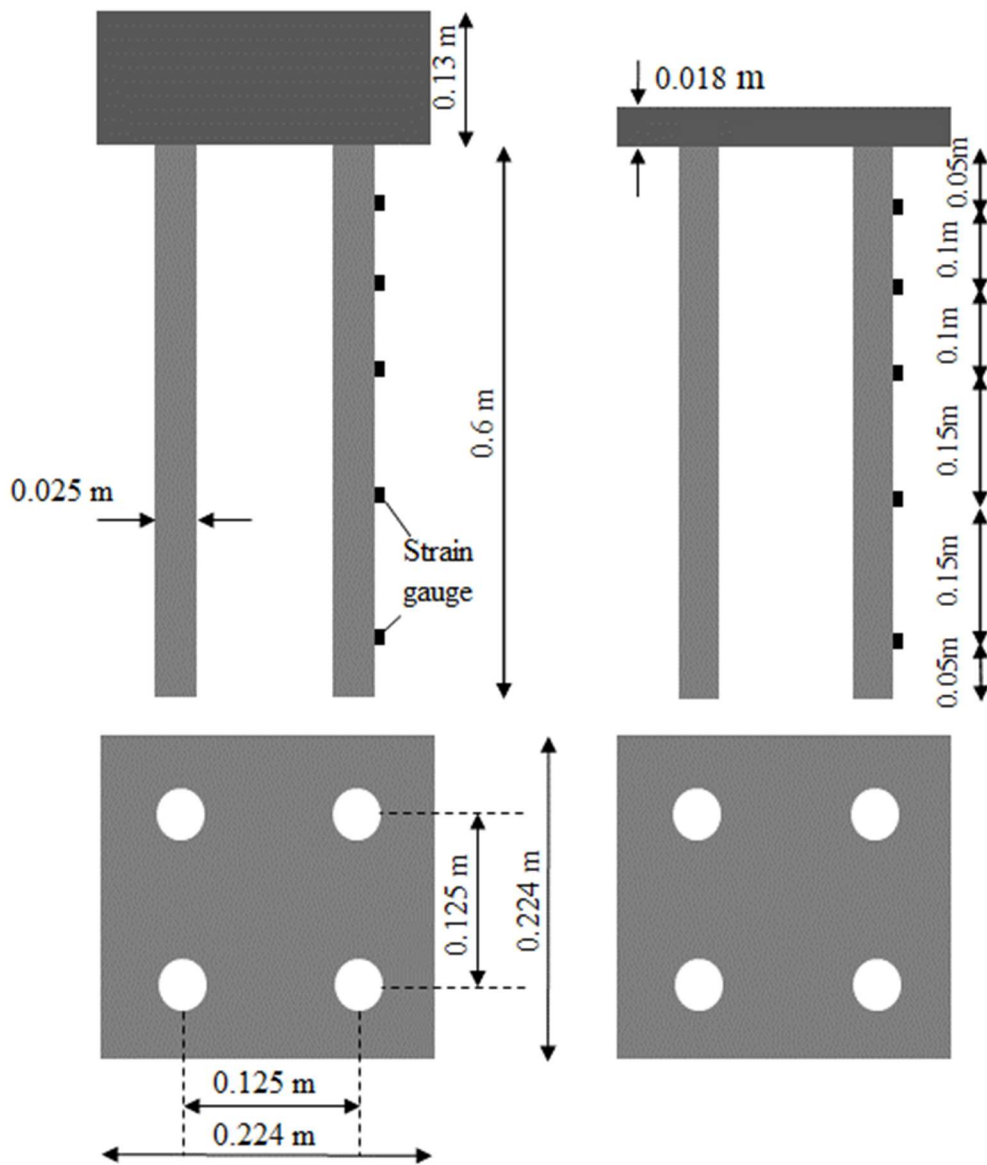


Fig. 6.12 Schematic diagram showing the (a) piled raft and (b) pile group models

6.5 LAMINAR BOX AND SHAKING TABLE

A flexible soil container is critical in modelling accurately, a prototype soil layer of infinite lateral extend. The container is required to support the soil while imposing no boundary condition that exists in the prototype condition. The general understanding is that the soil container can ideally have the same dynamic stiffness and natural frequency as that of the soil inside. Several researchers have designed laminar shear boxes with fundamental mode

frequency close to that of the soil bed (Durante 2015; Hokmabadi 2014; Meymand 1998). However, such a design would be configured for a certain model soil, for which the fundamental frequency is calculated. Another design concept for laminar boxes adopted widely in centrifuge testing involves the criteria of minimal resistance of the laminar box to soil movement. Several researchers have adopted this design philosophy for the design of large laminar boxes for 1-g tests by using roller bearings between the laminar ‘rings’.

In the present study, a laminar box with a length of 1.5 m, a width of 1 m and a depth of 1.2 m was fabricated using Aluminum tube sections of 50 mm x 50 mm. The box was housed in an outer frame for lifting and securing. Figure 6.13 presents the plan and elevation views of the laminar box. A 20mm stainless steel plate formed the base of the box. The laminar box has a translational single direction freedom of motion enforced by guide wheels attached to the outer frame. The laminar box can support a maximum lateral deflection of ± 150 mm. A shear pin was provided at the opposite ends of the laminar box to ‘lock’ the rings in a straight vertical line during model construction. A photograph of the laminar box bolted to the shaking table is presented in Fig. 6.14. The inner walls of the laminar box were lined with a Polystyrene sheet as an energy absorbent medium.

The MTS make 3 m x 3 m biaxial shaking table installed at the Structural Engineering Laboratory at IIT Madras was used in the experimental program. Figure 6.15 shows a photograph of the shaking table. The shaking table has a 10-ton payload capacity with a maximum overturning moment capacity of 30-meter tons. It can generate a maximum acceleration of 1 g with a maximum actuator stroke of 250 mm.

The operational frequency range of the equipment is from 1 Hz to 50 Hz. In this study, the shaking table was operated in the displacement control mode. Prior to the actual test, a calibration run was carried out with a dummy load in the laminar box, that had the equal to the test payload. The feedback command response varying with frequency is shown in Fig. 6.16. The input motion amplitude was adjusted using this response curve so as to control the actual applied displacement.

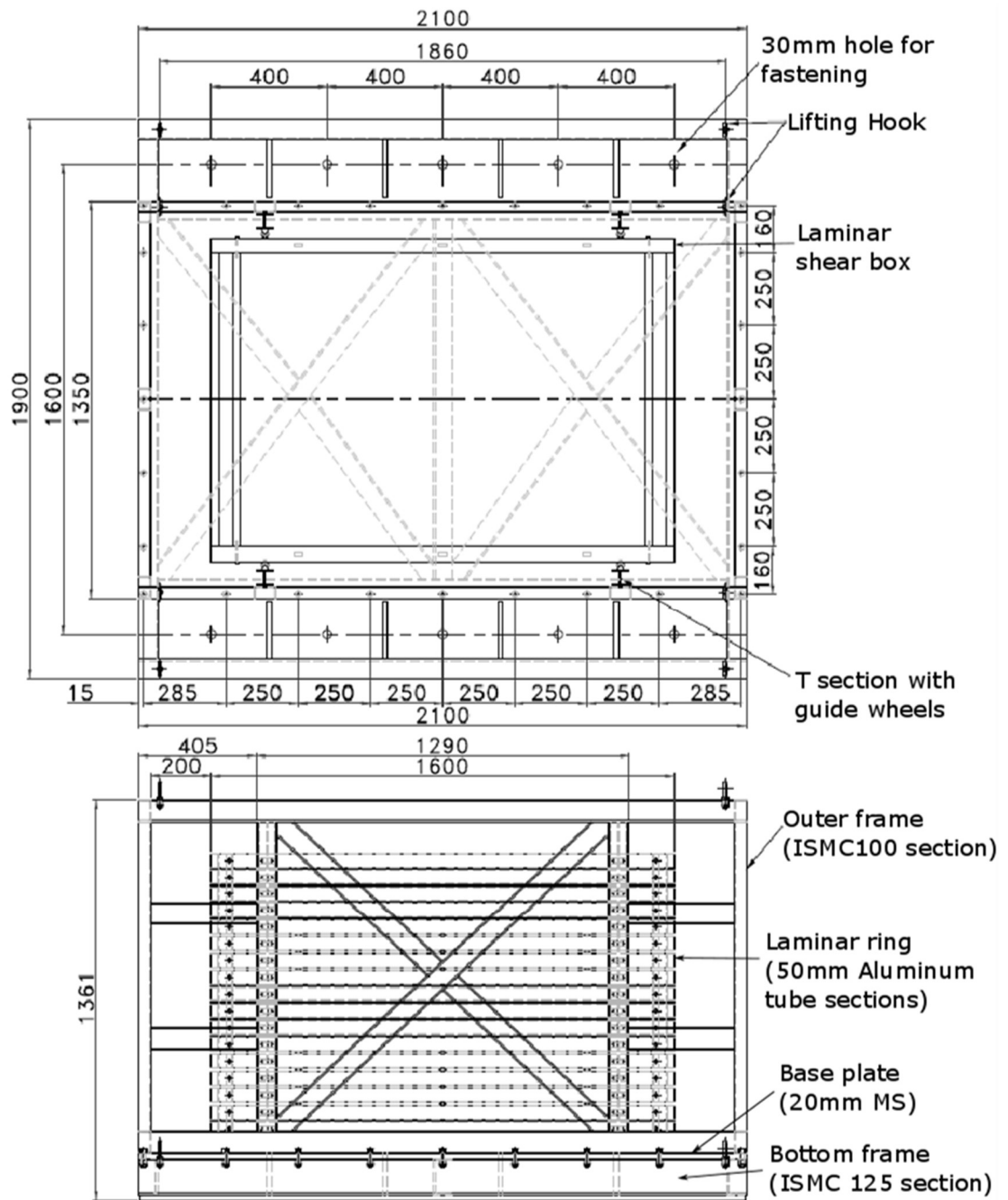


Fig. 6.13 Plan and elevation views of the laminar shear box and outer frame

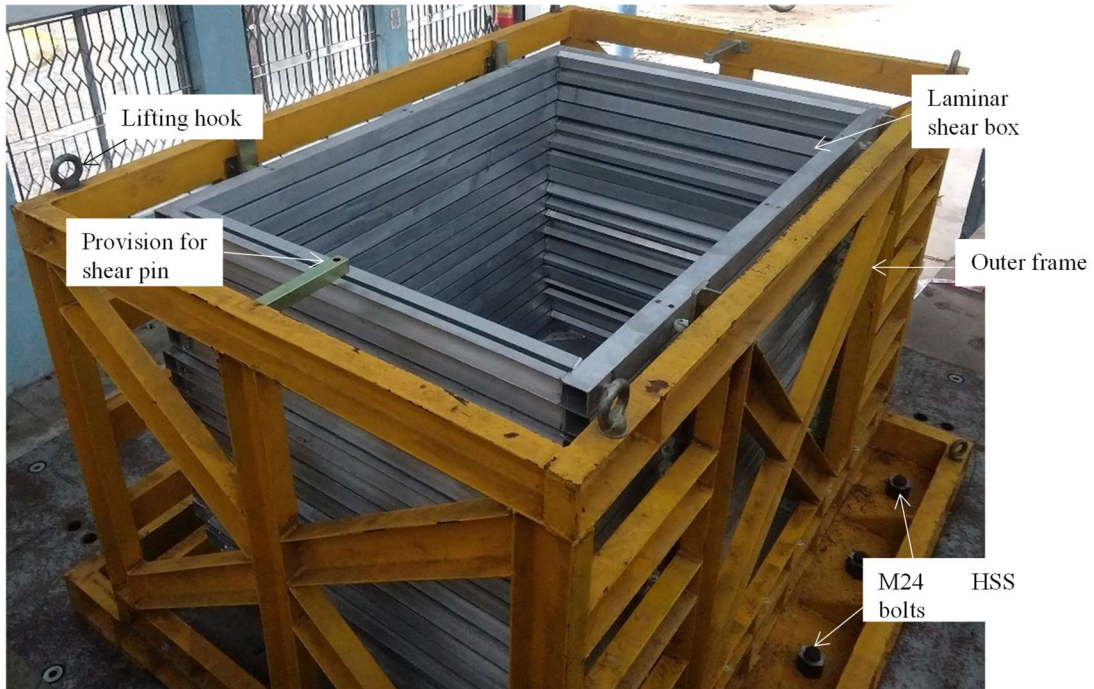


Fig. 6.14 The laminar shear box and the outer frame



Fig. 6.15 The biaxial shaking table at IIT Madras

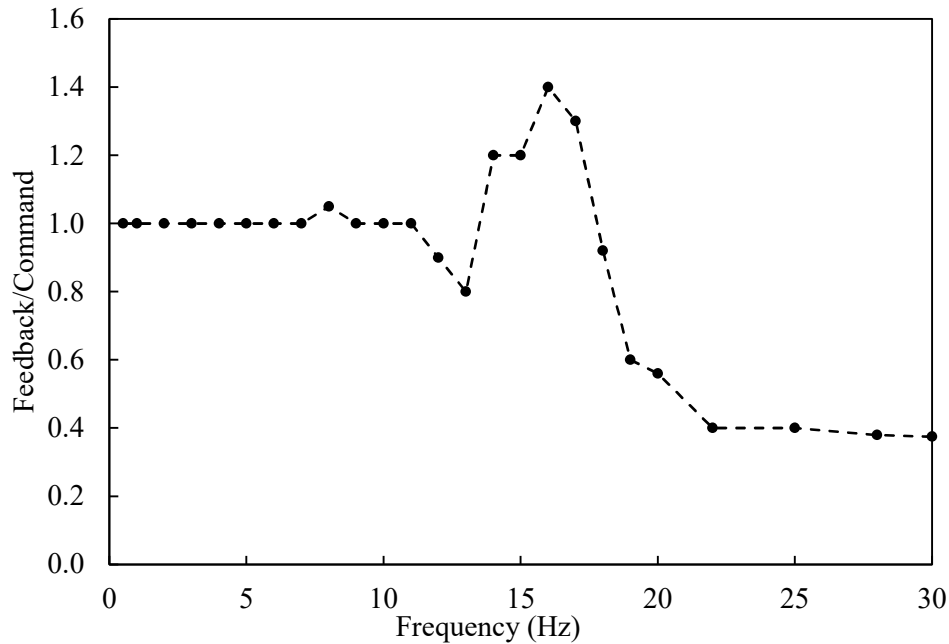


Fig. 6.16 Feedback to command ratio of displacement response

6.6 INSTRUMENTATION AND DATA ACQUISITION

The instrumentation scheme consisted of 10 accelerometers to record acceleration response and a set of strain gauges to measure bending strain in piles. The accelerometers consisted of five PCB make piezoelectric accelerometers and five inductive type HBM B12 accelerometers. The piezoelectric accelerometers had a resonant frequency of above 1500 Hz and an operating frequency range of 0.06 to 450 Hz. Photograph showing the piezoelectric accelerometers attached to the pile cap is presented in Fig. 6.17. The inductive type accelerometers, on the other hand, had a natural frequency of 500 Hz and an operating frequency range of 0 to 250 Hz. A schematic diagram showing the instrumentation is presented in Fig. 6.18.

To measure bending strain in the piles, five TML make 120 ohm strain gauges (Type FLAB-5-11-1LJC-F) were pasted on one pile in each of the pile groups. The strain gauges had a gauge length of 5 mm, gauge factor of 2.1 and a transverse sensitivity of 0.3 %. They were glued to the pile surface and protected using an epoxy coating. The transducers were connected to an MGC plus data acquisition system. The data was recorded in a laptop computer using the Catman program interface.

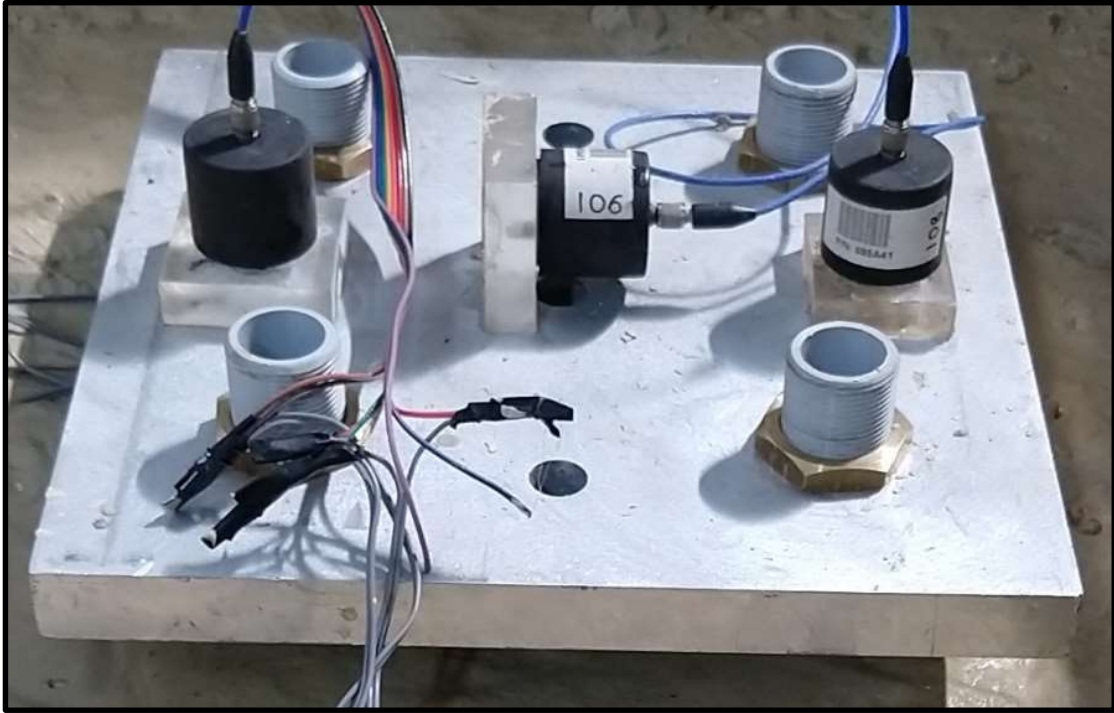


Fig. 6.17 Piezoelectric accelerometers attached to the pile cap

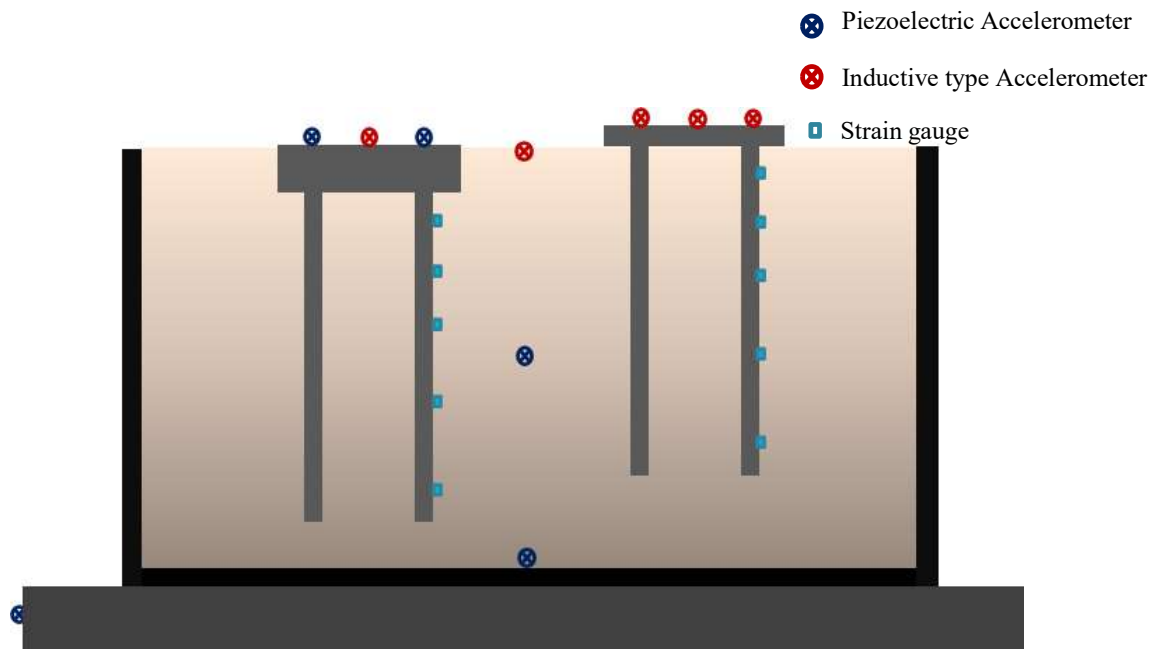


Fig. 6.18 Schematic diagram of the instrumentation scheme

6.7 MODEL CONSTRUCTION

The inner surfaces of the laminar box were first lined using a flexible tarpaulin membrane, in addition to the layer of polystyrene, to prevent leakage of water. The clay bed was prepared in two stages. The batching and mixing of dry Kaolinite powder, Bentonite powder and Fly Ash was carried out one day prior to the wet mixing. The lime powder was added just before wet mixing was commenced. The wet mixing was carried out in batches by adding dry mix into the water in a tank and blending using a handheld power mixer. Fig. 6.19 (a) shows the wet mixing process using a power mixer. The clay was then placed into the laminar box, and light tamping was applied to minimize air voids. The time elapsed from the commencement of mixing to the placing of the last batch was six hours. Fig. 6.19 (b) shows the finished clay bed.

The model piled raft and pile group were then carefully inserted into the clay bed. This procedure was carried out 6 hours after the placing was finished. A free headed single pile model was also placed in the clay bed along with the PG and PR models. The spacing between the PR and PG models was maintained at around 25 times the pile diameter to minimize the effects of interaction between the two. A layout of the foundation models in the shear box is presented in Fig. 6.20.



Fig. 6.19 (a) Wet mixing using power mixer, and (b) finished clay bed

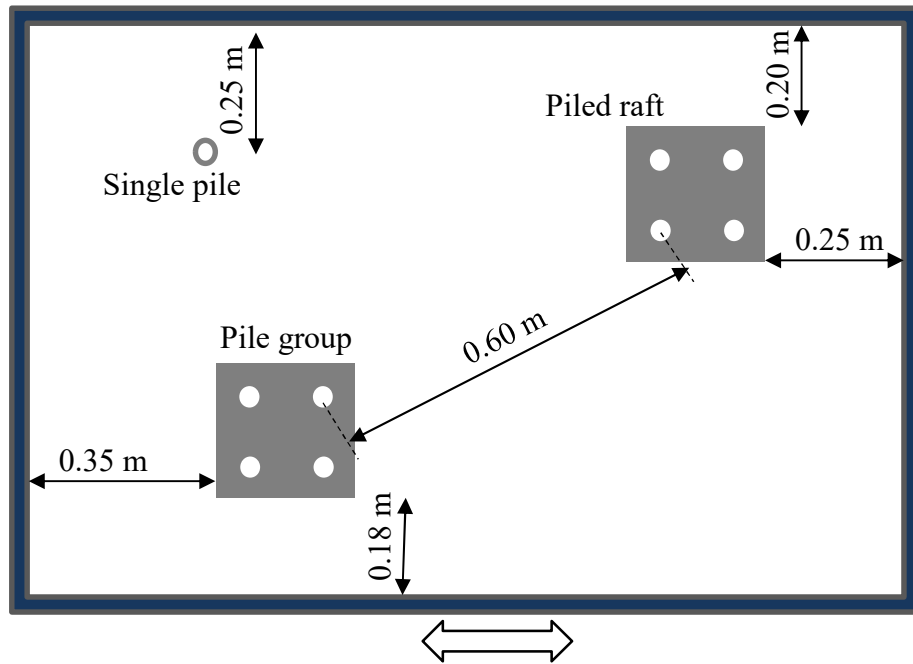


Fig. 6.20 Layout of the foundation models inside the laminar box

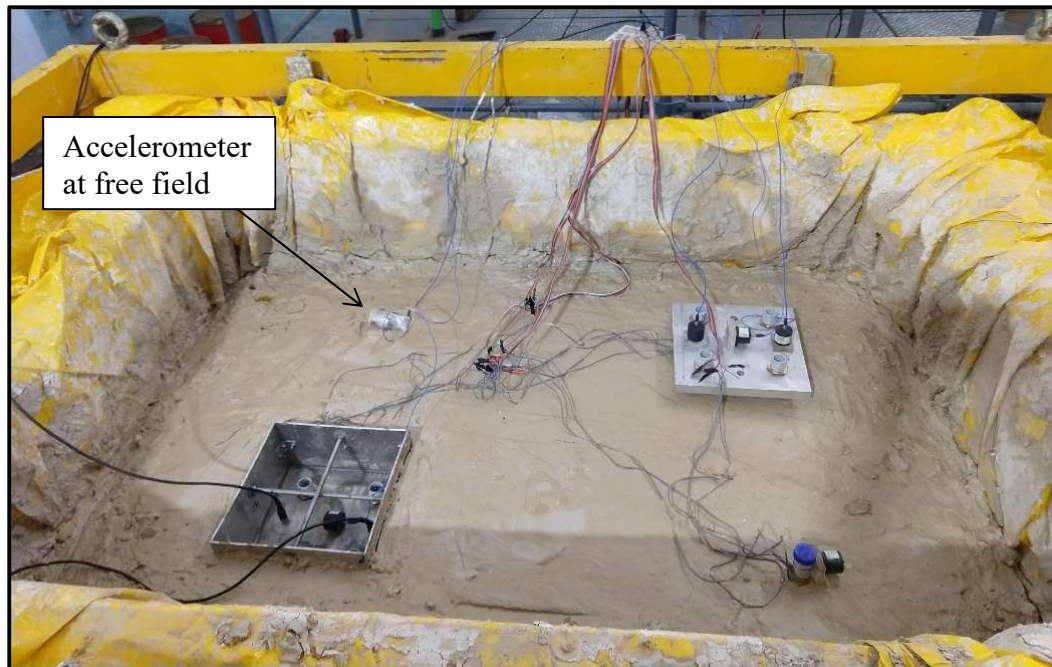


Fig. 6.21 The clay bed with instrumented foundation models

Confirmatory vane shear tests were conducted on samples collected from the mid depth and surface level of the clay bed. The samples were preserved in an air tight circular container of diameter 120 mm and height 50 mm. Vane shear tests were conducted at the time of the shaking

table test i.e. after a time duration of 36 hours. The undrained shear strength of the sample collected from the mid depth was found to be 2.5 kPa and the value for sample collected from the surface level was 2.1 kPa.

6.8 TEST PROGRAM

1-g shaking table experiments were carried out with the following foundations embedded in the clay bed.

- 2x2 piled raft with a raft embedment of 4 times the pile diameter
- 2x2 pile group without pile cap-soil contact

To evaluate the transfer functions in translation for vertically propagating shear waves, harmonic input motion with varying frequency was applied. A series of 14 sinusoidal signals with frequency varying from 0.1 Hz to 30 Hz was applied. The frequency around 17.5 Hz was skipped due to resonance effect of the shaking table system, observed during a previous trial run with a dummy load. Each signal consisted of 15 to 30 cycles with the input acceleration varying from 0.001 g to 0.2 g.

6.9 RESULTS AND DISCUSSION

The time histories of acceleration measured in the clay bed at the bottom, mid-level, and surface are presented in Fig. 6.22 (a), (b), and (c) for 5 Hz, 10 Hz and 15 Hz respectively. The ground response to vertically propagating shear waves, which results in increasing amplitude with distance from the base is evident. A steady-state amplitude can be observed in the time histories after a few initial cycles. The acceleration time histories recorded at the top of piled raft and pile group models are presented along with the free field motion for 2.5 Hz, 5 Hz and 7.5 Hz input motion in Fig. 6.23 (a), (b) and (c) respectively. The reduction in amplitude recorded at the foundation levels due to kinematic interaction is evident from Fig. 6.23 (c). The accelerometer at the clay surface was found to record erroneous values of the free field motion beyond frequency of 25 Hz, due to slippage. Hence these recordings were discarded.

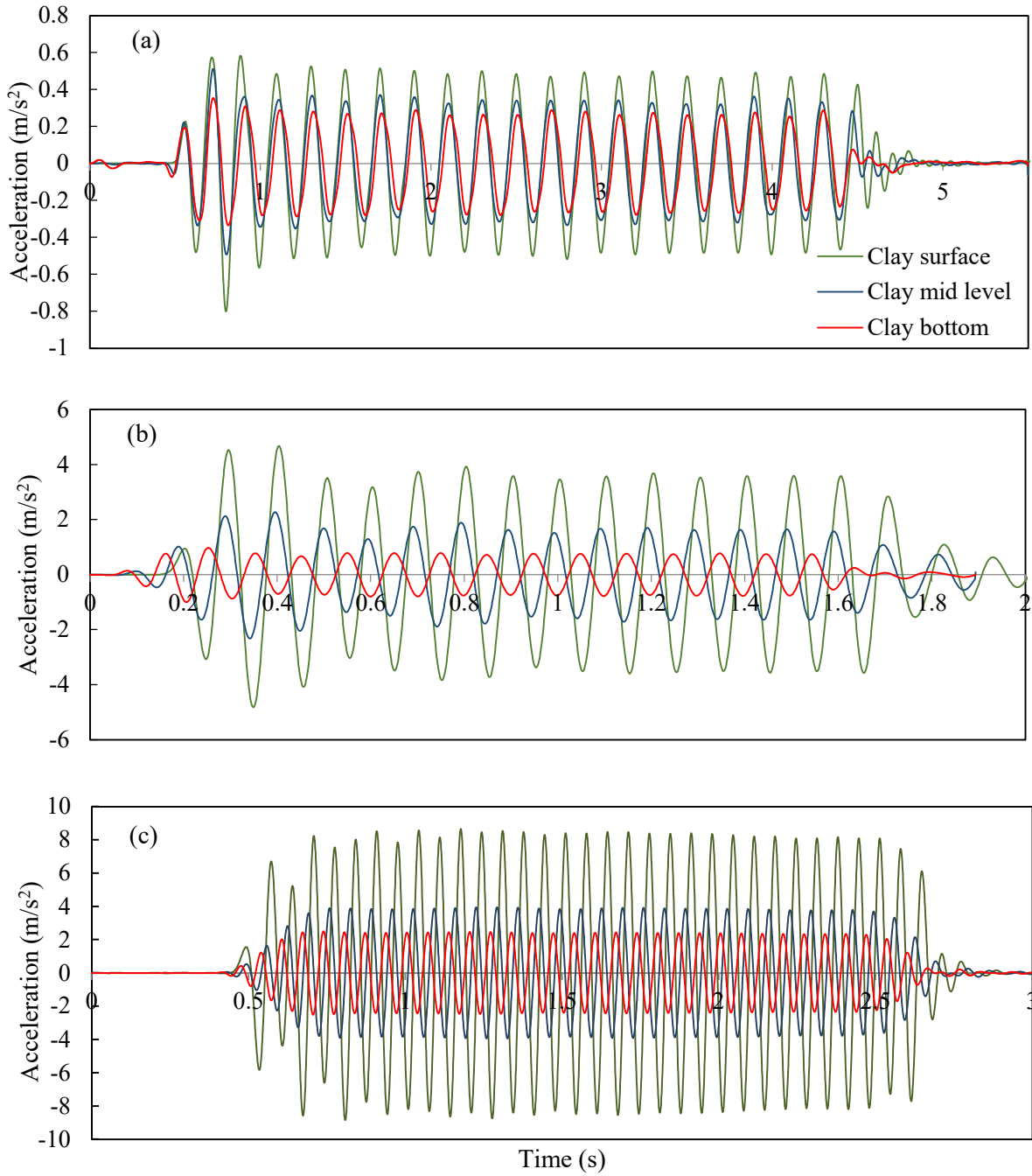


Fig. 6.22 Acceleration time histories recorded at various depths of the clay bed for (a) 5 Hz, (b) 10 Hz and (c) 15 Hz frequencies

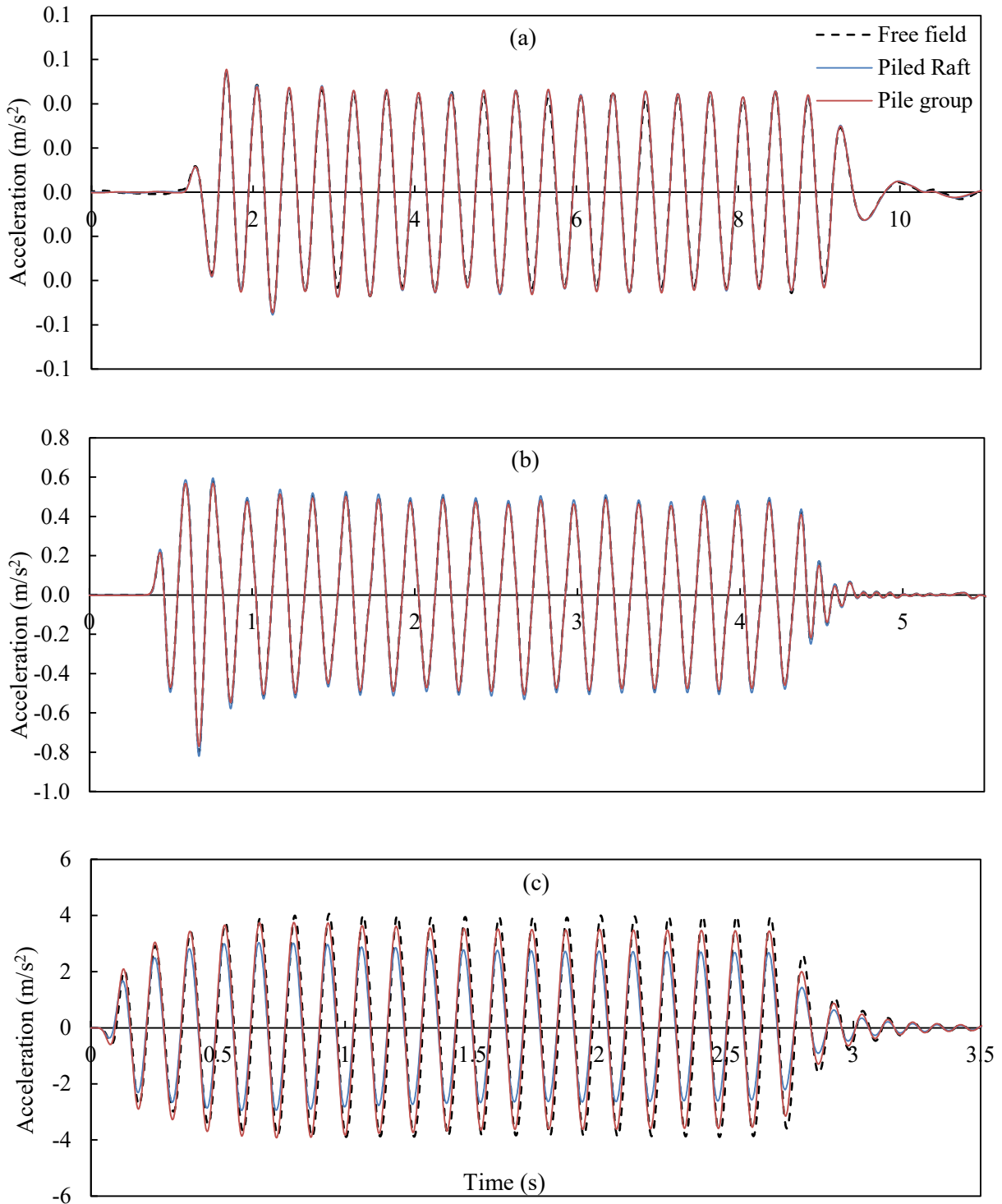


Fig. 6.23 Acceleration time histories recorded at the top of foundations for (a) 2.5 Hz, (b) 5 Hz and (c) 7.5 Hz frequencies

The steady state amplitude was used to calculate the transfer function in translation, I_u for the piled raft and pile group models. A bandpass filter was employed to filter mechanical noise

from the recorded accelerograms. A typical raw signal along with the filtered signal for 5 Hz is presented in Fig. 6.24.

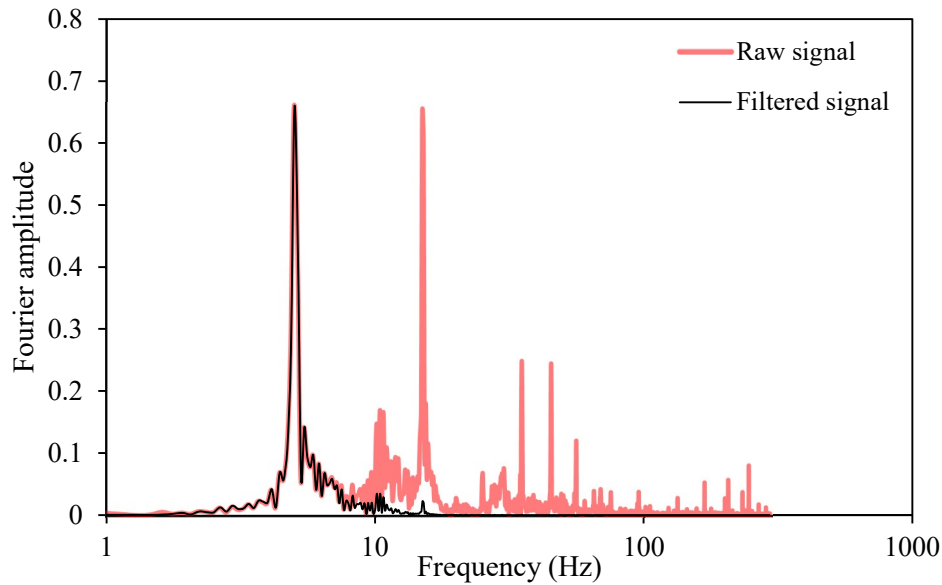


Fig. 6.24 Raw and filtered signal recorded at the free field for 5 Hz input motion

The kinematic response factor for the two foundations obtained from the experimental data is presented in Fig. 6.25. The response of the pile group was found to be higher across the frequency spectrum studied. It is interesting to note that the embedded raft keeps reducing the translational response with increasing frequency beyond a certain threshold frequency, which is close to 2.5 Hz in the present case. The reduction was found to be 35% and 41% at frequencies of 10 Hz and 15 Hz respectively. The trend followed the experimental kinematic response factors are in agreement with those obtained from numerical models described in Chapter 4.

The bending strains at five locations along the length of the instrumented piles were recorded using strain gauges. The maximum bending strain profile is obtained by assembling the maximum steady state strain amplitude of strains across the length of the pile.

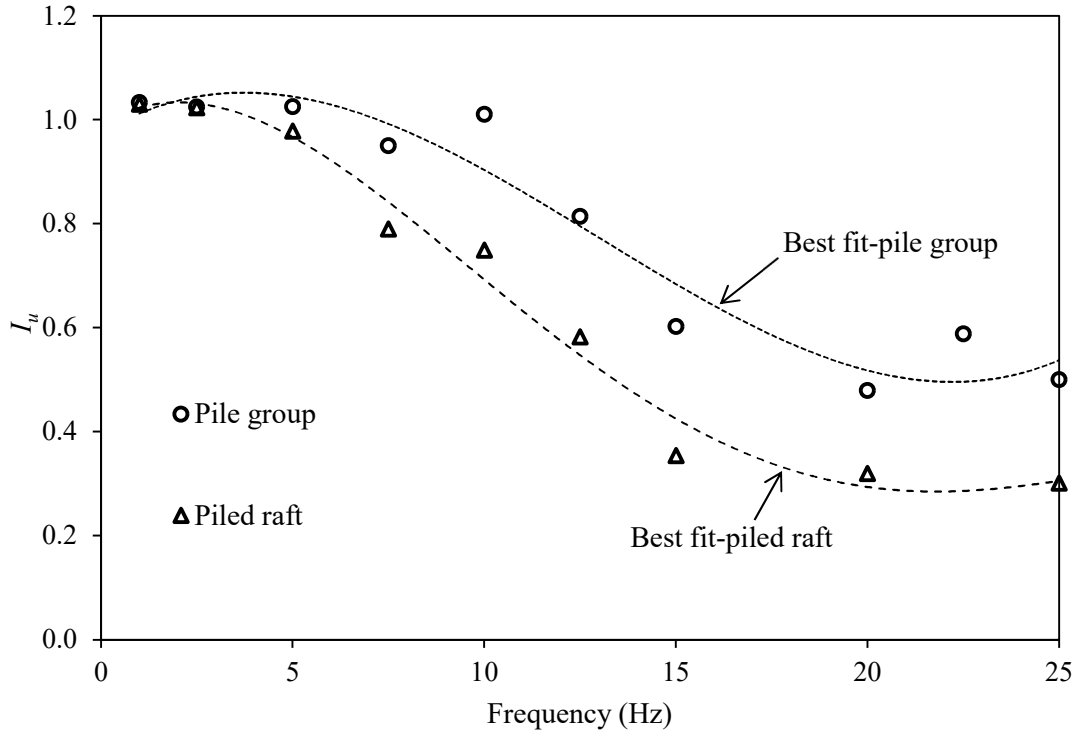


Fig. 6.25 Kinematic response factors in translation obtained from the experimental data

The typical bending strain profile obtained from the experiment for frequencies of 1 Hz, 2.5 Hz and 5 Hz are presented in Fig. 6.26 (a), (b) and (c) respectively. It is found that the pile head bending strains in the piled raft and pile group are comparable. In comparison to the pile group, piles in the piled raft model was found to experience lower bending strains in the active length of the pile. Although the piles are not socketed into hard strata, their tip rests in the relatively stiffer layer due to the difference in the setting and pouring time across depth in the clay bed. The increased bending strain at the pile base can be attributed to this reason. In order to assess the influence of raft on the bending moment, the normalized bending strain profile for the piled raft, ε'_{pr} defined as the ratio of bending strain of PR to bending strain of PG was calculated. Fig 6.27 presents the normalized bending strain of the piled raft plotted against normalized depth for frequencies in the range of 1 to 15 Hz. The normalized depth is defined as the ratio of distance from the pile head (h), to the total length of pile (l).

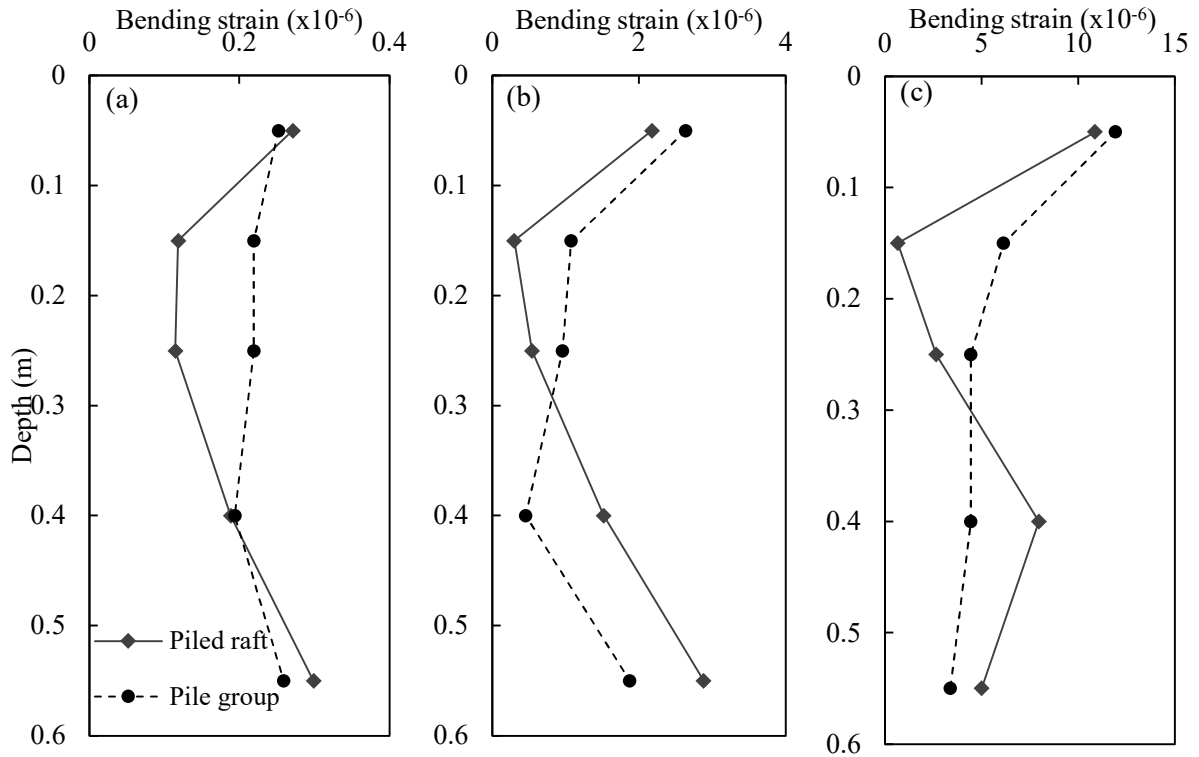
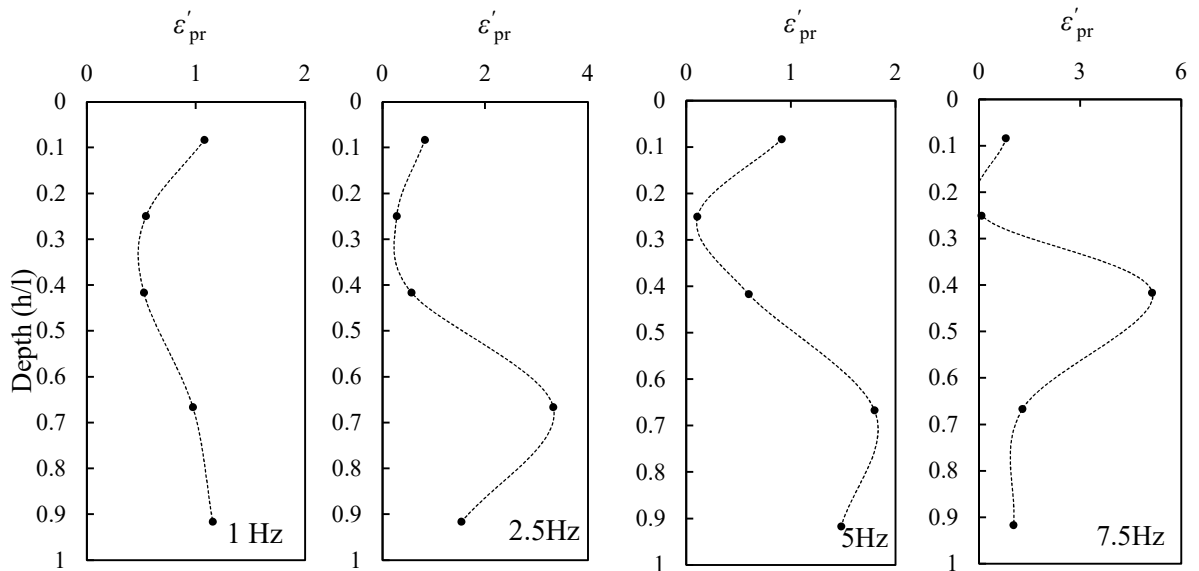


Fig. 6.26 Bending strain profile in PR and PG models for (a) 1 Hz, (b) 2.5 Hz, and (c) 5 Hz



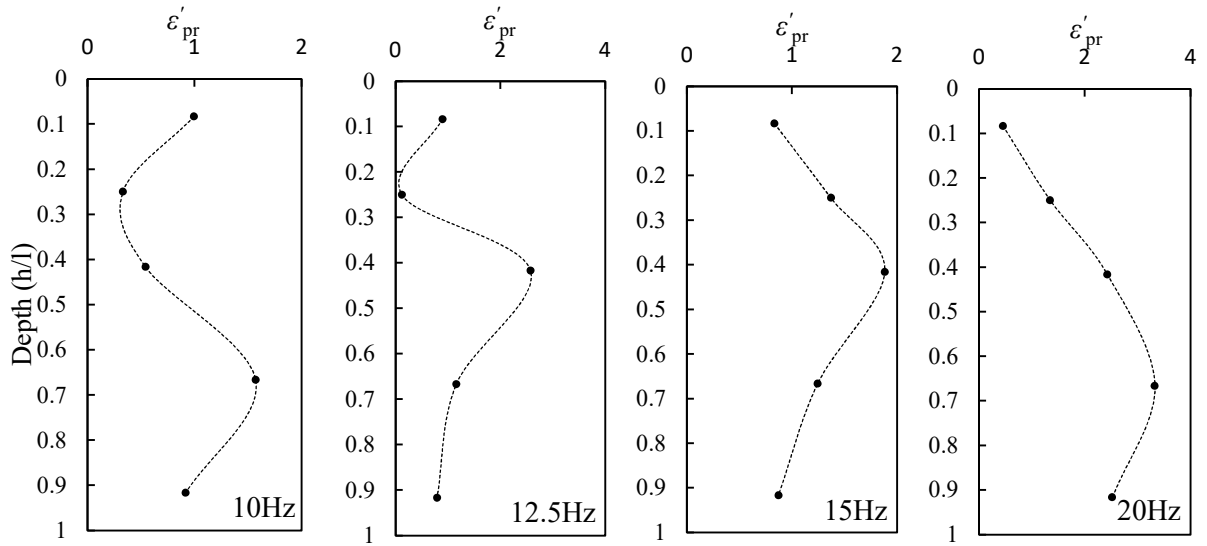


Fig. 6.27 Normalised bending strain profile of piled raft model with varying frequency of input motion

From Fig. 6.27 it is evident that the influence of raft embedment on the bending strain profile is a function of frequency. The bending strain near the pile head, that is a result of inertial interaction is not affected except for the input motion with 20 Hz frequency. The pile can be considered as flexible following the criteria stipulated by Poulos and Hull (1989), and Dobry et al. (1982). Following the equation proposed by (Ayothiraman and Boominathan 2013), the depth of fixity, of the pile soil system for dynamic loads can be estimated using

$$\frac{L_{fd}}{d} \approx 1.24 \left(\frac{E_p}{G_s} \right)^{0.29} \quad (6.6)$$

where L_{fd} is the depth of fixity, d is the diameter of pile, E_p represents the Young's modulus of pile material and G_s represents the shear modulus of soil. The depth of fixity of 0.23 m, corresponding to a normalised length of 0.38 was obtained using the Eq. 6.6. For frequencies below 15 Hz, the normalized bending strain obtained from the experimental results, up to a normalised depth of 0.3 are found to be below unity. In comparison to the pile group, a maximum increase in bending strain in the order of 5 times can be seen for the case with input frequency of 7.5 Hz. The most significant increase in bending strain caused by the embedment of raft is found to be below the depth of fixity across most frequencies.

6.10 CONCLUDING REMARKS

The seismic response of a piled raft and pile group is studied by conducting a 1-g shaking table test using model foundation-soil system in a laminar box. The effect of an embedded raft on the seismic response of a 2x2 pile group was evaluated experimentally by comparing the performance of a model piled raft and pile group embedded in a clay bed with shear wave velocity of 40 m/s, and density of 1517 kg/m³. A synthetic clay mix was adopted as the model soil after evaluation of its low strain shear modulus and modulus degradation behaviour using Bender element, and Cyclic Triaxial tests respectively. The model piles were composed of tube sections with outer diameter of 25 mm and length of 600 mm. The piled raft and pile group models had a similar 2x2 pile configuration with spacing to diameter ratio of 5.

The clay-pile system was subjected to harmonic input motion at the base, with frequencies ranging from 0.1 to 25 Hz and acceleration amplitudes varying from 0.001 g to 0.2 g. The acceleration response at the top of the foundation models, as well as at various location in the clay bed were recorded using accelerometers. The kinematic interaction factor in translation was then calculated from the experimental results. The response of the pile group was found to be higher across the frequency spectrum studied. It was found that the embedded raft resulted in a reduction in the translational response with increasing frequency beyond a certain threshold frequency, which was close to 2.5 Hz. A maximum reduction of 41% was found at a frequency of 15 Hz. The transfer function obtained from the experiment are in agreement with the trend obtained from numerical analyses, discussed in Chapter 4. The maximum bending strain profile in the piles from both piled raft and pile group models were obtained by assembling the maximum steady state strain amplitude of strains across the length of the pile. It is found that the pile head bending strains in the piled raft and pile group were close to each other up to a frequency of 15 Hz. However significant alteration in the kinematic bending strains were found in the piled raft model beyond the depth of fixity.

Findings from this chapter throw light on the effect of an embedded raft on the kinematic response of a piled raft. The reduction in transfer function observed from numerical analysis has been confirmed with experimental evidence. Seismic response of a foundation-structure system is however, a combination of both kinematic and inertial interactions. The next chapter discusses two case studies on seismic response of piled raft-structure systems.

CHAPTER 7

SEISMIC RESPONSE OF PILED RAFTS: CASE STUDIES

7.1 INTRODUCTION

Seismic response of a foundation-structure system involves both kinematic and inertial interaction effects. Practical piled raft designs often have asymmetric pile layout and varying pile geometry due to architectural or structural requirements (Mattsson et al. 2013; Uchida et al. 2012; Yamashita et al. 1994). Two case studies of piled raft foundations are discussed in this chapter. The first case is that of a single degree of freedom system supported by a 2x2 piled raft in layered soil. The model is an extension of the centrifuge experiment reported by Banerjee (2014). The second case study is that of a nuclear reactor building foundation proposed for the upcoming Nuclear Power Plant in a deep soil site in India. The foundation, consisting of a large piled raft with 271 piles, was analysed using site-specific soil properties.

7.2 CASE STUDY OF A 2X2 PILED RAFT IN CLAY

7.2.1 The Soil-Foundation-Structure System

Inertial interaction effects have been understood to exert significant shear forces and moments on foundations. Inertia from the superstructure can induce axial forces which can lead to pile head failure. The 2x2 piled raft in clay foundation discussed in section 4.2.4 is adopted in this case study. Four different piled raft models with pile diameter of 0.9 m, pile length of 13.5 m, and spacing to diameter (s/d) ratios of 4, 6, 8 and 10 were used for this study. A three-story framed building simplified as a single degree of freedom system with a fixed base period of 0.3 s, (following Storie et al. 2015) was adopted as the superstructure model for the analyses. The structure was modeled using beam elements with a lumped mass of 111.7 tonnes at the top. A schematic diagram showing the structure-foundation-soil system, along with a simplified three degree of freedom model, is presented in Fig. 7.1 (a) and (b) respectively. The superstructure-raft connection was modelled to transfer forces and moments in all directions, with a set of rigid links at the top surface of raft. The FE mesh of the model showing near field soil elements is presented in Fig. 7.1 (c)

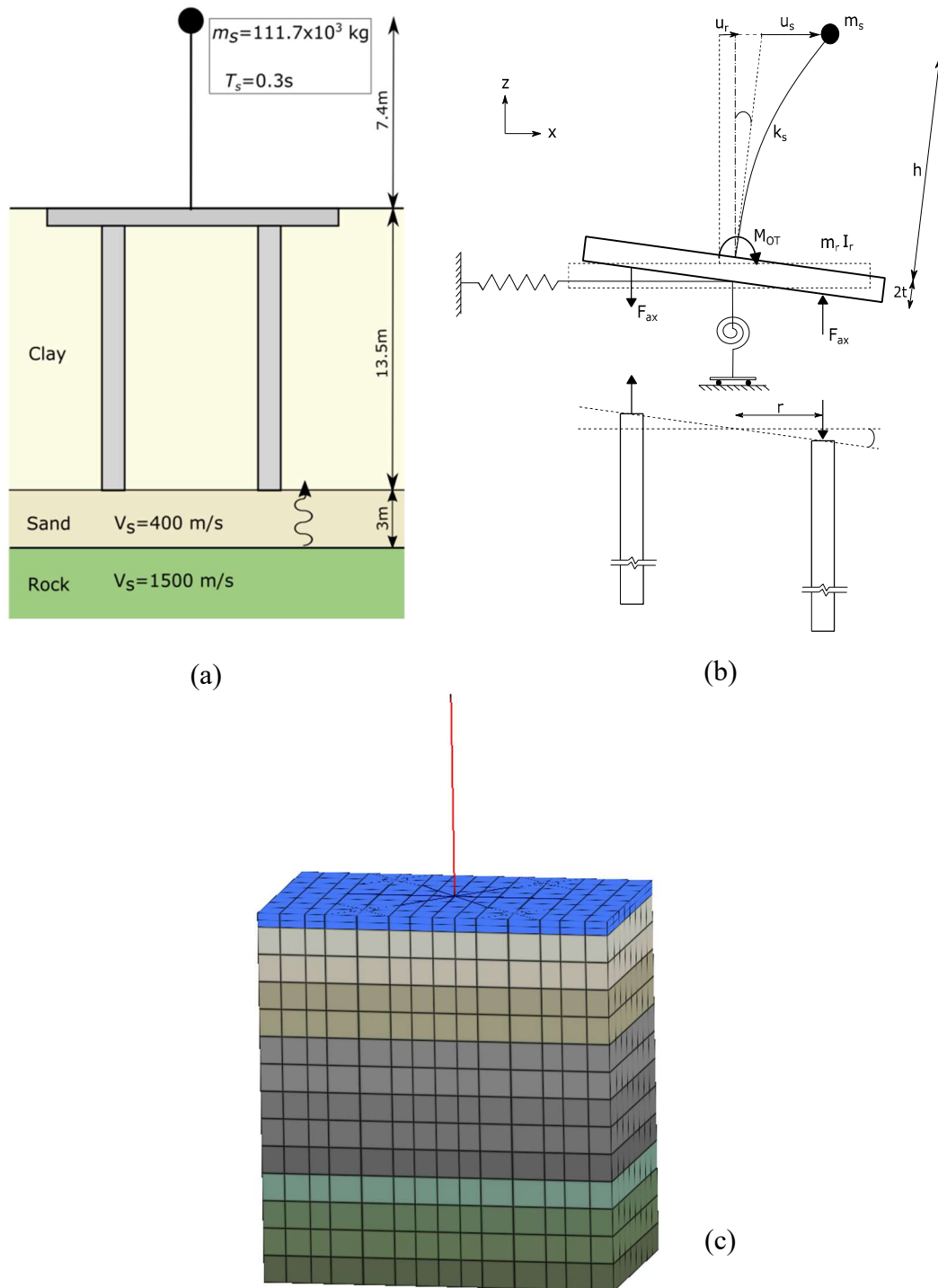


Fig. 7.1 (a) Schematic diagram and (b) simplified model of the structure-piled raft-soil system (c) FE model of the structure-PR-soil system

For the piled raft foundation considered in the present study, the raft can be considered to be a rigid body subjected to translational and rotational foundation input motion, as well as translational and rotational inertia forces from the superstructure. The role of piles in resisting

moments applied to the raft can be assumed to be primarily in the form of axial forces that generate resisting moments about the centre line of the raft (Di Laora et al. 2017). The symmetric pile arrangement in the present study would in principle form force couples about the centre line of the raft.

Considering the simplified model presented in Fig. 7.1 (b), the equation of motion of the raft in rotation, can be written as

$$m_s(h\ddot{u}_r + h\ddot{\theta}_r + \ddot{u}_s) + m_r(t\ddot{u}_r + t^2\ddot{\theta}_r) + I_r\ddot{\theta}_r + K_{ry}\theta_r + C_{ry}\dot{\theta}_r + \sum_{i=1}^n F_{axi}r_i = 0 \quad (7.1)$$

where m_s and u_s represents mass and displacement of the lumped mass; m_r , I_r , u_r , and θ_r represents mass, moment of inertia, displacement and rotation of the raft respectively; t represents half the raft thickness; F_{axi} is the axial force measured at the pile head of i^{th} pile, located at a distance of r from the centre line of the raft along the Y axis, and n represents the total number of piles.

The axial force exerted on piles, is investigated using a non-dimensional axial force factor defined as

$$f_p = \frac{\sum_{i=1}^n F_{axi}r_i}{M_{OT}} \quad (7.2)$$

where M_{OT} represents the maximum overturning moment exerted on the raft by the superstructure, and corresponds to the first term in Eq. (7.1). All the parameters, except r in Eq. (7.2) are time varying functions and hence the values at the instant of maximum overturning moment from the transient response, were obtained from the analysis. The actual overturning moment at any instant would be supplemented by moments due to translational and rotational inertia forces of the raft itself. The resistance to overturning moment, on the other hand, would be a combination of force couples from piles, along with resistance due to the bearing of raft from the bottom and sides. The non-dimensional axial force factor introduced would be an indicator of the contribution of axial forces developed in piles during shaking, towards resisting rocking at the raft level.

7.2.2 Input Motion

Transient response of the system was studied by the FVSM approach in the ACS SASSI program, by applying strong motion acceleration time histories from a near field event (Christchurch, 2011), and two far field events (Nepal, 2015, and Mexico, 2017), the details of which are presented in Table 7.1. The three acceleration time histories were scaled to 0.16g considering the peak ground acceleration in Zone III as per IS1893:2016 (BIS 2016). The time history and Fourier spectra of the scaled input earthquake motions are shown in Fig. 7.2 (a), (b) and (c) respectively. The input motions were applied at the top of the rock layer in the numerical analysis.

Table 7.1 Details of the earthquake motion scaled to 0.16g

Earthquake	Year	Recording Station	PHA (g)	M _w	Bracketed Duration (s)	Epicentral Distance (km)
Christchurch, New Zealand	2011	McQueen's Valley	0.147	6.3	4.7	15.0
Nepal Gorkha	2015	Kanti Path	0.163	7.8	44.2	59.9
Central Mexico	2017	UNAM	0.448	7.1	56.5	116.4

7.2.3 Results and Discussion

Response spectra obtained at the mass level was found to be affected by change in pile spacing, especially at closer spacing. Response spectra obtained for Christchurch 2011, Nepal 2015, and Mexico 2017 earthquakes are presented in Fig. 7.3 (a), (b), and (c) respectively. Increase in pile spacing to diameter ratio from 4 to 6 was found to bring about reduction in peak spectral acceleration by 17% to 26%, for Christchurch 2011, and Mexico 2017 input motions. One of the main reasons for this reduction is the increase in rocking stiffness of the piled raft with increase in pile spacing. Beyond a spacing ratio of 6, no significant variation in spectral ordinates was observed. The frequency content of response was also not altered by a change in pile spacing.

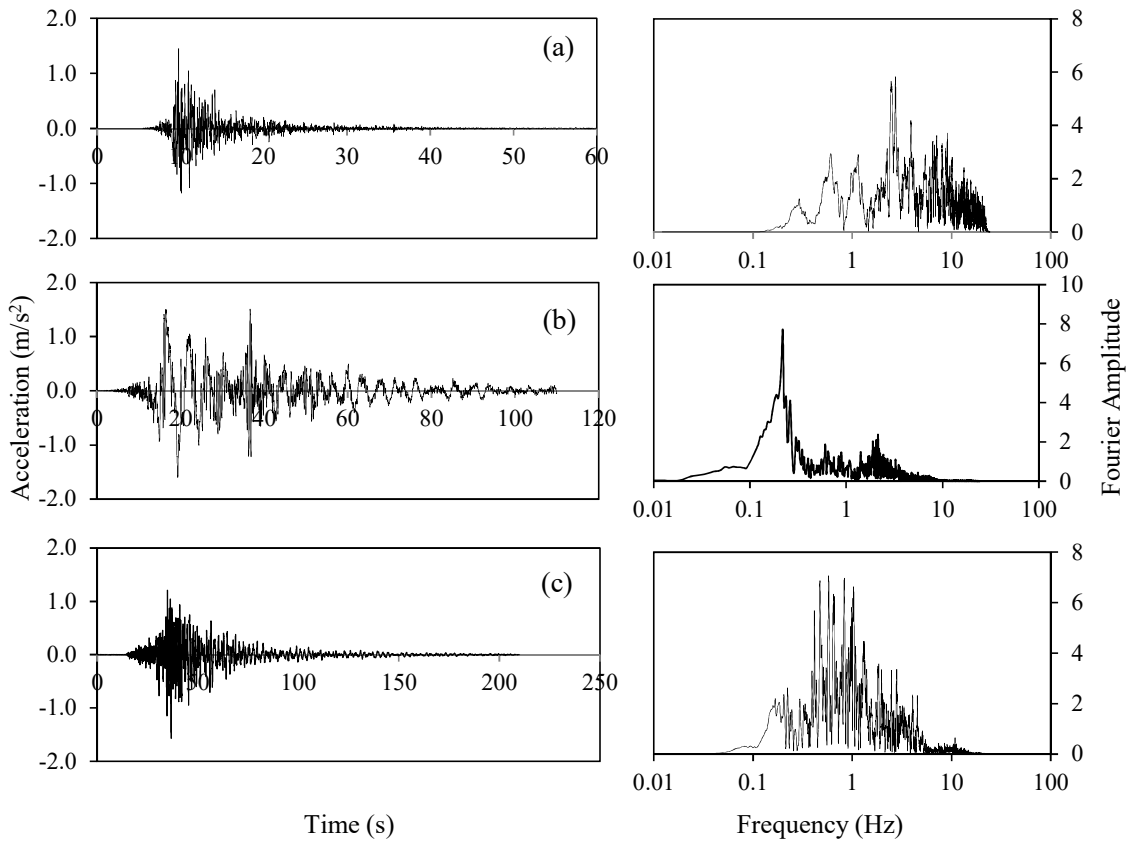
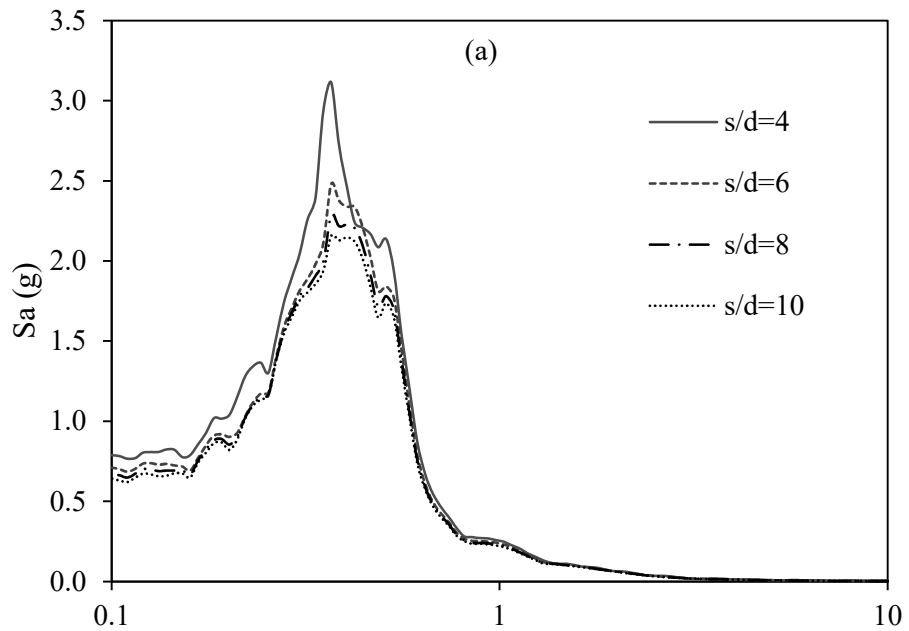


Fig. 7.2 Time history and Fourier spectra of scaled input motions from (a) Christchurch 2011, (b) Nepal 2015, and (c) Mexico 2017 earthquakes



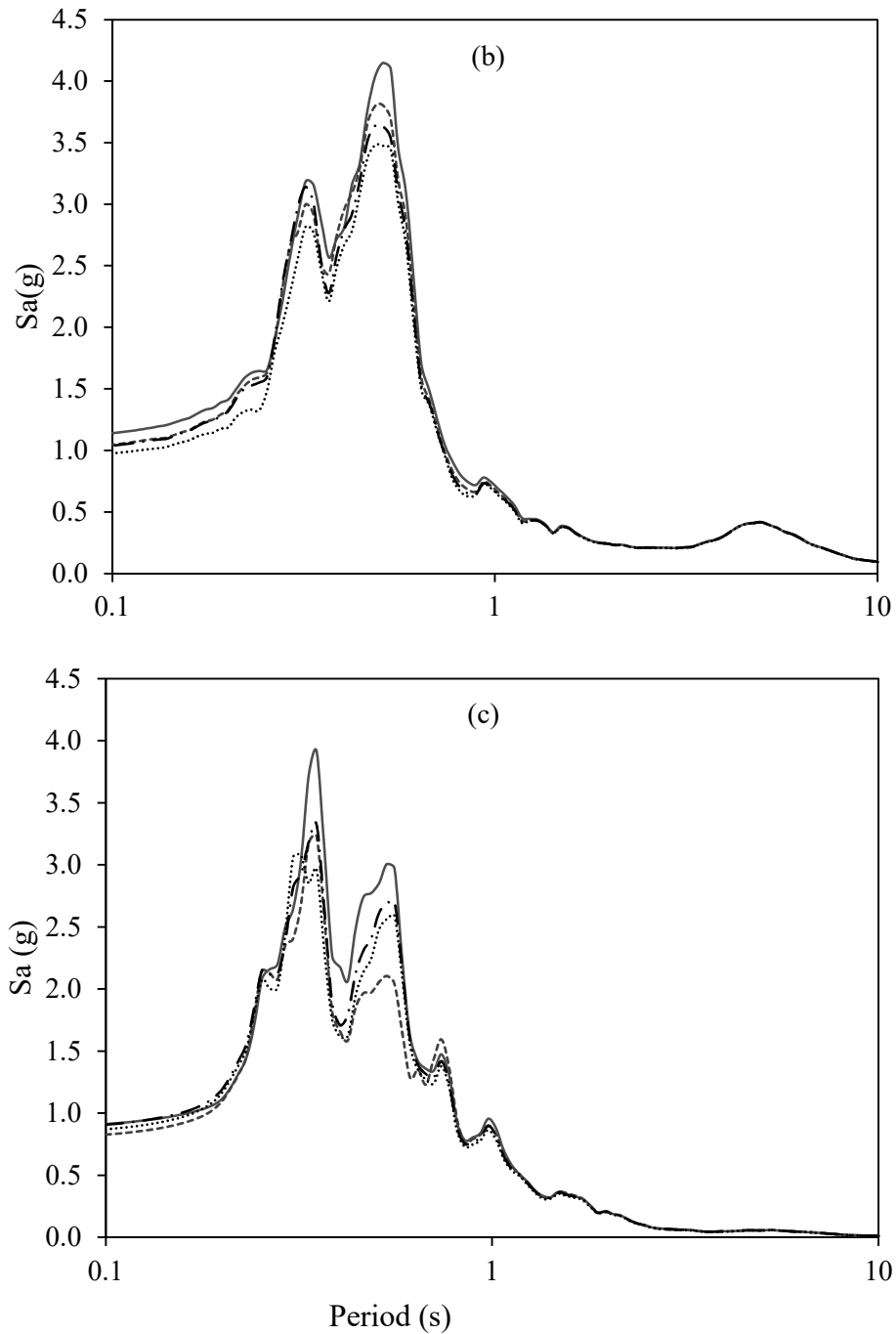


Fig. 7.3 Response spectra at the mass level for (a) Christchurch 2011, (b) Nepal 2015 and (c) Mexico 2017 earthquakes

The increase in f_p , with increase in pile spacing hints at an increased role of pile in resisting rotation at the raft level. On an average, the increase in f_p for increase in spacing from 4 to 6, 6 to 8, and 8 to 10 is 61%, 22% and 11% respectively. It was also found that the change in f_p ,

with increase in pile spacing is nonlinear. Studies on kinematic response of pile groups (Di Laora et al. 2017) have shown that rotation at the head of a pile group decreases with increasing pile spacing with a nonlinear trend. The nonlinear increase in pile axial force is therefore in agreement with the known rotation-pile spacing relationship. However, in the case of piled rafts, the resistance to rotation is offered by axial resistance of piles as well as resistance offered by the raft. The factor f_p does not isolate the effects of inertia forces offered by the massive raft, and the flexural resistance offered by the piles. Nevertheless, the parameter has the potential to identify the optimal pile arrangement in a piled raft considering stability during seismic shaking. The maximum bending moment profile in piles is presented in Fig. 7.5 for the three input motions. The maximum bending moment at the pile heads was observed to increase as spacing between piles decreases. The average difference between pile head bending moment for $s/d=4$ and $s/d=10$ is 27%. One reason for this observation is that the reducing force couple generated by piles to resist overturning moments (as indicated by the axial force factor) is partly compensated by an increase in flexural resistance provided by the piles.

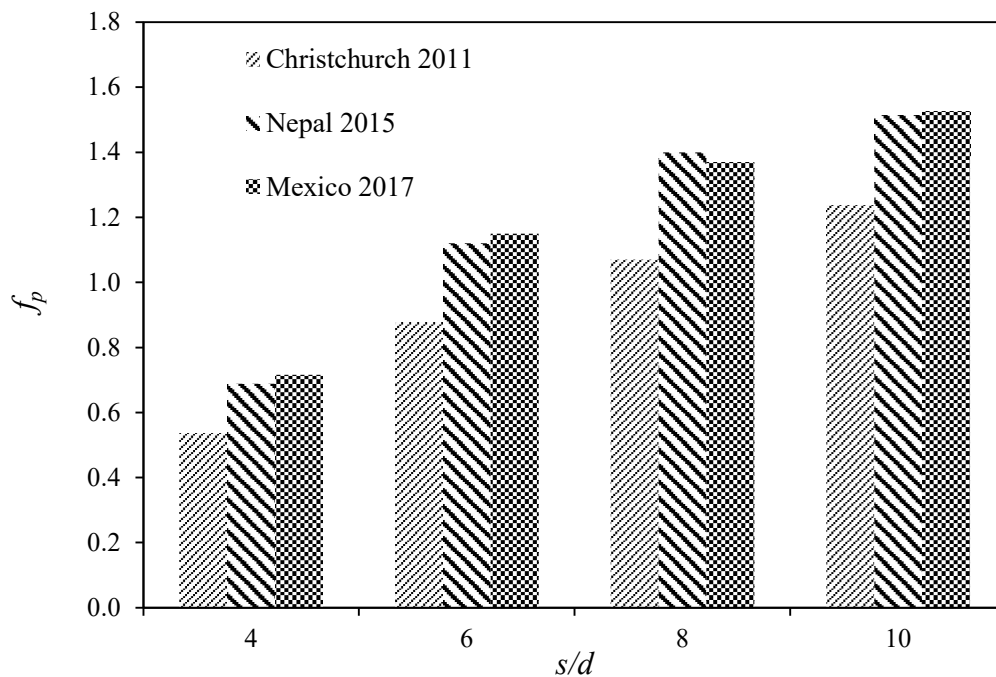


Fig. 7.4 Variation of axial force factor with pile spacing, for three earthquake input motion

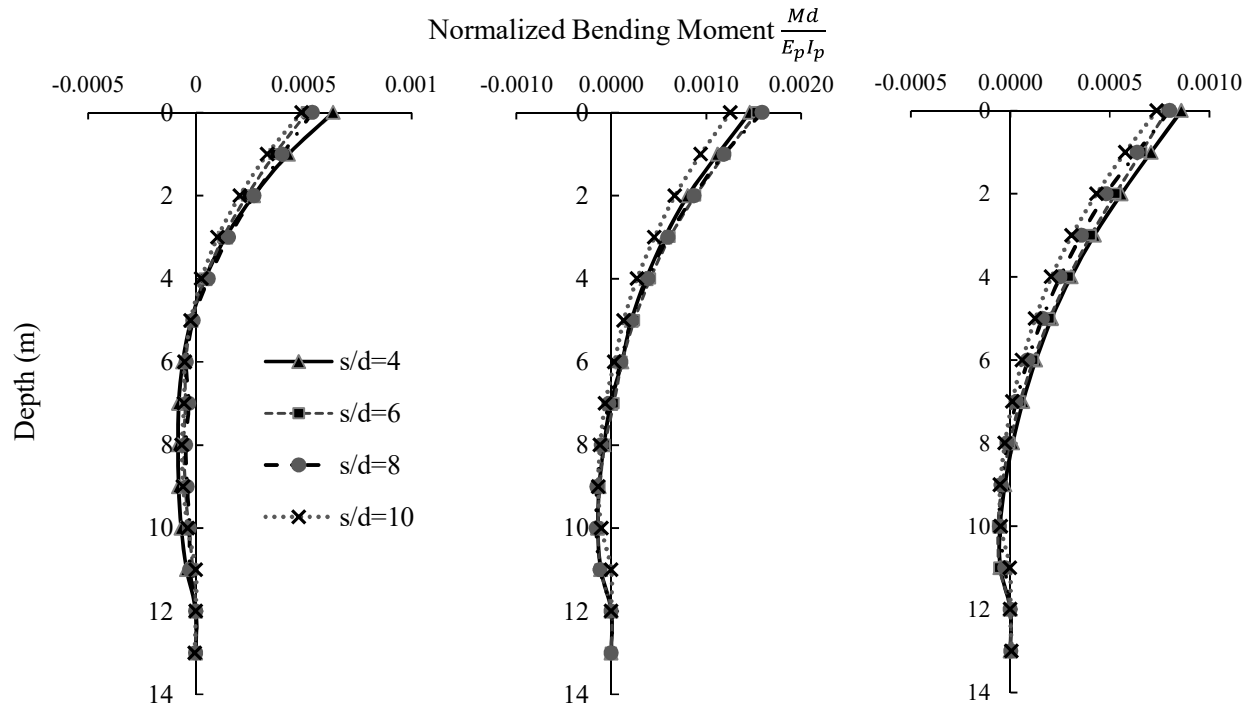


Fig. 7.5 Maximum BM profile in piles for (a) Christchurch 2011, (b) Nepal 2015 and (c) Mexico 2017 earthquakes

Placing piles near the periphery of the raft is found to have a clear advantage in terms of structural response as well as pile forces. Analysis of damages after the Mexico earthquake of 1985 have provided some valuable insights in this regard. Mendoza and Auvinet (1988) have reported the case study of an office building with a rectangular plan, on 70 friction piles. The building suffered from permanent tilt and large plastic deformations after the earthquake. The damage was attributed to two main reasons, the former being the high pre-earthquake stresses in the supporting soil under the slab foundation, and later being the absence of adequate peripheral piles. Pile arrangement in piled rafts has been the subject of many optimisation studies. The results from this case study show that seismic response, quantified by the axial force factor could be considered as a parameter in the optimisation of pile arrangement in a piled raft.

Summarizing, the case study of the piled raft supported oscillator provided insights into the response of piled rafts to combined kinematic and inertial loads. The next case study deals with a large piled raft system supported by a stiff improved soil layer. The influence of a stiff top layer on the kinematic response is evaluated.

7.3 CASE STUDY OF A LARGE PILED RAFT FOR A NUCLEAR BUILDING IN A DEEP SOIL SITE

7.3.1 Overview

Soil structure interaction is an important design consideration for nuclear power plants. Most nuclear power projects are located on rocky sites of low seismicity. However, there are cases in which nuclear power projects are located in soil sites (Mattsson et al. 2013; Wolf et al. 1981). The first nuclear power plant in India to be located in a deep soil site will be the 4x700 Megawatt Gorakhpur Nuclear Power Plant (GHAVP 1&2) being set up in Gorakhpur, in Haryana state, India. The site is located in the western part of Indo-Gangetic plain, known for its deep soil deposits. The alluvial deposit at the site is estimated to be around 320 m in depth.

The nuclear reactor building at the site has plan dimensions of roughly 100 m x 100 m. A piled raft foundation with 271 piles confined to the heavily loaded inner circular region was designed. The pile group consists of 44 peripheral piles of diameter 1.5 m and 227 interior piles of diameter 1.2 m. The dimensions of the building are presented in Fig. 7.6. To achieve a high factor of safety against liquefaction, top 5.5 m soil below the reactor building was improved by cement mixing. A study on the kinematic response of the large piled raft on improved ground is discussed in the following sections.

7.3.2 Soil Properties for SSI Analysis

The Haryana region of the IGP, in North Western India is covered to a large extent by quarternary sediments of alluvian or aeolian origin (Chopra 1990). The alluvial deposits have a thickness of around 200m at the southern region of Haryana state and increase to a few kilometers near the Siwalik Hills in the North making the region susceptible to liquefaction hazard from Himalayan earthquakes (Verma et al. 2012). To determine the dynamic soil properties of soil, laboratory experiments were conducted on undisturbed soil samples obtained from a borehole at the reactor building location. The undisturbed samples were extracted from boreholes using the Mezier sampling technique, and stored in sealed PVC tubes. The typical soil profile at the site along with corrected SPT N values is presented in Fig. 7.7.

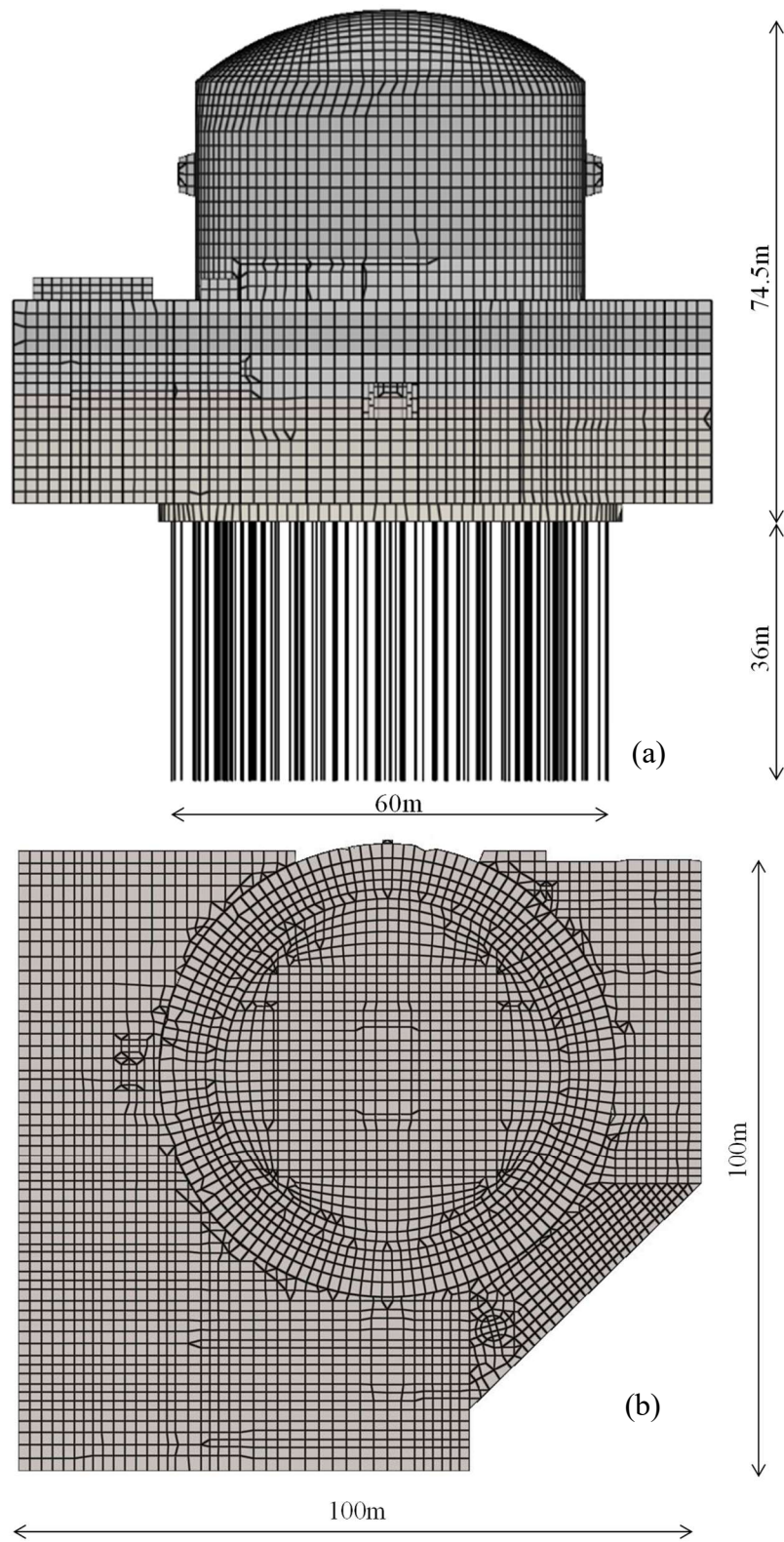


Fig. 7.6 (a) Elevation of the structure with foundation and (b) plan view at raft level

The soil profile at this site consists of deep deposits of silt and sand layers, in general. The soil at the site consists of 5.5 m of improved ground comprising cement mixed soil, followed by natural soil strata. In this study, laboratory tests were conducted on undisturbed soil samples (UDS) from the natural ground. The shear wave velocity profile was then arrived at by augmenting the laboratory test results with and in situ cross-hole test results. The UDS samples were extracted from four soil layers L1, L2, L3 and L4, covering depths from 6.5m to 32m, as shown in Fig. 7.7. A photograph of an intact sample and a trimmed sample placed on a testing apparatus is shown in Fig. 7.8. The grain size distribution of the soil at different depth is presented in Fig. 7.9 confirms the presence of high silt content in the soils. The index properties of soils are presented in Table 7.2.

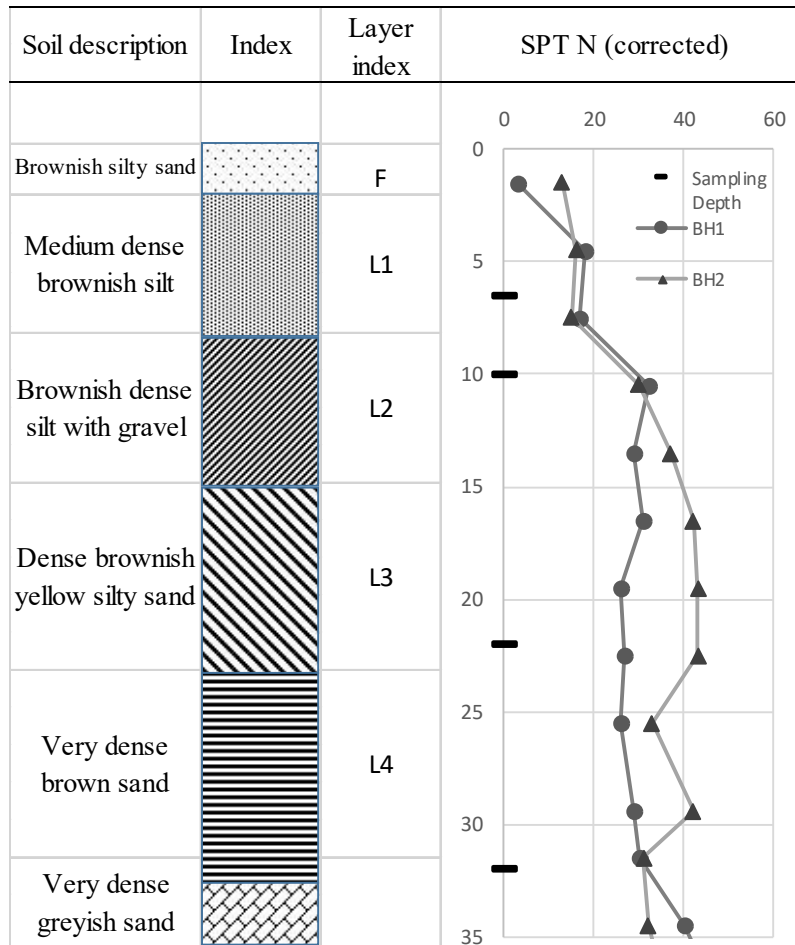


Fig. 7.7 Soil profile at the site



Fig. 7.8 Photographs of (a) intact sample from 10m depth and (b) the sample trimmed to size

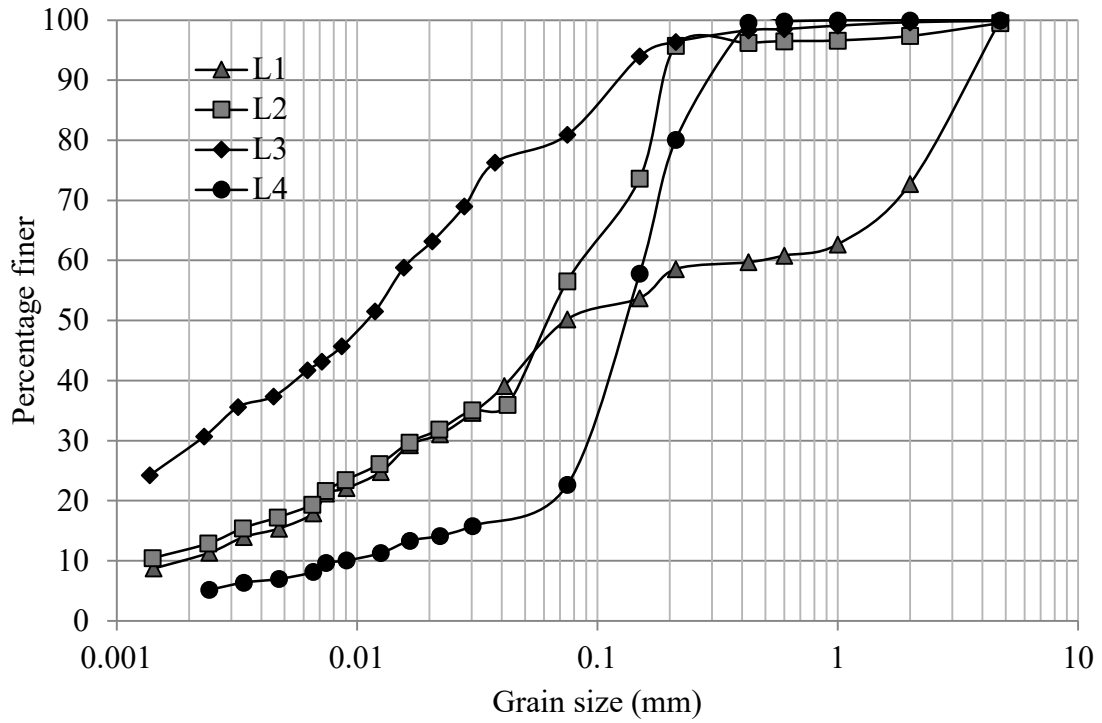


Fig. 7.9 Grain size distribution of the UDS sample from different depths

Table 7.2 Index properties of the soils

Particulars	Layer			
	L1	L2	L3	L4
Liquid Limit (%)	27	28	29	32
Plastic Limit (%)	24	23	22	26
PI (%)	3	5	7	6
Classification*	ML	ML	ML-CL	SM
Fines (%)	50.2	56.6	81.1	21.6
In-situ density (kN/m ³)	18.98	18.98	18.56	19.97
In-situ water content (%)	17.93	31.11	24.71	24.16

*as per unified soil classification system

The maximum shear modulus of the soil was determined using the bender element apparatus (Make: VJ Tech) as shown in Fig. 7.10. Two piezoelectric bender probes which can transmit and receiving shear waves were used to measure the shear wave velocity of the soil. The bender probes had a protruding depth of 2mm each and hence the effective length of the sample was maintained at around 96 mm. The samples were saturated progressively applying back pressure to ensure a Skempton's B parameter value greater than 0.95. The samples were then consolidated with effective cell pressures of 62, 94, 190 and 280 kPa for samples from L1, L2, L3 and L4 respectively. As the cell pressure in the bender element apparatus was pneumatically applied, two membranes were used to prevent the entry of air into the sample. Brignoli et al. (1996) observed that for shear wave velocity measurements, the most interpretable waveforms for 100mm long samples were obtained in the 3-10 kHz range. In this study, sinusoidal shear waves with a frequency of 5 kHz were generated from the bender element placed at the top of the sample and the bender element placed at the bottom was used to capture the arriving wave. The difference in the time of arrival of the first wave was recorded to determine the shear wave velocity, V_s of the soil. The low strain shear modulus, G_{max} was then determined using the standard expression:

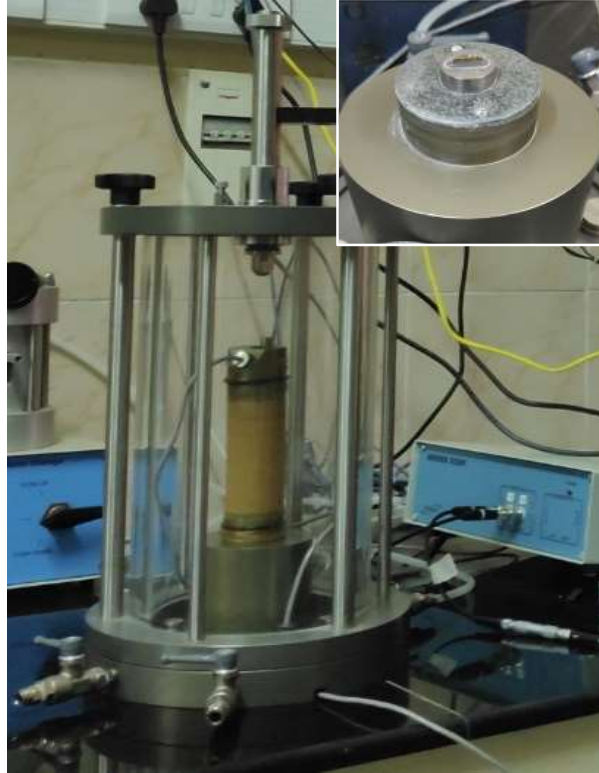


Fig. 7.10 Photographs of the Bender Element test setup (inset shows the bottom pedestal with bender)

$$G = \rho V_s^2 \quad (7.3)$$

Typical receiver signals obtained from test sample from a depth of 6.5 m, is presented in Fig. 7.11. The average shear wave velocity for the upper 30m, V_{s30} is estimated to be 234 m/s from the bender element test results. For the purpose of comparison, G_{max} is also estimated based on empirical correlations reported by Hardin (1978), Seed and Idriss (1970), and Chattaraj and Sengupta (2016). The study by Chattaraj and Sengupta (2016) was conducted on Kasai River sand in the West Bengal region, which also falls within the Indo Gangetic Plain. The shear wave velocity and the maximum shear modulus at different depths obtained from this study are presented along with predicted values in Table 7.3. It can be observed that the experimentally determined maximum shear modulus is in agreement with the SPT N profile at the site as shown in Fig. 7.7. The shear wave velocity profile determined from the laboratory tests was augmented by in situ cross-hole test results to arrive at the V_s profile for SSI analysis (NPCIL 2018).

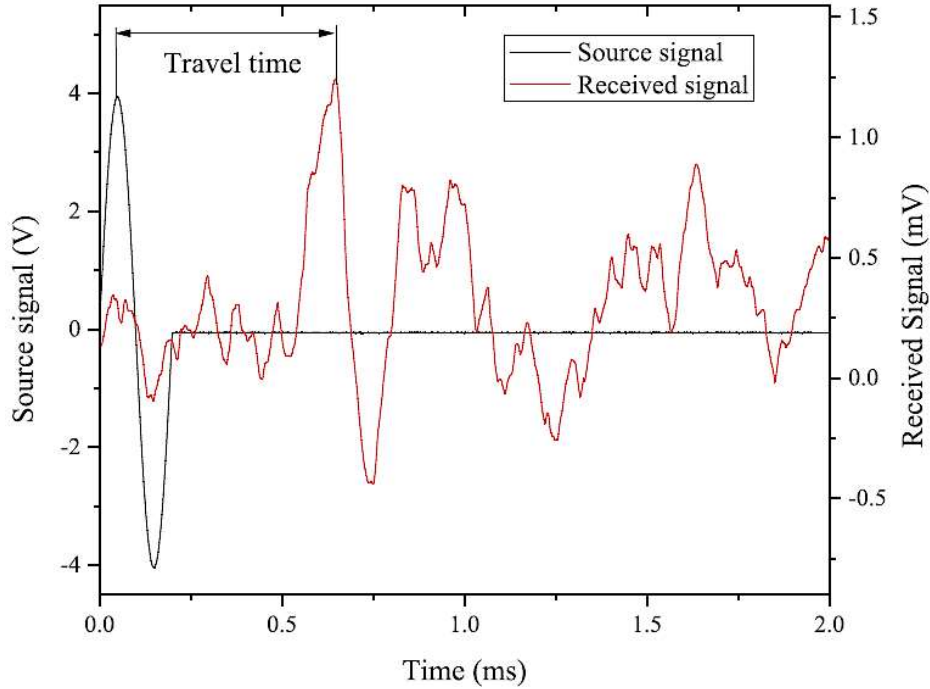


Fig. 7.11 Source and receiver signals recorded in the Bender scope

Table 7.3 Maximum shear modulus of soil at different depths

Depth (m)	V_s (m/s)	G_{max} (MPa)	G_{max} (MPa)	G_{max} (MPa)	G_{max} (MPa)
	Present study	Present study	Hardin (1978)	Seed & Idriss (1970)	Chattaraj & Sengupta (2016)
6.5	186	62	71	62	71
10	204	81	99	68	98
22	232	102	124	97	120
32	292	171	149	132	142

A ground improvement (GI) layer of 5.5 m thickness was proposed for the site considering the factor of safety against liquefaction. The soil below the reactor building was excavated, mixed with 5% by weight of cement, placed back and compacted by roller compaction. Based on tests conducted on soil samples collected from the field it was found that the cement soil mix had, on average, a maximum dry density of 18 kN/m^3 , and an optimum moisture content of 15% (personal communication from NPCIL). The final unit weight from in situ tests was found to

be 19.62 kN/m^3 , and this value was used in the SSI analysis. The 28-day unconfined compressive strength of the mix was determined to be between 1350 and 1450 kPa. Other details of the ground improvement are beyond the scope of this study, and are not discussed. Cross hole tests were conducted after the cement mixed soil layer was compacted in place. The soil profile with GI layer adopted for the SSI analysis, as well as the natural soil profile at the site is shown in Fig. 7.12.

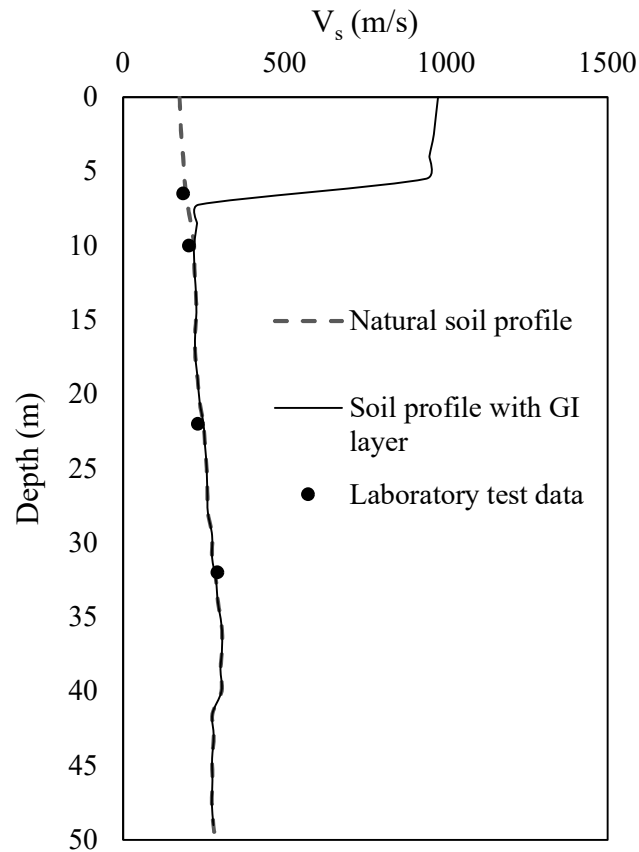


Fig. 7.12 Soil profile developed for SSI analysis

7.3.3 Piled Raft Foundation and Numerical Model

The foundation designed for the structure was a piled raft with 271 piles. The pile layout consisting of 44 peripheral piles of diameter 1.5 m, and 227 interior piles of diameter 1.2 m, is presented in Fig. 7.13. The raft was designed with a thickness of 3.5 m. The soil fill around the sides of the reactor building is not considered in the analysis.

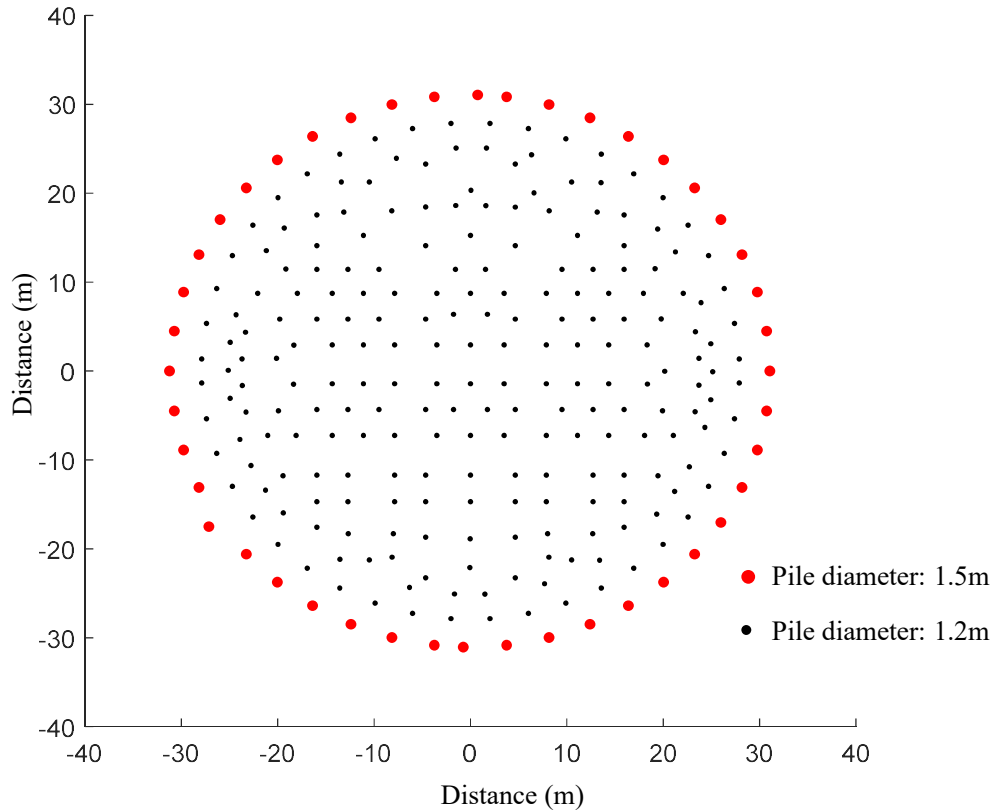


Fig. 7.13 Arrangement of piles in the piled raft

To study the kinematic response of the piled raft, a 3D numerical model was developed following the flexible volume sub structuring methodology. The superstructure was omitted from the model, and the raft was assigned a very low value of mass, such that inertial effects are avoided. Considering the large size of the structure, a simplified model with piles modelled using beam elements was developed. The finite element mesh of the piled raft used in the analysis is presented in Fig. 7.14. The raft was modelled using thick shell elements, maintaining the actual stiffness and geometry. The raft geometry is also grooved, which contributes to its stiffness. Conforming to the structural design, the raft was assigned an Elastic modulus of 33.5 GPa and a Poisson's ratio of 0.2. The piles were assigned an Elastic modulus of 30.2 GPa, a Poisson's ratio of 0.2, and a unit weight of 25 kN/m³. The number of interaction nodes in the model was 11276. The analysis was carried out in a workstation with 128 GB of RAM, and the time taken for each frequency of analysis was 2 hours and 20 minutes. Primary or secondary soil non linearity was not considered in this study.

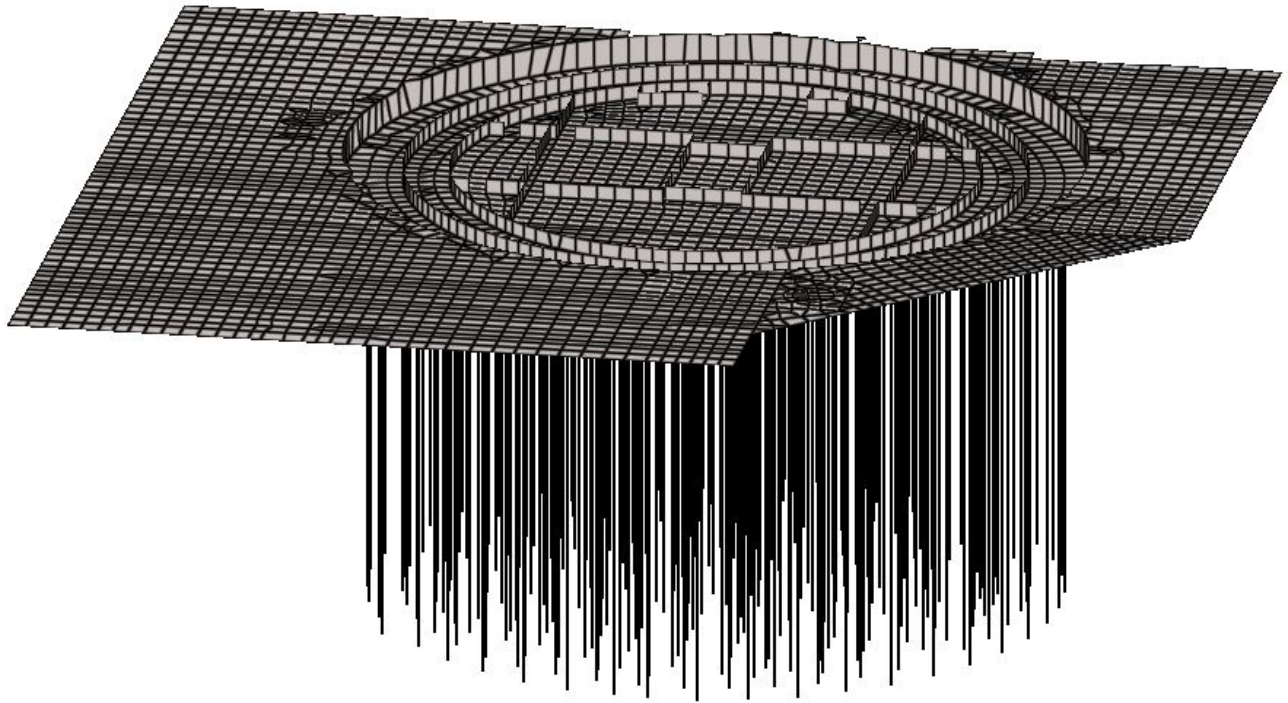


Fig. 7.14 Finite element model of the piled raft

7.3.4 Kinematic Response Characteristics of the Piled Raft

Harmonic Response

The transfer function in translation and rotation at the center of the raft was evaluated using the developed numerical model. The input motion was applied at the first soil layer. In order to identify the effect of a stiff cement treated soil layer, the kinematic response factors were analysed for the natural soil profile in addition to the actual soil profile with GI. Fig 7.15 (a) and (b) shows the variation of I_u and I_θ respectively, with frequency. The parameter I_θ was normalized with a diameter of 1.2 m, following Eq. 4.2. It is interesting to note that the presence of very stiff top layer with a depth equal to one sixth of the pile results in a much lesser filtering of ground motion. For example, at a frequency of 8 Hz the presence of a GI layer results in 40% higher translational motion. However, rotational component of foundation input motion is suppressed by the presence of the GI layer, in the practical range of earthquake frequencies.

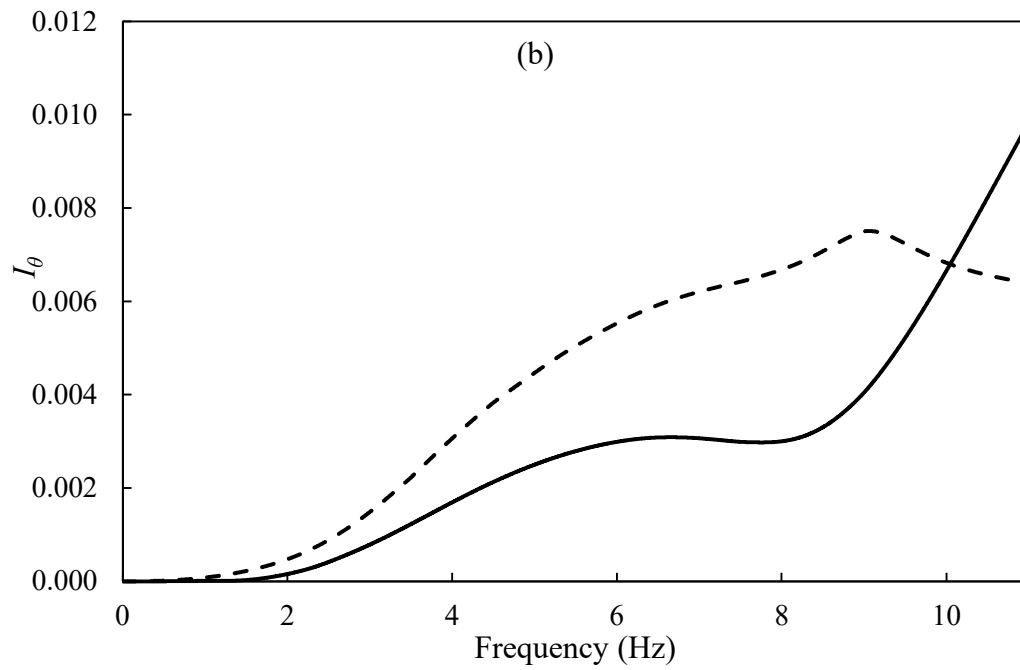
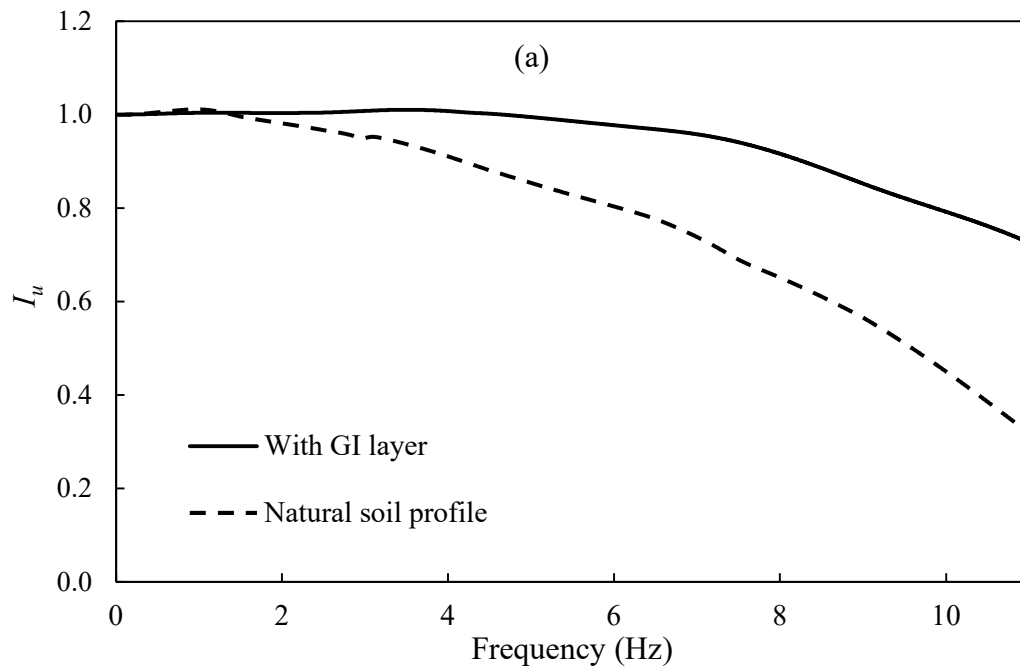


Fig. 7.15 Kinematic response factors for (a) translation and (b) rotation

Transient Response

The transient response of the foundation in the actual soil profile with GI was studied by applying the eight earthquake time histories described in Table 4.3. The response spectrum at the center of the raft was calculated for each input motion. Fig. 7.16 shows the spectral ratio curves for the time histories analysed. It is evident that beyond a period of 0.2s, the filtering effect is negligible.

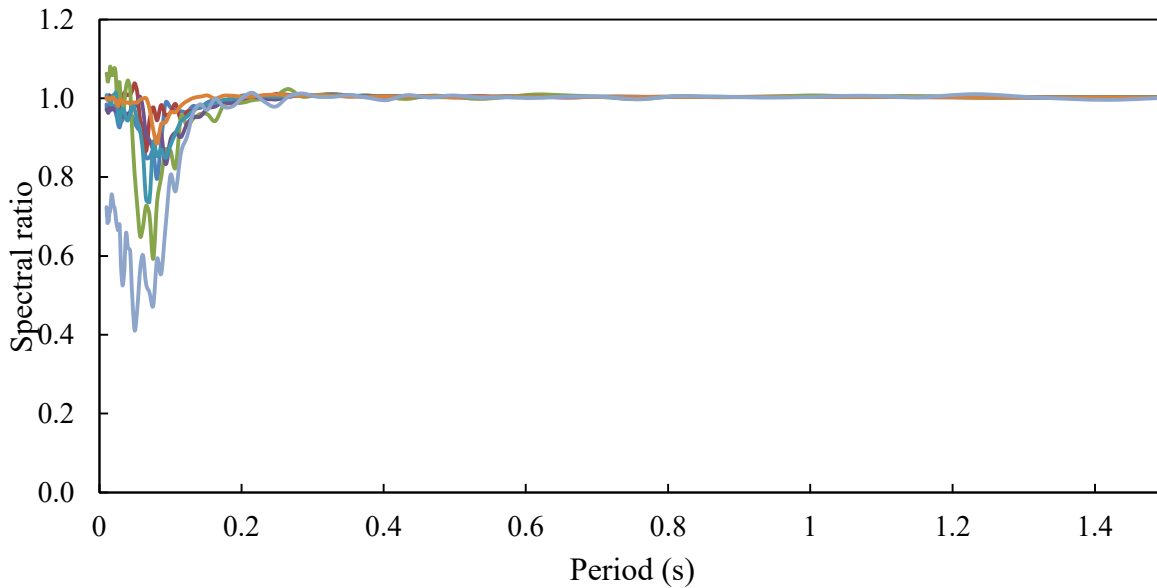


Fig. 7.16 Spectral ratio obtained for the input time histories

The soil profile in this case that consists of a stiff layer near the pile head contradicts the commonly assumed shear modulus variations adopted in previous studies (Gibson 1974; Karatzia and Mylonakis 2017; Vrettos 1991). Available studies on the spectral ratio (Iovino et al. 2019; Di Laora and de Sanctis 2013; Rovithis et al. 2019) have not considered a soil profile as in the case with GI layer.

For the purpose of comparison, the spectral ratio for the input motion described in Table 4.3, were also evaluated for the natural soil profile. A comparison of the spectral ratio obtained for a low frequency content motion (Norcia 2016) and a high frequency content motion (Christchurch 2011) is presented in Fig. 7.17 (a) and (b) respectively. A key finding is that the GI layer results in the critical period, T_{crit} being reduced by a factor of 0.3.

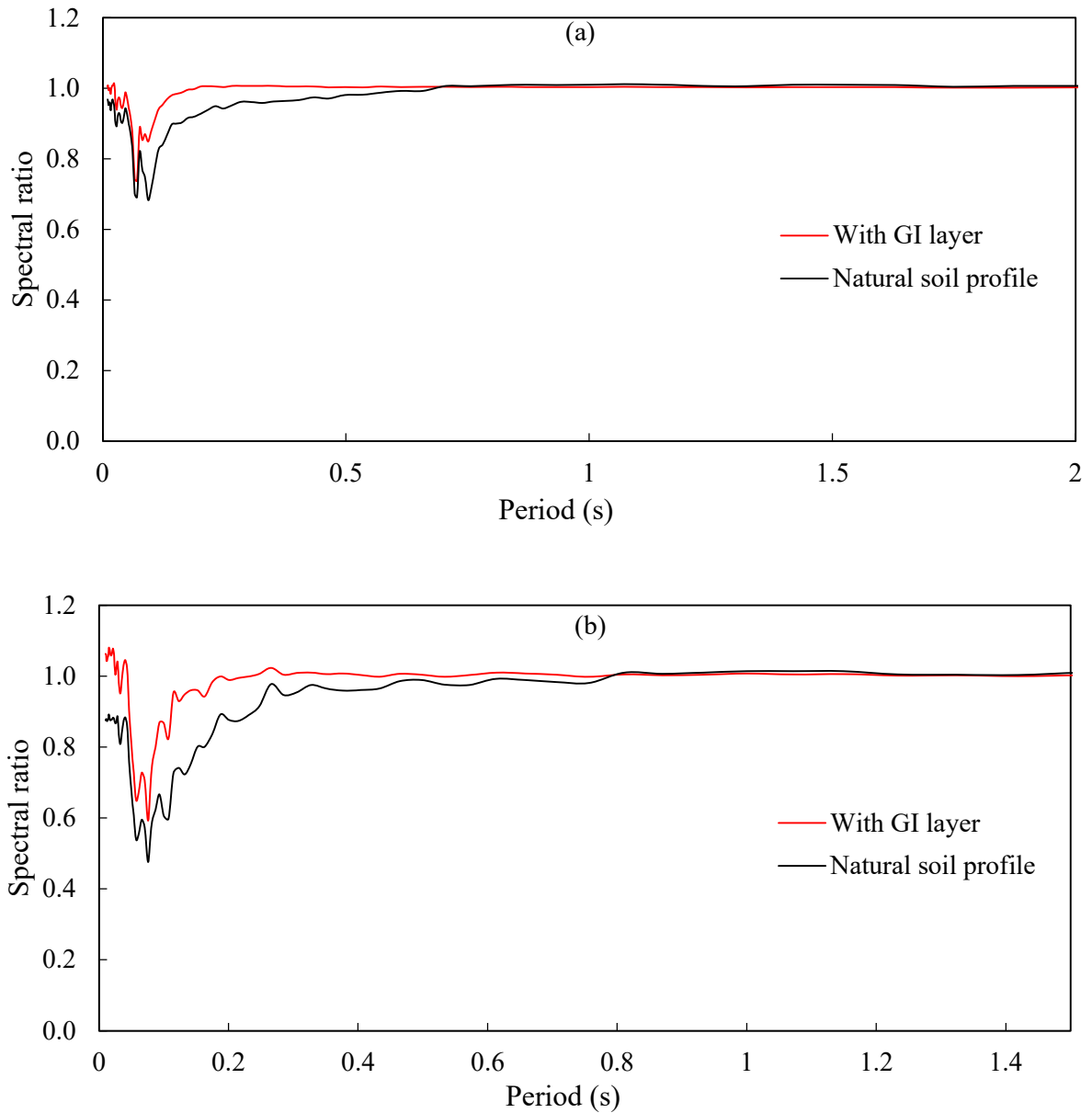


Fig. 7.17 Comparison of spectral ratio for (a) Norcia 2016 and (b) Christchurch 2011 input motions

The mean spectral ratio curve obtained from the analyses is presented in Fig. 7.18. For clarity, the critical structural periods are denoted as $T_{crit,nat}$ and $T_{crit,GI}$ for natural and improved soil profiles respectively. The corresponding spectral ratio ordinates at zero period are denoted by $\xi_{o,nat}$ and $\xi_{o,GI}$. Di Laora and de Sanctis (2013) reported that layer stiffness contrast had little influence on the structural periods T_{min} and T_{crit} (Refer section 4.3.1.2). The values of T_{min} and $T_{crit,GI}$ were found to be 0.07s and 0.18s respectively for the profile with GI layer. It is interesting

to note that the presence of a stiff GI layer does not alter the T_{min} value. On the other hand the threshold period, $T_{crit,nat}$ was found to be 0.70s for the foundation in natural soil profile. The ratio of $\xi_{o,GI}$ and $\xi_{o,nat}$ was found to be 1.13. Thus, the presence of a GI layer can result in a mild increase in the peak acceleration of the translational FIM.

These threshold periods are known to be largely independent of the input motion frequency content. However prediction of these structural periods using Eq. 4.12 requires an estimate of the active length (L_a) of pile. Iovino et al. (2019) modified the expression for T_{min} for inhomogeneous soil as

$$T_{min} = 1.2 \frac{L_a}{V_s} \quad (7.4)$$

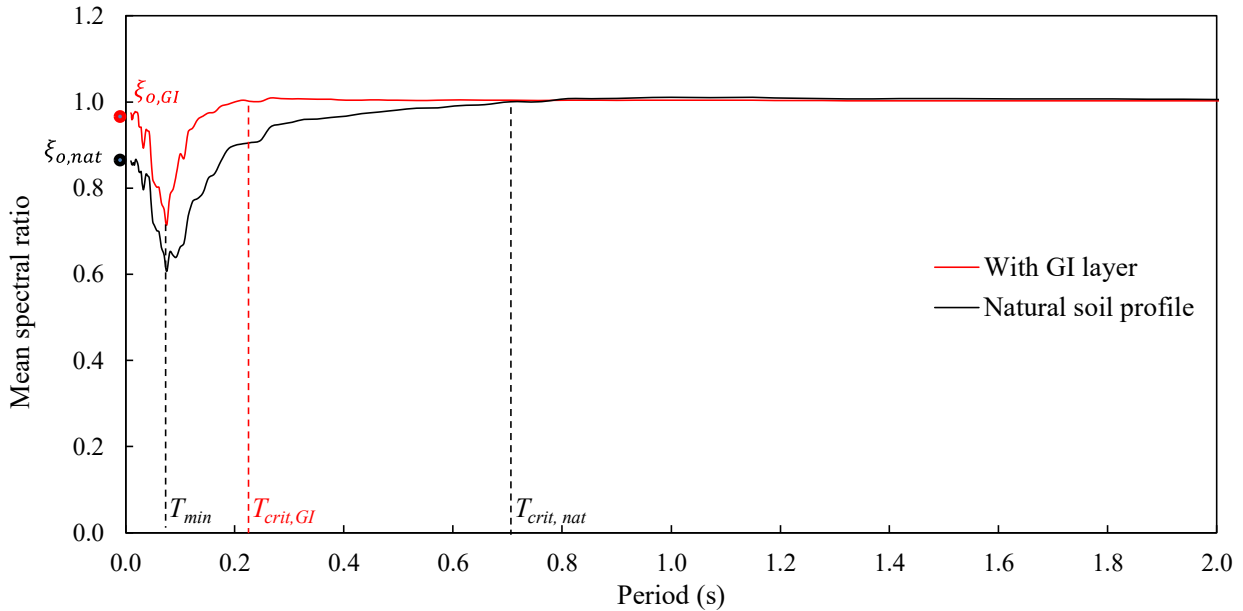


Fig. 7.18 Mean spectral ratio at the top of raft

Available formulations for active pile length of pile in inhomogeneous soil do not consider a soil profile as in the present case (Budhu and Davies 1987; Gazetas 1991; Gazetas et al. 1991; Di Laora and Rovithis 2015). The estimation of active length as 10 times the diameter was found to result in estimate of T_{min} and T_{crit} as 0.07s and 0.25s respectively, for the natural soil profile. However, the equations are not applicable to profiles such the one with GI. While making a comparison with predictive equations, one must also keep in mind that in the piled

raft analysed, the pile diameter and pile spacing are both non uniform. Nevertheless, from Fig 7.17 it can be concluded that the presence of a GI layer can result in a higher foundation input motion. The acceleration time history obtained from the seismic hazard analysis carried out at the site shows frequency content less than 5 Hz (NPCIL 2018), and therefore pile induced filtering can be expected to be minimal for the actual structure.

7.4 SUMMARY

Two case studies of soil-foundation-structure systems, one with a small piled raft and another with a large piled raft were evaluated in this chapter. The first case study dealt with the seismic response of a single degree of freedom system supported by a 2x2 piled raft in layered soil. The model is an extension of the centrifuge experiment reported by Banerjee et al. (2014), and discussed in section 4.2. Three different earthquake time histories with varying frequency content were applied as input ground motion. It was found that the response spectrum at the top of the raft is influenced by a change in pile spacing. Placing piles near the periphery of the raft is found to have a clear advantage in terms of structural response as well as pile forces. The maximum bending moment at the pile head was observed to increase mildly as the spacing between piles decreases. A novel non-dimensional axial force factor was proposed to quantify the role of piles in resisting overturning moments acting on a piled raft. Results from the study show that seismic response, quantified by the axial force factor could be considered as a parameter in the optimisation of pile arrangement in a piled raft.

The second case study dealt with a large piled raft foundation designed for an upcoming nuclear reactor building in India. The foundation system consists of a large 100m x 100m raft supported by 271 piles. The soil profile at the location was developed from Bender Element tests on undisturbed soil samples collected from boreholes, and cross-hole test results. The presence of a stiff cement mixed soil layer in the top 5.5m was found to pose a unique challenge as available studies on kinematic pile response did not consider a soil profile with stiffer layer on top. It was found that the presence of a stiff GI layer at the top can result in a higher foundation input motion in terms of translation for the superstructure. However, the presence of the GI layer was found to reduce the rocking component of FIM. The spectral ratio at the centre of the raft was also evaluated. The presence of a GI layer was found to reduce the threshold structural period, T_{crit} by a factor of 0.25.

CHAPTER 8

SUMMARY AND CONCLUSIONS

8.1 SUMMARY

Pile foundations subjected to dynamic loads form a complex soil structure interaction problem involving kinematic and inertial effects. The concept of piled raft has been accepted as an economical alternative to conventional pile foundations for heavily loaded structures. The present study investigated soil-piled raft interaction using numerical and experimental techniques. Observed damage from post-earthquake surveys has shown that pile supported structures are vulnerable to damage from seismic loads. From a detailed review of literature, it was found that most of the work on dynamic soil-pile interaction ignored the embedment effect of the pile cap. The primary motive of the research undertaken was to study soil structure interaction effects in piled raft foundations. The problems of kinematic soil-piled raft interaction and foundation response to dynamic loads were studied separately.

A substructure based numerical methodology was adopted to rigorously model the three-dimensional mechanisms governing the dynamic response of piled rafts. The FVSM methodology was implemented in the ACS SASSI program to study SSI in this research. An algorithm to partition the finite element domain into substructures was developed and implemented in Matlab. The methodology was evaluated using two levels of verification problems. Since the analysis follows the linear/equivalent linear soil modelling, the results from the study are suitable for situations where the soil is subjected to small strain levels.

The influence of raft embedment and pile layout on the kinematic response factors were investigated by a comprehensive study covering two foundation soil systems. The 2x2 piled raft-clay model used to simulate a centrifuge shaking table tests was extended to a parametric study to analyse the influence of pile layout on kinematic response factors. Pile spacing was found to have a profound impact on the rocking at the raft level in the piled raft models. The influence of raft embedment depth on the kinematic response of piled rafts was then investigated by carrying out a comprehensive parametric study on piled rafts with 3x3 and 5x3

pile configurations, embedded in homogenous and layered soil profiles. A clear trend of increasing filtering of translational response with increasing raft embedment was found from kinematic response factor plots.

The influence of ground contacting pile cap on the dynamic impedance of a pile group was investigated by studying the case study of a pile supported compressor unit in Hazira, India. Results from a lateral dynamic load test on a full scale test pile at the site are presented. The resonant frequency was observed to decrease below natural frequency observed from free vibration tests, with increasing force intensity due to nonlinear pile-soil interaction. A 3D model of a capped pile model as well as the 2x2 piled raft was then employed in a parametric study on vertical and horizontal dynamic stiffness. A unique feature of this study is the investigation of the ratio of load carried by piles in the piled raft or the load ratio in vertical and horizontal modes of vibration. The frequency dependent variation in the vertical load ratio found from this study can have implications in the design of piled rafts for dynamic loads.

The problem of seismic response of a piled raft in clay was investigated through a 1-g shaking table tests with instrumented piled raft and pile group models in clay, conducted at the 3 m x 3 m shaking table facility. The model was designed to simulate in prototype scale a hypothetical 2x2 pile group and a 2x2 piled raft in a homogeneous clay. A synthetic clay mix was adopted as the model soil after evaluation of its low strain shear modulus and modulus degradation behaviour using laboratory element tests. The clay-pile system was subjected to harmonic input motion at the base, with frequencies ranging from 0.1 to 25 Hz, and the transfer function for translation was calculated for the two foundation models.

The numerical analysis was also extended to two case studies involving piled raft foundations. The first case study dealt with the seismic response of an idealized single degree of freedom system supported by a 2x2 piled raft in layered soil. Three different earthquake time histories with varying frequency content were applied as input ground motion. The response spectra and pile forces were then compared for models with various pile placing. The second case study dealt with a large 100m x 100m piled raft foundation designed for an upcoming nuclear building in India. The soil-foundation system was modelled using actual soil properties from laboratory tests on undisturbed soil samples. The influence of the proposed stiff improved soil layer at the top 5.5 m was investigated.

8.2 CONCLUSIONS

8.2.1 SSI Analysis using the FVSM Based 3D Models

An algorithm to develop three dimensional models for the FVSM methodology and its subsequent execution using the ACS SASSI code was developed in this study. Results from 3D models of single and group piles were compared with available analytical solutions for impedances and kinematic response factors and a close match was found. Further, a centrifuge shaking table test with clay-piled raft system was simulated with strain compatible soil properties. The numerical models with piles modelled using the central beam and rigid links technique were found to provide a reasonable comparison with experimental results.

8.2.2 Kinematic Response of Piled Rafts

From studies on 2x2 piled raft-clay models, it was found that the translational and rocking response of piled rafts and pile groups do not differ considerably at low frequencies. However, the ratio of translational response of piled raft to pile group was found to increase with increasing pile spacing in the direction of motion at intermediate to high frequencies. The rocking response at the raft level was significantly affected by the pile arrangement.

The influence of raft embedment depth on the kinematic response of piled rafts were then investigated by carrying out a comprehensive parametric study on a piled rafts with 3x3 and 5x3 pile configurations, embedded in homogenous and layered soil profiles. A clear trend of increasing filtering of translational response with increasing raft embedment was found from kinematic response factor plots. For the 5x3 pile configuration, a dip in translational response was found at an a_o value of 0.2 where the response of piled raft with raft thickness equal to $5d$ was 0.42 times that of the pile group. An increasing embedment depth was found to increase the rocking response for the 3x3 piled rafts. However, this effect diminished when the number of piles in the direction of motion was increased. Transient response of the piled raft models was studied by applying eight different ground motion time histories and studying the spectral ratio curves. Embedment of the raft was found to influence all of the critical parameters that define the spectral ratio curve. The most significant effect was the decrease in peak acceleration, as well as shifting of the critical period T_{crit} . A reduction of peak acceleration in tune of 23-30% can be seen when the embedment increases from zero to $5d$. A comparison of the maximum bending moment profiles in piled raft and pile group models showed that that a raft embedment

of $5d$ can cause an increase in the pile head bending moment by 1.3 to 1.6 times. Thus, an additional conservatism in seismic design can be brought in by considering the additional filtering on input ground motion by an embedded raft, especially for large pile groups. However, caution should be exercised when there is a chance of scour or loss of contact around the side walls.

8.2.3 Dynamic Response of Piled Rafts

The presence of a circular ground contacting cap on a single pile was found to have a significant influence on the stiffness and damping coefficients. The alteration in impedance functions due to an embedded raft is found to become prominent when the pile-soil stiffness ratio, E_p/E_s was reduced from 1000 to 100. In the case of the 2x2 piled raft, the dynamic interaction for vertical vibration was found to exhibit characteristics of a dynamic system. Amplitude and phase of the dynamic interaction factor was found to be strongly influenced by both pile-soil modulus ratio and area ratio of piled raft. Available prediction equations for horizontal dynamic interaction factor, were found to produce large deviations in predicted amplitude and phase for the piled rafts considered in the present study.

The ratio of load carried by the pile in a capped pile was found to be primarily dependent on the relative pile-soil stiffness and frequency of vibration, in the vertical mode of vibration. However, for 2x2 piled rafts the load ratio was found to be influenced by both frequency and pile spacing in the vertical mode of vibration. When compared to static loading, a decrease of up to 40% in the load carried by piles was observed for dynamic loading in stiff soil profiles. Thus the design of a piled raft for high frequency dynamic loads has to consider the deviation from static load sharing at high frequencies. Load ratio in horizontal mode of vibration was found to be mildly affected by frequency of loading, for both capped pile and piled raft models.

8.2.4 Experimental Evidence

The kinematic response factor in translation was then calculated from the experimental results. It was found that the embedded raft resulted in a reduction in the translational response with increasing frequency beyond a certain threshold frequency, which was close to 2.5 Hz. A maximum reduction of 41% was found at a frequency of 15Hz. The kinematic response factor obtained experimentally was in agreement with the trend obtained from numerical analyses.

The pile head bending strains in the piled raft and pile group were found to be close to each other up to a frequency of 15 Hz. However, alteration in the kinematic bending strains was found in the piled raft model beyond the depth of fixity.

8.2.5 Case Studies of Piled Raft-Structure Systems

A novel non-dimensional axial force factor was proposed to quantify the role of piles in resisting overturning moments acting on a piled raft. The axial force factor was found to vary with increasing pile spacing with non-linear trend, due to pile-soil-pile and raft-soil-pile interactions.

From the study on a large piled raft in a deep soil site, it was found that an improved top soil layer significantly alters the kinematic response factors in translation and rotation, when compared to the natural soil profile. From a transient ground motion analysis using eight different earthquake time histories, it was found that the improved layer causes a reduction in the critical structural period by a factor of 0.25, and an increase in the peak horizontal acceleration by a factor of 1.13.

8.3 RECOMMENDATIONS FOR FUTURE RESEARCH

Some recommendations for future investigations are:

The present study adopted numerical analysis in the frequency domain, considering material nonlinearity by approximate methods. The response of soil-foundation-structure systems to high intensity seismic shaking involves additional secondary nonlinearity at the vicinity of the foundation. These effects can be simulated only by nonlinear analysis in the time domain that can model effects such as pile soil slip, and loss of soil-foundation contact. The lateral earth pressure acting on the sidewalls of the raft can also be a subject of investigation.

The piled raft models considered in this study fall in the category of small piled rafts. Investigations on the dynamic response of piled raft systems can be extended to large piled rafts. The present study did not investigate pile-soil systems with varying flexural behaviour of the pile. It would be useful to study separately the influence of foundation embedment on piled rafts with rigid and flexible piles.

Closed form analytical expressions can be arrived at to calculate kinematic response factors for pile groups with embedded pile caps. Empirical equations for spectral ratio parameters could be derived based on the results from numerical simulations such as those discussed in this thesis. Parameters such as the axial force factor could be considered for practical seismic design guidelines for piled rafts.

It would be useful to execute experimental studies using 1-g and N-g models to measure the pile forces in axial, shear and bending, during seismic shaking. The effects of loss of contact and pile soil slip can be experimentally simulated by high strain testing.

REFERENCES

- Abdoun, T., Dobry, R., O'Rourke, T. D., and Chaudhuri, D.** (1996). Centrifuge modeling of seismically-induced lateral deformation during liquefaction and its effect on a pile foundation. *Proc. of the Japan-US Workshop on Earthquake Resistant Design of Lifeline Facilities and Countermeasures Against Soil Liquefaction*, 6, 525–539.
- Ali, O. S., Aggour, M. S., and McCuen, R. H.** (2017). Dynamic soil–pile interactions for machine foundations. *International Journal of Geotechnical Engineering*, **11**(3), 236–247.
- Alnuaim, A. M., El Nagggar, H., and El Nagggar, M. H.** (2015a). Performance of micropiled raft in sand subjected to vertical concentrated load: centrifuge modeling. *Canadian Geotechnical Journal*, **52**(1), 33–45.
- Alnuaim, A. M., El Nagggar, H., and El Nagggar, M. H.** (2017). Evaluation of piled raft performance using a verified 3D nonlinear numerical model. *Geotechnical and Geological Engineering*, **35**(4), 1831–1845.
- Alnuaim, A. M., El Nagggar, M. H., and El Nagggar, H.** (2015b). Performance of micropiled raft in clay subjected to vertical concentrated load: centrifuge modeling. *Canadian Geotechnical Journal*, **52**(12), 2017–2029.
- Alnuaim, A. M., El Nagggar, M. H., and El Nagggar, H.** (2016). Numerical investigation of the performance of micropiled rafts in sand. *Computers and Geotechnics*, **77**, 91–105.
- Alnuaim, A. M., El Nagggar, M. H., and El Nagggar, H.** (2018). Performance of micropiled rafts in clay: Numerical investigation. *Computers and Geotechnics*, **99**, 42–54.
- Amorosi, A., Boldini, D., and Di Lernia, A.** (2017). Dynamic soil-structure interaction: a three-dimensional numerical approach and its application to the Lotung case study. *Computers and Geotechnics*, **90**, 34–54.
- Anoyatis, G.** (2013). *Contribution to kinematic and inertial analysis of piles by analytical and experimental methods*. PhD Thesis, University of Patras, Rio, Greece.
- Anoyatis, G., Di Laora, R., Mandolini, A., and Mylonakis, G.** (2013). Kinematic response of single piles for different boundary conditions: analytical solutions and normalization schemes. *Soil Dynamics and Earthquake Engineering*, **44**, 183–195.

- Arango-Greiffenstein, I.** (1971). *Seismic stability of slopes in saturated clay*. Ph. D. Thesis, University of California Berkely, California, U.S.A.
- ASCE.** (2013). *Minimum Design Loads for Buildings and Other Structures (ASCE/SEI 7-10)*. American Society of Civil Engineers, Reston, Virginia, U.S.A.
- ASCE.** (2017). *Seismic Analysis of Safety-Related Nuclear Structures (ASCE/SEI 4-16)*. American Society of Civil Engineers, Reston, Virginia, U.S.A.
- ATC.** (1978). *Tentative Provisions for the Development of Seismic Regulations for Buildings,(ATC-3-06)*. National Bureau of Standards-Special Publication 510, Washington, DC.
- ATC.** (2005). *Improvement of nonlinear static seismic analysis procedures (FEMA 440)*. Applied Technology Council, Redwood City, California.
- Ayothiraman, R., and Boominathan, A.** (2013). Depth of fixity of piles in clay under dynamic lateral load. *Geotechnical and Geological Engineering*, **31**(2), 447–461.
- Ayothiraman, R., Boominathan, A., and Krishna Kumar, S.** (2012). Lateral dynamic response of full-scale single piles: Case studies in India. In *Full-scale testing and foundation design: Honoring Bengt H. Fellenius* (pp. 710–721).
- Banerjee, S, Goh, S. H., and Lee, F. H.** (2014). Earthquake-induced bending moment in fixed-head piles in soft clay. *Géotechnique*, **64**(6), 431–446.
- Banerjee, S.** (2009). *Centrifuge and Numerical Modelling of Soft Clay-Pile-Raft Foundations Subjected To Seismic Shaking*. Doctoral Dissertation, National University of Singapore.
- Banerjee, S., Goh, S. H., and Lee, F. H.** (2007). Response of Soft Clay Strata and Clay-Pile-Raft Systems To Seismic Shaking. *Journal of Earthquake and Tsunami*, **01**(3), 233–255. <https://doi.org/10.1142/S1793431107000146>
- Banerjee, S., and Lee, F. H.** (2013). Centrifuge shaking table tests on a single pile embedded in clay subjected to earthquake excitation. *International Journal of Geotechnical Engineering*, **7**(2), 117–123.

- Berger, E., Mahi, S. A., and Pyke, R.** (1977). Simplified method for evaluating soil-pile-structure interaction effects. *Proc. of Offshore Technology Conference (OTC'77)*, Houston, Texas.
- Bharathi, M., Dubey, R. N., and Shukla, S. K.** (2019). Experimental investigation of vertical and batter pile groups subjected to dynamic loads. *Soil Dynamics and Earthquake Engineering*, **116**, 107–119.
- Biot, M. A.** (1962). Mechanics of deformation and acoustic propagation in porous media. *Journal of Applied Physics*, **33**(4), 1482–1498.
- BIS.** (1981). *Guide for lateral dynamic load test on piles (IS 9716: 1981)*. Bureau of Indian Standards, New Delhi.
- BIS.** (2000). *IS-456: Plain and Reinforced concrete-Code of Practice*. Bureau of Indian Standards, New Delhi.
- BIS.** (2014a). *Criteria for earthquake resistant design of structures- part 2: liquid retaining tanks (IS 1893-2)*. Bureau of Indian Standards, New Delhi.
- BIS.** (2014b). *Criteria for earthquake resistant design of structures - part 3: bridges and retaining walls (IS 1893-3)*. Bureau of Indian Standards, New Delhi.
- BIS.** (2015). *Criteria for earthquake resistant design of structures part 4: industrial structures including stack-like structures (IS 1893-4)*. Bureau of Indian Standards, New Delhi.
- BIS.** (2016). *Criteria for Earthquake Resistant Design of Structures Part I General Provisions and Buildings (IS 1893-1)*. Bureau of Indian Standards, New Delhi.
- Biswas, S., and Manna, B.** (2018). Experimental and Theoretical Studies on the Nonlinear Characteristics of Soil-Pile Systems under Coupled Vibrations. *Journal of Geotechnical and Geoenvironmental Engineering*, **144**(3), 4018007.
- Blaney, G. W., Kausel, E., and Roesset, J. M.** (1976). Dynamic stiffness of piles. *Proc. 2nd Int. Conf. Numer. Meth. Geomech, Blacksburg, 1976*, 1001–1012.
- Bochert, J. S., Schau, H., and Schmitt, T.** (2015). Seismic soil-structure interaction of a nuclear building : Comparison of two different methods. *Proc. of 23rd International Conference on Structural Mechanics in Reactor Technology, Manchester UK*, 248.

- Bolisetti, C., Whittaker, A. S., and Coleman, J. L.** (2018). Linear and nonlinear soil-structure interaction analysis of buildings and safety-related nuclear structures. *Soil Dynamics and Earthquake Engineering*, **107**, 218–233.
- Boominathan, A., and Ayothiraman, R.** (2006). Dynamic response of laterally loaded piles in clay. *Proceedings of the Institution of Civil Engineers-Geotechnical Engineering*, **159**(3), 233–241.
- Boominathan, A., and Ayothiraman, R.** (2007). An experimental study on static and dynamic bending behaviour of piles in soft clay. *Geotechnical and Geological Engineering*, **25**(2), 177.
- Boominathan, A., Ayothiraman, R., and Elango, J.** (2002). Lateral vibration response of full scale single piles. *Proc. of 9th International Conference on Piling and Deep Foundations, France*, 141–146.
- Boominathan, A., Kumar, S. K., and Subramanian, R. M.** (2015). Lateral dynamic response and effect of weakzone on the stiffness of full scale single piles. *Indian Geotechnical Journal*, **45**(1), 43–50.
- Boominathan, A., Varghese, R., and Nair, S. K.** (2018). *Soil–structure interaction analysis of pile foundations subjected to dynamic loads*. pp 45-61. In **Krishna, A. M., Dey, A., & Sreedeeep, S.** (eds) *Geotechnics for Natural and Engineered Sustainable Technologies*, Springer.
- Boulanger, B. R. W., Curras, C. J., Member, S., Kutter, B. L., Wilson, D. W., Member, A., and Abghari, A.** (1999). Seismic soil-pile-structure interaction experiments and analyses. *Journal Of Geotechnical And Geoenvironmental Engineering*, **125**, 750–759.
- Boulanger, R. W., Kutter, B. L., Brandenburg, S. J., Singh, P., Chang, D., and University of California, D. C. for G. M.** (2003). *Pile foundations in liquefied and laterally spreading ground during earthquakes: centrifuge experiments & analyses (UCD/CGM-03/01)*. Center for Geotechnical Modeling, Department of Civil and Environmental Engineering, University of California, Davis, California.

- Brandenberg, S. J., Boulanger, R. W., Kutter, B. L., and Chang, D.** (2005). Behavior of pile foundations in laterally spreading ground during centrifuge tests. *Journal of Geotechnical and Geoenvironmental Engineering*, **131**(11), 1378–1391.
- Bray, J. D.** (1991). *The effects of tectonic movements on stresses and deformations in earth embankments*. Doctoral Dissertaion, University of California, Berkely.
- Brignoli, E. G. M., Gotti, M., and Stokoe, K. H.** (1996). Measurement of shear waves in laboratory specimens by means of piezoelectric transducers. *Geotechnical Testing Journal*, **19**(4), 384–397.
- Budhu, M., and Davies, T. G.** (1987). Nonlinear analysis of laterality loaded piles in cohesionless soils. *Canadian Geotechnical Journal*, **24**(2), 289–296.
- Burr, J. P., Pender, M. J., and Larkin, T. J.** (1997). Dynamic response of laterally excited pile groups. *Journal of Geotechnical and Geoenvironmental Engineering*, **123**(1), 1–8.
- C S I (Computers and Structures).** (2009). *SAP2000: Integrated finite element analysis and design of structures basic analysis reference manual*. Computers and Structures, Inc., Berkeley, California, USA.
- Café, P. F. M.** (1991). *Dynamic response of a pile-supported bridge on soft soil*. M.S Thesis, University of California, Davis.
- Chandra, S., Saha, R., and Haldar, S.** (2014). Inelastic seismic behavior of soil – pile raft – structure system under bi-directional ground motion. *Soil Dynamics and Earthquake Engineering*, **67**, 133–157. <https://doi.org/10.1016/j.soildyn.2014.08.012>
- Chang, D., Boulanger, R. W., Brandenberg, S. J., and Kutter, B. L.** (2006). Dynamic analyses of soil-pile-structure interaction in laterally spreading ground during earthquake shaking. In *Seismic Performance and Simulation of Pile Foundations in Liquefied and Laterally Spreading Ground* (pp. 218–229).
- Chattaraj, R., and Sengupta, A.** (2016). Liquefaction potential and strain dependent dynamic properties of Kasai River sand. *Soil Dynamics and Earthquake Engineering*, **90**, 467–475.

- Chatterjee, K., Choudhury, D., and Poulos, H. G.** (2015). Seismic analysis of laterally loaded pile under influence of vertical loading using finite element method. *Computers and Geotechnics*, *67*, 172–186.
- Chau, K. T., Shen, C. Y., and Guo, X.** (2009). Nonlinear seismic soil–pile–structure interactions: shaking table tests and FEM analyses. *Soil Dynamics and Earthquake Engineering*, *29*(2), 300–310.
- Chen, J. C.** (1980). *Analysis of Local Variation in Free-Field Seismic Ground Motions*. Doctoral Dissertaion, University of California, Berkely.
- Chopra, S.** (1990). A geological cum geomorphological framework of Haryana and adjoining areas for landuse appraisal using LANDSAT imagery. *Journal of the Indian Society of Remote Sensing*, *18*(1–2), 15–22.
- Clancy, P., and Randolph, M. F.** (1993). An approximate analysis procedure for piled raft foundations. *International Journal for Numerical and Analytical Methods in Geomechanics*, *17*(12), 849–869.
- Clough, R. W., and Seed, H. B.** (1963). Earthquake resistance of sloping core dams. *Journal of the Soil Mechanics and Foundations Division*, *89*(1), 209–244.
- Coleman, J. L., Bolisetti, C., and Whittaker, A. S.** (2016). Time-domain soil-structure interaction analysis of nuclear facilities. *Nuclear Engineering and Design*, *298*, 264–270. <https://doi.org/10.1016/j.nucengdes.2015.08.015>
- Cooley, J. W., and Tukey, J. W.** (1965). An algorithm for the machine calculation of complex Fourier series. *Mathematics of Computation*, *19*(90), 297–301.
- Cunha, R. P., Poulos, H. G., and Small, J. C.** (2001). Investigation of design alternatives for a piled raft case history. *Journal of Geotechnical and Geoenvironmental Engineering*, *127*(8), 635–641.
- Curras, C. J., Boulanger, R. W., Kutter, B. L., and Wilson, D. W.** (1999). Seismic soil-pile-structure interaction in soft clay. *Earthquake Geotechnical Engineering*, 965–970.

- de Almeida Barros, P. L., Labaki, J., and Mesquita, E.** (2019). IBEM-FEM model of a piled plate within a transversely isotropic half-space. *Engineering Analysis with Boundary Elements*, **101**, 281–296.
- de Sanctis, L., Maiorano, R. M. S., and Aversa, S.** (2010). A method for assessing kinematic bending moments at the pile head. *Earthquake Engineering & Structural Dynamics*, **39**(10), 1133–1154.
- de Sanctis, L., and Mandolini, A.** (2006). Bearing capacity of piled rafts on soft clay soils. *Journal of Geotechnical and Geoenvironmental Engineering*, **132**(12), 1600–1610.
- de Sanctis, L., and Russo, G.** (2008). Analysis and performance of piled rafts designed using innovative criteria. *Journal of Geotechnical and Geoenvironmental Engineering*, **134**(8), 1118–1128.
- Dhandapani, Y., Sakthivel, T., Santhanam, M., Gettu, R., and Pillai, R. G.** (2018). Mechanical properties and durability performance of concretes with Limestone Calcined Clay Cement (LC3). *Cement and Concrete Research*, **107**, 136–151.
- Di Laora, R., and Mandolini, A.** (2011). Some remarks about Eurocode and Italian code about piled foundations in seismic area. *Proc. of Athina 2011 XV ECSMGE: Geotechnics of Hard Soils Soft Rocks*.
- Di Laora, R. and de Sanctis, L.** (2013). Piles-induced filtering effect on the foundation input motion. *Soil Dynamics and Earthquake Engineering*, **46**, 52–63.
- Di Laora, R., Grossi, Y., de Sanctis, L., and Viggiani, G. M. B.** (2017). An analytical solution for the rotational component of the Foundation Input Motion induced by a pile group. *Soil Dynamics and Earthquake Engineering*, **97**(March), 424–438. <https://doi.org/10.1016/j.soildyn.2017.03.027>
- Di Laora, R., and Mandolini, A.** (2011). Some aspects of the design of pile foundations under seismic motion. *Rivista Italiana Di Geotecnica*, **1**, 3–74.
- Di Laora, R., Mandolini, A., and Mylonakis, G.** (2012). Insight on kinematic bending of flexible piles in layered soil. *Soil Dynamics and Earthquake Engineering*, **43**, 309–322.

- Di Laora, R., and Rovithis, E.** (2015). Kinematic bending of fixed-head piles in nonhomogeneous soil. *Journal of Geotechnical and Geoenvironmental Engineering*, *141*(4), 4014126.
- Dinh, D., Nguyen, C., Kim, D., and Jo, S.** (2013). *Settlement of Piled Rafts with Different Pile Arrangement Schemes via Centrifuge Tests*. *139*(October), 1690–1698. [https://doi.org/10.1061/\(ASCE\)GT.1943-5606.0000908](https://doi.org/10.1061/(ASCE)GT.1943-5606.0000908).
- Dobry, R., and Gazetas, G.** (1988). Simple method for dynamic stiffness and damping of floating pile groups. *Geotechnique*, *38*(4), 557–574.
- Dobry, R., and O’Rourke, M. J.** (1983). Discussion of “Seismic Response Of End-bearing Piles” by Raul Flores-Berrones and Robert V. Whitman (April, 1982). *Journal of Geotechnical Engineering*, *109*(5), 778–781.
- Dobry, R., Vicente, E., O’Rourke, M., and Roesset, M.** (1982). Horizontal stiffness and damping of single piles. *Journal of Geotechnical and Geoenvironmental Engineering*, *108*(GT3).
- Durante, M. G.** (2015). *Experimental and numerical assessment of dynamic soil–pile–structure interaction*. Ph. D. Thesis, Universita’ degli Studi di Napoli Federico II, Napoli.
- Durante, M. G., Di Sarno, L., Mylonakis, G., Taylor, C. A., and Simonelli, A. L.** (2016). Soil–pile–structure interaction: experimental outcomes from shaking table tests. *Earthquake Engineering & Structural Dynamics*, *45*(7), 1041–1061.
- El-Marsafawi, H., Han, Y. C., and Novak, M.** (1992). Dynamic experiments on two pile groups. *Journal of Geotechnical Engineering*, *118*(4), 576–592.
- El Naggari, M. H., and Novak, M.** (1995). Nonlinear lateral interaction in pile dynamics. *Soil Dynamics and Earthquake Engineering*, *14*(2), 141–157.
- Elkasabgy, M., and El Naggari, M. H.** (2013). Dynamic response of vertically loaded helical and driven steel piles. *Canadian Geotechnical Journal*, *50*(5), 521–535.
- Elkasabgy, M., and El Naggari, M. H.** (2018). Lateral Vibration of Helical and Driven Steel Piles Installed in Clayey Soil. *Journal of Geotechnical and Geoenvironmental Engineering*, *144*(9), 6018009.

- Emani, P. K., and Maheshwari, B. K.** (2009). Dynamic impedances of pile groups with embedded caps in homogeneous elastic soils using CIFEEM. *Soil Dynamics and Earthquake Engineering*, **29**(6), 963–973. <https://doi.org/10.1016/j.soildyn.2008.11.003>
- EN 1998-5.** (2004). *Eurocode 8: Design of structures for earthquake resistance-Part 5: Foundations, retaining structures and geotechnical aspects (EN 1998-5)*. British Standards, London.
- Fan, K., Gazetas, G., Kaynia, A., Kausel, E., and Ahmad, S.** (1991). Kinematic Seismic Response of Single Piles and Pile Groups. *Journal of Geotechnical Engineering*, **117**(12), 1860–1879. [https://doi.org/10.1061/\(ASCE\)0733-9410\(1991\)117:12\(1860\)](https://doi.org/10.1061/(ASCE)0733-9410(1991)117:12(1860))
- Finn, W. D. L.** (1987). Centrifuge model studies of piles under simulated earthquake lateral loading. *Geotech. Special Pub.*, **11**, 21–38.
- Fioravante, V., Giretti, D., and Jamiolkowski, M.** (2008). *Physical modeling of raft on settlement reducing piles*. pp 206-229 In Laier, J. E., Crapps, D. K., & Hussein, M. H. (eds) *From research to practice in geotechnical engineering*, ASCE Publications.
- Flores-Berrones, R., and Whitman, R. V.** (1982). Seismic Response of end-bearing piles. *Journal of the Geotechnical Engineering Division*, **108**, 554–569.
- Fukuwa, N., and Wen, X.** (2007). Efficient soil-structure interaction analysis method of a large-scale pile group. *Proc. of the Fourth US-Japan Workshop on Soil Structure Interaction, Tsukuba*.
- Gazetas, G., Anastasopoulos, I., Adamidis, O., and Kontoroupi, T.** (2013). Nonlinear rocking stiffness of foundations. *Soil Dynamics and Earthquake Engineering*, **47**, 83–91.
- Gazetas, G.** (1984). Seismic response of end-bearing single piles. *International Journal of Soil Dynamics and Earthquake Engineering*, **3**(2), 82–93.
- Gazetas, G.** (1991). Foundation vibrations. In *Foundation engineering handbook* (pp. 553–593). Springer.
- Gazetas, G., and Dobry, R.** (1984a). Horizontal response of piles in layered soils. *Journal of Geotechnical Engineering*, **110**(1), 20–40.

- Gazetas, G., and Dobry, R.** (1984b). Simple radiation damping model for piles and footings. *Journal of Engineering Mechanics*, **110**(6), 937–956.
- Gazetas, G., Fan, K., Kaynia, A., and Kausel, E.** (1991). Dynamic interaction factors for floating pile groups. *Journal of Geotechnical Engineering*, **117**(10), 1531–1548.
- Ghiocel, D. M.** (2019). Sensivity Studies for Nuclear Island Founded on Piles Including Effects of Seismic Motion Spatial Variation and Local Nonlinear Soil Behavior. *Proc. of Structural Mechanics in Reactor Technology (SMiRT-25), Charlotte, NC, U.S.A.*
- Ghiocel Predictive Technologies.** (2014). *ACS SASSI: An Advanced Computational Software for 3D Dynamic Analysis Including Soil-Structure Interaction*. Ghiocel Predictive Technologies, Inc., Pittsford, NY, U.S.A
- Gibson, R. E.** (1974). The analytical method in soil mechanics. *Geotechnique*, **24**(2), 115–140.
- Gle, D. R., and Woods, R. D.** (1984). Suggested procedure for conducting dynamic lateral-load tests on piles. In *Laterally loaded deep foundations: analysis and performance*. ASTM International.
- Goh, S. H., and Zhang, L.** (2017). Estimation of peak acceleration and bending moment for pile-raft systems embedded in soft clay subjected to far-field seismic excitation. *Journal of Geotechnical and Geoenvironmental Engineering*, **143**(11), 4017082.
- Gohl, W. B.** (1991). *Response of pile foundations to simulated earthquake loading: experimental and analytical results*. Ph.D. Thesis, University of British Columbia, Canada.
- Goit, C. S., and Saitoh, M.** (2018). Single pile under vertical vibrations in cohesionless soil. *Géotechnique*, **68**(10), 893–904.
- Gupta, B. K., and Basu, D.** (2018). Dynamic analysis of axially loaded end-bearing pile in a homogeneous viscoelastic soil. *Soil Dynamics and Earthquake Engineering*, **111**(March), 31–40. <https://doi.org/10.1016/j.soildyn.2018.04.019>
- Gupta, V. K., and Trifunac, M. D.** (1991). Seismic response of multistoried buildings including the effects of soil-structure interaction. *Soil Dynamics and Earthquake Engineering*, **10**(8), 414–422.

- Gutierrez, J. A., and Chopra, A. K.** (1978). A substructure method for earthquake analysis of structures including structure-soil interaction. *Earthquake Engineering & Structural Dynamics*, **6**(1), 51–69.
- Hamada, J.** (2016). Bending moment of piles on piled raft foundation subjected to ground deformation during earthquake in centrifuge model test. *Japanese Geotechnical Society Special Publication*, **2**(34), 1222–1227. <https://doi.org/10.3208/jgssp.JPN-119>
- Hamayoon, K., Morikawa, Y., Oka, R., and Zhang, F.** (2016). 3D dynamic finite element analyses and 1 g shaking table tests on seismic performance of existing group-pile foundation in partially improved grounds under dry condition. *Soil Dynamics and Earthquake Engineering*, **90**, 196–210.
- Han, Y.** (2008). Study of vibrating foundations considering soil-pile-structure interaction for practical applications. *Earthquake Engineering and Engineering Vibration*, **7**(3), 321.
- Han, Y. C., Wang, S., Chan, P., and Sprinkhuysen, A.** (1999). Design of an elevated compressor table top structure considering soil-pile-structure interaction. *Proc. of the Annual Conf. CSCE, Regina, Saskatchewan*, 291–300.
- Han, Y., and Novak, M.** (1988). Dynamic behaviour of single piles under strong harmonic excitation. *Canadian Geotechnical Journal*, **25**(3), 523–534.
- Hardin, B. O.** (1978). The nature of stress-strain behavior for soils. *From Volume I of Earthquake Engineering and Soil Dynamics--Proceedings of the ASCE Geotechnical Engineering Division Specialty Conference, June 19-21, 1978, Pasadena, California.*
- Hokmabadi, A. S., Fatahi, B., and Samali, B.** (2014). Assessment of soil–pile–structure interaction influencing seismic response of mid-rise buildings sitting on floating pile foundations. *Computers and Geotechnics*, **55**, 172–186.
- Hokmabadi, A. S., Fatahi, B., and Samali, B.** (2015). Physical modeling of seismic soil-pile-structure interaction for buildings on soft soils. *International Journal of Geomechanics*, **15**(2), 4014046.
- Hokmabadi, A. S.** (2014). *Effect of Dynamic Soil-pile Structure Interaction on Seismic Response of Mid-rise Moment Resisting Frames*. University of Technology, Sydney.

- Horikoshi, K.** (1995). Optimum design of piled raft foundations. *PhD Thesis, The Univ. of Western Australia.*
- Horikoshi, K., Matsumoto, T., Hashizume, Y., and Watanabe, T.** (2003). Performance of piled raft foundations subjected to dynamic loading. *International Journal of Physical Modelling in Geotechnics*, **3**(2), 51–62. <https://doi.org/10.1680/ijpmg.2003.030205>
- ICC.** (2018). *International building code*. International Code Council, ICC Country Club Hills, IL, U.S.A.
- Iovino, M., Di Laora, R., Rovithis, E., and de Sanctis, L.** (2019). The Beneficial Role of Piles on the Seismic Loading of Structures. *Earthquake Spectra*, **35**(3), 1141–1162.
- Japanese Road Association.** (1996). *Specification for Highway Bridges, Part V, Seismic Design*. Japan Rpad Association, Tokyo, Japan.
- Jaya, K. P., and Prasad, A. M.** (2004). Dynamic behaviour of pile foundations in layered soil medium using cone frustums. *Geotechnique*, **54**(6), 399–414. <https://doi.org/10.1680/geot.54.6.399.45426>
- Jeremic, B., Jie, G., Preisig, M., and Tafazzoli, N.** (2009). Time domain simulation of soil-foundation-structure interaction in non-uniform soils. *Earthquake Engineering and Structural Dynamics*, **38**(5), 699–718. <https://doi.org/10.1002/eqe.896>
- JSCE.** (2007). *Standard specifications for concrete structures - design (JSCE 15)*. Japan Society of Civil Engineers, Tokyo, Japan.
- Kagawa, T., and Kraft, L. M.** (1981). Lateral pile response during earthquakes. *Journal of Geotechnical and Geoenvironmental Engineering*, **107**(ASCE 16735).
- Kana, D. D., Boyce, L., and Blaney, G. W.** (1986). *Development of a scale model for the dynamic interaction of a pile in clay.*
- Kanellopoulos, K., and Gazetas, G.** (2019). Vertical static and dynamic pile-to-pile interaction in non-linear soil. *Géotechnique*, *April*, 1–16. <https://doi.org/10.1680/jgeot.18.p.303>

- Kang, M., Baneree, S., Lee, F.-H., and Xie, H. P.** (2012). Dynamic Soil-Pile-Raft Interaction in Normally Consolidated Soft Clay During Earthquakes. *Journal of Earthquake and Tsunami*, **06**(03), 1250031. <https://doi.org/10.1142/S1793431112500315>
- Karatzia, X., and Mylonakis, G.** (2017). Horizontal stiffness and damping of piles in inhomogeneous soil. *Journal of Geotechnical and Geoenvironmental Engineering*, **143**(4), 4016113.
- Katzenbach, R, Arslan, U., and Moormann, C.** (2000). Piled raft foundation projects in Germany. In J. . Hemsley (Ed.), *Design applications of raft foundations* (p. 323). Thomas Telford.
- Katzenbach, R, Arslan, U., Moormann, C., and Reul, O.** (1998). Piled raft foundation: interaction between piles and raft. *Darmstadt Geotechnics*, **4**(2), 279–296.
- Katzenbach, Rolf, and Choudhury, D.** (2013). ISSMGE Combined Pile-Raft Foundation Guideline. *International Society for Soil Mechanics and Geotechnical Engineering*, July, 23.
- Kausel, E.** (1981). *An explicit solution for the Green functions for dynamic loads in layered media (Research report R81-13)*. Department of Civil Engineering, School of Engineering, Massachusetts Institute of Technology, Cambridge, MA, U.S.A
- Kausel, E., and Roesset, J. M.** (1975). Dynamic stiffness of circular foundations. *Journal of the Engineering Mechanics Division*, **101**(6), 771–785.
- Kavvas, M., and Gazetas, G.** (1993). Kinematic seismic response and bending of free-head piles in layered soil. *Geotechnique*, **43**(2), 207–222.
- Kaynia, A. M., and Kausel, E.** (1982). Dynamic behavior of pile groups. *Proc. of Second International Conference on Numerical Method in Offshore Piling, 1982*.
- Kaynia, A. M.** (1982). *Dynamic stiffness and seismic response of pile groups*. Ph. D. Thesis, Massachusetts Institute of Technology, Cambridge, MA, U.S.A.

- Kim, J., Lee, E., Lee, D., Lee, C., Kim, J., Lee, E., Lee, D., Lee, C., and Yang, S.** (2016). Influence of Radius of Central Soil Column in POINT Module of the SASSI Program on Seismic Response of Foundation. *Journal of Earthquake Engineering*, **Jan(00)**, 1–13. <https://doi.org/10.1080/13632469.2016.1264321>
- Kim, S., Asce, A. M., and Stewart, J. P.** (2003). *Kinematic Soil-Structure Interaction from Strong Motion Recordings*. April, 323–335.
- Kline, S. J.** (2012). *Similitude and approximation theory*. Springer Science & Business Media.
- Kokusho, T.** (2017). *Innovative earthquake soil dynamics*. CRC Press.
- Koyamada, K., Miyamoto, Y., and Tokimatsu, K.** (2006). Field investigation and analysis study of damaged pile foundation during the 2003 Tokachi-Oki Earthquake. In *Seismic Performance and Simulation of Pile Foundations in Liquefied and Laterally Spreading Ground* (pp. 97–108).
- Kubo, K.** (1969). Vibration test of a structure supported by pile foundation. *Proceedings of 4th World Conference on Earthquake Engineering, Santiago, Chile*, A6:1-12.
- Kumar, A., and Choudhury, D.** (2018). Development of new prediction model for capacity of combined pile-raft foundations. *Computers and Geotechnics*, **97**, 62–68.
- Kumar, A., Choudhury, D., and Katzenbach, R.** (2016). Effect of Earthquake on Combined Pile–Raft Foundation. *International Journal of Geomechanics*, **16(5)**, 04016013. [https://doi.org/10.1061/\(ASCE\)GM.1943-5622.0000637](https://doi.org/10.1061/(ASCE)GM.1943-5622.0000637)
- Kumar, E. M., and Ramamurthy, K.** (2017). Influence of production on the strength, density and water absorption of aerated geopolymer paste and mortar using Class F fly ash. *Construction and Building Materials*, **156**, 1137–1149.
- Lee, JinHyung, Kim, Y., and Jeong, S.** (2010). Three-dimensional analysis of bearing behavior of piled raft on soft clay. *Computers and Geotechnics*, **37(1–2)**, 103–114.
- Lee, Junhwan, Park, D., Park, D., and Park, K.** (2015). Estimation of load-sharing ratios for piled rafts in sands that includes interaction effects. *Computers and Geotechnics*, **63**, 306–314.

- Leung, Y. F., Klar, A., Ph, D., Asce, M., Soga, K., Ph, D., and Asce, M.** (2010). *Theoretical Study on Pile Length Optimization of Pile*. February, 319–330.
- Liingaard, M., Andersen, L., and Ibsen, L. B.** (2007). Impedance of flexible suction caissons. *Earthquake Engineering & Structural Dynamics*, **36**(14), 2249–2271.
- Liu, C. L., and Ai, Z. Y.** (2017). Vertical harmonic vibration of piled raft foundations in layered soils. *International Journal for Numerical and Analytical Methods in Geomechanics*, **41**(17), 1711–1723. <https://doi.org/10.1002/nag.2696>
- Liu, H. S., and Chen, K. J.** (1991). Test on behavior of pile foundation in liquefiable soils. *Proc. of 2nd International Conference on Recent Advances in Geotechnical Engineering and Soil Dynamics, St. Louis, USA*, Vol. 1, 233-235.
- Liu, L., and Dobry, R.** (1995). Effect of liquefaction on lateral response of piles by centrifuge model tests. *Proc. of Workshop on New Approaches to Liquefaction Analysis 1991, Washington, D.C*
- Liu, Y., and Zhang, L.** (2018). Seismic response of pile–raft system embedded in spatially random clay. *Géotechnique*, 1–8.
- Liu, Y., and Zhang, L.** (2019). Seismic response of pile–raft system embedded in spatially random clay. *Géotechnique*, **69**(7), 638–645.
- Luan, L., Zheng, C., Kouretzis, G., Ding, X., and Poulos, H.** (2020). A new dynamic interaction factor for the analysis of pile groups subjected to vertical dynamic loads. *Acta Geotechnica*. <https://doi.org/10.1007/s11440-020-00989-7>
- Lysmer, J., & Kuhlemeyer, R. L.** (1969). Finite dynamic model for infinite media. *Journal of the Engineering Mechanics Division, ASCE*, **95**(4), 859–878.
- Lysmer, John, Tabatabaie-Raissi, M., Tajirian, F., Vahdani, S., and Ostadan, F.** (1981). *SASSI: A system for analysis of soil-structure interaction*. Geotechnical Engineering Group, University of California, Berkeley, California
- Maeso, O., Aznárez, J. J., and García, F.** (2005). Dynamic impedances of piles and groups of piles in saturated soils. *Computers & Structures*, **83**(10), 769–782. <https://doi.org/https://doi.org/10.1016/j.compstruc.2004.10.015>

- Maiorano, R. M. S., de Sanctis, L., Aversa, S., and Mandolini, A.** (2009). Kinematic response analysis of piled foundations under seismic excitation. *Canadian Geotechnical Journal*, **46**(5), 571–584.
- Makris, N., and Gazetas, G.** (1993). Displacement phase differences in a harmonically oscillating pile. *Geotechnique*, **43**(1), 135–150.
- Makris, N., and Gazetas, G.** (1992). Dynamic pile-soil-pile interaction. Part II: Lateral and seismic response. *Earthquake Engineering & Structural Dynamics*, **21**(2), 145–162.
- Mandolini, A., Russo, G., and Viggiani, C.** (2005). Pile foundations: Experimental investigations, analysis and design. *Proceedings of the International Conference on Soil Mechanics and Geotechnical Engineering*, **16**(1), 177.
- Manna, B., and Baidya, D. K.** (2010a). Dynamic nonlinear response of pile foundations under vertical vibration-Theory versus experiment. *Soil Dynamics and Earthquake Engineering*, **30**(6), 456–469. <https://doi.org/10.1016/j.soildyn.2010.01.002>
- Manna, B., and Baidya, D. K.** (2010b). Nonlinear Dynamic Response of Piles under Horizontal Excitation. *Journal of Geotechnical and Geoenvironmental Engineering*, **136**(12), 1600–1609. [https://doi.org/10.1061/\(asce\)gt.1943-5606.0000388](https://doi.org/10.1061/(asce)gt.1943-5606.0000388)
- Manna, B., and Baidya, D.** (2009). Dynamic vertical response of model piles—experimental and analytical investigations. *International Journal of Geotechnical Engineering*, **3**(2), 271–287.
- Margason, E.** (1977). Pile bending during earthquakes. *Proc., Sixth World Conference on Earthquake Engineering, Sarita Prakashan, 1690*, II.
- Maiorano, R. M. S., de Sanctis, L., Aversa, S., & Mandolini, A.** (2009). Kinematic response analysis of piled foundations under seismic excitation. *Canadian Geotechnical Journal*, **46**(5), 571-584
- Martinelli, M., Burghignoli, A., and Callisto, L.** (2016). Dynamic response of a pile embedded into a layered soil. *Soil Dynamics and Earthquake Engineering*, **87**, 16–28. <https://doi.org/10.1016/j.soildyn.2016.03.021>

- Matsumoto, T., Fukumura, K., Horikoshi, K., and Oki, A.** (2004). Shaking table tests on model piled rafts in sand considering influence of superstructures. *International Journal of Physical Modelling in Geotechnics*, *4*(3), 21–38.
- Mattsson, N., Menoret, A., Simon, C., and Ray, M.** (2013). Case study of a full-scale load test of a piled raft with an interposed layer for a nuclear storage facility. *Géotechnique*, *63*(11), 965–976.
- Mayoral, J. M., Alberto, Y., Mendoza, M. J., and Romo, M. P.** (2009). Seismic response of an urban bridge-support system in soft clay. *Soil Dynamics and Earthquake Engineering*, *29*(5), 925–938. <https://doi.org/10.1016/j.soildyn.2008.10.007>
- Mayoral, J. M., Flores, F. A., and Romo, M. P.** (2011). Seismic response evaluation of an urban overpass. *Earthquake Engineering & Structural Dynamics*, *40*(8), 827–845. <https://doi.org/10.1002/eqe.1062>
- Mayoral, J. M., and Romo, M. P.** (2015). Seismic response of bridges with massive foundations. *Soil Dynamics and Earthquake Engineering*, *71*, 88–99. <https://doi.org/10.1016/j.soildyn.2015.01.008>
- Mendoza, M. J., and Auvinet, G.** (1988). The Mexico earthquake of September 19, 1985—behavior of building foundations in Mexico City. *Earthquake Spectra*, *4*(4), 835–853.
- Mendoza, M. J., and Romo, M. P.** (1996). Geoseismic Instrumentation of a Friction Pile-Box Foundation. *Proc. of the Eleventh World Conference on Earthquake Engineering, Acapulco, Mexico*.
- Mendoza, M. J., and Romo, M. P.** (1998). Performance of a friction pile-box foundation in Mexico City clay. *Soils and foundations*, Elsevier, *38*(4), 239–249.
- Mendoza, M. J., Romo, M. P., Orozco, M., and Dominguez, L.** (2000). Static and Seismic Behavior of a Friction Pile-Box Foundation in Mexico City Clay. *Soils And Foundations*, *40*(4), 143–154.
- Mendoza, M. J., Romo, M. P., Orozco, M., and Mendoza, M. J.** (2004). Behavior of a Friction-Piled Box Foundation for an Urban Bridge in Mexico City Clay. *Proc. of the Fifth International Conference on Case Histories in Geotechnical Engineering, New York*.

- Meyerhof, G. G.** (1953). Some recent foundation research and its application to design. *The Structural Engineer*, **31**(6), 151–167.
- Meymand, P. J.** (1998). *Shaking table scale model tests of nonlinear soil-pile-superstructure interaction in soft clay*. Ph. D Thesis, University of California Berkeley, California, U.S.A.
- Michaelides, O., Gazetas, G., Bouckovalas, G., and Chryssikou, E.** (1998). Approximate non-linear dynamic axial response of piles. *Geotechnique*, **48**(1), 33–53.
- Militano, G., and Rajapakse, R.** (1999). Dynamic response of a pile in a multi-layered soil to transient torsional and axial loading. *Geotechnique*, **49**(1), 91–109.
- Mizuno, H., and Iiba, M.** (1992). Dynamic effects of backfill and piles on foundation impedance. *Proc. of the Tenth World Conference on Earthquake Engineering*, 1823–1828.
- Moncarz, P. D., and Krawinkler, H.** (1981). *Theory and application of experimental model analysis in earthquake engineering*. The John A. Blume Earthquake Engineering Center Report.
- Moss, R. E. S., Crosariol, V., and Kuo, S.** (2010). Shake table testing to quantify seismic soil-structure-interaction of underground structures. *Proc. of the Fifth International Conference of Geotechnical Earthquake Engineering and Soil Dynamics, Missouri*
- Mucciacciaro, M., and Sica, S.** (2018). Nonlinear soil and pile behaviour on kinematic bending response of flexible piles. *Soil Dynamics and Earthquake Engineering*, **107**, 195–213.
- Mylonakis, G.** (1995). *Contributions to the static and seismic analysis of pile-supported bridge piers*. Ph.D. Thesis. State University of New York, Buffalo, U.S.A.
- Mylonakis, G.** (2001). Simplified model for seismic pile bending at soil layer interfaces. *Soils and Foundations*, **41**(4), 47–58.
- Mylonakis, G., and Gazetas, G.** (1999). Lateral vibration and internal forces of grouped piles in layered soil. *Journal of Geotechnical and Geoenvironmental Engineering*, **125**(1), 16–25.

- Mylonakis, G., Nikolaou, A., and Gazetas, G.** (1997). Soil — Pile — Bridge Seismic Interaction : Kinematic and Inertial Effects . Part I : Soft Soil. *Earthquake Engineering & Structural Dynamics*, **26**(October 1995), 337–359. [https://doi.org/10.1002/\(SICI\)1096-9845\(199703\)26](https://doi.org/10.1002/(SICI)1096-9845(199703)26)
- Nagai, H.** (2019). Simplified method of estimating the dynamic impedance of a piled raft foundation subjected to inertial loading due to an earthquake. *Computers and Geotechnics*, **105**(May 2018), 69–78. <https://doi.org/10.1016/j.compgeo.2018.09.014>
- Nakai, S., Kato, H., Ishida, R., and Mano, H.** (2004). Load Bearing Mechanism of Piled Raft Foundation during Earthquake. *Proc. of the Third UJNR Workshop on Soil-Structure Interaction*, 18.
- Nakai, S., Mano, H., and Matsuda, T.** (2001). An Analysis for Stress Distribution of Piled Raft Foundations under Seismic Loading. *Proceedings 2nd US-Japan Workshop on Soilstructure Interaction, Tsukuba City, Japan*, 1–33.
- Nam, K., Lee, S., Kim, K., Chung, C., Mo, M., and Sung, H.** (2001). *Optimal pile arrangement for minimizing differential settlements in piled raft foundations*. **28**, 235–253.
- NEHRP.** (1997). *Recommended provisions for seismic regulations Structures, new buildings and other Structures*. Building Seismic Safety Council, Washington, DC.
- New Zealand Standard (NZS) 1170.5.** (2004). *Structural Design Actions Part 5: Earthquake Actions-New Zealand*. Standards New Zealand Wellington, NZ.
- Nikolaou, A., Mylonakis, G., and Gazetas, G.** (1995). *Kinematic Bending Moments in Seismically Stressed Piles*. Report. NCEER-95-0022. <http://hdl.handle.net/10477/673%0A>
- Nikolaou, S., Mylonakis, G., Gazetas, G., and Tazoh, T.** (2001). Kinematic pile bending during earthquakes: analysis and field measurements. *Géotechnique*, **51**(5), 425–440. <https://doi.org/10.1680/geot.51.5.425.39973>
- Nikolaou, Stella, Mylonakis, G., Gazetas, G., and Tazoh, T.** (2001). Kinematic pile bending during earthquakes: analysis and field measurements. *Geotechnique*, **51**(5), 425–440.
- Nogami, T., and Novak, M.** (1977). Resistance of soil to a horizontally vibrating pile. *Earthquake Engineering & Structural Dynamics*, **5**(3), 249–261.

- Nogami, T., Jones, H. W., and Mosher, R. L.** (1991). Seismic response analysis of pile-supported structure: assessment of commonly used approximations. *Proc. of the Third International Conference on Recent Advances in Geotechnical Engineering and Soil Dynamics, University of Missouri-Rolla, Missouri*, 931–940.
- Nogami, T., and Novák, M.** (1976). Soil-pile interaction in vertical vibration. *Earthquake Engineering & Structural Dynamics*, **4**(3), 277–293.
- Novak, M., Wi, H. E., and Sharnouby, B. E. L.** (1984). *Static and Dynamic Behaviour of Pile Groups*. 645–651.
- Novak, M.** (1974). Dynamic stiffness and damping of piles. *Canadian Geotechnical Journal*, **11**(4), 574–598.
- Novak, M.** (1980). Approximate approach to contact effects of piles. *Special Technical Publication on Dynamic Response of Pile Foundations: Analytical Aspects*.
- Novak, M., and Aboul-Ella, F.** (1978). Impedance functions of piles in layered media. *Journal of the Engineering Mechanics Division*, **104**(3), 643–661.
- Novak, M., Aboul-Ella, F., and Nogami, T.** (1978). Dynamic soil reactions for plane strain case. *Journal of the Engineering Mechanics Division*, **104**(4), 953–959.
- Novak, M., and El Sharnouby, B.** (1983). Stiffness constants of single piles. *Journal of Geotechnical Engineering*, **109**(7), 961–974.
- Novak, M., and F. Grigg, R.** (1976). Dynamic experiments with small pile foundations. *Canadian Geotechnical Journal*, **13**(4), 372–385.
- Novak, M., and Han, Y. C.** (1990). Impedances of soil layer with boundary zone. *Journal of Geotechnical Engineering*, **116**(6), 1008–1014.
- Novak, M., and Sharnouby, B. El.** (1984). Evaluation of dynamic experiments on pile group. *Journal of Geotechnical Engineering*, **110**(6), 738–756.
- NPCIL.** (2018). *Geotechnical input parameters for Seismic Soil Structure Interaction (SSSI) analysis and proposed soil profile including Best Estimate (BE), Lower Bound (LB) and Upper Bound (UB) values to be used in ACS SASSI*. Nuclear Power Corporation of India Ltd., Mumbai, India.

- Ostadan, F.** (1983). *Dynamic Analysis of Soil-Pile-Structure Systems*. Ph. D. Thesis, University of California, Berkeley.
- Ostadan, F., and Deng, N.** (2012). *SASSI 2010 Version 1.0 User's Manual*.
- Padrón, L. A.** (2009). *Numerical model for the dynamic analysis of pile foundations*. Ph. D. thesis, Univesidad de Las Palmas de Gran Canaria.
- Padrón, L. A., Aznárez, J. J., and Maeso, O.** (2007). BEM-FEM coupling model for the dynamic analysis of piles and pile groups. *Engineering Analysis with Boundary Elements*, **31**(6), 473–484. <https://doi.org/10.1016/j.enganabound.2006.11.001>
- Padrón, L. A., Mylonakis, G. E., and Beskos, D. E.** (2009). Importance of footing–soil separation on dynamic stiffness of piled embedded footings. *International Journal for Numerical and Analytical Methods in Geomechanics*, **33**(11), 1439–1448.
- Pal, A. S., and Baidya, D. K.** (2018). Dynamic Analysis of Pile Foundation Embedded in Homogeneous Soil Using Cone Model. *Journal of Geotechnical and Geoenvironmental Engineering*, **144**(8), 06018007. [https://doi.org/10.1061/\(asce\)gt.1943-5606.0001927](https://doi.org/10.1061/(asce)gt.1943-5606.0001927)
- Phanikanth, V. S., Choudhury, D., and Reddy, G. R.** (2013). Behavior of single pile in liquefied deposits during earthquakes. *International Journal of Geomechanics*, **13**(4), 454–462.
- Pitilakis, D., Dietz, M., Muir, D., Clouteau, D., and Modaressi, A.** (2008). *Numerical simulation of dynamic soil – structure interaction in shaking table testing*. **28**, 453–467. <https://doi.org/10.1016/j.soildyn.2007.07.011>
- Poulos, H. G.** (2001). Piled raft foundations: design and applications. *Géotechnique*, **51**(2), 95–113. <https://doi.org/10.1680/geot.2001.51.2.95>
- Poulos, H. G., Small, J. C., and Chow, H.** (2011). Piled raft foundations for tall buildings. *Geotechnical Engineering Journal of the SEAGS & AGSSEA*, **42**(2), 78–84.
- Poulos, H. G., Small, J. C., Ta, L. D., Sinha, J., and Chen, L.** (1999). Comparison of some methods for analysis of piled rafts. *International Conference on Soil Mechanics and Foundation Engineering*, 1119–1124.

- Poulos, H. G., and Bunce, G.** (2008). *Foundation design for the Burj Dubai—the world's tallest building*.
- Poulos, H. G., and Hull, T.** (1989). The role of analytical geomechanics in foundation engineering. *Foundation Engineering: Current Principles and Practices, ASCE, Reston, 2*, 1578–1606.
- Poulos, H. G., and Davis, E. H.** (1980). *Pile foundation analysis and design*. Wiley (John) & Sons, Limited
- Rahmani, A., Taiebat, M., Liam Finn, W. D., and Ventura, C. E.** (2016). Evaluation of substructuring method for seismic soil-structure interaction analysis of bridges. *Soil Dynamics and Earthquake Engineering, 90*, 112–127. <https://doi.org/10.1016/j.soildyn.2016.08.013>
- Rajapakse, R., and Shah, A. H.** (1989). Impedance curves for an elastic pile. *Soil Dynamics and Earthquake Engineering, 8*(3), 145–152.
- Randolph, M. F.** (1994). Design methods for pile groups and piled rafts. *International Conference on Soil Mechanics and Foundation Engineering*, 61–82.
- Rathje, E. M., Abrahamson, N. A., and Bray, J. D.** (1998). Simplified frequency content estimates of earthquake ground motions. *Journal of Geotechnical and Geoenvironmental Engineering, 124*(2), 150–159.
- Reul, O.** (2004). Numerical Study of the Bearing Behavior of Piled Rafts. *International Journal of Geomechanics, 4*(2), 59-68.
- Roesset, J. M., and Angelides, D.** (1980). Dynamic stiffness of piles. In *Numerical methods in offshore piling* (pp. 75–81). Thomas Telford Publishing.
- Roesset, J. M., and Kausel, E.** (1976). Dynamic soil structure interaction. *Proc. of the 2nd International Conference on Numerical Methods in Geomechanics, Blacksburg, Va.(USA)*.
- Rollins, K. M., and Sparks, A.** (2002). Lateral resistance of full-scale pile cap with gravel backfill. *Journal of Geotechnical and Geoenvironmental Engineering, 128*(9), 711–723.

- Romo, M. P., Mendoza, M. J., and Garcia, S. R.** (2000). Geotechnical Factors in Seismic Design of Foundations State of the Art Report. *Proc. of the 12th World Conference on Earthquake Engineering, Auckland, New Zealand.*
- Roscoe, K. H.** (1968). Soils and model tests. *Journal of Strain Analysis*, **3**(1), 57–64.
- Rovithis, E., Di Laora, R., Iovino, M., & de Sanctis, L.** (2019). A numerical study on the filtering action of piles in the soft clay of Maliakos Gulf, Central Greece. *Proc. of the 17th International Conference on Computational Methods in Structural Dynamics and Earthquake Engineering, COMPDYN 2019, National Technical University of Athens. Vol. 1, pp 1975-1985*
- Roy, J., Kumar, A., and Choudhury, D.** (2018). Natural frequencies of piled raft foundation including superstructure effect. *Soil Dynamics and Earthquake Engineering*, **112**, 69–75.
- Russo, G., and Viggiani, C.** (1998). Factors controlling soil-structure interaction for piled rafts. *Proc. of Int. Conf. on Soil-Structure Interaction in Urban Civil Engineering*, 297–322.
- Schnabel, P. B.** (1972). SHAKE a computer program for earthquake response analysis of horizontally layered sites. *EERC Report, Univ. of California, Berkeley.*
- Scott, R. F., Liu, H. P., and Ting, J.** (1977). Dynamic pile tests by centrifuge modeling. *Proc. of 6th World Conference on Earthquake Engineering, New Delhi, India, pp 4–50.*
- Seed, H. B., and Idriss, I. M.** (1970). Soil moduli and damping factors for dynamic response analysis. Rep. No. EERC 70-10. *Earthquake Engineering Research Centre, Berkeley, CA.*
- Shadlou, M., and Bhattacharya, S.** (2014). Dynamic stiffness of pile in a layered elastic continuum. *Geotechnique*, **64**(4), 303.
- Sharnouby, B. El, and Novak, M.** (1984). Dynamic experiments with group of piles. *Journal of Geotechnical Engineering*, **110**(6), 719–737.
- Sica, S., Mylonakis, G., and Simonelli, A. L.** (2011). Transient kinematic pile bending in two-layer soil. *Soil Dynamics and Earthquake Engineering*, **31**(7), 891–905.
- Simone, S. V. D. E.** (1966). Suggested Design Procedures for Combined Footings and Mats. *Journal of The American Concrete Institute*, **10**(63), 1041–1057.

- Small, J. C., and Zhang, H. H.** (2006). *Behavior of Piled Raft Foundations Under Lateral and Vertical Loading*. 2(1), 29–45. [https://doi.org/10.1061/\(ASCE\)1532-3641\(2002\)2](https://doi.org/10.1061/(ASCE)1532-3641(2002)2)
- Spyrakos, C. C., and Xu, C.** (2004). Dynamic analysis of flexible massive strip-foundations embedded in layered soils by hybrid BEM–FEM. *Computers & Structures*, 82(29–30), 2541–2550.
- Stewart, J. P., Crouse, C. B., Hutchinson, T. C., Lizundia, B., Naeim, F., and Ostadan, F.** (2012). *Soil-Structure Interaction for Building Structures (NIST GCR 12-917-21)*. National Institute of Standards and Technology, MD, U.S.A.
- Stewart, J. P., Seed, R. B., and Fenves, G. L.** (1999). Seismic soil-structure interaction in buildings. II: Empirical findings. *Journal of Geotechnical and Geoenvironmental Engineering*, 125(1), 38–48.
- Storie, L. B., Knappett, J. A., and Pender, M. J.** (2015). Centrifuge modelling of the energy dissipation characteristics of mid-rise buildings with raft foundations on dense cohesionless soil. *Proc. of 6th International Conference on Earthquake Geotechnical Engineering, Christchurch*.
- Sultan, H. A., and Seed, H. B.** (1967). Stability of sloping core earth dams. *Journal of Soil Mechanics & Foundations Division, ASCE*.
- Tabatabaie, M.** (2013). Accuracy of the Subtraction Model Used in SASSI. *Proc. of the 22nd International Conference on Structural Mechanics in Reactor Technology, San Francisco, U.S.A.*
- Tabatabaiefar, S. H. R.** (2012). *Determining seismic response of mid-rise building frames considering dynamic soil-structure interaction*. Ph.D. Thesis, University of Technology, Sydney.
- Tajimi, H.** (1966). Earthquake response of foundation structures (in Japanese) report. *Faculty of Science and Engineering, Nihon University Tokyo*, 1.
- Tajimi, H.** (1969). Dynamic analysis of a structure embedded in an elastic stratum. *Proc. 4th World Conf. on Earthq. Engng*, 53–69.

- Tazoh, T.** (1988). Seismic observations and analysis of grouped piles. *Shimizu Technical Research Bulletin*, *7*, 17–32.
- Ting, J. M., and Scott, R. F.** (1984). Static and dynamic lateral pile group action. *Proc. 8th. World Conf. EQ Eng., San Francisco*, *3*, 641–648.
- Tokimatsu, K., Mizuno, H., and Kakurai, M.** (1996). Building damage associated with geotechnical problems. *Soils and Foundations*, *36*(Special), 219–234.
- Turner, B. J., Brandenberg, S. J., and Stewart, J. P.** (2017). *Influence of kinematic SSI on foundation input motions for pile-supported bridges (PEER Report No. 2017/08)*. Pacific Earthquake Engineering Research Center, California, U.S.A.
- Uchida, A., Yamada, T., Odajima, N., and Yamashita, K.** (2012). Piled raft foundation with grid-form ground improvement subjected to the 2011 earthquake. *9th International Conference on Urban Earthquake Engineering/4th Asia Conference on Earthquake Engineering, Tokyo Institute of Technology, Tokyo*, 151–156.
- Ulrich, E. J., Shukla, S. N., Secretary, C., Baker Jr, C. N., Ball, S. C., Bowles, J. E., Colaco, J. P., Davisson, X. I. T., Focht Jr, J. A., and Gaynor, M.** (1988). Suggested analysis and design procedures for combined footings and mats. *ACI Structural Journal*, *85*(3), 304–324.
- Varghese, R., Boominathan, A., and Banerjee, S.** (2019). Seismic Response Characteristics of a Piled Raft in Clay. *Journal of Earthquake and Tsunami*, *13*(1). <https://doi.org/10.1142/S1793431119500052>
- Vasilev, G., Parvanova, S., Dineva, P., and Wuttke, F.** (2015). Soil-structure interaction using BEM-FEM coupling through ANSYS software package. *Soil Dynamics and Earthquake Engineering*, *70*, 104–117. <https://doi.org/10.1016/j.soildyn.2014.12.007>
- Vaziri, H., and Han, Y.** (1991). Full-scale field studies of the dynamic response of piles embedded in partially frozen soils. *Canadian Geotechnical Journal*, *28*(5), 708–718.
- Vaziri, H., and Han, Y.** (1993). Impedance functions of piles in inhomogeneous media. *Journal of Geotechnical Engineering*, *119*(9), 1414–1430.

- Verma, K. ., Gaur, M. ., and Saini, H. .** (2012). *Geology and Mineral Resources of Haryana*.
<https://doi.org/ISSN 0579 4706>
- Viggiani, C., Mandolini, A., and Russo, G.** (2014). *Piles and pile foundations*. CRC Press.
- Vrettos, C.** (1991). Time-harmonic Boussinesq problem for a continuously non-homogeneous soil. *Earthquake Engineering & Structural Dynamics*, **20**(10), 961–977.
- Waas, G.** (1972). *Linear Two-dimensional Analysis of Soil Dynamics Problems in Semi-infinite Layered Media*. Ph.D. Thesis, University of California, Berkeley.
- Waas, G., and Hartmann, H. G.** (1981). Pile foundations subjected to dynamic horizontal loads. *Proc. of the European Simulation Meeting on Modeling and Simulation of Large Scale Structural Systems*.
- Wen, X., Zhou, F., Fukuwa, N., and Zhu, H.** (2015). A simplified method for impedance and foundation input motion of a foundation supported by pile groups and its application. *Computers and Geotechnics*, **69**, 301–319.
- Wilson, D.** (1998). *Dynamic centrifuge tests of pile supported structures in liquefiable sand*
Ph. D. Thesis, University of California, California, USA.
- Wilson, E. L.** (1965). Structural analysis of axisymmetric solids. *Aiaa Journal*, **3**(12), 2269–2274.
- Wolf, J. P., Von Arx, G. A., De Barros, F. C. P., and Kakubo, M.** (1981). Seismic analysis of the pile foundation of the reactor building of the NPP Angra 2. *Nuclear Engineering and Design*, **65**(3), 329–341.
- Wolf, J. P., Meek, J. W., and Song, C.** (1992). Cone models for a pile foundation. *Proceedings of the Conference on Piles Under Dynamic Loads, New York, USA*.
- Wu, G., and Finn, W. . D. L.** (1997a). Dynamic elastic analysis of pile foundations using finite element method in the frequency domain. *Canadian Geotechnical Journal*, **34**(1), 34–43.
<https://doi.org/10.1139/cgj-34-1-34>
- Wu, G., and Finn, W. D. L.** (1997b). Dynamic nonlinear analysis of pile foundations using finite element method in the time domain. *Canadian Geotechnical Journal*, **34**(1), 44–52.

- Wu, G., Finn, W. D. L., and Dowling, J.** (2015). Quasi-3D analysis: Validation by full 3D analysis and field tests on single piles and pile groups. *Soil Dynamics and Earthquake Engineering*, *78*, 61–70.
- Wu, W. B., Wang, K. H., Zhang, Z. Q., and Leo, C. J.** (2013). Soil-pile interaction in the pile vertical vibration considering true three-dimensional wave effect of soil. *International Journal for Numerical and Analytical Methods in Geomechanics*, *37*(17), 2860–2876.
- Xu, B., Lu, J.-F., and Wang, J.-H.** (2010). Dynamic responses of a pile embedded in a layered poroelastic half-space to harmonic lateral loads. *International Journal for Numerical and Analytical Methods in Geomechanics*, *34*(5), 493–515. <https://doi.org/10.1002/nag.814>
- Yamashita, K., Kakurai, M., and Yamada, T.** (1994). Investigation of a piled raft foundation on stiff clay. *International Conference on Soil Mechanics and Foundation Engineering*, 543–546.
- Yamashita, K., Hamada, J., Onimaru, S., and Higashino, M.** (2012a). Seismic behavior of piled raft with ground improvement supporting a base-isolated building on soft ground in Tokyo. *Soils and Foundations*, *52*(5), 1000–1015.
- Yamashita, K., Hamada, J., Onimaru, S., and Higashino, M.** (2012b). Seismic behavior of piled raft with ground improvement supporting a base-isolated building on soft ground in Tokyo. *Soils and Foundations*, *52*(5), 1000–1015. <https://doi.org/10.1016/j.sandf.2012.11.017>
- Yamashita, K., Hamada, J., and Tanikawa, T.** (2016a). Static and seismic performance of a friction piled raft combined with grid-form deep mixing walls in soft ground. *Soils and Foundations*, *56*(3), 559–573. <https://doi.org/10.1016/j.sandf.2016.04.020>
- Yamashita, K., Hamada, J., and Tanikawa, T.** (2016b). Static and seismic performance of a friction piled raft combined with grid-form deep mixing walls in soft ground. *Soils and Foundations*, *56*(3), 559–573.
- Yamashita, K., Shigeno, Y., Hamada, J., and Chang, D.-W.** (2018). Seismic response analysis of piled raft with grid-form deep mixing walls under strong earthquakes with performance-based design concerns. *Soils and Foundations*, *58*(1), 65–84.

- Yuksekol, Y., Matsumoto, T., and Shimono, S.** (2015). Shaking Table Tests of Piled Raft and Pile Group Foundations in Dry. *Proceedings of 6th International Conference on Earthquake Geotechnical Engineering, 1-4 November, Christchurch, New Zealand. ICEGE, November.*
- Zeng, X., and Rajapakse, R.** (1999). Dynamic axial load transfer from elastic bar to poroelastic medium. *Journal of Engineering Mechanics*, **125**(9), 1048–1055.
- Zhang, L., Goh, S. H., and Liu, H.** (2017a). Seismic response of pile-raft-clay system subjected to a long-duration earthquake: centrifuge test and finite element analysis. *Soil Dynamics and Earthquake Engineering*, **92**(November 2016), 488–502. <https://doi.org/10.1016/j.soildyn.2016.10.018>
- Zhang, L., Goh, S. H., and Liu, H.** (2017b). Seismic response of pile-raft-clay system subjected to a long-duration earthquake: centrifuge test and finite element analysis. *Soil Dynamics and Earthquake Engineering*, **92**, 488–502.
- Zhang, W., Esmailzadeh Seylabi, E., and Taciroglu, E.** (2017). Validation of a three-dimensional constitutive model for nonlinear site response and soil-structure interaction analyses using centrifuge test data. *International Journal for Numerical and Analytical Methods in Geomechanics*, **41**(18), 1828–1847.
- Zheng, C., Kouretzis, G. P., Sloan, S. W., Liu, H., and Ding, X.** (2015). Vertical vibration of an elastic pile embedded in poroelastic soil. *Soil Dynamics and Earthquake Engineering*, **77**, 177–181. [https://doi.org/https://doi.org/10.1016/j.soildyn.2015.05.010](https://doi.org/10.1016/j.soildyn.2015.05.010)
- Zhou, X.-L., and Wang, J.-H.** (2009). Analysis of pile groups in a poroelastic medium subjected to horizontal vibration. *Computers and Geotechnics*, **36**(3), 406–418.

LIST OF PUBLICATIONS BASED ON THIS THESIS

REFEREED JOURNALS

1. **Varghese, R., Boominathan, A., & Banerjee, S.** (2020). Stiffness and load sharing characteristics of piled raft foundations subjected to dynamic loads. *Soil Dynamics and Earthquake Engineering*, **133**, 106117.
2. **Varghese, R., Amuthan, M. S., Boominathan, A., & Banerjee, S.** (2019). Cyclic and postcyclic behaviour of silts and silty sands from the Indo Gangetic Plain. *Soil Dynamics and Earthquake Engineering*, **125**, 105750.
3. **Varghese, R., Boominathan, A., & Banerjee, S.** (2019). Seismic response characteristics of a piled raft in clay. *Journal of Earthquake and Tsunami*, **13**(01), 1950005.

BOOK CHAPTERS AND CONFERENCE PROCEEDINGS

1. **Varghese, R., Boominathan, A., & Banerjee, S.** (2019). Numerical Analysis of Seismic Response of a Piled Raft Foundation System. *Soil Dynamics and Earthquake Geotechnical Engineering*. Springer, Singapore. 227-235
2. **Boominathan, A., Varghese, R., & Nair, S. K.** (2018). Soil–structure interaction analysis of pile foundations subjected to dynamic loads. *Geotechnics for Natural and Engineered Sustainable Technologies*. Springer, Singapore. 45-61
3. **Boominathan, A., Srinivas, A., Varghese, R.** (2019). Response of a Critical Structure to a Spatially Varying Ground Motion *Proceedings of 7th International Conference on Earthquake Geotechnical Engineering, Rome, Italy, 2019*
4. **Varghese, R., Boominathan, A., & Banerjee, S.** (2019). Pile Induced Filtering of Seismic Ground Motion in Homogeneous Soil *Proceedings of 5th International Conference on Modeling & Simulation in Civil Engineering, Kollam, Kerala, 2019*
5. **Varghese, R., Boominathan, A., & Banerjee, S.** (2018). Kinematic Response Characteristics of a Piled Raft Foundation *Proceedings of 43rd Annual of the Deep Foundations Institute at Anaheim California, USA during Oct 24-27, 2018*

6. **Varghese, R., Boominathan, A., & Banerjee, S.** (2017). Substructure based Numerical Simulation of Seismic Response of a Piled Raft System. *Proceedings of 3rd International Conference on Performance Based Design in Earthquake Geotechnical Engineering (PBD-III), 2017, Vancouver, Paper no. 195.*

CURRICULUM VITAE

NAME : Ramon Varghese

DATE OF BIRTH : 22 June 1990

EDUCATIONAL QUALIFICATIONS

2012 Bachelor of Technology

Institution : T.K.M College of Engineering, University of Kerala

Specialization : Civil Engineering

2014 Master of Technology

Institution : S.V. National Institute of Technology, Surat

Specialization : Soil Mechanics and Foundation Engineering

Doctor of Philosophy (Ph.D.)

Institution : Indian Institute of Technology, Madras

Specialization : Soil Dynamics and Earthquake Engineering

DOCTORAL COMMITTEE

CHAIRPERSON

Dr Manu Santhanam

Professor and Head

Department of Civil Engineering

GUIDES

Dr A. Boominathan

Professor

Department of Civil Engineering

Dr Subhadeep Banerjee

Associate Professor

Department of Civil Engineering

MEMBERS

Dr Sathish Kumar S. R.

Professor

Department of Civil Engineering

Dr Robinson R. G.

Professor

Department of Civil Engineering

Dr Nallayarasu S.

Professor

Department of Ocean Engineering